An Investigation of the Reaction Kinetics of Photocatalytic Wastewater Treatment using Suspended Titanium Dioxide Catalyst

by

William Joseph Hotz Jr.

Bachelor of Science, Civil Engineering
Rensselaer Polytechnic Institute, 2013

and

Claudia Carolina León Chávarri

Bachelor of Engineering, Industrial Engineering
Universidad de Lima, 2012

Submitted to the Department of Civil and Environmental Engineering Partial Fulfillment of the Requirements for the Degree of
Master of Engineering in Civil and Environmental Engineering\
at the
Massachusetts Institute of Technology

June, 2014

Signature of Author: Signature redacted
Department of Civil and Environmental Engineering
May 9, 2014

Certified by: Signature redacted
Edward Eric Adams
Senior Lecturer, Senior Research Engineer of Civil and Environmental Engineering
Thesis Supervisor

Accepted by: Signature redacted
Heidi M. Nepf
Chair, Departmental Committee for Graduate Students

An Investigation of the Reaction Kinetics of Photocatalytic Wastewater Treatment using Suspended Titanium Dioxide Catalyst

by

William J. Hotz Jr.

and

Claudia Carolina León Chávarri

Submitted to the Department of Civil and Environmental Engineering on
May 9, 2014 in Partial fulfilment of the requirements
For the Degree of Master of Engineering in Civil and Environmental Engineering

ABSTRACT

The goal of wastewater treatment is to remove compounds that may be harmful to the natural ecosystem or to humans. Although traditional treatment is fairly effective in meeting water quality standards, current technologies face the challenge of balancing a high removal of these damaging compounds with the addition of chemicals as a part of the very same removal process. In addition, new types of pollutants resistant to conventional treatment techniques are being found in wastewater streams at increasing concentrations. Moreover, traditional treatment technologies, require a large input of energy, emit greenhouse gases, and thus have a detrimental impact on the ecosystems that they intend to preserve.

In response to this dilemma, over the past few decades, the scientific community has devoted a special effort in the development of a new technology that harnesses natural sunlight to trigger the water treatment process. Photocatalytic oxidation, as this form of advanced oxidation process (AOP) is known, is characterized by the generation of hydroxyl radicals – one of the most oxidizing agents known in environmental chemistry – which easily attack all types of organic pollutants found in wastewater. However, while this process seems very promising, there are no standard design parameters to accurately model and predict the behavior of a photocatalytic reactor, a situation that prevents its use in full-scale treatment plants.

The photocatalytic oxidation of *Escherichia coli*, methanol, cinnamic acid, and sulfamethoxazole was tested on a laboratory-scale for dependence upon three initial variables. Based on experimental data, a direct dependence was found between the oxidation rate constants and the initial conditions of catalyst concentration and radiation intensity. Experimental results also show that the dependency upon initial pollutant concentration is highly related to the structure of the contaminant. This thesis studies a photocatalytic process using suspended titanium dioxide (TiO_2) catalyst. This document reviews the methodology followed to create the experimental framework and conduct the data analysis.

Thesis Supervisor: Edward Eric Adams
Title: Senior Research Engineer

ACKNOWLEDGEMENTS

We would like to thank the following people for their invaluable support and guidance over the last nine months:

Eric Adams, for serving as our advisor and providing his insights as we explored this new topic. Without his encouragement and direction, it would have been impossible to complete this project in the allotted time.

Javier Marugán, for proposing the topic of this research and guiding us during the literature review process. We would also like to thank him for proposing the numerical model used in Section 5, without which we would have likely struggled to produce anything remotely useful.

Ruud Timmers, for teaching us all about the (Ruud-made) reactor, its operation, and all of the sample analysis methods. His guidance greatly reduced the amount of time that would have been required to learn everything, and become competent in the experimentation process.

The entire lab group at Universidad Rey Juan Carlos in Madrid, for their hospitality and putting up with us while we conducted the experiments. By lending us their expertise, they greatly improved our overall productivity.

Lauren Maclean, for helping to organize our travels to Spain, providing support (and food), and most of all for maintaining order of the M. Eng Room.

And last, but not least, our fellow M. Eng'ers for their friendship and general support as we all rode the "struggle bus" together.

Mom, Dad, Lin, Nana, and the rest of the family, thank you so much for all of the support and encouragement throughout the last nine months, and my through entire life. There is no doubt that I would not have gotten to this point without you.

- Love, B

I would like to thank my whole family and friends for their unconditional love and support throughout this journey. Special thanks to my Mom, Dad and Tofy, for their encouragement and for sharing their time and technical advice whenever I needed it. All your texts, e-mails and videocalls have meant the world to me and I dedicate the fruits of my work to you, for making it possible.

- All my love, Calu

TABLE OF CONTENTS

LIST OF FIGURES

LIST OF TABLES

1 INTRODUCTION

Access to adequate water sources is a major problem that affects nations all over the world (UNICEF, 2013). While the specific problem varies in each country, it is possible to categorize the main issue as having either limited access or substandard access to this vital resource. Furthermore, this situation is expected to become more severe as climate change and water scarcity occur worldwide (USEPA, *Climate Change* 2013). Water and wastewater treatment is considered to be a traditional approach to facing inadequate water supply (WHO, 2013 & USEPA, *Water: SDWA* 2013). The quality of treated wastewater can directly affect human health either through direct contact, or indirectly since treated wastewater is often discharged into a receiving water body that may also act as a drinking water source. Wastewater treatment is the process, or group of processes, by which contaminants present in an influent are removed in order to provide a safe effluent according to water quality regulations which relate to the intended use of the liquid. Usually, the primary goal of wastewater treatment is to remove organic material and malign nutrients from the water body before it is discharged into the environment (USEPA, *Water: SDWA* 2013).

In the last few decades, however, the composition of wastewater streams has changed due to the introduction of new chemicals, such as pharmaceuticals and personal care products, that humans use daily (USEPA, *Water: CEC* 2013). These compounds, labeled as emerging pollutants, are potentially harmful and have recently been found in increasing concentrations in the effluent of municipal wastewater streams (AWRA, 2013) and have become an area of major concern for environmental scientists and engineers (USEPA, *Water: CEC* 2013). The growing use of these products, along with their resistance to traditional biological treatment has led to the need for an additional treatment step to remove these persistent chemicals.

Scientific research shows that it is possible to reduce the concentration of emerging pollutants, such as pharmaceuticals and personal care products, through oxidizing reactions that degrade even the most complex organic molecule structures to carbon dioxide (Stinson, n.d. & Science Daily, 2013). As a result, a great deal of emphasis has been placed on the study of a group of more effective oxidation techniques classified as advanced oxidation processes (AOPs). In practice, AOPs typically used in wastewater treatment are ozonation and UV-radiation. While these processes are effective, they are also very costly in terms of capital investment and operational energy requirements.

Fortunately, a sustainable solution to this challenge is being developed in the form of photocatalytic oxidation. Photocatalytic oxidation is an AOP alternative that uses natural sunlight to activate a semiconductor metal oxide catalyst which in turn generates oxidizing agents able to degrade pollutants and inactivate pathogens typically resistant to traditional treatment (University of Rhode Island, 2011 & Bennett, 2014). This process is non-selective in regards of target pollutant, does not require the addition of extra chemicals (the catalyst can be reused and

does not leave the system) and is expected to demand low operational costs; therefore, it has created high expectations among environmental scientists and engineers (Kaan et al., 2013).

Although this process of photocatalytic water treatment is complex, it can be observed as a system composed of three sub-processes: solar radiation, reaction kinetics, and reactor design. Due to the complexity of the reaction kinetics, this research will focus solely on this sub-process. A number of experiments were conducted on a lab-scale solar reactor, testing representative target pollutants (*E. coli*, methanol, cinnamic acid, and sulfamethoxazole) and varied catalyst concentrations and light intensities.

This study follows the research on photocatalytic AOP that is currently being conducted on a laboratory scale at Universidad Re Juan Carlos in Spain. Although other laboratory and pilot-plant studies have focused on bacterial inactivation, this study intends to test and model photocatalytic degradation of organic chemical pollutants. This thesis suggests that kinetic behavior can be modeled, allowing for the technology to be applied to full-scale wastewater treatment facilities.

1.1 BACKGROUND CONCEPTS

This section will review the most predominant concepts that will be utilized throughout this document. It will also acknowledge some of the primary sources discussing the theory behind photocatalytic advanced oxidation.

1.1.1 Typical Wastewater Treatment Process

A typical wastewater treatment plant (WWTP) employs a number of treatment steps (Figure 1.1) to remove natural organic matter and other components that may be harmful to the natural environment.

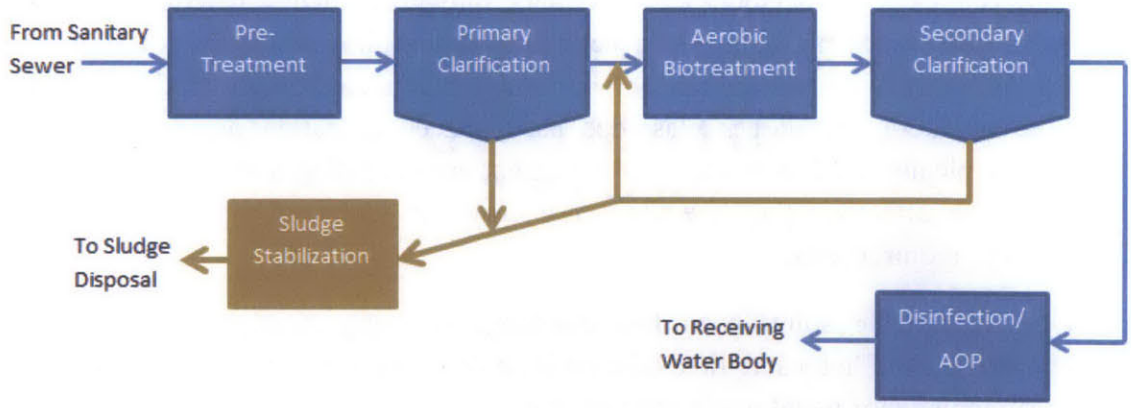

Figure 1.1 Traditional Wastewater Treatment Flow Process

Below is a brief description of the main treatment steps from raw wastewater to treated effluent water.

1.1.1.1 Pre-Treatment

The first step in the wastewater treatment process involves the removal of objects of considerable size and density by physical means such as screening and grit removal. Screening removes any large items (i.e. sticks or garbage) that may damage pumps and other equipment. Grit removal is achieved as dense solids, such as sand and gravel, quickly settle out. The pre-treatment stage does not account for significant removal of organic compounds.

1.1.1.2 Primary Treatment

In the primary treatment stage, settling basins utilize low fluid velocity and high retention times to allow for the settlement of lower density solids as well as the floatation of other constituents of municipal wastewater. The lower density solids that settle typically consist of both inorganic solids and organic matter. This material is called primary sludge and is removed from the settling tank while the primary wastewater moves on to secondary treatment. Occasionally, chemicals may be added in this step in order to promote coagulation, flocculation, and precipitation of particulates. The overall benefit of chemically enhanced primary treatment is reducing the loading on the secondary treatment process, increasing its efficiency.

1.1.1.3 Secondary Treatment

This is the step in which the majority of the dissolved organic matter is removed from the municipal wastewater. The organic material is degraded through biological respiration. This microbial activity can occur in either a suspended state, or in a fixed film. Methods of fixed film biological treatment include rotating biological contactors and trickling filters. However, the most common form of secondary treatment is the activated sludge process, which includes an aerated biological treatment step combined with secondary clarification. For this reason, the following discussion will focus on the activated sludge process.

Biological Treatment

This stage of treatment is responsible for degrading the dissolved organics that did not settle out during primary treatment. The primary treated wastewater is introduced into an environment containing a high microbial population and an immense supply of oxygen to promote high respiration rates. The oxygen is typically introduced into the wastewater through the process of vigorous mechanical mixing or through air bubbled through the tank via diffusers. The microbes use the oxygen as an electron acceptor in order to oxidize the organic matter within the wastewater, typically quantified as Biochemical Oxygen Demand (BOD) or Volatile Suspended Solids (VSS). After an appropriate retention time, the mixture is transferred to a settling tank.

Secondary Settling

After the mixture of wastewater and microorganisms leaves the aeration tanks, it enters a secondary settling tank. Much like primary settling, low fluid velocity and high retention times allow the solids to settle to the bottom of the tank. However, in secondary settling, the material that is being removed is the engorged microorganisms (biomass). A portion of this settled material, called activated sludge, is recirculated back into the aeration process to promote a healthy microorganism population. The remainder of the activated sludge is removed from the secondary treatment process (waste activated sludge). There are many possible fates of waste activated sludge, the most common being disposal via landfill and anaerobic digestion.

1.1.1.4 Nutrient Removal

Occasionally, the treatment process will not meet the plant effluent requirements for the removal of nutrients, such as nitrogen. There are currently two primary processes utilized for the removal of nitrogen:

Enhanced Secondary Treatment

The biological process within secondary treatment may be altered such that there are aerobic and anaerobic/anoxic zones to promote the removal of nitrogen through nitrification and denitrification.

Tertiary Treatment

There are a number of technologies that can be classified as tertiary treatment, some of which are biological nitrogen removal, biological phosphorus removal, and media filtration. It is important to note that the majority of WWTPs do not have a tertiary treatment step, and thus advanced oxidation will be discussed as if no additional nutrient removal was achieved.

1.1.1.5 Disinfection/Advanced Oxidation

Disinfection and advanced oxidation are the last treatment steps in the wastewater treatment process. While there are a number of options at this stage, the most commonly employed processes include chlorination, ozonation, and ultraviolet radiation. The goal of this treatment step is to inactivate any pathogens that may prove harmful if allowed to enter the ecosystem. This process is not responsible for the removal of organic matter.

1.1.2 Emerging Pollutants

Emerging pollutants (contaminants of emerging concern) are classified as chemical compounds that have only recently been recognized as pollutants and of which the scientific community currently has a limited understanding. The U.S. EPA categorizes the following as contaminants of emerging concern: pharmaceuticals and personal care products; steroids and hormones; pesticides; nonlyphenols, octylphenol, and alkylphenol ethoxylate (APEs) compounds;

polybrominated biphenyl ether (PBDE) fire retardants; polynuclear aromatic hydrocarbons (PAHs) (EPA, 2010).

The presence and behavior of these compounds when released into the environment had previously been unknown or not deemed relevant. However, recent reports on these contaminants have raised concern for the potential risks posed to the environment and to public health. Their discovery is also partly due to the advances in monitoring technology, suggesting that some these compounds may have been present in the water for many decades, but at concentrations too low to have previously measured.

Emerging pollutants pose a risk to the environment mainly due to their resistance to removal through traditional treatment techniques. The accumulation of these pollutants in fish and drinking water supplies then poses a risk to public health due to possible adverse allergic effects. Due to the lack of consensus on factual data or methods to analyze the data sampled thus far, it is typical to find these compounds unregulated and that their impact in the environment remains uncertain or non-conclusive (Petrovic et al., 2003).

Another characteristic that is particular to this category of chemicals is the already high and ever increasing rates of production and demand; which bring as a consequence a continuous inflow of these pollutants in the environment, making them behave as persistent chemical compounds even when they are not expected to (Petrovic et al., 2003).

1.1.3 Pathogens of Concern

Pathogens are disease-causing microorganisms that can be commonly found in natural water bodies. In the National Primary Drinking Water Regulations, the U.S. EPA has identified four primary pathogens of concern: *Cryptosporidium*, *Giardia lamblia*, *Legionella* and enteric viruses. The EPA also list Maximum Contaminant Levels (MCL) for indicators such as total coliforms and fecal coliforms, which relate to the presence of bacterial microorganisms (e.g.: *Escherichia coli*).

Each of these pathogens is highly dangerous, even in very low concentrations, and some of them are highly resistant to traditional disinfection practices (WHO, 2006). The primary purpose of the disinfection step of water and wastewater treatment is to inactivate these pathogens, thus removing the health risk. However, complete inactivation is often very difficult due to the very low initial pathogen concentration and due to the fact that some are more resistant to traditional treatment than others.

1.1.4 Advanced Oxidation Process (AOP)

Commonly abbreviated AOP, advanced oxidation processes are a type of chemical reaction that generates hydroxyl radicals in quantities. These radicals interact with organic compounds present in a system of interest (e.g. wastewater) and cause them to degrade into CO_2 through the process

of mineralization. The aforementioned reactions are possible because of the high oxidation reduction potential (ORP) of the hydroxyl radicals ($E_{\bullet OH}$ = +2.80V), second highest after flourine (E_F = 3.03 V) (Suib, 2013).

The chemical mechanisms that prevail are usually hydrogen abstraction and electrophilic addition (Schwarzenbach et al., 2003). The degradation of the compounds' structures is a sequence (that can be reasonably predicted) where the molecules are repeatedly oxidized and ultimately reduced to CO_2 (as shown on Figure 1.2). Besides the effectiveness of AOPs on compounds that previous treatment steps do not remove (either because of their complexity or for being in low concentrations), it is also of great importance to note that in this process virus and bacteria become inactivated.

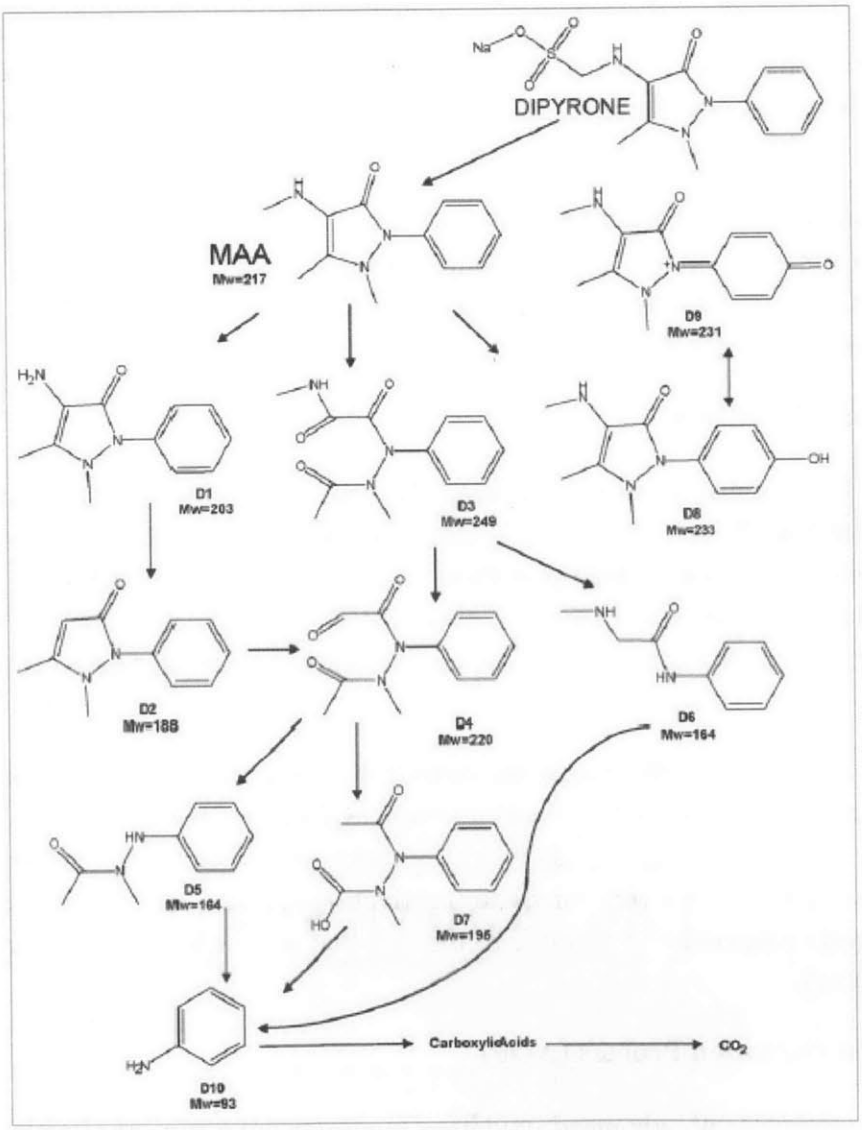

Figure 1.2 Oxidation Degradation Sequence of Dipyrone (Malato et al., 2009)

1.1.4.1 Heterogeneous Photocatalytic AOP

The designation of this technology provides a brief understanding of this AOP mechanism:

- *Photo-* is the Greek word for light.
- *–catalytic* means that this process requires the use of a *catalyst*, a compound whose presence (not consumption) favors a chemical reaction.
- *Oxidation* is the name of a specific chemical reaction, one that degrades even complex pollutants, such as emerging pollutants, into compounds of lesser complexity.

This process is considered to be heterogeneous because it occurs at the boundary between the solid phase of the catalyst and the aqueous phase of the solution being treated (Braslavsky et al., 2011). Heterogeneous photocatalytic advanced oxidation occurs when hydroxyl radicals (•OH) are generated due to the interaction between a semiconductor (titanium dioxide (TiO_2) in this case) and the photons emitted by a light source (natural sunlight or artificial). When photons of energy equal to or greater than the semiconductor's vacant band gap hit its surface, electron/hole pairs (e^-/h^+) are generated in the valence band (Malato et al., 2009). In turn, these e^- and h^+ will interact with water, and create an unstable intermediate product called hydrogen peroxide (H_2O_2) which will spontaneously divide itself into a pair of •OH radicals (Malato et al., 2009).

There are two primary methodologies for applying photocatalysis; supported and suspended catalysts. In supported catalyst systems, the catalyst is typically fixed upon glass beads or cylinders within the reactor tubes (Gelover et al., 2004). Suspended catalyst systems simply use a uniform suspension within the water sample. Although fixed catalyst systems are typically of lower efficiency (and have higher head loss) than suspended catalyst systems, the amount of research on fixed catalyst systems is growing due to fact that the suspended catalyst would have to be removed post-treatment (Malato et al., 2009).

Prominent researchers

During the literature review phase of this research, some publications were fundamental to understanding the theoretical background of the photochemistry involved in this photocatalytic oxidation technique as well as application attempts previously undertaken within the research community. It is important to acknowledge the fact that a major proportion of current investigation efforts have been made by the Plataforma Solar de Almería team in Spain, currently directed by Dr. Sixto Malato Rodríguez. Other essential references include Malato et al. (2009), Malato, J. B. (2007), Caslake et al. (2004), Legrini et al. (1993), Agulló-Barceló, M. I. P.-L. (n.d.), Pablos et al. (2012). Efforts to model the reaction kinetics within the photocatalytic oxidation process can be largely attributed to the works of Javier Marugán, Rafael Van Grieken, and Christina Pablos (2010).

1.2 SIGNIFICANCE OF PHOTOCATALYSIS

The relevance and eventual success of solar photocatalytic water treatment is founded on the three pillars of sustainability, namely social viability, environmental viability, and economic viability.

1.2.1 Social Viability

Despite centuries of technological development to provide acceptable water quality in a cost effective manner, access to clean water and sanitation remains a problem that affects people on a global scale. The lack of safe water sources causes well known problems that need to be addressed: "1.2 billion people lack access to safe drinking water, 2.6 billion have little or no sanitation, millions of people die annually – 3900 children a day – from diseases transmitted through unsafe water or human excreta" (Malato et al., 2009).

Knowing that clean water is becoming scarce; being able to mitigate this shortage, and thus improving the quality of life of billions of people around the world, is mandatory and perhaps a moral obligation of the scientific and engineering community.

1.2.2 Environmental Viability

The goal of wastewater treatment is to remove compounds that may be harmful to the natural ecosystem and could indirectly pose a risk to human health. Current technologies face the problem of balancing a high removal of those damaging compounds and the addition of chemicals as part of the very same removal process. Traditional advanced oxidation technologies require large amounts of energy, and indirectly emit greenhouse gases, having a detrimental impact on the ecosystem that they intend to preserve. Therefore, an adequate process should address the following two problems:

1.2.2.1 Downsides of Traditional Treatment

Although traditional treatment is fairly effective in meeting water quality standards, removal of organic compounds is often incomplete and requires the addition of potentially harmful chemicals.

Partial Removal

Figure 1.2 displays the oxidation degradation process representative of a complex organic molecule. Using traditional biological treatment processes, complex molecules may not be fully degraded to CO_2 and water, leaving the intermediate compounds untreated. If not removed, some of these compounds may give rise to additional threats to the receiving water body. Additionally, intermediate compounds may react with other chemical inputs to be transformed into even more potent compounds, as described below.

Disinfection Byproducts

The most commonly used method for the disinfection of secondary effluent is chlorination. The wide use of chlorination is due to its low operational costs; however, the hydrolyzed forms of the chlorine are free to react with any remaining natural organic matter to form chlorinated compounds that may be harmful to the environment (EPA, 2000).

Other traditional disinfection/advanced oxidation methods include ultraviolet radiation and ozonation. Similar to chlorination, oxidation by UV and ozone can also form disinfection by-products. Additionally, both processes require larger amounts of energy, when compared to chlorination.

1.2.2.2 Presence of Emerging Pollutants in Wastewater

As stated in Section 1.1.2, in recent years it has been noted that wastewater streams include higher and higher concentrations of complex organic molecules. These compounds, known as contaminants of emerging concern (CEC), or emerging pollutants, include a wide range of herbicides, pesticides, pharmaceuticals and personal care products (PPCPs), and industrial substances. These compounds are resistant to conventional wastewater treatment, making them persistent in the natural environment through WWTP effluent. Some ecological risks include the disruption of the reproduction cycle of fish, and accumulation in higher order predators. Emerging pollutants also have many potential adverse health effects, including allergic reactions, dermal irritation, or worse.

The subject of this research is environmentally relevant as a means to identify methods of wastewater treatment that can efficiently remove pollutants while "minimizing the use of chemicals and impact on the environment" (Malato et al., 2009).

1.2.3 Economic viability

Having already explained each of the treatment steps involved in a traditional wastewater treatment process in Section 1.1.1, it is important to note the high capital investment that is required to install and operate a conventional wastewater treatment facility. The technologies used are specific to the target pollutants that are expected to compose the influent wastewater and large amounts of energy are needed to power up a series of pumps, heaters and other equipment, especially during secondary and tertiary treatment steps, as well as in the most commonly used advanced oxidation processes.

Although photocatalytic AOPs have a high capital cost, given the fact photocatalysis is powered by sunlight, this appears to be a promising alternative method for treating water at lower cost and with less energy. At the same time, photocatalytic AOP reduces cost by minimizing the use of chemicals and impact on the environment.

1.3 ULTIMATE GOAL FOR SOLAR PHOTOCATALITIC AOP

The primary objective for the research field of photocatalytic advanced oxidation is to ultimately apply this technology to large-scale municipal and industrial applications. Figure 1.3 is a simple diagram that shows the probable layout of a large-scale reactor.

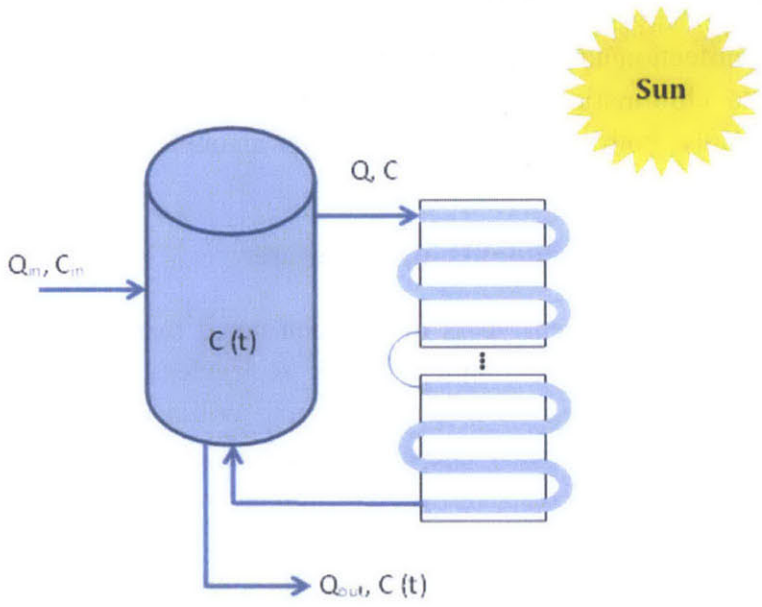

Figure 1.3 Field Application Scheme of a Photocatalytic Solar Reactor

Although there is no standard design process for the construction of photocatalytic wastewater treatment facilities, this technology has shown positive results at treating real effluents with outdoor reactors at different operational scales. Some examples of the facilities currently in operation are:

- Volkswagen plant: Two laboratory and bench-scale experiments were conducted at the German manufacturer's factories in Wolfsburg (Germany) and Taubaté (Brazil) (Dillert et al., 1999). Driven by the promising results, a pilot plant was installed in the Wolfsburg industrial unit during the summer of 1998.

- Tunisia plant: A study conducted by Freudenhammer et al. (1997) on photocatalytic treatment of textile wastewater in Mediterranean countries, reported in 1997, lead to the construction of a pilot plant in Menzel Temime. The project, funded by the European Commission, was chosen based on the appealing cost-effective performance of the initial studies.

- SOLARDETOX plant: Full size demonstration plant built in Madrid, Spain, and run by a consortium that is coordinated by Plataforma Solar de Almería research group. This

facility is "intended to identify any pre or post-processing requirements, potential operating problems, and capital and operating costs" (Malato et al., 2009).

- El Ejido plant: Another Spanish full size plant which began operation in 2004, treating agricultural wastewater contaminated with pesticides from the industry.

Despite the lack of large scale applications, the typical configuration may consist of two main components: the storage/equalization tank and the photo-reactors. Since the flow within a wastewater treatment facility can vary significantly throughout the day, the equalization tank will serve to maintain a constant flow to the photo-reactors. In addition, if sized adequately, the equalization tank might be capable of storing the untreated water while conditions are not favorable for photocatalyic oxidation (i.e. night or low insolation). The water is then pumped from the equalization tank through the reactor setup, which may consist of any number of reactors, in series or parallel. Whatever the configuration, the sizing of the large-scale reactor will ultimately be dependent on the pollutant loading and the solar energy per volume per time used by the reactor.

1.3.1 Developing the Technology

As with any emerging field of study, modelling is an essential step toward developing this technology from the lab-scale to the large-scale. To achieve this, models must be developed for solar radiation, and reaction kinetics, and hydraulics. The following describes of each of these models and their importance; however, this study does not address all of these items. For the scope of work, see Section 1.4.

1.3.1.1 Solar Radiation Model

As mentioned previously, the interaction of photons with the photocatalyst is essential to the degradation of organic molecules within the water stream. In fact, studies show that the oxidation rate is directly related to the radiation entering the system (Malato et al., 2009). These photons must have a certain minimum energy (maximum wavelength) to activate the photocatalyst. Therefore, it is essential to model the number of photons, at or above this certain energy level, that are entering the irradiance tubes. The flux of these photons through the tube walls also depends greatly on the position of the sun in the sky as well as the weather conditions at any given time of the day. For the solar radiation model to accurately predict the number of photons entering the reactor and interacting with the photocatalyst it must:

- Determine the position of the sun as a function of longitude, latitude, date, and time.
- Determine the total radiation and spectral distribution at the Earth's surface, considering climatological variables.
- Model radiation transport within the solar reactor, using the Radiative Transfer Equation.

- Define the distribution of the rate of photon absorption within the irradiance tubes (required for the kinetic model).

1.3.1.2 Reaction Kinetics Model

The goal of photocatalysis is to remove chemicals and pathogens from wastewater (secondary effluent) through chemical oxidation. The removal of these constituents is dependent on the reaction kinetics occurring within the reactor, and therefore must be modeled to achieve efficient operation. The reaction kinetics model is the most complex portion of this project because it is dependent on many different variables. In general, the reaction kinetics can be dependent on the initial concentration of the reactant, concentration of the catalyst, water pH, temperature, radiant flux and wavelength, and oxygen content of the water (Malato et al., 2009). To accurately represent the degradation kinetics, the model must:

- Define possible degradation routes of target pollutants.
- Define the best fit rate and order of the kinetics degradation process based on experimental data.
- Model the dependency of the reaction kinetics as a function of pollutant concentration, catalyst concentration and radiation intensity.
- Include other pertinent water quality parameters such as pH, conductivity, oxygen content, turbidity.

1.3.1.3 Hydraulic Model

The fluid dynamics model is needed to aid in the scaling process and will be used to ensure that certain flow requirements are met. The effective operation of the photocatalytic reactor requires that the fluid within each of the irradiance tubes achieve turbulent flow and a state of complete mixing. This model will use the reactor geometry and the flow rate to ensure that these requirements are met for a range of operating conditions. The hydraulic model may be used to combine the kinetic model (with the solar model embedded) into a single model in which all of the parameters may be entered, achieving a single output for the pollutant concentration. This can be done with certain commercial computational fluid dynamics packages, such as ANSYS FLUENT. Steps involved with the hydraulic model include:

- Verify that complete mixing is maintained throughout each of the reactor tubes.
- Verify that the flow remains turbulent.
- Combine the numerical models for the Reaction kinetics.

1.4 THESIS OBJECTIVE

The objective of this study is to investigate photocatalytic degradation using natural sunlight as a viable AOP option for use in full scale wastewater treatment facilities. Empirical data are analyzed to determine the effects of varying the initial pollutant concentration, catalyst concentration, and the intensity of irradiation. Additionally these experimental results are used in an attempt to calibrate a numerical kinetic model. The calibration of this numerical model is the first step toward producing a kinetic model that can be applied to a number of pollutants, as would more accurately represent real-world conditions.

2 EXPERIMENTATION

During January 2014, a series of experiments were conducted using the photoreactor located at Mostoles campus of Universidad Rey Juan Carlos in Spain. Under the direction of Dr. Ruud Timmers, the photocatalytic oxidation of methanol, cinnamic acid, sulfamethoxazole, and E. coli was explored with the goal of determining how the rate of decay of each contaminant is affected by a number of variables. In total, 28 runs (A through AB), each consisting of two simultaneous experiments (labeled Pump 1 and Pump 2), were conducted. This section will detail the processes of solution preparation, reactor preparation, reactor operation, and sample analysis.

2.1 EXISTING LABORATORY SET-UP

This section details the infrastructure of the experimental setup used during the experimentation period.

2.1.1 Radiation Source

The experimental setup at URJC utilizes a 5,000 Watt xenon arc lamp as the primary radiation source. In addition, a number of the experiments were also conducted outside using natural solar radiation. Figure 2.1, displays the measured radiation spectrum for both the Xenon lamp and natural solar radiation.

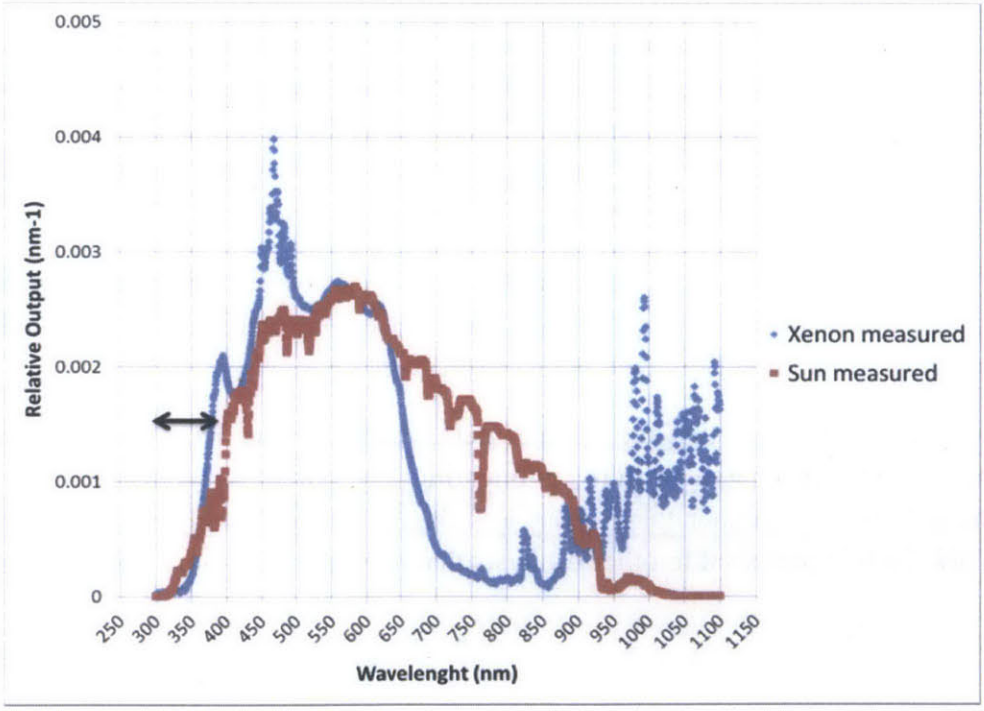

Figure 2.1 Measured Spectra (Marugán & Timmers, 2013)

Although at first glance it appears that these two radiation sources shown are somewhat different, there are two factors that make the artificial light source comparable to natural sunlight:

- Experimental data shows that the relative activity of TiO_2 is at its highest in wavelengths between 300 nm and 390 nm (Malato et al., 2009). Figure 2.2, presented in the following section, illustrates this relationship.
- In Figure 2.1, it is important to note the similar behavior in the UV band of the solar spectrum. This range is represented by the black arrow and shows that both the Xenon arc lamp and the natural solar radiation behave similarly in the 300 nm to 390 nm range.

For the purposes of representing the varying solar conditions that may occur during daily operation of a large-scale reactor, the radiation intensity of the Xenon lamp can be adjusted.

2.1.2 Photocatalyst

In order to generate •OH radicals at high rates, it is of utmost importance to use the most highly active catalyst possible. Studies on a vast array of semiconductor materials suggest that, under comparable conditions, the TiO_2 catalyst is the most active compound available. These observations can be explained by analyzing the energetic separation between the valence and conduction band (bandgap energy) of TiO_2, shown in the table in Figure 2.2. This low bandgap energy allows photons with wavelengths 390 nm and lower to activate the TiO_2, suggesting that utilizing the sun as the primary source of radiation is both economical and ecologically sensible. Catalysts that are capable of absorbing a larger portion of the solar spectrum would be more effective in the process of photocatalysis. However, when tested, these catalysts experienced certain degree decay, reducing the oxidation efficiency after repeated experimentation (Malato et al., 2009). Malato et al. (2009) also suggest that TiO_2 is preferred due to its resistance to chemical breakdown, safety, and low cost.

Additionally, TiO_2 is an abundant compound that presents a low solubility in water as well as a strong resistance to chemical breakdown and photocorrosion, making it a safe and low cost option when compared to other semiconductors (Malato et al., 2009).

Malato et al. (2009) indicates that the optimal performance of the TiO_2 catalyst occurs at pH levels where the surface charge of zero, eliminating any attraction/repulsion forces between particles; the pH must be greater than 4, but less than 7. Since this pH range includes typical wastewater pH, TiO_2 is preferred to other catalysts that may require a more acidic environment.

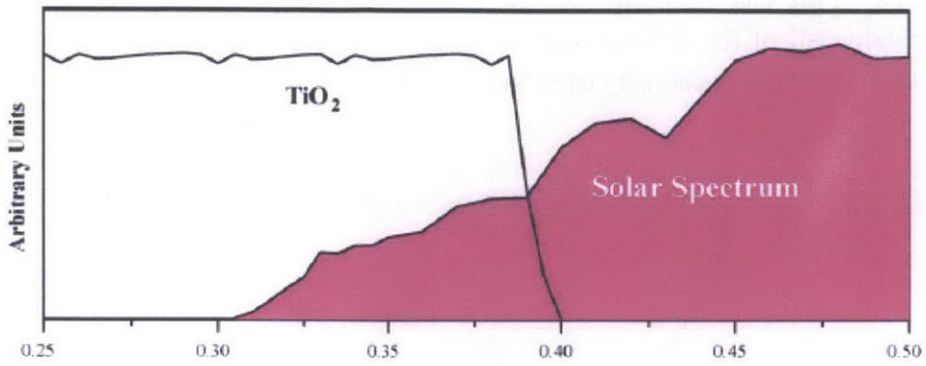

Semiconductor	VB (V vs. NHE ± 0.1 V)	CB (V vs. NHE ± 0.1)	E_g (eV)	Band gap wavelength (nm)
TiO_2	+3.1	-0.1	3.0	380
SnO_2	+4.1	+0.3	3.9	318
ZnO	+3.0	-0.2	2.8	440
ZnS	+1.4	-2.3	3.7	336
WO_3	+3.0	+0.2	2.8	443
CdS	+2.1	-0.4	2.5	497
CdSe	+1.6	-0.1	1.7	730
GaAs	+1.0	-0.4	1.4	887
GaP	+2.2	-1.0	2.3	540

Fig 2.2 TiO_2 Absorbance Spectrum Compared with Solar Spectrum and Band Position (Water at pH 1) for some Common Semiconductor Photocatalysts (Malato et al., 2009)

Due to the reasons expressed above, TiO_2 is the preferred option for large scale photocayalytic water treatment. Additionally, the use of suspended catalyst has proven to be more effective than fixed catalyst. Therefore, suspended TiO_2 is also the catalyst of choice for the experimentation at URJC.

2.1.3 Reactor Design

The reactor located at URJC is a portable lab-scale reactor which could be used indoors for artificial light experimentation, and also outdoors for natural light experimentation. The following will describe the type as well as the pertinent parameters of this lab-scale photocatalytic reactor.

2.1.3.1 Reactor Type

There are two primary categories of reactors that can be used for solar photocatalysis: concentrating and non-concentrating. Reactors are placed into one of these categories based upon the concentration factor. A concentrating collector is defined by a concentration factor greater than unity, while a concentration factor of one signifies a non-concentrating collector. The reactor at URJC used for the experimentation is classified as a non-concentrating compound parabolic collector (CPC). A cross-section of a non-concentrating CPC is shown in Figure 2.3. Non-concentrating CPCs are the preferred design for solar photocatalytic reactors because they

have no moving parts, are easy to maintain, and utilize 100% of direct and diffuse light (Malato et al., 2009). Utilizing all of the diffuse light is essential in considering reactor performance on the field scale, because of the variability of natural solar conditions and weather patterns.

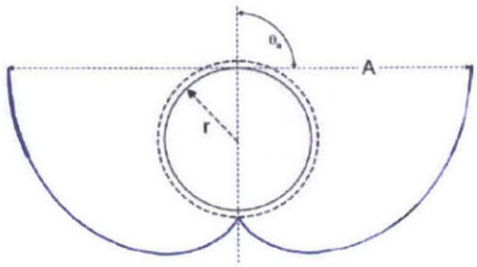

Figure 2.3 CPC Cross-section (Malato et al., 2009)

2.1.3.2 Reactor Parameters

The reactor setup also allows for the variation of a number of physical parameters that must remain fixed in order to produce consistent results. One primary parameter that must remain consistent throughout each of the tests is the time for which a parcel of the fluid is subjected to irradiation. This time can be affected by a number of controls, such as the fluid flow rate and the total volume of the fluid in the irradiance tubes. The irradiance time will then be defined as the irradiance tube volume divided by the fluid flow rate. Based on information from URJC, the typical flow rate used is around 9-10 liters per minute and the liquid volume can be varied between 0.75 and 3.5 liters. For the purposes of maintaining a large sample size throughout the testing, it would be beneficial to use a fairly high fluid volume. These parameters as well as other reactor dimensions are provided in Table 2.1. For the experimentation, the reactor was modified to run two experiments in parallel, each only using two tubes of the lab reactor.

Table 2.1 – Reactor Parameters

Reactor Measurements				
Number of Reflectors/Irradiance Tubes	1 to 4			
Width of Reflector	8.26	(3.25)	cm	(in)
Length of Reflector	38	(15.00)	cm	(in)
Minimum Radiation Area	314	(48.70)	cm^2	(in^2)
Maximum Radiation Area	1256	(194.70)	cm^2	(in^2)
Inner Diameter of Tube	2.6	(1.00)	cm	(in)
Tube Length	38	(15.00)	cm	(in)
Tube Volume	202	(0.05)	mL	(US gal)
Maximum Reservoir Volume	2000	(0.53)	mL	(US gal)
Maximum Reactor Volume (4 Tubes)	3500	(0.92)	mL	(US gal)
Minimum Reactor Volume (1 Tube)	750	(0.20)	mL	(US gal)
Typical Reactor Flow Rate	9 to 10	(2.4 to 2.6)	L/min	(gpm)

(Dr. Ruud Timmers, 2014)

As mentioned previously, the radiation power can also be varied for each of the experiments. Varying the power of the xenon lamp is essential to predicting the behavior of the photocatalytic degradation under natural solar conditions.

2.2 DESIGN OF EXPERIMENTS

2.2.1 Experimental Variables

Three model compounds of increasing complexity were tested. These pollutants include methanol, cinnamic acid, and sulfamethoxazole. Methanol has the most basic structure of all the tested compounds and therefore represents simple organic compounds commonly found in municipal wastewater. Cinnamic acid represents a constituent of humic acids (both containing carboxyls), slightly more complex compounds that typically occur in urban or industrial wastewater streams. Moreover, cinnamic acid is commonly found in olive mill wastewater (Mantzavinos & Kalogerakis, 2005). Finally, sulfamethoxazole, the most complex compound tested, represents typical pollutants found in hospital wastewater streams. Sulfamethoxazole is a complex organic compound that is commonly used as an antibiotic drug. It has been shown to be resistant to traditional wastewater treatment processes, appearing in 19% of 139 streams sampled in the U.S. (Kolpin et al., 2002).

Three different concentrations of each of the compounds mentioned above were tested under various conditions to monitor the removal behavior. The other independent variables that were modified throughout the tests include catalyst concentration and radiation power. The first experiments using methanol were conducted as blanks to define a baseline condition used to display the potential of photocatalysis.

As mentioned earlier, the presence of pathogens in wastewater is of great concern. Several reports have displayed the effectiveness of AOPs in the inactivation of pathogens. Currently, a study by Marugán et al. (2010) has observed the inactivation of *E. coli* using TiO_2 photocatalysis. The effectiveness of photocatalytic inactivation has also been predicted, by Malato et al. (2009), to be as effective as typical AOPs, e.g. ozonation and UV radiation. Due to the short window for experimentation, only two experiments were conducted for the inactivation of *E. coli*.

A brief outline of the schedule of experiments is located in Section 2.2.3, and a more detailed schedule of events is shown as Table 2.4.

2.2.2 Water Quality Parameters

Due to the fact that simulated wastewater already contains dissolved carbon, the URJC research group recommended testing for the degradation of the three target compounds in deionized water to reduce any "noise" in the results. However, simulated wastewater was used during the *E. coli* experimentation, to more accurately represent the inactivation of pathogens and degradation of trace emerging pollutants.

Chemical oxygen demand (COD) and total organic carbon (TOC) were monitored throughout the experiments because of their direct relation to the concentration of the organic pollutants. The concentration of cinnamic acid can be measured directly using a spectrophotometer; however, for more complex solutions containing numerous compounds, directly measuring the concentrations would be far costly. Therefore, bulk concentrations must be interpreted through TOC measurements. By measuring the TOC throughout the degradation process, it was then possible to determine the amount of TOC that has been mineralized to inorganic carbon (mostly in the form of CO_2). The remaining TOC represents the organic carbon contributed by the initial pollutant and any intermediary compounds within the degradation pathway. This provides valuable information on the degree to which the compounds are being fully oxidized through processes similar to that shown in Figure 1.2. For the parameters and respective testing methods that will be used at URJC, see Table 2.2.

Table 2.2 – Water Quality Parameters and Testing Methods

Parameter	Testing Method
COD	Potassium dichromate with UV spectrometry
TOC	TOC analyser, measuring the CO_2 using infrared, based on catalytic combustion of the sample at 650°C

(Marugán, 2013)

As described earlier, the pH of the test fluid will reflect the neutral pH for the optimal use of the TiO_2 photocatalyst.

2.2.3 Design of Experiments (Factorial design)

An initial approach to study the interactions of these factors was to use a full factorial design model, using three levels for each factor to be tested in any experiment. The values for each level of catalyst and the light intensity were conveniently chosen from known characteristics of wastewater influents as well as data from the literature review.

The concentration levels of the target pollutants were defined as equivalent TOC concentrations, based on characteristic oxygen demand of wastewater streams. The average reported chemical oxygen demand of untreated water was first converted to the corresponding organic carbon concentration, and this value was subsequently further converted in terms of pollutant to be added to each prepared test solution.

For the catalyst, the concentration levels were formulated as a proportion of the optimal catalyst concentration reported by Marugán et al. (2010) for the solar reactor at URJC. Current literature shows that optimal catalyst concentrations are likely to be highly dependent on the specific geometry affecting the photon path length within the reactor (Malato et al., 2009).

Table 2.3 shows the values of the variables and levels considered for the experimentation.

Table 2.3 Experiment Design Factors

Photocatalytic water treatment process			
Variable	Variable values	Levels per experiment	Level values
Pollutant concentration	Methanol Cinnamic acid	3 concentrations	4 mM of TOC 6 mM of TOC 8 mM of TOC
	Sulfamethoxazole	2 concentrations	20 ppb 0.1 ppb
	Escherichia coli	2 concentrations	10^9 CFU/100 mL 10^6 CFU/100 mL
Catalyst concentration	TiO_2	3 concentrations	0.05 g/L 0.10 g/L 0.20 g/L
Average UV Radiation	W/m^2	3 intensities	Natural Sunlight 46..2 74.2 83.7

To account for all the possible interactions, however, it would have been necessary to run a total of 108 experiments, something that was impossible due to budget and time restrictions. Therefore, it was necessary to delimit the design, as shown in the final experimentation schedule in Table 2.4.

The most relevant considerations introduced in the experimentation design were the following:

- Exploit the fact that, although it was only one machine, in reality we had 2 independent reactors and parallel tests could be run in the devices.
- Make blank tests with methanol to have a baseline oxidation process (i.e. not enhanced by a catalyst or sunlight).
- Run only two levels of light intensity for each target pollutant (e.g. methanol test were run with either 83.7 W/m^2 or 74.2 W/m^2, and cinnamic acid with 74.2 W/m^2 or 46.2 W/m^2).
- Focus initial work only on the systems which degradation process require long runs (i.e. methanol and cinnamic acid).
- Run at least one experiment with natural sunlight for pharmaceuticals and bacteria.

Table 2.4 Final Experimentation Schedule

Date	Experiment	Target	[TOC]	[TiO_2]	[Light]
JAN.08	A	Methanol	100 mM	0.1 g/L	---
	B	Methanol	100 mM	---	---
JAN.09	C	Methanol	100 mM	0.1 g/L	83.7 W/m^2
	D	Methanol	100 mM	---	83.7 W/m^2
	E	Methanol	200 mM	---	83.7 W/m^2
	F	Methanol	50 mM	---	83.7 W/m^2
JAN.10	G	Methanol	4 mM	---	83.7 W/m^2
	H	Methanol	4 mM	0.1 g/L	74.2 W/m^2
	I	Methanol	8 mM	0.1 g/L	74.2 W/m^2
	J	Methanol	6 mM	0.1 g/L	74.2 W/m^2
JAN.13	K	Methanol	4 mM	0.05 g/L	74.2 W/m^2
	L	Methanol	8 mM	0.05 g/L	74.2 W/m^2
	M	Methanol	6 mM	0.05 g/L	74.2 W/m^2
JAN.15	N	Cinnamic acid	4 mM	0.1 g/L	74.2 W/m^2
JAN.16	O	Cinnamic acid	8 mM	0.1 g/L	74.2 W/m^2
	P	Cinnamic acid	6 mM	0.1 g/L	74.2 W/m^2
	Q	Cinnamic acid	4 mM	0.05 g/L	74.2 W/m^2
JAN.17	R	Cinnamic acid	8 mM	0.05 g/L	74.2 W/m^2
JAN.20	S	Cinnamic acid	6 mM	0.05 g/L	74.2 W/m^2
	T	Cinnamic acid	4 mM	0.2 g/L	74.2 W/m^2
JAN.21	U	Cinnamic acid	8 mM	0.2 g/L	74.2 W/m^2
	V	Cinnamic acid	6 mM	0.2 g/L	74.2 W/m^2
JAN.22	W	Cinnamic acid	4 mM	0.2 g/L	46.2 W/m^2
JAN.23	X	Cinnamic acid	8 mM	0.2 g/L	46.2 W/m^2
	Y (1)	Artificial WW with *E. coli*	Low	0.2 g/L	Natural
	Y (2)	Artificial WW with *E. coli*	High	0.2 g/L	Natural
JAN.24	Z	Cinnamic acid	6 mM	0.2 g/L	46.2 W/m^2
JAN.29	AA (1)	Sulfamethoxyzole	Low	0.2 g/L	46.2 W/m^2
	AA (2)	Sulfamethoxyzole	High	0.2 g/L	46.2 W/m^2
JAN.30	AB (1)	Artificial WW with *E. coli*	Low	0.2 g/L	Natural
	AB (2)	Artificial WW with *E. coli*	High	0.2 g/L	Natural

2.3 SOLUTION PREPARATION

Prior to conducting each experiment, the test solution of 1.5 liters must be carefully prepared. As the goal is to represent a concentration of pollutant representative of what may be found in typical wastewater facilities, the methanol and cinnamic acid were compared with regards to total organic carbon.

The first step to preparing each of the solutions is to fill a 1 L volumetric flask and a 0.5 L volumetric flask about half-way with the micro-filtered "Milli-Q" water.

2.3.1 Solutions for Artificial Light Experiments

Maintaining constant radiation flux throughout an experiment is essential to gathering consistent results for the degradation of the model compounds of concern. For this reason, all of the experiments focusing on methanol, cinnamic acid, and sulfamethoxazole were tested under artificial radiation.

2.3.1.1 Methanol

The methanol solutions were prepared by adding a defined amount of 99% pure methanol stock solution to each of the flasks using a pipette. The volume of methanol to be added to each liter of test solution was calculated using the following equation:

$$\frac{mL\ CH_3OH}{L\ solution} = TOC\left[\frac{10^{-3} mol\ C}{L\ solution}\right] \times \frac{1\ mol\ CH_3OH}{1\ mol\ C} \times \frac{32.04\ g\ CH_3OH}{1\ mol\ CH_3OH} \times \frac{1\ mL\ CH_3OH}{0.7918\ g\ CH_3OH} \qquad \text{Eq. 2-1}$$

Due to the limited precision of the pipettes, the volume of methanol added to the 1 L and 0.5 L did not always match the 2:1 ratio. For this reason, the table below summarizes the target TOC concentrations and the volume of methanol added to each of the flasks to obtain the target concentration.

Table 2.5 Methanol Solution Preparation Summary

Target TOC	CH_3OH in 1 L flask	CH_3OH in 0.5 L flask
200 mM	8.093 mL	4.046 mL
100 mM	4.046 mL	2.023 mL
50 mM	2.023 mL	0.634 mL
8 mM	0.324 mL	0.162 mL
6 mM	0.243 mL	0.121 mL
4 mM	0.162 mL	0.081 mL

2.3.1.2 Cinnamic Acid

The cinnamic acid (CA) solutions were prepared by adding a finite amount of 99% pure, solid cinnamic acid. After properly weighing the appropriate amount using an electronic balance, the solid was added to each of the flasks. The following equation was used to determine the mass of cinnamic acid needed to produce the required TOC concentration of 4, 6, and 8 mM:

$$Mass\ CA\ (mg) = TOC(mM) \times \frac{148.16\ mg\ CA}{1\ mmol\ CA} \times \frac{1\ mmol\ CA}{9\ mmol\ Carbon} \times 1.5\ L\ H_2O \qquad \text{Eq. 2-2}$$

To reduce error, it was imperative that all of the cinnamic acid be flushed out of the weighing vessel and into the flask. To speed up the preparation process, the mass of cinnamic acid was added to a one liter flask, and 0.5 L of pure Milli-Q water was then combined with the one liter solution upon the homogenization step, to be described later.

Due to the low solubility of cinnamic acid, 546 $^{mg}/_{L}$ at 25°C (USEPA, 2014), it was necessary to use an ultrasonic bath device to speed up the dissolving process. The bath applies ultrasonic waves to break up any remaining particles and heat to speed up the dissolution process. Even with this process, complete dissolution of the 8 mM solutions could take upwards of one hour.

2.3.1.3 Sulfamethoxazole

The experimental concentrations for the antibiotic sulfamethoxazole (SMX) were based on a study by Brown et al. (2006), which found maximum and minimum concentrations of 1000 and 400 nanograms per liter in the wastewater influent of four treatment plants. These values are also in agreement with the concentrations found in natural waters in the study by Kolpin et al. (2002) mentioned previously. For simplicity, Pump 1 was chosen to contain 20 ppb and Pump 2 contained a concentration of 100 ppt sulfamethoxazole. Sulfamethoxazole is found as a solid at standard conditions and therefore multiple dilutions are required to achieve these concentrations. The dilution process is as follows:

Pump 1 (20 $^{\mu g}/L$): 2 mg Sulfamethoxazole added to 100 mL Milli-Q, then 1 mL of this solution is added to each liter of the test solution

Pump 2 (100 $^{ng}/L$): 0.5 mL of the solution for Pump1 added to 100 mL Milli-Q, then 1 mL of this solution is added per liter of test solution

For these experiments, the sulfamethoxazole stock solutions were prepared by the lab group at URJC. This preparation information was provided by Dr. Timmers.

The goal of these solutions was to be representative of wastewater influent, therefore sulfamethoxazole was not compared to the methanol and the cinnamic acid concentrations based upon organic carbon content. If this were the case, sulfamethoxazole concentrations would be five orders of magnitude larger than the maximum concentration found in Brown et al. (2006).

2.3.2 Solution for Natural Light Experiments

The goal of the natural radiation experiments was to obtain results that would hopefully prove that photocatalytic oxidation processes can be a viable large-scale technology for tertiary wastewater treatment. The results were not intended to be used for the modeling aspects of this project. During the experimentation period, only two experiments were conducted using natural radiation. Due to the limited number of experiments using natural light, each half of the reactor was designated to test high and low concentrations (Pump 1: Low ; Pump 2: High).

2.3.2.1 Simulated Wastewater

The use of simulated wastewater is essential if the inactivation of bacteria (in this case E. coli) is to be tested. Use of Milli-Q water causes osmotic stress on the cell wall of the bacteria due to high ion concentration gradients (Marugán et al., 2010). The added stress due to high pumping rates in the reactor often causes the bacteria to be destroyed. The recipe for the synthetic wastewater, as specified in the OECD Guidelines, is as follows:

Table 2.6 Composition of Synthetic Municipal Wastewater

Chemical component	Concentration (mg/L)
Peptone	160
Meat extract	110
Urea	30
Potassium phosphate (K_2HPO_4)	28
Sodium chloride (NaCl)	7
Calcium chloride ($CaCl_2.2H_2O$)	4
Magnesium sulfate ($Mg_2SO_4.7H_2O$)	2

(OECD Guidelines, 1999)

After preparing one liter of the simulated wastewater solution, it must be autoclaved for two hours in order to properly disinfect the solution. Double concentrations were used for the Experiments Y and AB, resulting in a TOC of 200 mg/L (Kositzi et al., 2003).

2.3.2.2 Bacteria Culture

The culture used for experiments Y and AB were prepared by the lab group at URJC; thus, the following information on its preparation was provided by Dr. Timmers.

Escherichia coli K12 strains, equivalent to ATCC® product 23631 and complying with CECT (Coleccion Española de Cultivos Tipo) were used to prepare the bacterial suspensions. Liquid cultures were prepared by inoculation in a Luria-Bertani nutrient medium (Miller's LB Broth,

Scharlab) and incubated at 37 degrees Celsius for 24 hours, with constant stirring on a rotary shaker. The reaction suspensions were prepared by centrifuging 5 mL of the liquid culture with concentration of 10^9 CFU/mL to recover the bacteria. This was then suspended in sterile deionized water (Milli-Q1, 18.2MV cm). It was decided that the reaction liquid for Pump 1 would have a concentration of 10^3 CFU/mL (3logCFU/mL) and Pump 2 would have a concentration of 10^6 CFU/mL. The following equations were used to determine the amount of the initial culture to achieve these concentrations.

Pump 1 (10^6 CFU/mL): 1 mL of the initial 10^9CFU/mL solution was added per liter of test solution

Pump 2 (10^3 CFU/mL): The initial solution of 10^9 CFU/mL was diluted 100 times through serial dilution of 0.5 mL to 4.5 mL Milli-Q (x3), then 1 mL of the third dilution was added per liter of test solution

2.3.2.3 Emerging Pollutant Cocktail

While sulfamethoxazole is an adequate representative of a single pharmaceutical chemical that can be present in wastewater streams, real influent wastewaters often contain not one, but a mix of chemical compounds. During the oxidation process, all these chemicals compete for the oxidizing hydroxyl radicals present in the water, thus reducing the individual decay rates of each compound.

It was decided that each of the pumps would receive different concentrations of the pharmaceuticals. Much like the *E. coli* concentrations, Pump 1 would receive the "high" concentration of 20 ppb and Pump 2 would test a "low" concentration of 1 ppb. The following dilution procedures began with a stock solution of methanol with pharmaceutical concentrations of 1 gram per liter.

Pump 1 (20 μg/L): 2 mL of the 1 g/L stock solution was added to 100 mL of Milli-Q, then 1 mL of this solution was added per liter of test solution

Pump 2 (1 μg/L): 5 mL of the solution for Pump 1 was added to 100 mL of Milli-Q, then 1 mL of this solution was added per liter of test solution

In total, fifteen different pharmaceuticals and herbicides were used to comprise the emerging pollutant cocktail. The table below contains basic information on these compounds.

Table 2.7 Compounds Found in the Emerging Pollutant Cocktail

Abbreviation	Pharmaceutical Name	Chemical Formula	Molecular Weight (g/mol)
4-AAA	4-Acetamidoantipyrine	$C_{13}H_{15}N_3O_2$	245.28
ACF	Clofibric Acid	$C_{10}H_{11}ClO_3$	214.65
ATN	Atenolol	$C_{14}H_{22}N_2O_3$	266.34
CFN	Caffeine	$C_8H_{12}N_4O_2$	194.19
CZP	Carbamazepine	$C_{15}H_{12}N_2O$	236.27
DCF	Diclofenac	$C_{14}H_{11}Cl_2NO_2$	296.15
GFZ	Gemfibrozil	$C_{15}H_{22}O_3$	250.33
HCT	Hydrochlorothiazide	$C_7H_8ClN_3O_4S_2$	297.74
IBP	Ibuprofen	$C_{13}H_{18}O_2$	206.28
IPT	Isoproturon	$C_{12}H_{18}N_2O$	206.28
MTM	Metamitron	$C_{10}H_{10}N_4O$	202.21
PGT	Progesterone	$C_{21}H_{30}O_2$	314.46
RNT	Ranitidine	$C_{10}H_{11}N_4O_3S_2$	314.4
SMX	Sulfamethoxazole	$C_{10}H_{11}N_3O_3S$	253.28
SPD	Sulpiride	$C_{15}H_{23}N_3O_4S$	341.43

2.3.3 Photocatalyst

The TiO_2 photocatalyst is a light white powder that must be carefully measured with an electronic balance. The catalyst concentrations that were used throughout the experimentation period were 0.0, 0.05, 0.1, and 0.2 grams per liter. These concentrations were chosen based around the optimal catalyst concentration of 0.1 g/L, for this particular reactor, found by Marugán et al. (2010). The selected mass of TiO_2 was added during the homogenization phase of the experiment, which will be described in greater detail later in this section.

2.4 REACTOR AND SAMPLING PREPARATION

As with any scientific experimentation, there are a number of parameters that must be held constant while varying only a single parameter. This section will discuss the key aspects of the experimental setup and the procedures required for each essential piece of equipment.

2.4.1 Radiation

As previously discussed, the radiation source used for the indoor experiments was a cinema projector lamp with a 5,000 Watt xenon arc lamp. As the lamp is fixed to the bench, there are only two means through which the radiation flux from the lamp can be modified. The first is the amperage control. On the side of the lamp housing, below the power, switch is an unmarked dial that can be used to increase or decrease the output of the lamp. Changes in the amperage can be

read on the meter located above the power switch. The amperage was set at 130 A for experiments C-G; 110 A for I-V; and 100 A for W, X, Z, and AA. This results in average radiation intensities of 83.7, 74.2, and 46.2 W/m^2 respectively.

2.4.2 Positioning the Photoreactor

As the photoreactor is on wheels, it is essential that it is positioned properly at consistent distance from the reactor. There is a long board that should be placed on the floor between two "L" brackets at the end of the projector table and set against the line drawn on the floor. This ensures that the reactor is always located in the center of the projector beam. This board also has measurements on it to allow the reactor to be moved toward or away from the light source. For experiments W, X, Z, and AA the reactor was positioned 132 cm from the base of the reactor table. For the remainder artificial light experiments, the reactor was placed at a distance of 104.5 cm.

When the photoreactor is squared up to and set at the appropriate distance from the projector, a carpenter's level should be used to make sure that the portion of the reactor containing the irradiation tubes is vertical.

2.4.2.1 Natural Radiation

For the experiments with natural solar radiation, the position of the reactor is paramount to ensure that the reactor receives the maximum amount of direct radiation as the sun moves across the sky. Ideally, the solar reactor would adjust in two dimensions to receive the maximum possible radiation, but as the reactor is not capable of continuous adjustment, a fixed position must be chosen. This decision can also be validated on the basis of cost effectiveness when considering large scale application, to be discussed later.

Sun position data can be found through many online sources, such as the Sun Position tool located at sunearthtools.com, given as the elevation angle and the azimuth angle. By observing the annual range of the position of the sun, the median position of the sun must be obtained to determine the optimal fixed position of the reactor. Below is a plot of the sun position for the URJC Mostoles campus obtained from sunearthtools.com.

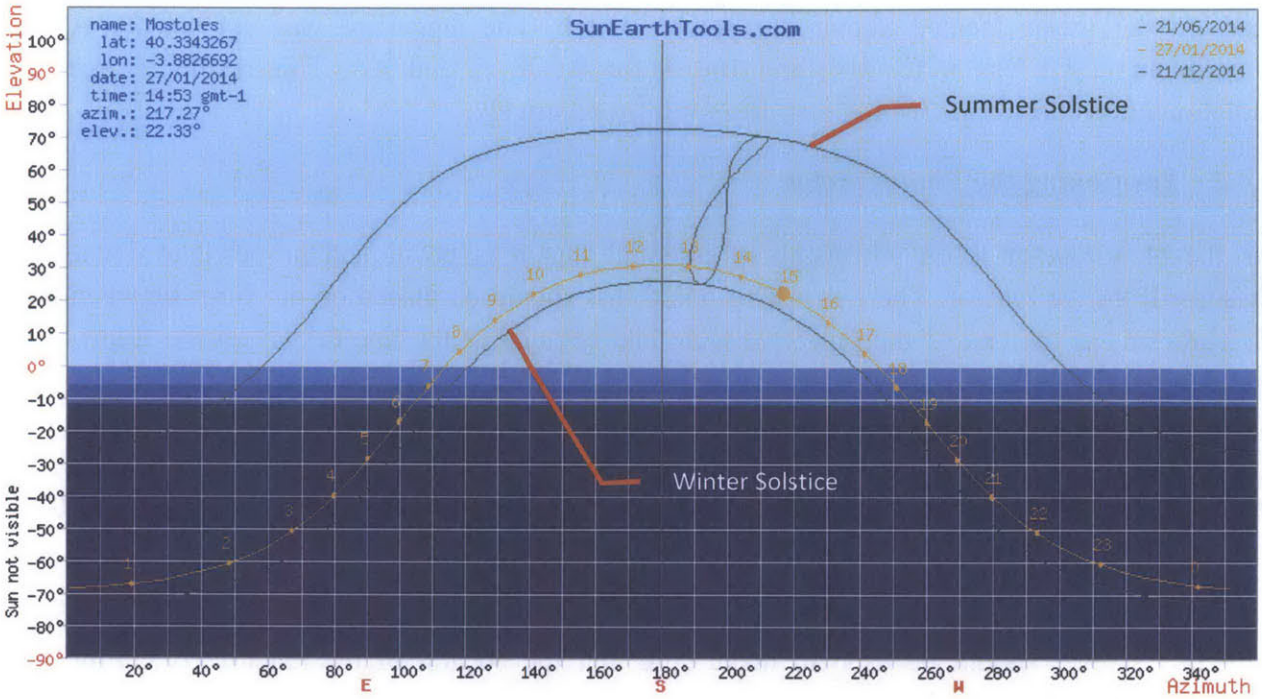

Figure 2.4 Sun Position Chart in Cartesian Coordinates as Provided by Sunearthtools.com

This chart shows that the maximum elevation of the sun will occur with an azimuth of 180 degrees, due South, signifying that that reactor must be fixed with the reactor face perpendicular to the South. The angle of the reactor face can then be determined by observing the maximum elevation angle (at an azimuth of 180 degrees) on the spring and fall equinox. This angle also happens to be the latitude of the location of the reactor. The equinox represents the two days in the year when the fixed reactor will be 90 degrees to the sun, and thus achieve maximum direct radiation. At the Mostoles campus, the optimal angle for year round use of a fixed position reactor would be 40 degrees from the horizontal.

The angle of the reactor for the outdoor experiment AB was chosen to be 22 degrees (112 degrees from the horizontal) due to the average predicted position of the sun throughout the experiment. The position of the sun throughout this day, January 27th, is shown in Figure 2.4.

2.4.3 Radiation Measurement

To appropriately account for the effect of the radiation on the decay rate of the contaminant in question, the radiation must be measured with a spectrometer. These measurements were conducted using the Blue-Wave miniature spectrometer and SpectraWiz software, developed by StellarNet Inc. The spectrometer utilizes a fiber optic cable to measure radiation in the range of 300-1150 nm. For these experiments, the data was collected in flux terms of watts per square meter.

The measurement procedures for the artificial and natural radiation experiments are fundamentally different. The artificial radiation experiments utilize a constant source of radiation, and thus require measurement at a single point in time. However, the radiation must be measured at a number of points across the face of the reactor (portion containing the irradiation tubes) to account for any spatial variation in radiation flux. Thus, a nine-by-nine grid of 81 measurement points was developed by Dr. Timmers in order to determine the average radiation reaching the reactor tubes. Each horizontal line of nine measurement points corresponds to the edge of a parabolic reflector and at the centerline of an irradiation tube. When conducting tests at the same lamp power and distance, the total radiation need only be measured once. But when either the lamp power or the distance is modified, the radiation must be measured again. From these measurements, the average UV radiation in W/m^2 can be determined by integrating the measured spectra over the UV wavelength range and averaging these values for the 45 points of the grid over the two reactor tubes.

During experimentation using natural solar radiation, it can be assumed that the radiation flux is uniform over the face of the reactor, and thus can be measured from a single point. However, measurements from this point must be taken at given intervals to account for the temporal variation in the solar radiation flux due to cloud cover or the position of the sun. Measurements were taken every two minutes during the first outdoor experiment (Y) and every five minutes during experiment AB.

2.4.4 Preparation for Sampling

A series of samples must be taken at defined intervals in order to track the decay of the pollutant(s) over the experiment. Therefore, it is important to define the times at which the samples will be taken, before beginning the experimentation. Due to the nature of exponential decay (which was predicted to be approximately the case for photocatalitic oxidation), the rate of decay will begin high and decrease over time. Thus, it was decided to gather samples at smaller intervals at the beginning and increase these intervals as the experiment progresses. For example, the two-hour cinnamic acid experiments required sampling at time 0, 5, 10, 20, 30, 45, 60, 75, 90, and 120-minutes.

Due to the close proximity of the first three samples, it is beneficial to set up the sampling station prior to the start of the experiment. This includes gathering all of the required materials: sample vials and caps, 10 mL syringes (2 to 3 per reactor), syringe filters, a beaker of Milli-Q water, an empty beaker for waste water, and a timer. The function of each of these materials will be described later in the sampling portion of the following section. The most important process to prepare for sampling is to clearly label each of the vials with the experiment letter, sample time, and reactor number. This will reduce confusion during and after the experiment.

It is also important to know what the sample size will be, which can be roughly determined based upon the tests that will be run. Sample size varies for each pollutant, depending on the amounts

that are required to successfully run the desired tests. For methanol, for example, it is required to take at least 7 mL samples; whereas for cinnamic acid the required sample size is15 mL.

2.5 EXPERIMENTAL PROCEDURE

This section will discuss the experimental procedures followed for the operation of the lab-scale reactor at URJC, a schematic of which is shown in Figure 2.5.

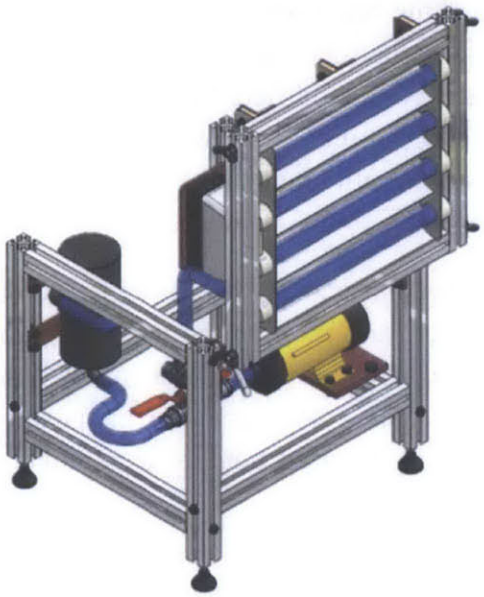

Figure 2.5 Lab-scale Reactor Schematic

2.5.1 Homogenization

The first step is to make sure that the lamp is on and at the correct amperage, and to position the reactor. As the lamp requires some time (about 10 minutes) to warm up, it is recommended to have the lamp on before beginning the homogenization process. Additionally, the reflector must be completely covered in aluminum foil to prevent any oxidation during the homogenization.

At this point, the test solution and the TiO_2 catalyst may be added to each reservoir. At this point the homogenization process has begun. This process should last about five minutes for each of the experiments.

2.5.2 Beginning the Experiment/Sampling

At the end of the homogenization, the aluminum foil must be removed, the timer started, and the first samples must be taken (time = 0). After gathering the samples into the syringes the sample must be forced through a disposable particulate filter placed on the end of the syringe. It is important to rest the filter on the opening of the vial (with label matching the sample number) to

reduce the possibility of filter malfunction. The same filter may be used if multiple syringes are required for the same sample, but different filters must be used for the two reactors.

After the samples have been filtered and the vials sealed, the syringes must be flushed with Milli-Q in preparation for the next wave of sampling.

2.5.2.1 Bacterial Experiments

For bacterial tests it is important to utilize an extra syringe to take a small sample that must remain unfiltered for the plating process (to be described later). One cannot filter the majority of the sample in a syringe and use the rest for plating, because this is believed to concentrate the remaining portion of the sample.

Additionally, the syringe cleaning process differs for bacterial tests. Prior to the Milli-Q flush step (same as without bacteria), the syringes must be flushed three times with ethanol. However, in this step the ethanol does not need to be wasted, instead it can be reused.

2.6 CONCLUDING THE EXPERIMENT

Before the reactor can be cleaned at the end of each experiment, the solution must be drained from the reactor by opening the valves below each of the reservoirs. But first one must make sure that the pumps are off and there is a container for the solution to drain into. It is beneficial to tip the reactor from side to side (holding for about 15 seconds) to help drain any remaining solution from the reactor tubes.

2.6.1 Flushing

Thoroughly flushing the reactor after each experiment is essential to reduce erroneous results, increasing the repeatability of the experiment. Depending on the solution being tested, different flushing procedures may be required. Additionally, after a number of tests a noticeable fogging of the reactor tubes may develop (where flushing is no longer sufficient) and a more thorough cleaning may be required.

2.6.1.1 Methanol

As a result of the high solubility of methanol and its oxidation product formaldehyde, the flushing procedure at the conclusion of methanol experiments is simple. The reactor should be flushed three times with Milli-Q water, thoroughly draining after each flush.

2.6.1.2 Cinnamic Acid

In contrast with methanol, the low solubility of cinnamic acid results in a tendency for it to sorb to the solid phase, sticking to the irradiation tubes. Therefore, flushing with Milli-Q is not sufficient to remove the cinnamic acid. Gmelin (1859) clearly notes that nitric acid (HNO_3)

easily dissolves cinnamic acid. As a result of this relationship, a 10% nitric acid solution was used to flush the reactor before the conventional three flushes with Milli-Q. The nitric acid may be reused for multiple experiments.

Note: Due to the interactions between the cinnamic acid and the nitric acid, it is important to store the nitric acid in a non-rigid vessel, or to maintain a loose cap on a glass vessel to prevent the build-up of any potentially dangerous pressure.

2.6.1.3 Sulfamethoxazole

Due to the very low concentrations of sulfamethoxazole, the flushing procedure for these tests only requires flushing with Milli-Q water a total of three times.

2.6.1.4 Bacteria

When experimenting with solutions containing bacteria, it is essential that all possible remaining bacteria are inactivated. Thus, the reactor must be flushed three times with pure ethanol. So as to not waste ethanol, the same volume of ethanol may be used for all flushing after bacterial testing. To then remove any remaining ethanol, the standard Milli-Q flushing procedure must be followed.

2.6.1.5 Cleaning the Reactor

After conducting a number of experiments with the reactor, a film may begin to develop on the inside of the reactor tubes which cannot be removed by flushing with nitric acid. This fogging of the tubes will reduce the amount of light entering the tubes, reducing the degradation rates of further experiments, and thus must be removed manually. To do this, the reactor must be carefully dismantled under the supervision of the reactor's designer Dr. Ruud Timmers. Once the tubes have been removed, they can be cleaned with soap and a simple test tube cleaning brush.

2.7 SAMPLE ANALYSIS

For the purpose of studying the photocatalytical degradation process, different tests were performed on the samples taken during experiments A through AB, with reactor Pumps 1 and 2, to analyze the pollutants concentrations under the varied conditions provided in Table 2.3. Table 2.8 below summarizes the tests conducted on each target pollutant, and the following sections detail the procedural methods.

Table 2.8 Sample Analysis Tests Performed per Target Pollutant

Test	Methanol	Cinnamic acid	SMX	Bacteria
Absorbance	X	X		
Total Organic Carbon	X	X		
Chemical Oxygen Demand	X	X		
Micropollutant Measurement			X	
Colony Forming Unit Count				X

2.7.1 Absorbance (Abs) Measurement

The task of measuring the concentration of a chemical compound in a sample can be done through an absorbance test. The task of measuring the absorbance in the previously taken samples was done on a Biochrom Libra S22 UV/Vis Spectrophotometer. The procedure for this test, which was conducted on methanol and cinnamic acid samples only, is the following:

a) For a given experiment, take enough test tubes to account for each sample that will be tested, and an additional of one extra test tube per set of reactor samples. For example, to run an absorbance test for experiment N, Pumps 1 and 2, it will be necessary to use one test tube per sample, as well as 2 extra vials: one for the N-1 samples set, and another for N-2 samples set.

b) Fully cover all tubes with aluminum foil to prevent additional photocatalytic degradation of the samples over the duration of the testing procedure.

c) If possible, but not necessarily, label the vials to reference the corresponding sample that each will contain.

d) Next, prepare the vials. For the spectrophotometer to work correctly, it is required to prepare a volume of 3 mL of diluted sample.

    a. Prepare the blank test tubes: For blank tube, take one vial and add 3 mL of pure Milli-Q water. Close tightly using a cap with sealing membrane.

    b. Prepare the sample test tubes: For the sample tubes, prepare dilution mixes according to the dilution composition stated in Table 2.9. It is important to note that absorbance readings for the methanol experiments are actually measuring

formaldehyde, the oxidation product of methanol. These concentrations will then be related to methanol concentration as described in Section 3.2.1.1.

Table 2.9 Methanol and Cinnamic Acid Absorbance Test Parameters

Target Pollutant	Methanol	Cinnamic acid
Compound tested	Formaldehyde	Cinnamic acid
Test wave length	412 nm	272 nm
Dilution rate	10:1	20:1 for 8 mM 10:1 for 4 and 6 mM
Dilution composition	1.5 mL Ammonium Phosphate buffer (pH 6) 1.5 mL Sample 0.03 mL Acetylacetone	20:1 0.15 mL Sample 10:1 0.3 mL Sample Remainder Milli-Q

c. After preparing all tubes, it is required to do the following: in the case of formaldehyde tubes, wait no less than 60 minutes for the acetylacetone reagent to take effect; and, in the case of cinnamic acid tubes, homogenize the sample by shaking it using a vortex shaker.

e) Begin testing one tube at a time, starting with the blank test tube to calibrate the machine. For each diluted sample, do as follows:

a. Pour the contents on a pristine and dry cuvette and lightly shake it to remove any air bubbles. After making sure that there are no air bubbles present in the cuvette, place it on the spectrophotometer.

b. On a computer, start the Libra Sample Analyzer software and set the adequate test wave length (412 nm for formaldehyde and 272 nm for cinnamic acid).

c. Test the cuvette by clicking on "Calibrate" in the case of the blank calibration test and "Abs" for all the other samples. The absorbance measurement will be automatically reported on the main window of the program.

f) Since absorbance is a relative value and samples were diluted, the real concentration of the chemical corresponds to the measured absorbance value converted to concentration using a calibration curve for each distinct chemical and multiplied by its corresponding dilution rate.

2.7.1.1 Methanol Data Processing

The absorbance test provided the samples' formaldehyde molar concentrations by using the formaldehyde calibration curve shown in Appendix A.. Using the stoichiometric relationship of

methanol and formaldehyde (1 mol of methanol consumed per 1 mol of formaldehyde produced) from the balanced equation 3-1, it was possible to calculate the concentration of methanol consumed by the photocatalytic oxidation process. Knowing the initial methanol molar concentration, the remaining methanol concentration was found by subtracting the consumed moles of methanol from the initial methanol value.

Molar carbon concentrations were found to be equivalent to the molar formaldehyde concentrations based upon the chemical formulas of compounds. Table 2.10 displays the equivalencies between the absorbance data and the molar concentrations of methanol, formaldehyde, and carbon as calculated for Experiment H, Pump 2.

Table 2.10 Experiment H Pump 2 Absorbance Data

Time	Abs [-]	CHOH [mM]	CH_3OH [mM]	CH_3OH [mM C]
0	0.000	0.000	4.000	4.000
5	0.007	0.049	3.951	3.951
10	0.017	0.119	3.881	3.881
15	0.018	0.126	3.874	3.874
20	0.025	0.175	3.825	3.825
30	0.033	0.231	3.769	3.769
45	0.031	0.217	3.783	3.783

2.7.1.2 Cinnamic Acid Data Processing

From a chemical perspective, cinnamic acid is an organic compound from the carboxylic acid family. Its condensed chemical formula $C_6H_5CHCHCO_2H$ can also be written as $C_9H_8O_2$, corresponding to a molar weight of 148.16 g/mol.

For experiments N through Z (sans Y), the absorbance test provided the cinnamic acid mass concentrations. Using the molar weight of cinnamic acid and the carbon molar ratio (9 mol of carbon content per 1 mol of cinnamic acid), it was possible to compute the concentration of cinnamic acid present in the water samples in terms of moles of carbon. Table 2.11 lists the equivalencies between the absorbance data and the molar concentrations of cinnamic acid and carbon as calculated for Experiment N, Pump 1.

Table 2.11 Experiment N Pump 1 Absorbance Data

Time	Abs [-]	$C_9H_8O_2$ [mg/L]	$C_9H_8O_2$ [mM C]
0	0.788	66.575	4.044
5	0.663	56.014	3.403
10	0.582	49.171	2.987
20	0.521	44.017	2.674
30	0.418	35.315	2.145
45	0.382	32.274	1.960
60	0.349	29.486	1.791
75	0.340	28.725	1.745
90	0.325	27.458	1.668
120	0.290	24.501	1.488

2.7.2 Total Organic Carbon (TOC) Measurement

Measuring the Total Organic Carbon (TOC) of each sample was done using a computerized test machine with autosampler (Shimadzu Corporation, Kyoto, Japan). The system was composed of a TOC-V CSN TOC Analyzer coupled with the Shimadzu ASI-V autosampler with a capacity for 68 vials per run. This test, which was conducted on methanol and cinnamic acid samples only, consisted of the following:

a) Take enough 24 mL vials to account for each sample that will be tested, as well as extra vials to rinse the machine's needles between experiment sets. For example, to run a TOC test for given experiment, Pumps 1 and 2, it will be necessary to use 3 extra vials to rinse the needles at the beginning of the TOC test of Pump 1, between Pump 1 and Pump 2, and after Pump 2.

b) Label the vials to reference the corresponding sample that each will contain. Rinsing vials do not require to be labeled though.

c) Match these vials with caps that have top holes covered with sealing membranes. For the test, the TOC Analyzer will require to introduce a needle through the vial's cap to extract the sample, thus.

d) Next, prepare the vials. For the autosampler to work correctly, it is required to fill a volume of no less than 15 mL in each vial.

    a. Prepare the rinsing vials: For each rinsing vial, take one vial and add 15 mL of pure Milli-Q water. Close tightly using a cap with sealing membrane.

    b. Prepare the sample vials: In this test, the samples will be diluted on a 1:3 ratio. For each sample to be tested, take the corresponding labeled vial and fill it with

10 mL of Milli-Q water. Next, add 5 mL of the pure sample that will be tested. Close tightly using a cap with sealing membrane.

c. Once all vials have been prepared, double check that all caps are tightly closed and lightly shake the vials.

e) At this moment, open the ASI-V autosampler and place the vials in order on the sampler wheel, taking note of the position number where they are being placed (a number marked 1 through 68 corresponds to each position in the machine). Make sure that the samples have been correctly positioned and close the autosampler. If this has been done correctly, the ASI-V sampler wheel should automatically position itself on the "Start test" position.

f) On a computer, run the TOC Analyzer software and create a Test Sheet. On the form, generate a list of the vials that have been introduced on the ASI-V autosampler. One by one, type in the sample label and choose an adequate TOC calibration curve. Calibration curves have to be previously created and can be found on a calibration library (procedure to generate the curve is detailed in Appendix A).

g) Still on the software, click on the autosampler icon to be directed to the ASI-V window. There, match each line of the Test Sheet (vial label described in step f) to the corresponding autosampler number (vial number described in step e). Once the position numbers have been correctly entered, save the changes.

h) Before running the test, verify that no more samples need to and can be included in the current test run. It is very important to check this, because, once the test has begun, it should not be stopped until it finishes. Always try to use the system at its full capacity.

i) On the main window, click on the "Start test" button to begin the TOC measurement test. The time for this process varies according to the number of vials that are being sampled per run by the machine.

j) Once the machine has performed the test, the TOC measurements will be reported on the Test Sheet on mg/L concentrations.

k) Because the samples were diluted, the real TOC measurement corresponds to the reported value multiplied by 3.

2.7.2.1 Total Organic Carbon Data in mM of Carbon

The measured TOC data was reported in terms of carbon mass concentration (mg/L). Because of this, obtaining the molar carbon concentration was done by factoring in the molar weight of a mol of carbon.

$$1 \text{ mol of Carbon} = 12 \text{ g of Carbon} \qquad \text{Eq. 2-3}$$

Thus, TOC data was converted to the equivalent mM of carbon by dividing the mass concentrations by the molar weight of carbon.

2.7.3 Chemical Oxygen Demand (COD) Measurement

The task of measuring Chemical Oxygen Demand (COD) of a sample was done using mercuric sulfate reagent test kits for low COD range (0-150 mg/L). This test, which was conducted on methanol and cinnamic acid samples only, consisted of the following steps:

a) Prior to performing the COD test, define what dilution rate, if any, is required. This should be done to prevent wasting test vials by introducing samples that are not within the COD range of the kit. To do this, estimate the expected COD concentration of the sample using its previously measured TOC for reference. If dilution is required, it is important to make sure that the dilution rate is compatible with the precision of the available pipettes, to avoid introducing error on the measurement during the dilution process.

b) Before preparing the vials, pre-heat the incubator reactor where the samples will later be placed. The oxidation reaction rate should be favored by the high temperature, making it critical to process the samples at an adequate temperature, which is 150°C. The pre-heating process can take several minutes. Thus, conditioning the incubator prior to preparing the vials is a very important step and it can shorten the overall time of the testing procedure.

c) While the machine is pre-heating, it is time to prepare the test vials. The test kit vials come pre-filled with an oxidizing reagent that need to be mixed with a volume of 2 mL of diluted sample to complete the required COD test volume.

    a. Mark the test kit vials caps that will be used and slightly open them.

    b. Prepare a blank vial: Take one test kit vial and fully open the cap. Add 2 mL of pure Milli-Q water and close tightly the cap. This will be the reference vial.

    c. Prepare the sample vials: For each sample to be tested, one test kit vial will be used. Using the dilution rate defined previously, calculate the amount of pure Milli-Q water and pure sample that will be required. Take one test kit vial and fully open the cap. First, add the required amount of pure Milli-Q water but do not mix. Following, add the required amount of sample. Close the cap tightly.

    d. Once all vials have been prepared, double check that all caps are tightly closed.

    e. One by one, shake the vials to make sure that the sample and the reagent are well mixed. When doing this, it is necessary to follow some safety measures. One, hold the vial by its neck and as closely to the cap as possible. The reaction is

exothermal and the vial's body will rapidly heat up. Two, make sure that the cap is pointing to an occupied place. The reaction can generate pressure which a loose cap might not be able to contain.

d) At this moment, place the vials in the incubator which should be set at a temperature of 150°C. Once all the vials are in place, activate the machine timer, which should be set for 90 minutes. Due to the long lapse required for the oxidation, it is advisable to run the COD test as a batch process and use the incubator at its full capacity.

e) After the 90 minutes period, remove the vials from the incubator and place them on a cooling rack for no less than 15 minutes. Note that the reactor will begin a cooling sequence automatically after incubating period is over.

f) To get the COD measurements, test the cooled samples using a photometric colorimeter. Following the specific instructions for the machine, select the COD range and calibrate it using the blank vial. One by one, place the sample vials in the colorimeter and record the COD readings.

g) If the sample was diluted, the real COD measurement corresponds to the multiplied value of the reading by the dilution rate.

2.7.4 Micropollutant Measurement

The task of measuring the presence of specific micropollutants in a sample was done using a Varian 325 LC-MS/MS triple quadrupole mass spectrometer, equipped with a vortex electrospray ionization interface (vESI) and a Pursuit XRs Ultra 2.8 C18 100 x 2.0 column (Agilent Technologies, Santa Clara, USA). A volume of 10 mL of undiluted sample was delivered for the external party to measure the compounds presence in the water.

This test method was used to detect the concentration of the pharmaceuticals and herbicides listed in Table 2.6, which were present only in the experiments AA and AB, as indicators for the removal of representative complex organic micropollutants.

2.7.5 Bacterial Analysis

The task of estimating the presence of bacteria in a sample can be done by measuring viable cells on cultivated plates, using a procedure known as Colony-Forming Units (CFU) count. Considering its applicability, this test was conducted on bacterial experiments Y and AB only. The serial dilution and counting procedure is the following:

a) First, define the dilution series that will be conducted per experiment test. This is necessary to estimate the amount of materials that will be used for the procedure. Table 2.12 and 2.13 describe the dilution series for Experiments Y and AB, respectively.

Table 2.12 Dilution Series for Experiment Y

Time	No dilution		d1 (by 10^1)		d2 (by 10^2)		d3 (by 10^3)	
Reactor	1	2	1	2	1	2	1	2
0		x					x	
10		x			x		x	
20	x	x	x				x	
30	x	x	x		x		x	
45	x	x	x		x		x	
60	x	x	x		x		x	
75	x	x	x		x		x	
90	x	x	x		x		x	
120	x	x						

Table 2.13 Dilution Series for Experiment AB

Time	No dilution		d1 (by 10^1)		d2 (by 10^2)		d3 (by 10^3)	
Reactor	1	2	1	2	1	2	1	2
0		x					x	
5		x			x		x	
10		x			x		x	
20	x	x	x		x		x	
30	x	x	x		x		x	
45	x	x	x					
60	x	x	x					
75	x	x						
90	x	x						
120	x	x						

b) Prior to performing the serial dilutions, it is mandatory to sterilize all the equipment and instruments that will be used in the process. To do so, introduce a safety factor into the estimated amount of Eppendorf's tubes, Eppendorf's racks, pipette tips and pure water from step (a). Compartment those using boxes and jars, and place these boxes and jars in an autoclave's baskets. Put the baskets in the machine, and begin the sterilization procedure.

c) When the autoclave has finished the sterilization cycle, transfer the jars and boxes immediately to a functioning hood. It is of utmost importance that this hood is adequate for performing biological testing procedures.

d) Working in the hood, take a rack and place rows of open Eppendorf's tubes for each sample that will be tested and its respective dilutions. At this moment, fill the dilution Eppendorf's with 0.9 mL of sterilized pure water and close the lids.

e) After taking each sample from the solar reactor, without filtering it, pour 1.9 mL of the liquid in an empty and sterilized Eppendorf's tube and close it. These will be the d0 tubes.

f) After filling all the tubes, methodically begin the decimal dilution process.

   a. For the d1 tubes, add 0.1 mL of d0 sample on the first row of Eppendorf's with 0.9 mL of water. Close the lid and homogenize using the centrifuge.

   b. For the d2 tubes, add 0.1 mL of d1 sample on the second row of Eppendorf's with 0.9 mL of water. Close the lid and homogenize using the centrifuge.

   c. For the d3 tubes, add 0.1 mL of d2 sample on the third row of Eppendorf's with 0.9 mL of water. Close the lid and homogenize using the centrifuge.

g) Now that the dilution mixes have been prepared, the samples have to be plated on LB nutrient agar plates (Miller's LB Agar, Scharlab) following the instructions listed Table 2.14 for the number of drops and sample volumes per drop.

Table 2.14 Plating Volumes and Number of Drops

Dilution series	Number of drops	Volume per drop
d1000	1	1000 µL
d100	6	100 µL
d0	8	10 µL
d1	8	10 µL
d2	8	10 µL
d3	8	10 µL

Sample plates have to be left to dry within the hood, only cap plates after the sample has dried.

h) Take the closed plates to an incubator which has to be preset at 37°C to cultivate the bacteria. This process takes 24 hours.

i) After the incubation period has passed, take the cultivated plates and count the number of viable cells that have formed.

2.7.5.1 *E. coli* Data Processing

This procedure for processing the information from the CFU count has been adapted from information provided by Dr. Ruud Timmers, one of the leading photocatalysis researchers at URJC.

After the counting process is complete, the number of CFU per drop can be transformed into a concentration value. To do this, the CFU number for a given drop is multiplied by the dilution factor, then divided by the drop volume in mL. For example, a CFU count of three in a drop of 100 μL and a dilution of one will result in a concentration of nearly 30 CFU/mL (1.5 log(CFU)/mL).

3 RESULTS AND DISCUSSION

Over the course of the 28 experiments using the lab-scale reactor at URJC, a vast amount of data was collected. This data consists of contaminant concentration, total organic carbon (TOC) obtained at various points in time during each experiment. Tests for chemical oxygen demand (COD) were conducted for a majority of the methanol and cinnamic acid experiments and are included in appendix data sheets when applicable. However, these COD results were not analyzed as they were not essential for the determination of the initial pollutant decay behavior.

This section contains the data that was collected for each run, normalized by the intended initial concentration of the variable in question (C/C_0). This section will provide the experimental results of each experimental run (including TOC when applicable) and will make a note of any observable trends and other conclusions.

3.1 ESCHERICHIA COLI

E. coli was introduced into the test solution for the two natural sunlight experiments (Y and AB) to more closely represent the field application of photocatalysis. For each experiment different initial concentrations were used for each half of the reactor (Pump 1 and Pump 2), 3 log(CFU)/mL for Pump 1 and 6 log(CFU)/mL for Pump 2.

3.1.1 Observations on *E. coli* Inactivation

Although the results from the plating process for experiment Y were inconclusive due to various procedural errors, the results from experiment AB help to confirm the viability of this technology for large scale disinfection.

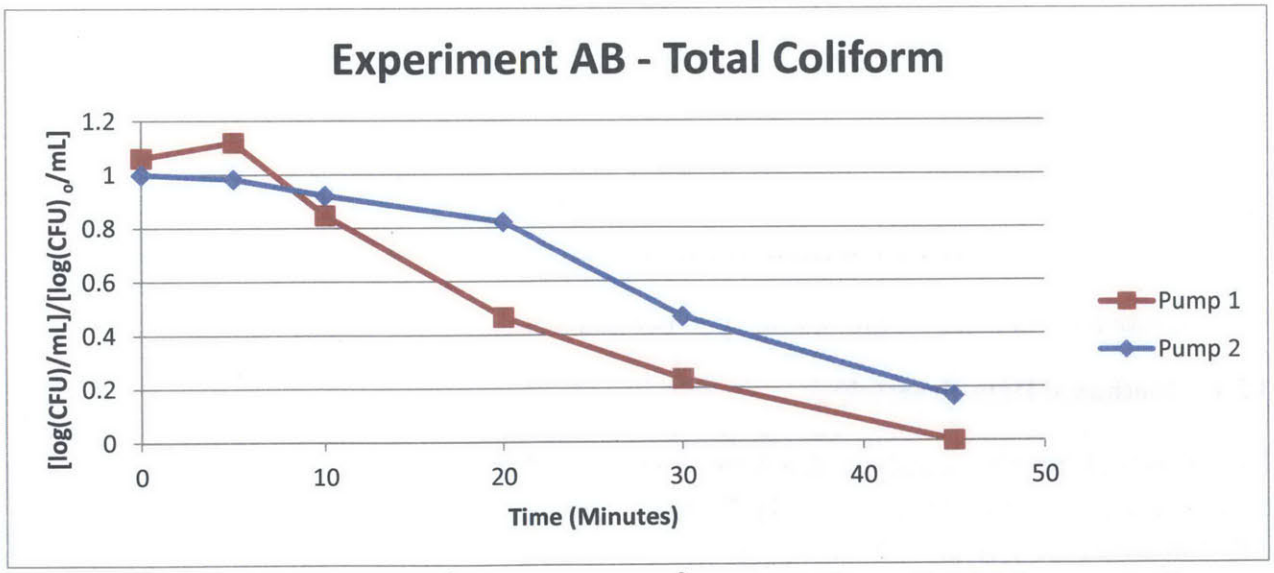

Figure 3.1 Experiment AB: 10^6 (Pump 1) and 10^3 CFU/mL (Pump 2) initial concentrations, 0.2 g/L TiO_2, natural light

Figure 3.1 displays the concentration of CFU for Pump 1 and Pump 2 of Experiment AB. As previously mentioned, this test was conducted with natural light, a catalyst concentration of 0.2 g/L, and at both high and low *E. coli* concentrations (10^6 and 10^3 CFU/mL) for Pumps 1 and 2 respectively. From this chart, it can be observed that the rate of decay for both the Pump 1 and Pump 2 samples are very similar, suggesting that the rate of inactivation is not dependent on the initial concentration of *E. coli*. Additionally, the inactivation of *E. coli* is consistent with the trends observed in a study by Marugán et al. (2010). The data plotted on a semi-log scale shows three regions: smooth decay, log-linear decrease and a decelerated decay towards the end of the reaction (clearly shown by Pump 1). Some other factors that may have influenced this behavior are the competition for hydroxyl radicals (the sample contained emerging pollutants and organic compounds in the artificial wastewater, the TOC is around 200 mg/L), and a decrease in solar radiation over time.

3.2 METHANOL

Following the schedule presented in Table 2.4, a total of thirteen experiments (A through M) were conducted to study the decay of methanol as a result of photocatalytic treatment. Over the course of these experiments, initial concentration of methanol, catalyst concentration, and radiation flux were varied to detect the interactions of these independent variables and their impact on the water treatment process. The samples taken in the experimentation process were tested to quantify the concentration of the pollutant and identify the rate of degradation.

From a chemical perspective, methanol is an organic compound and the most basic form in the alcohol group. When oxidized, alcohols form aldehydes; and methanol, as shown in equation 3-1, produces formaldehyde.

$$2\,CH_3OH + O_2 \rightarrow 2\,CHOH + 2\,H_2O \qquad \text{Eq. 3-1}$$

The formaldehyde can be further mineralized into carbon dioxide and water, as shown in equation 3-2 and 3-3.

$$CHOH + H_2O_2 \rightarrow CHOOH + H_2O \qquad \text{Eq. 3-2}$$

$$CHOOH + H_2O_2 \rightarrow CO_2 + 2H_2O \qquad \text{Eq. 3-3}$$

These reactions (3-2 and 3-3) are not likely to occur under conditions of neutral pH.

3.2.1 Methanol Data Processing

To understand the photocatalytic degradation process of methanol, it is necessary to relate the data obtained from the Absorbance, TOC tests. However, as these values were all reported in different concentration units, it was required to compute equivalent measurements on a reference unit base of comparison. Given the fact that the goal of photocatalysis is the mineralization of the target pollutant, it was chosen to convert the available data to molar units of organic carbon as a

mean to track down effectiveness of the oxidation process. Refer to Sections 2.7.1.1 and 2.7.2.1 for the procedures used for processing the raw absorbance and TOC measurements.

3.2.2 Observations on Methanol Results

After converting absorbance and TOC data to molar carbon concentrations, the experiment results were analyzed to quantify the effectiveness of photocatalytic oxidation. An initial analysis allowed for some preliminary conclusions in regards of the degree of methanol removal and the mineralization of the pollutant treated by photocatalysis. The experimental data for each of the experiments is located in Appendix B.

3.2.2.1 Observations on Photocatalytic Oxidation

The initial experiments conducted with methanol illustrate that photocatalysis does require the interaction of the catalyst and the light source, as photochemistry science proposes. This means that no other processes play role in methanol oxidation, and that the observed oxidation is only due to photocatalysis.

Figures 3.2 through 3.3 accompanying this section show that, when the polluted water does not receive radiation or no catalyst has been added to the system, there is no methanol degradation even after a relatively long period of time (60 minutes). Such behavior demonstrates that, for photocatalytic oxidation to take place, it is indeed required to have the interaction between catalyst and light source. Whenever either of these components is missing, no oxidation occurs.

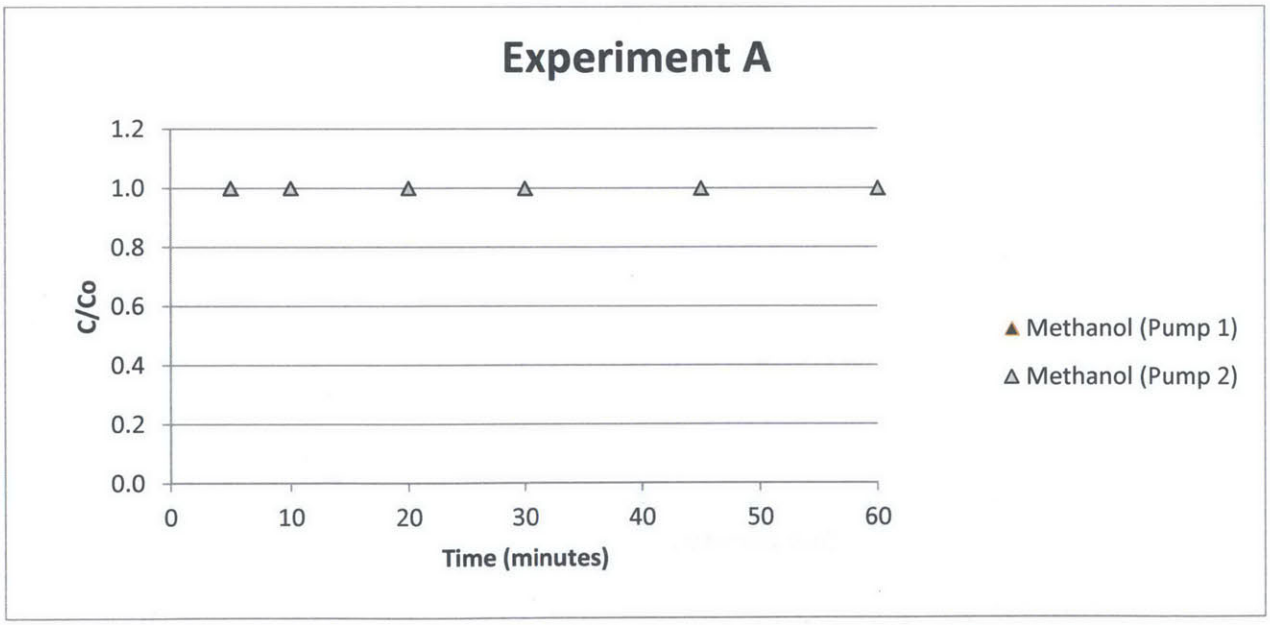

Figure 3.2 Experiment A: 100 mM TOC as Methanol, 0.1 g/L of TiO_2 and No Light

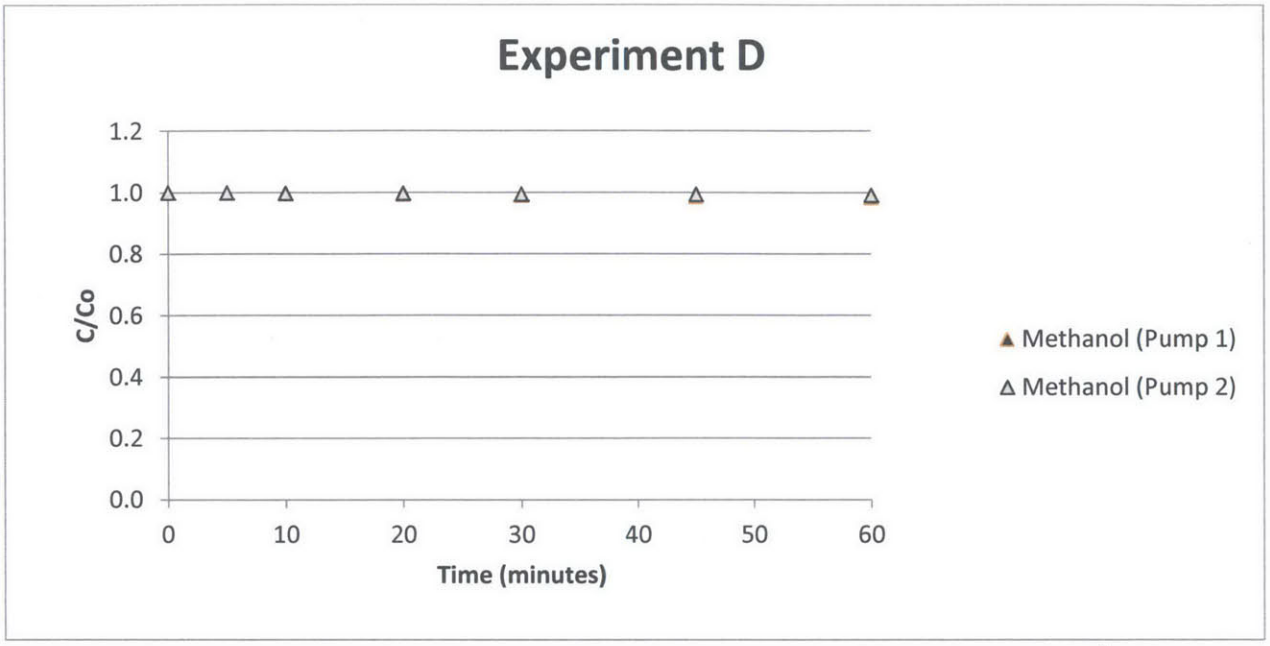

Figure 3.3 Experiment J: 200 mM TOC as Methanol, 0.0 g/L TiO_2 and 83.7 W/m^2 of Light

On the other hand, when TiO_2 is added to the polluted water, and the system is put in the presence of a light source, the pollutant is effectively attack and begins being removed. Figure 3.4 portrays a decreasing of methanol content over time as the water is being treated using 0.1 g/L of TiO_2 and powering the xenon lamp at 130 A (83.7 W/m^2).

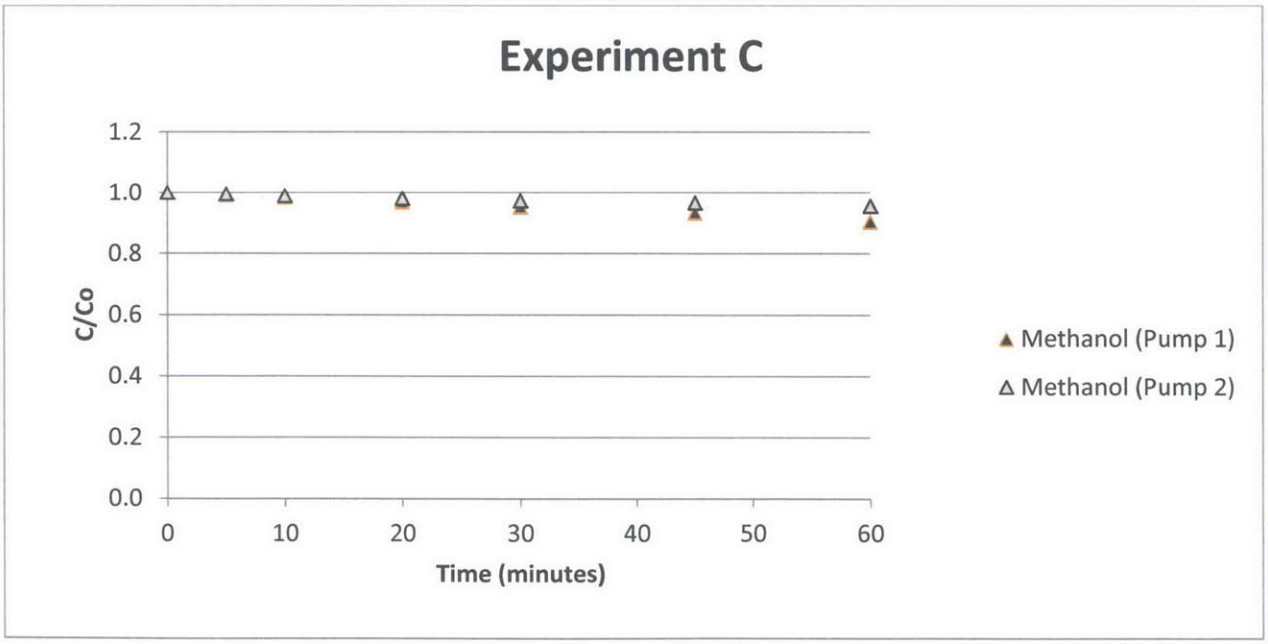

Figure 3.4 Experiment C: 100 mM TOC as Methanol, 0.1 g/L of TiO_2 and 83.7 W/m^2 of Light

3.2.2.2 Observations on Methanol Oxidation

The first step to assess the success of photocatalytic treatment is to monitor the evolution of the target pollutant. In the case of methanol, the study should verify that the methanol is disappearing from the water system as a result of photocatalytic oxidation. For the purpose of comparing the behavior of methanol in experiments that start with varying initial concentrations, all the results are presented as a concentration percentage normalized to the initial target TOC.

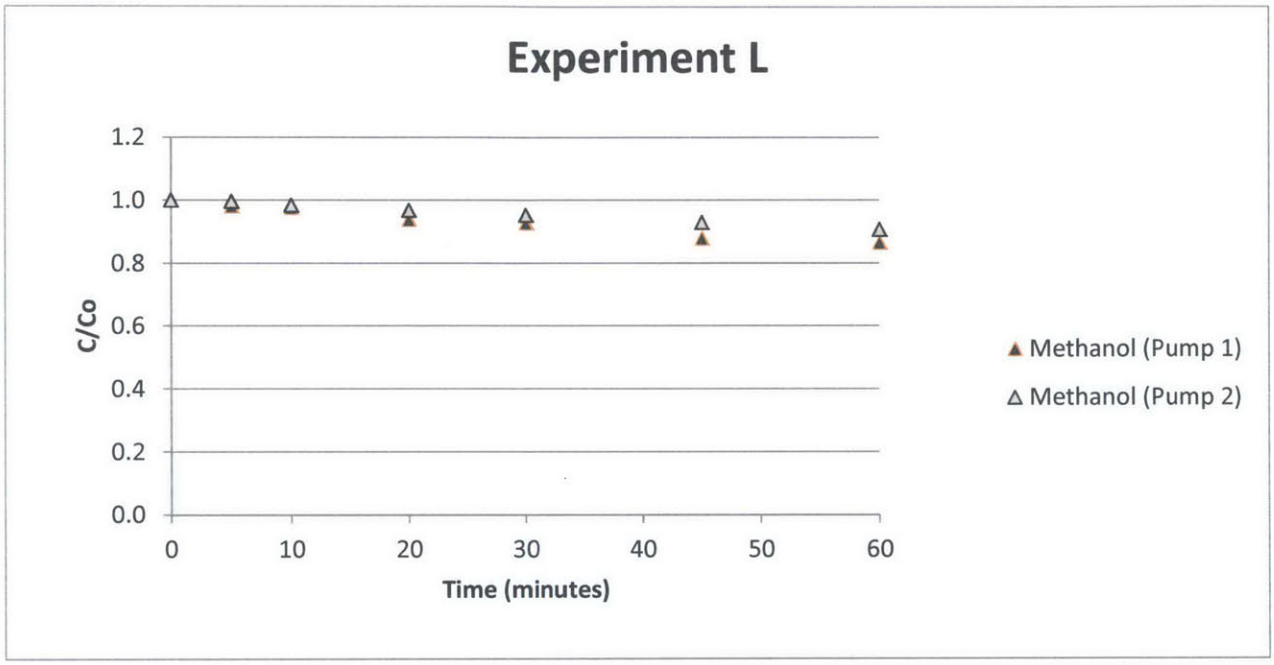

Figure 3.5 Experiment L: 8 mM TOC as Methanol, 0.05 g/L of TiO_2 and 74.2 W/m^2 of Light

Even though there is some observed decay of methanol, it is at a very slow rate. It is possible that the slow removal may be due to the molecule structure as well as due to acid base chemistry within the solution. These reasons for this low removal rate are further explored in Section 4.2.1.

3.2.2.3 Observations on TOC Decay

In addition to the reaction shown in Equation 3-1, the mineralization of methanol requires the formaldehyde molecules to undergo two more oxidation steps (Eq. 3-2 and 3-3) to become fully degraded to carbon dioxide. Thus, the best way to monitor the mineralization of methanol is by monitoring the organic carbon content in the water samples, as portrayed on Figure 3.6 below. However, complete mineralization is not expected under conditions of neutral pH, as was the case with these experiments. The oxidation reactions 3-2 and 3-3 require acidic pH to proceed.

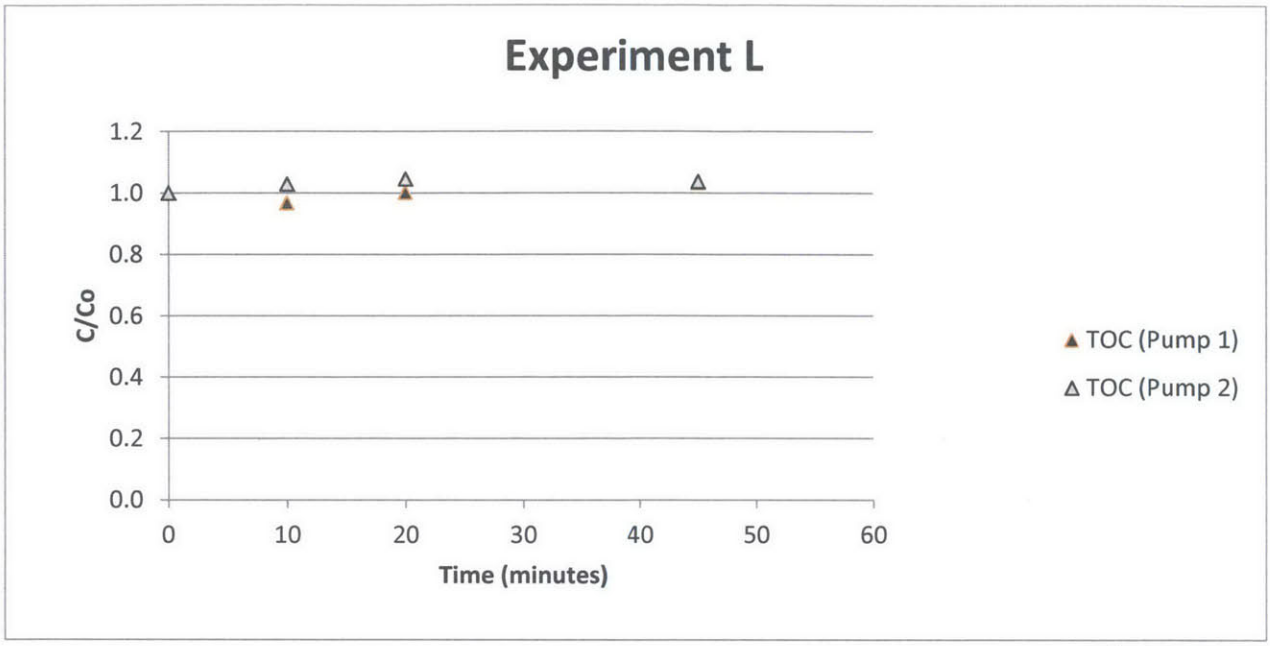

Figure 3.6 Experiment L: 8 mM TOC as Methanol, 0.05 g/L of TiO_2 and 74.2 W/m^2 of Light

3.3 CINNAMIC ACID

A total of twelve experiments were conducted to explore the decay of cinnamic acid under conditions of varying contaminant concentration, catalyst concentration, and radiation flux. These experiments include N through Z with the exception of Experiment Y, which was conducted using natural light. The three parameters that were monitored throughout these tests include absorbance, total organic carbon, and chemical oxygen demand. For these tests, the absorbance and TOC test results needed to be converted into concentrations of organic carbon (mM C). To make these conversions, the raw data was processed in the following way.

3.3.1 Cinnamic Acid Data Processing

Same as for the analysis of methanol photo-oxidation, the study of cinnamic acid degradation by photocatalysis relates the data obtained from the absorbance, TOC and COD tests. Thus, these measurements needed to be processed similar to those of methanol and converted to molar units of organic carbon.

3.3.2 Observations on Cinnamic Acid Results

Monitoring the fate of cinnamic acid throughout an experiment is essential to determining the degree to which photocatalytic oxidation is able to degrade this particular contaminant. The experimental data gathered in each of the cinnamic acid experiments is located in Appendix C.

3.3.2.1 Observations on Cinnamic Acid Oxidation

Figure 3.7 contains data collected from Experiment X with an initial TOC (as cinnamic acid) of 8 mM C, a catalyst concentration of 0.2 g/L TiO2, and an irradiation intensity of 46.2 W/m^2. The cinnamic acid concentration is normalized to the initial target TOC for the purposes of comparing numerous tests with different initial concentrations.

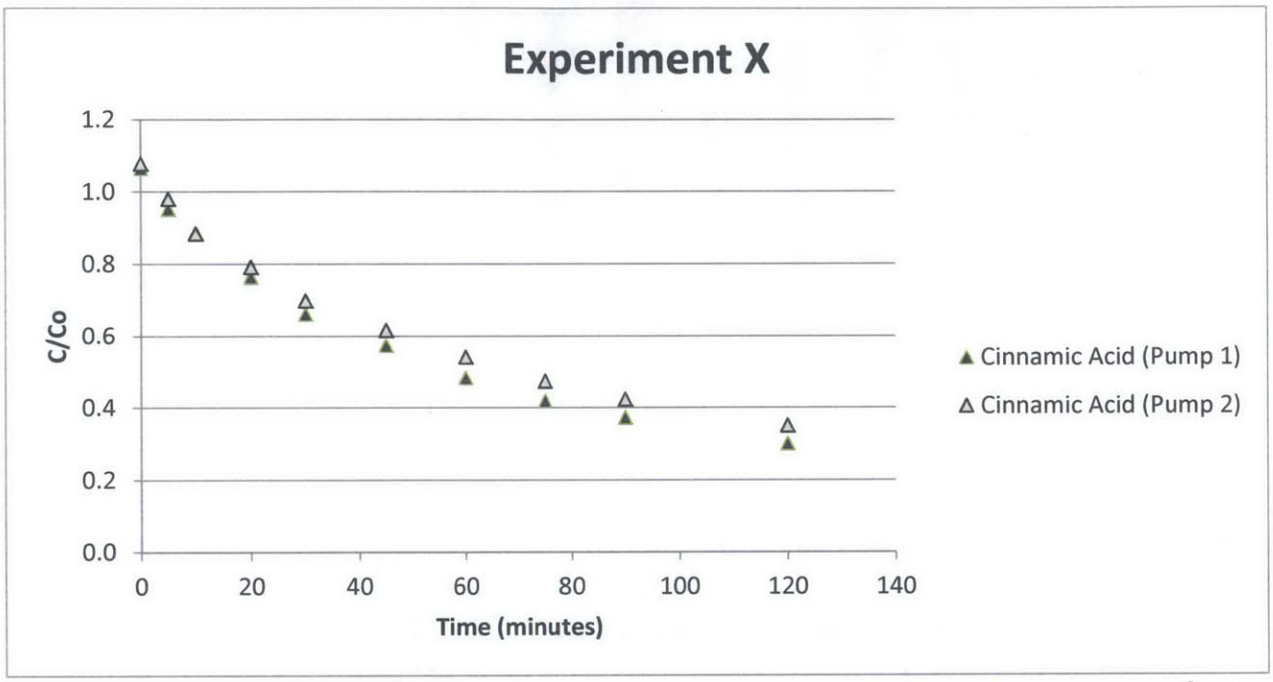

Figure 3.7 Experiment X: 8 mM TOC as Cinnamic Acid, 0.2 g/L of TiO_2 and 46.2 W/m^2 of Light

One important observation that can be made from the decay of cinnamic acid in Experiment X is the slight divergence in the values of Pump 1 and Pump 2. In fact, closer analysis shows that Pump 1 has exhibited 70 percent removal after two hours, while Pump 2 has only shown 65% removal. This suggests that the rate of decay for the reactors may not be equivalent to each other. This could be a result of the slightly different initial concentrations, but is most likely due to the heterogeneity of irradiation on the reactor. This unequal distribution of photons entering each of the reactors was observed in the form of a shadow being cast over a portion of the irradiance tubes of Pump 2. Further analysis of the radiation distribution shows that Pump 1 received an average radiation of 53.7 W/m^2 while Pump 2 received an average of 38.8 W/m^2. The shadowing was a result of the focus of the light source. This trend can be observed throughout each of the cinnamic acid tests, and can be seen in Figure 3.8, where the percent removal for Pump 1 of any experiment is higher than the value in Pump 2 for that particular experiment (with the exception of Experiment R). Upon further inspection of Experiment R, however, it is clear that the 120 minute value for the absorbance of Pump 1 was erroneous.

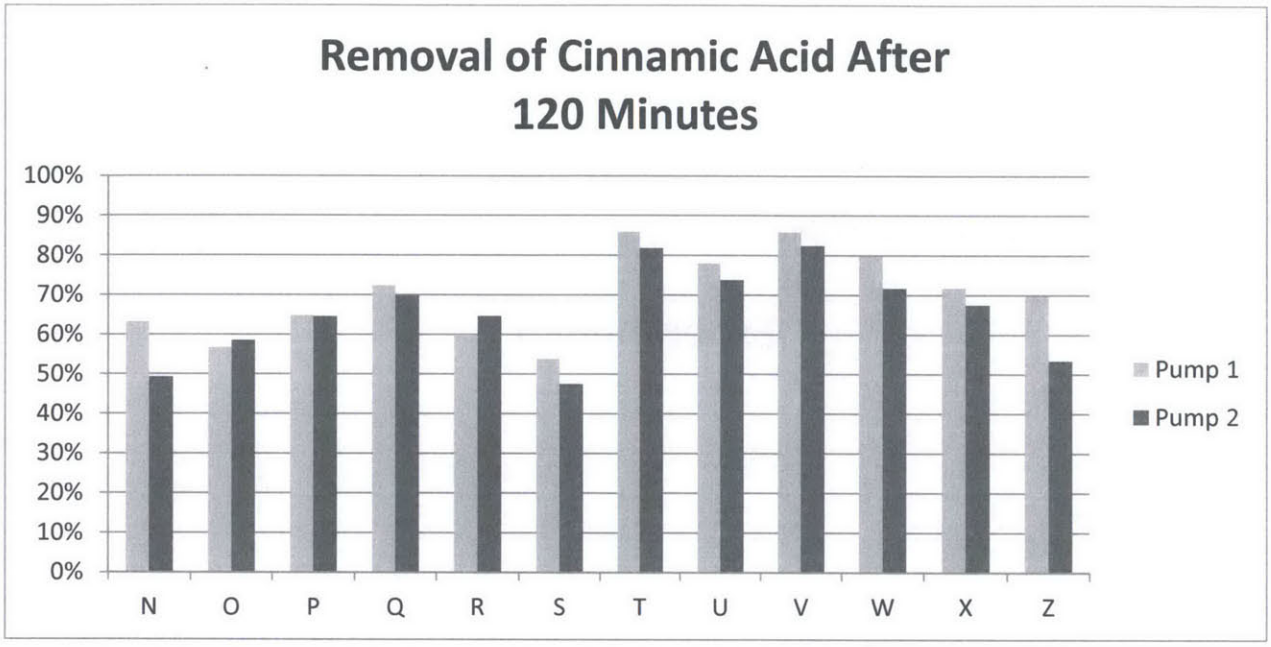

Figure 3.8 Removal of Cinnamic Acid after 120 minutes for Experiments N-Z (sans Y)

Within this chart, a number of patterns can be observed for the removal efficiency of cinnamic acid. For example, it is clear that Experiments T, U, and V experienced a higher removal of cinnamic acid than Experiments N through S, which is understandable considering N through S have lower catalyst concentrations. Additionally, it is clear that tests W, X, and Z experience less removal than T through V, and this is likely a result of the lower light intensity. Although some trends can be observed, they are only based upon removal at the end of each experiment. The following section, the Decay Rate Constant Analysis section, will analyze the decay rate constant which is typically more descriptive of the decay throughout an experiment and is therefore less susceptible to error.

3.3.2.2 Observations on TOC Oxidation

The monitoring of total organic carbon is essential to observing the decay behavior of the cinnamic acid. By definition, TOC measures all of the organic carbon in the test solution, which includes the organic carbon within the cinnamic acid itself as well as any organic carbon within any intermediary oxidized compounds. The decay of TOC suggests that a portion of the cinnamic acid molecules have been oxidized forming intermediate compounds, and that these molecules further degrade into carbon dioxide and water. This process, although for a different initial compound, is represented in Figure 1.2.

Figure 3.9 displays the decay of TOC as measured in Experiment Z normalized to the initial target TOC concentration. This experiment tested an initial concentration of 6 mM TOC, 0.2 g/L TiO_2, as well as a reduced radiation intensity of 46.2 W/m^2. This test was also conducted for four hours instead of two.

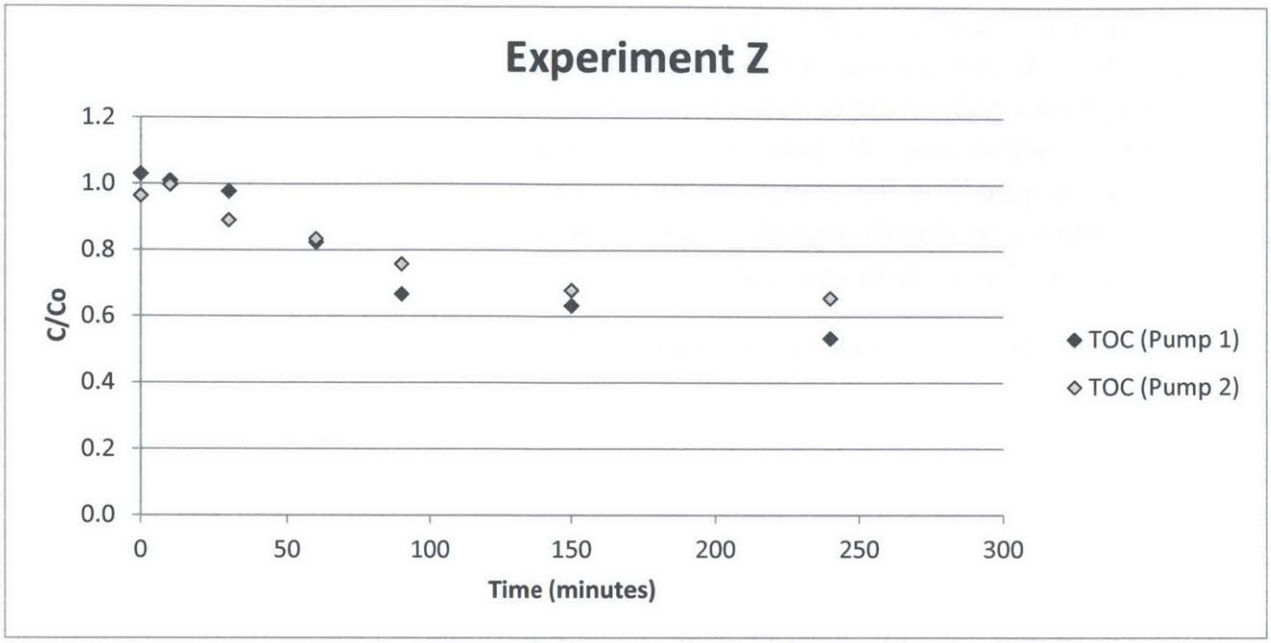

Figure 3.9 Experiment Z: 6 mM TOC as Cinnamic Acid, 0.2 g/L of TiO_2 and 46.2 W/m^2 of Light

In this experiment, the shadowing of the Pump 2 portion of the reactor is again apparent, likely causing a reduced decay in comparison to Pump 1. However, the primary observation that can be made from this chart is that nearly 40 percent of the initial TOC has been mineralized into carbon dioxide after 240 minutes of irradiation. Figure 3.10 displays the percent of mineralized carbon after 90 minutes for Experiments N through Z (sans Y).

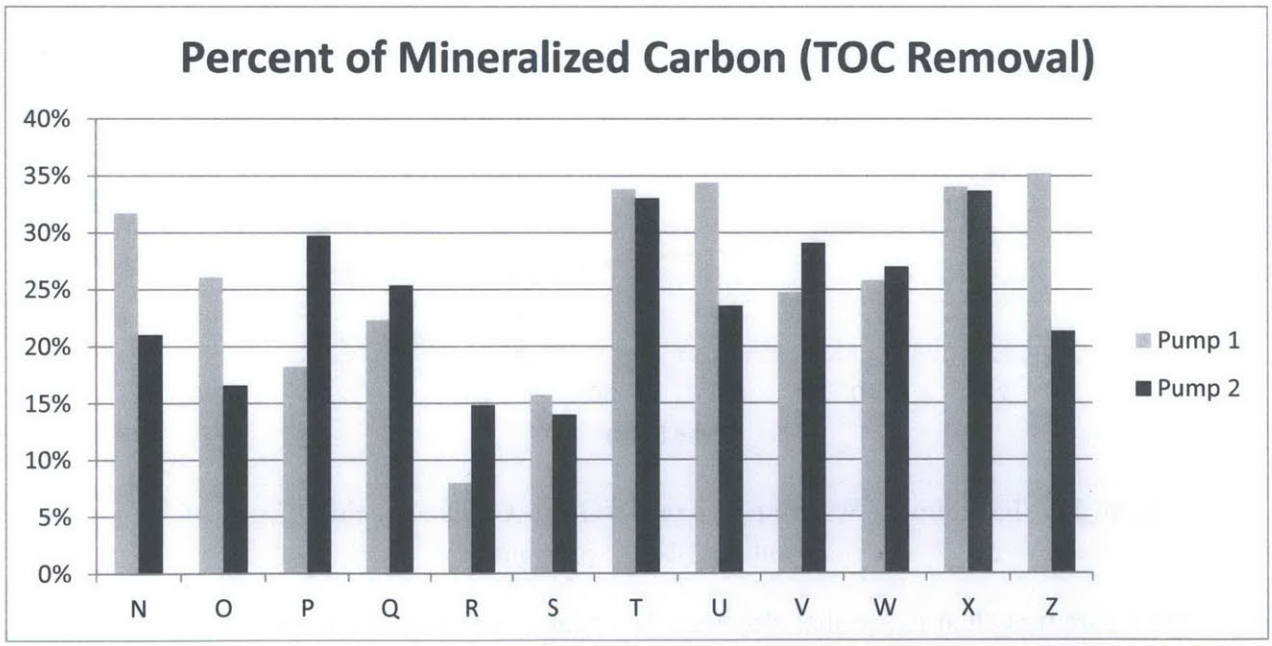

Figure 3.10 Removal of Organic Carbon after 90 minutes for Experiments N-Z (sans Y)

From this figure it is much more difficult to determine any specific trends. In fact, the previously observed trend of higher removal in Pump 1 versus Pump 2 is only seen in seven out of twelve experiments. Additionally, it can be seen observed that Experiment R displays the lowest amount of mineralized carbon after 90 minutes, this is understandable as it is the highest initial concentration, coupled with the lowest catalyst concentration. This supports the photocatalytic concept that removal is directly related to the amount of oxidizing agents in relation the initial concentration of molecules to be oxidized.

3.3.2.3 Compiled Observations for Cinnamic Acid Experiments

As was previously mentioned, the degradation pathway of cinnamic acid can be simplified into the following: cinnamic acid degrades into intermediate compounds, which are then degraded into carbon dioxide (shown as Eq. 3-4).

$$[A] \rightarrow [B] \rightarrow \ldots \rightarrow CO_2 + H_2O \qquad \text{Eq. 3-4}$$

Therefore, by treating the TOC measurements as the sum of the organic carbon contributed by cinnamic acid and by the bulk intermediates, and by having direct measurements of organic carbon contributed by cinnamic acid, it is possible to obtain values for the organic carbon contained in the bulk intermediate stage. The following figure (Figure 3.11) displays how this concept may be applied for any given set of measurements.

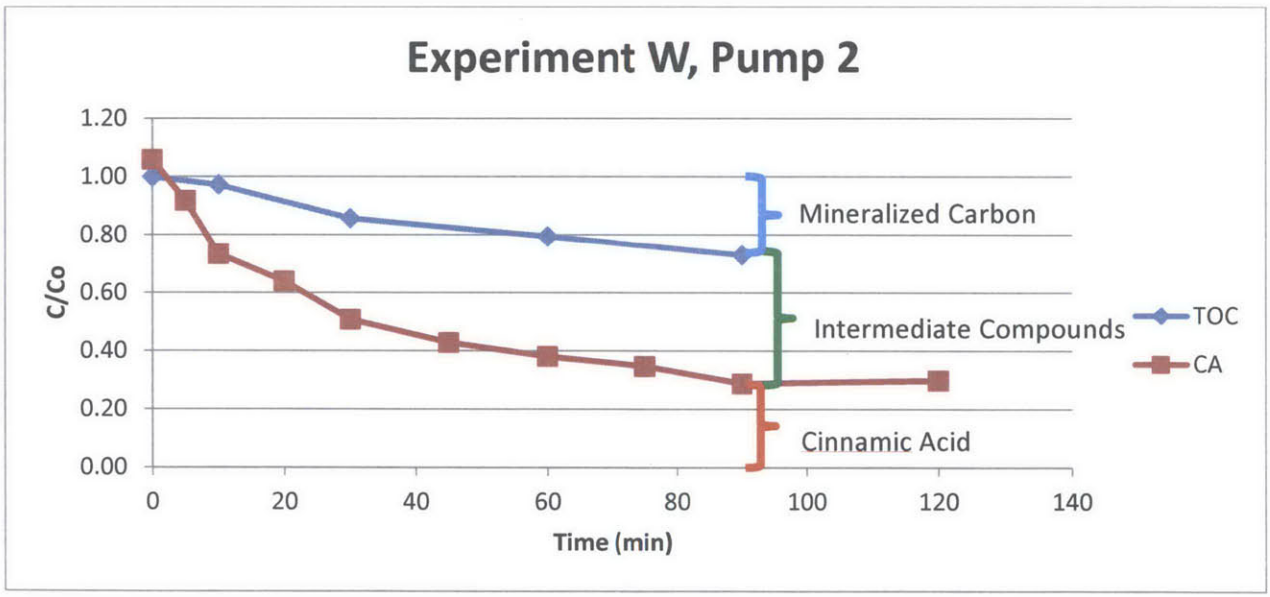

Figure 3.11 Experiment W Pump 2: 4 mM TOC as Cinnamic acid, 0.2 g/L of TiO_2 and 46.2 W/m^2 of Light

From this figure it is clear to see that although the organic carbon in the form of cinnamic acid is reduced by nearly 70 percent, the intermediate compounds remain the dominant source of organic carbon after 90 minutes. Figure 3.12 displays the breakdown of these values at 90 minutes for Experiments N through Z (san Y).

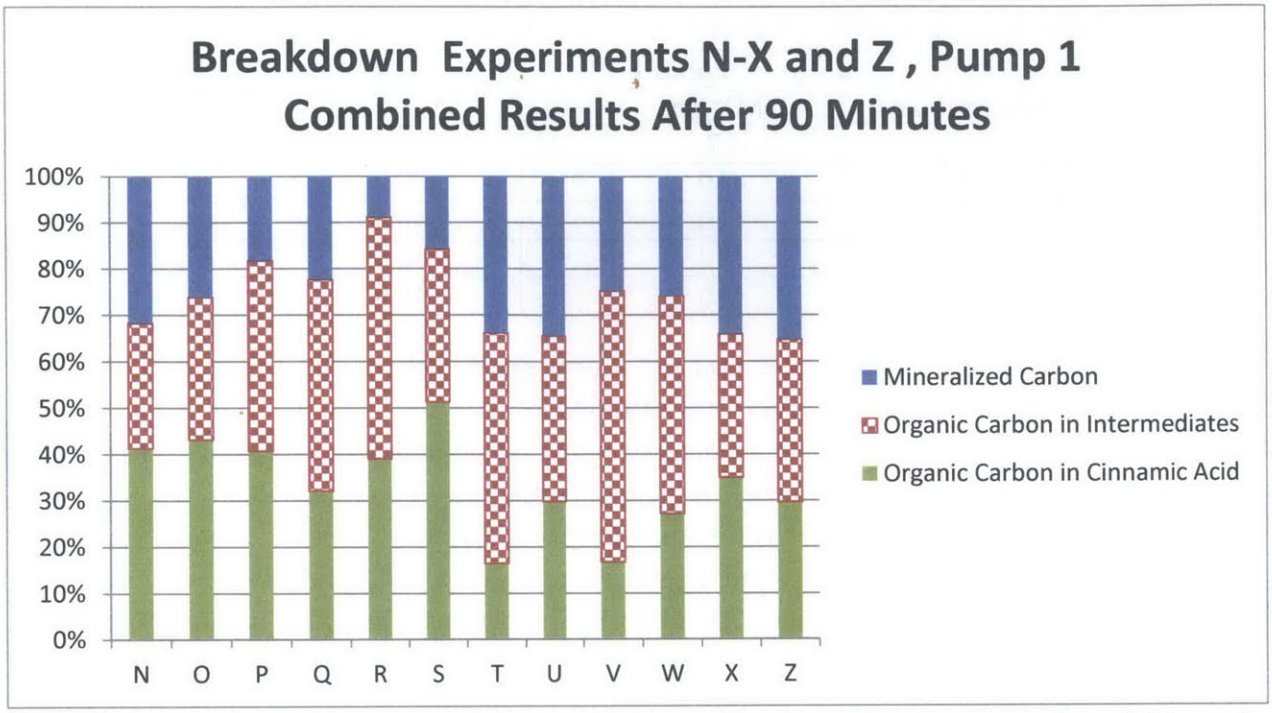

Figure 3.12 Mineralized Carbon, and Organic Carbon in Intermediate Compounds and Cinnamic Acid after 90 Minutes for Experiments N-Z (sans Y)

A careful analysis of Figure 3.12 shows generally lower amounts of mineralized carbon, as well as generally similar organic carbon (as cinnamic acid), for Experiments Q through S when compared to Experiments N through P. This trend is likely due to the decrease in catalyst concentration, causing a reduced availability of hydroxyl radicals. Under these conditions, the radicals more selectively attack the molecules with a greater amount of sites available for oxidation. The decrease in mineralized carbon and increase in cinnamic acid that can also be observed when comparing Experiments T through V to Experiments N through P.

The decrease in radiation observed in Experiments W, X, and Z (when compared to T-V) does not seem to effect the amount of mineralized carbon, but instead reduces the overall reduction of organic carbon found in cinnamic acid.

3.4 SULFAMETHOXAZOLE

Due to limited time with the reactor, only a single run (AA) was conducted with sulfamethoxazole as the sole contaminant. The goal for this single experiment was to have a concentration of 100 ng/L (ppt) in the "Pump 1" half of the reactor and 20 µg/L (ppb) in the "Pump 2" half of the reactor, with catalyst concentration and irradiation power of 0.2 g/L and 46.2 W/m^2 respectively. The measurements collected by the mass spectrometer are located in Figure 3.3.

Table 3.1 Experiment AA Reported Concentration of Sulfamethoxazole

	Pump 1		Pump 2	
Time (minutes)	SMX ppt	std	SMX ppb	std
0	77	18	<0.9	
2	<10		<0.9	
4	<10		<0.9	
6	<10		<0.9	
8	<10		<0.9	

It is clear from these results that there was significant error in the initial concentration of the Pump 1 solution, given that the target concentration of 100 ppt is only just outside of the standard error for this measurement. It even appears that no sulfamethoxazole was ever added to Pump 2, or that the amount added was below the detectable limit. The values that read <10 ppt or <0.9 ppb signify concentration values below the machine's detection limit. However, despite the erroneous initial concentrations, the rapid degradation observed in the first two minutes of the Pump 1 experiment is very important. Although this experiment provides no information on intermediate compounds, it is clear that the sulfamethoxazole is rapidly degraded.

Fortunately, the experiment AB, with natural sunlight, tested the degradation of sulfamethoxazole within a complex solution. As previously mentioned, the solutions tested in experiment AB consisted of synthetic wastewater, *E. coli* bacterium, as well as a cocktail of emerging pollutants (listed in Table 2.7) at an initial concentration of 1 microgram per liter (ppb). With this experiment it is possible to observe the degradation behavior of sulfamethoxazole in a solution with numerous other compounds competing for the hydroxyl radicals. Below is a plot of the various compounds, normalized to their respective concentrations at time zero, with sulfamethoxazole as the large Xs.

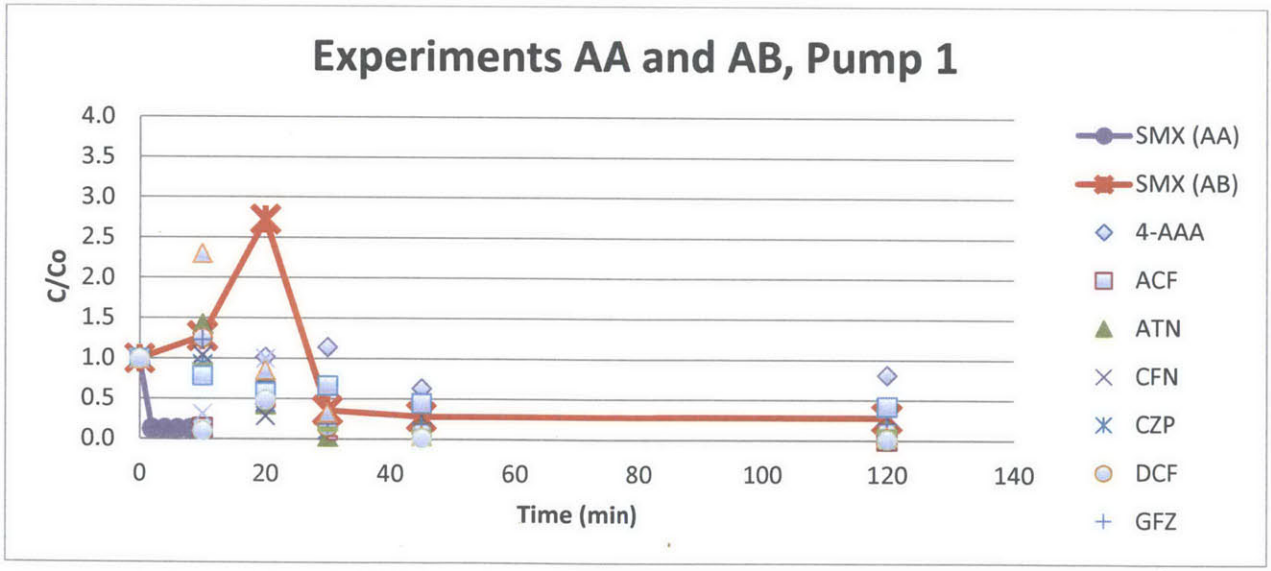

Figure 3.13 Experiments AA Pump 1: 100 ppt Initial Concentration, 0.1 g/L TiO_2, W/m^2 Light and AB Pump 1: 1000 ppt Initial Concentration, 0.2 g/L TiO_2, natural light

From the results of this experiment (AB Pump 1), a nearly 75% removal of sulfamethoxazole can be observed after 45 minutes of the experiment. Similarly, the results for AB Pump 2 show a 50% reduction of sulfamethoxazole (from 15.8 ppb to 7.3 ppb) after 60 minutes. The rate of removal in AB Pump 1 is significantly lower than seen in AA Pump 1. This is to be expected due to the fact that the irradiation power is lower than in experiment AA Pump 1. This significant difference is suspected to be the result of high competition for hydroxyl radicals. This competition could be a result of the lower radiation (which limits the formation of hydroxyl radicals) as well as the presence of more contaminants.

The data for the decay of the higher initial concentration (20 ppb) emerging pollutant cocktail is shown in Figure 3.14. These measurements were normalized to the initial measured concentrations.

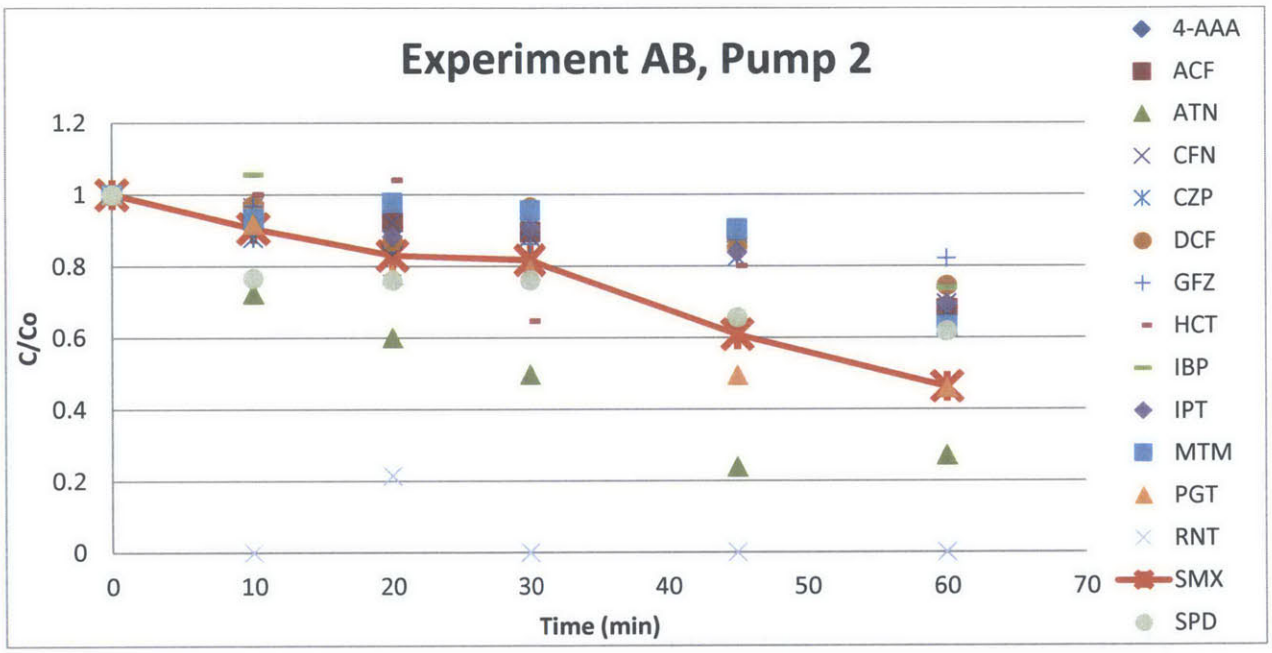

Figure 3.14 Experiment AB Pump 2: 20 ppb Initial Concentration, 0.2 g/L TiO_2, natural light

Here it can be seen that the sulfamethoxazole has been removed by more than 50 percent after a time of 60 minutes, despite the intense competition for hydroxyl radicals. Within Figure 3.14, it is easy to see that not every one of the emerging pollutants is being degraded at the same rate. This suggests that the hydroxyl radicals may experience a propensity for attacking some contaminants rather than others. This likely has to do with the structure of the molecules and the bond strength between atoms.

3.5 TEMPERATURE

An electronic temperature sensor took temperature measurements each second that the reactor was plugged in. Therefore, it was possible to monitor the temperature throughout each of the experiments. Although this data was not used for any analysis, or for the modelling, some brief

conclusions can be made. Over all of the methanol experiments, the change in temperature throughout the experiment was typically around 20°C. The change in temperature for the cinnamic acid experiments was typically less, around 10°C, due to the fact that the initial temperature was generally higher than for methanol as a result of using the sonic bath. For the outdoor experiments, a smooth temperature curve, like that shown in Figure 3.15, does not occur. This is likely a result of the varying radiation, as well as the colder ambient conditions.

Another interesting observation that can be made is that there exists a linear portion of the temperature curve toward the beginning of the experiment. This likely represents the homogenization phase in which the reactor is covered in aluminum foil. This trend can also be observed in the majority of the indoor experiments.

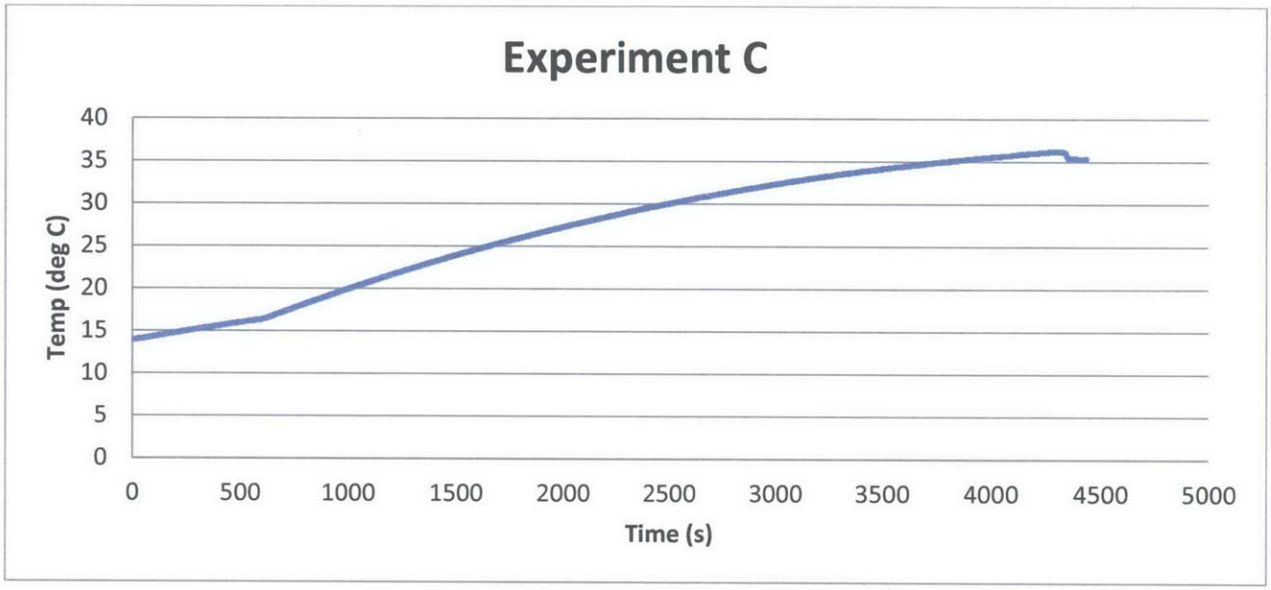

Figure 3.15 Temperature Curve for Experiment C

3.6 QUALITATIVE ERROR ANALYSIS

As with any scientific experimentation, there are always sources of error. Thus, it is important to indicate these possible sources, and to eventually quantify the error. The following will list possible areas of the experimentation process in which error may have been introduced as well as attempt to quantify some of this error.

3.6.1 Possible Sources

The first step in the experimentation process that could produce error is in the process of the solution preparation. This could be simply due to error within the calculation for the mass of contaminant added to the solution, or to errors in measurement of the contaminant itself. While calculation errors seem unlikely, it is highly possible that the initial concentrations of the test solutions showed reasonable error as a result of measurement errors. These initial concentration

errors were used to create the error bars shown on the model fitting charts in Section 5. Theoretically, this process can be applied to each of the model fitting charts, but was only included in the plots in Section 5 as a method for qualitatively determining the degree to which the model fits the experimental data. As an example, the mean error of the initial cinnamic acid and TOC (compared to the target concentrations) are -3.6 and -6.0 percent, with standard deviations of 23.0 and 14.4 percent, respectively. For a more detailed breakdown of the initial concentration errors for each of the contaminants, see Appendix D.

During each experiment, there are many other areas in which human error may have resulted in erroneous measurements. It is possible that the reactor may have been out of line, or at a slightly different distance from the light source itself; however, it is not likely that this produced a noticeable effect. The sampling is another area where human error is likely to have occurred. This could have happened in two main ways: taking the sample at the incorrect time, or switching the two samples by placing a sample from Pump 2 into the vial for Pump 1. For example, the trends shown in Figure 3.16 suggest that the values for Pump 1 and Pump 2 at 60 minutes may have been switched. Similar results have also been observed in the methanol datasets.

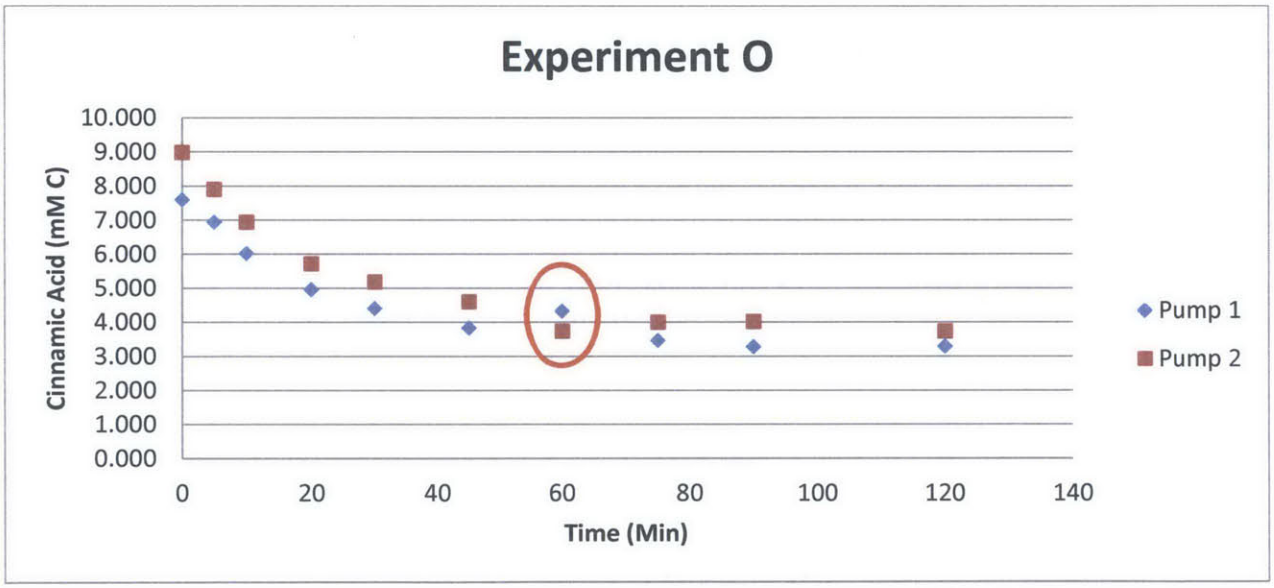

Figure 3.16 Experiment O, Possible Switching of Pump 1 and 2 Samples

The sample analysis is the last area of experimentation that could produce error. Due to the fact that very low concentrations were being tested, any human error in the testing procedure could have significant effects. Conducting the absorbance, TOC and COD tests required sample dilution by as much as twenty times. Error here could result from inaccurate sample dilution or from incorrect notation of the dilution factor that was used. Additionally, use of the pipette could have introduced error in two different ways: precision of the instrument or operation error. For example, Figure 3.17 displays one of these errors. Although it is difficult to tell whether the error

was made in the absorbance or TOC measurements, it is suspected that the TOC is in error as the intended TOC is almost exactly double.

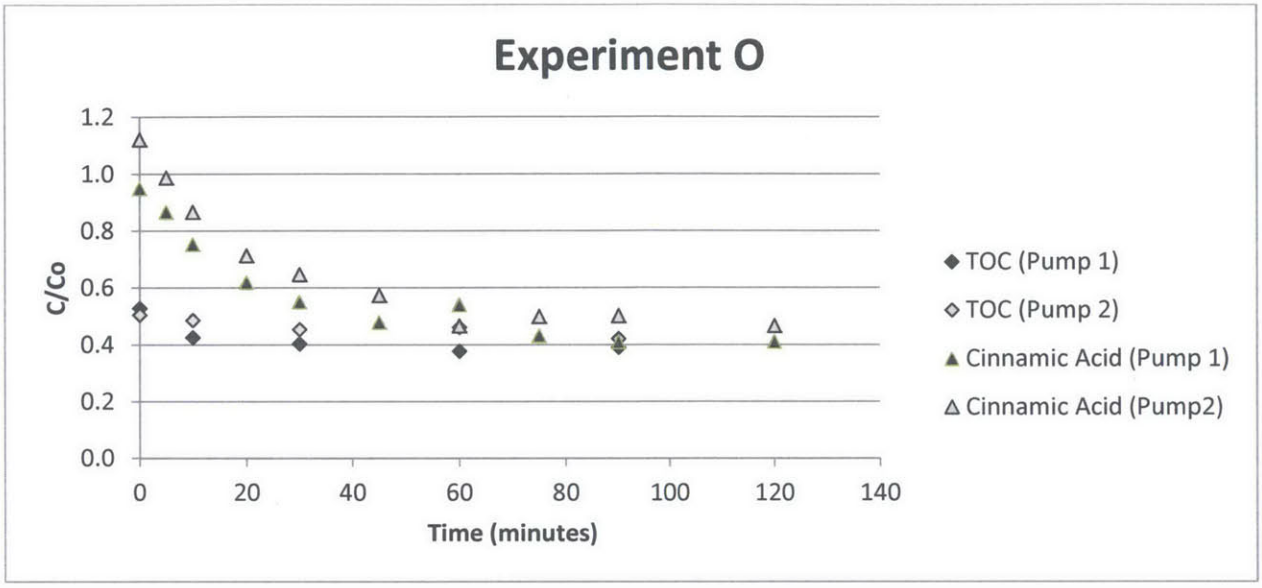

Figure 3.17 Experiment O, Possible Error in Dilution/Dilution Recordkeeping

Finally, possible error may have also been introduced in the sample analysis phase due to the machines themselves. For example, the research group at URJC found the TOC sampler to have an error of 0.1000 mg/L. Although the TOC error may be small, the error for the mass spectrometer ranged as high as 220% for some of the 1 mg/L samples.

Additionally, a few of the given samples were tested twice (the second time by Dr. Timmers), to check for consistency; however, it is not quite clear that this error is due to human error or machine error.

4 ANALYSIS OF DECAY RATE CONSTANTS

In order to evaluate photocatalytic oxidation as a viable advanced oxidation option for larger scale wastewater treatment, it was essential that the degradation of the contaminants in question be further analyzed. This section will discuss the process used to qualitatively analyze the effect of varying initial concentration, catalyst concentration, and radiation power, as well as the results of said analysis. The decay constants found for the methanol and cinnamic acid experiments will be analyzed for these qualitative trends. Unfortunately, the few experiments with sulfamethoxazole and *E. coli* make it impossible to perform an analysis of the decay constant trends.

4.1 APPROACH

The experimental results for contaminant concentration and total organic carbon (TOC) with respect to time can be examined to determine the decay behavior of each individual constituent. Classically, the decay behavior of a single compound can be described by an "order" of the reaction; such as 0^{th}, 1^{st}, and 2^{nd} order. For each reaction model, there exists a decay rate constant. The order of the reaction gives insight into the way or ways in which this decay rate constant can be influenced by a number of variables (or none). For a given decay reaction without intermediate steps, $aA + bB \rightarrow cC$, the rate law can be written as:

$$r = \frac{d[A]}{dt} = -k[A]^x[B]^y \qquad \text{Eq. 4-1}$$

The x and y exponents are typically used to define the order of the reaction, and can be determined experimentally. The decay rate constant, the parameter of concern for this analysis, is also empirically derived and is often dependent on other parameters such as catalyst presence and light irradiation.

4.1.1 Zero Order Kinetics

A reaction order of zero signifies that the sum of the exponents for reactant A and B is equal to zero and that the rate of decay of A is linear and equal to the decay constant k. The technique for determining if a reaction follows zero order kinetics is rather simple. If the plot of the concentration data vs. time follows a linear trend, then this reaction is zero order. The equation below defines this line, where the slope is equivalent to the decay rate constant and the point at which the line crosses the y-axis is equal to the initial concentration of A.

$$[A] = -kt + [A]_0 \qquad \text{Eq. 4-2}$$

A good linear fit signifies that the reaction rate is independent of the contaminant concentration.

4.1.2 First Order Kinetics

A first order reaction will have an exponent for reactant A equal to one (exponent for B equal to zero). To determine if the particular experimental data exhibits first order decay, the data can be linearized by plotting the natural logarithm of the concentration of A vs. time. With this linearization technique, the slope of this line will be equivalent to the decay rate constant and the y-intercept is equal to the natural logarithm of the initial concentration of A. This equation is shown below.

$$ln[A] = -kt + ln[A]_0 \qquad \text{Eq. 4-3}$$

A good linear fit for the first order linearization signifies that the rate of decay at any given moment is dependent on the concentration of A at that time. This is commonly referred to as exponential decay.

4.1.3 Second Order Kinetics

A reaction can be classified as second order if it is monotonic (only A) with an exponent of two, or if the exponents of A and B are both one. Diatomic second order reactions are more difficult to model, due to the dependence on both A and B. For this reason, A was assumed to be the only reactant for this analysis. Thus, the experimental data can be linearized according to the following equation.

$$\frac{1}{[A]} = \frac{1}{[A]_0} + kt \qquad \text{Eq. 4-4}$$

By plotting the inverse of the concentration of A vs. time, the slope of the line represents the decay constant and the y-intercept represents the inverse of the initial concentration.

4.2 RESULTS AND CONCLUSIONS

For photocatalytic application, one can conclude that the decay rate constant is essentially dependent upon the number of hydroxyl radicals available and the number of sites for these radicals to oxidize the contaminant in question. Further, the concentration of hydroxyl radicals is dependent on the catalyst concentration and the radiation intensity. It is for this reason that these variables will be examined.

4.2.1 Methanol Experiments

To analyze the methanol data, the concentration values were processed using the linearization techniques detailed in Section 4.1 and a linear regression was applied to each of the resulting data sets. By examining the visual trends and taking into consideration the coefficient of determination (R^2) for each linearized set of values, it was found that the methanol system

(experiments A through M) is likely to behave as a zero order kinetic reaction. The best fit 0^{th}, 1^{st}, and 2^{nd} order rate constants and R^2 values are located in Appendix E.

4.2.1.1 Contaminant Concentration

Considering that the photocatalytic oxidation depends on the interaction of the initial pollutant, the catalyst, and the radiation energy, it was expected to find that the rate of decay varied when these factors were set at different levels. To better understand the photochemical system, the previously estimated zero order decay rates were plotted to determine any qualitative trends that arise with the varying conditions set for each experiment.

Effect of Initial Concentration

Kinetic chemistry theory indicates that a zero order reaction is not dependent on the initial concentration of the chemical of interest. To test this, the estimated decay rates of methanol data sets were compared on the basis of catalyst concentration and light intensity levels. Figure 4.1 illustrates the decay rate constants for Pump 1 Experiments H through M in subsets of two TiO_2 concentrations and a specific radiation intensity.

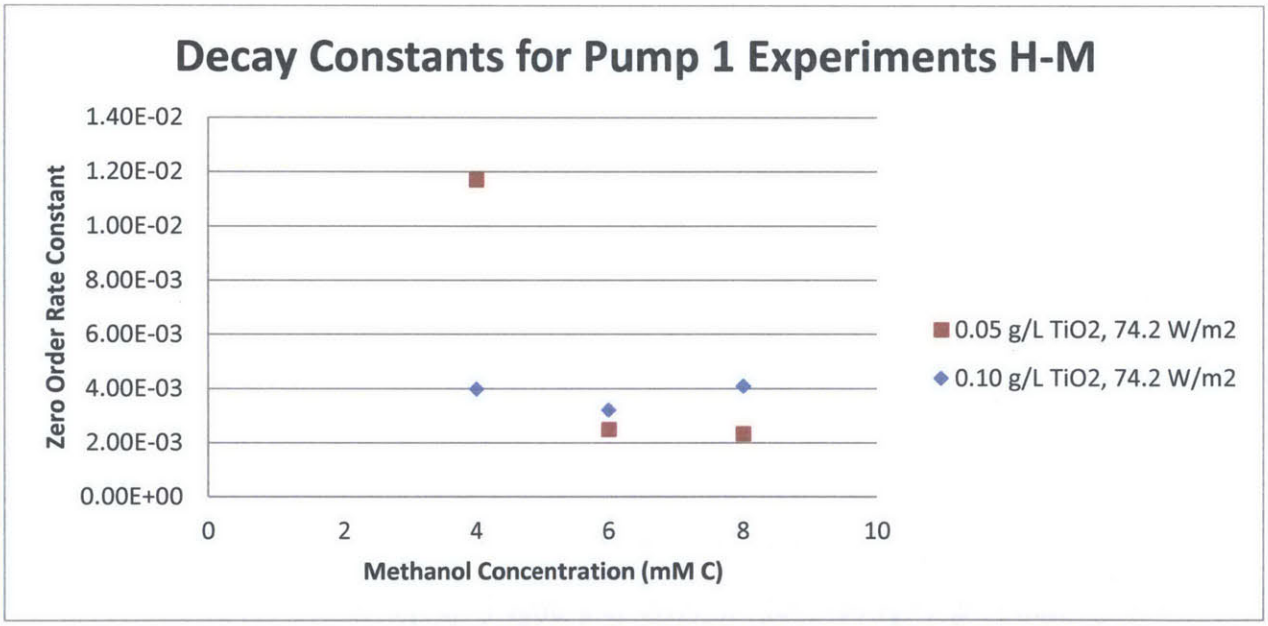

Figure 4.1 Effect of Initial Methanol Concentration on Oxidation Rate

In the plot, it is possible to note that the experiments with 0.10 g/L of catalyst behave as anticipated by kinetics theory and do not show much variability as a result of changing initial methanol concentration. Even though the 0.05 g/L data is not as consistent (with a single outlier of extremely high decay rate at low methanol concentration), it is clear from the two other methanol concentrations that the photocatalytic degradation maintains a fairly constant rate regardless of the initial concentration of the target pollutant.

It is noticeable also that, two out of three times, the decay rates of the experiments conducted with a high catalyst concentration (0.10 g/L) exceed the rates at which methanol decays when catalyst concentration level was low (0.05 g/L). Given the direct relation between catalyst concentration and availability of hydroxyl radicals, this trend is once more consistent with kinetics theory as a faster rate of decay should be observed when the availability of the oxidizing agents is greater.

Similar behavior was observed in the Pump 2 decay rates.

Effect of Catalyst Concentration

Analyzing the same data (experiments H through M), Figure 4.2 shows decay rates in subsets of three initial methanol concentrations (in equivalent TOC values) and a 74.2 W/m^2 radiation intensity. This graph is useful to evaluate trends on decay rates as a result of varying the catalyst concentration.

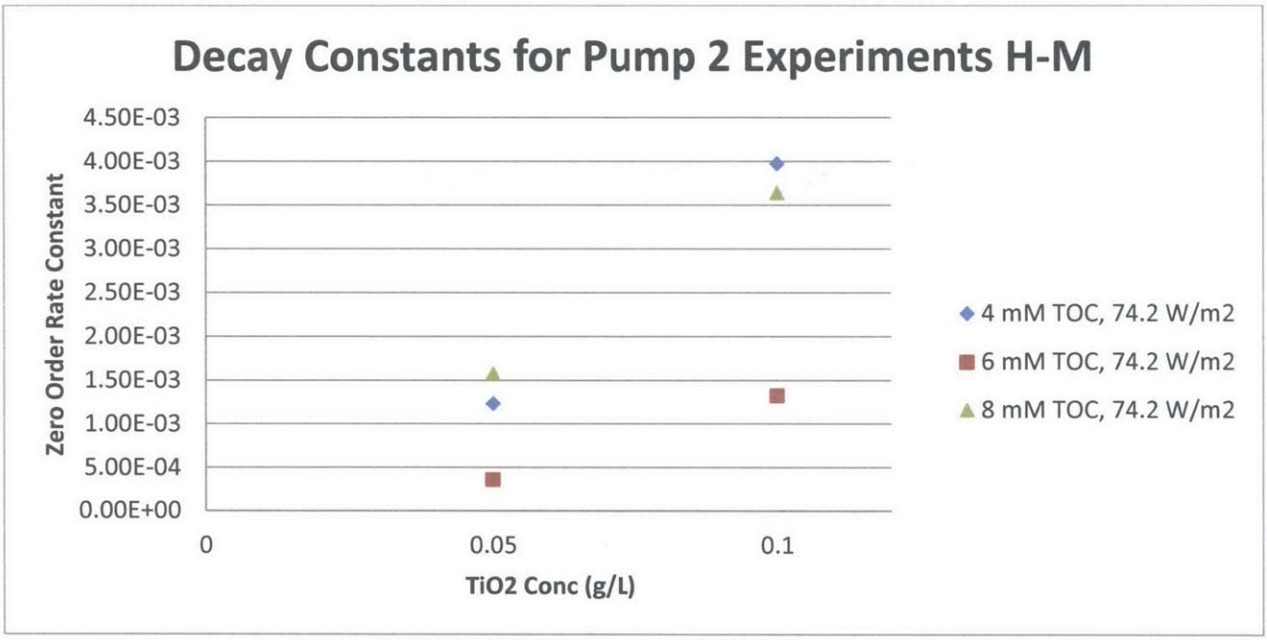

Figure 4.2 Effect of TiO_2 Concentration on Oxidation Rate Constants

As previously indicated, in photocatalysis there is a directly proportional relationship between the catalyst concentration and the generation of hydroxyl radicals; a correspondence that explains that higher oxidation rates are observed as a result of increasing the TiO_2 content per volume of water. As Figure 4.2 clearly shows, methanol is consistently becoming degraded at a faster pace when TiO_2 concentration doubles, even though the degree by which this accelerated rate occurs does not show a regular trend.

Pump 1 experiments revealed a similar behavior, with an exceptionally low decay of the 4 mM TOC sample at 0.1 g/L TiO_2 concentration.

Effect of Radiation Intensity

Although the effect of radiation flux is of high relevance in understanding photocatalytic processes, the experiments conducted did not include a set of experiments in which the initial contaminant and catalyst concentration remained constant while varying the radiation intensity. Thus, no conclusions can be made on the effect of radiation intensity on the decay rate constants for the methanol experiments.

4.2.1.2 TOC Concentration

Given the fact that the intention in applying photocatalytic oxidation is to remove the organic pollutants from the water stream, the trends on the total organic carbon decay are of great relevance to predict the overall effectiveness that this technology may show in real applications.

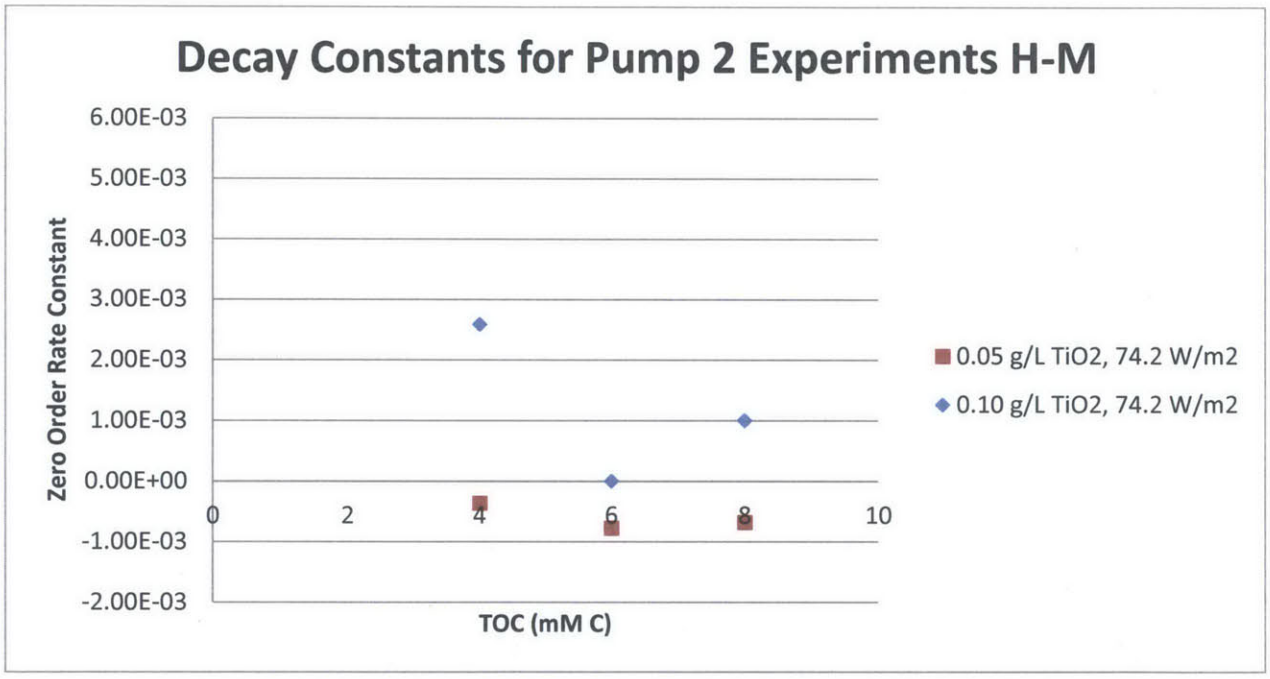

Figure 4.3 Effect of Initial TOC on TOC Oxidation Rate Constants

Figures 4.3 and 4.4 show, with the exception of an outlier point on each graph, that estimated TOC decay rates were nearing zero, a value which was consistent to the observed TOC measurements being always around an average value and presenting not great variation.

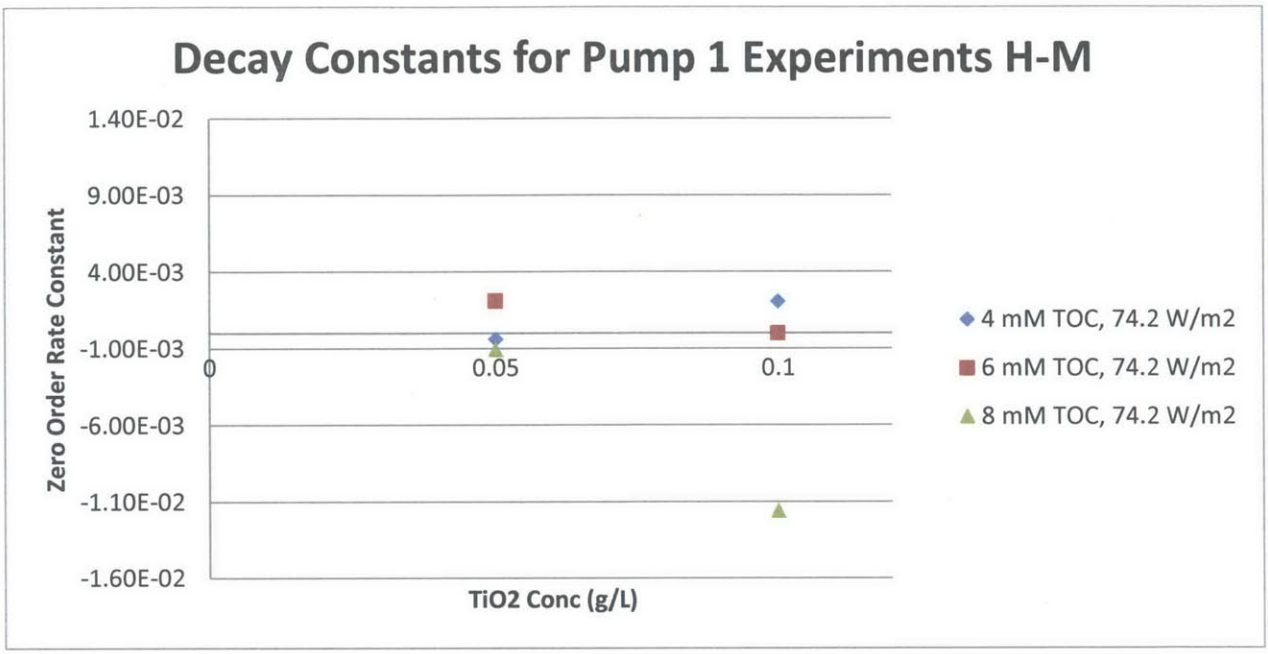

Figure 4.4 Effect of TiO_2 Concentration on TOC Oxidation Rate Constants

It is possible to conclude that the organic content was maintained at a constant level throughout the duration of all experiments. Even though methanol was being degraded to formaldehyde, formaldehyde appeared to not degrade any further. This forces one to consider other reaction parameters that govern the oxidation of these compounds and which had not been monitored during the tests. An analysis of the structure of the methanol and formaldehyde molecules as well as an investigation on acid-basic chemistry shed light to some possible kinetic factors that were missing in the design of the methanol experiments:

- One relevant element in photochemical reactions is the interaction between the oxidizing agent and the parts of the target molecule that are susceptible to become oxidized. In this sense, molecules with linear structures are much more difficult to attack than, for example, those with benzene rings. In a similar fashion, molecules with a large molecular surface have higher probabilities to interact with the oxidizing agents than those with a small area. Applying this knowledge to the study of methanol degradation, it is noted that the molecules of methanol and formaldehyde are poor candidates for photocatalytic treatment.

- In the reactions where methanol is degraded, the acidity/basicity of the environment in which the reactions occurring play a major role. Empirical data shows that, for this family of compounds, an acidic environment enhances the reaction rate, whereas a neutral pH diminishes the process speed. In the case of the methanol experiments conducted, the environment was governed by the use of neutral Milli-Q water, which decreased the effect of photocatalysis and prevented reducing TOC levels.

4.2.2 Cinnamic Acid Experiments

After utilizing the linearization methods described above to determine the order of the reactions occurring for the cinnamic acid tests (experiments N-X and Z), it was found that the data exhibited an order between first and second order kinetics. These 0^{th}, 1^{st}, and 2^{nd} order rate constants are located in Appendix F. For simplicity, the results will be analyzed based upon the calculated first order decay rate constants. Further, due to the monitoring of cinnamic acid concentration and TOC, the decay of both constituents will be analyzed. In general, it can be seen that the decay rate constants of cinnamic acid are higher than that of methanol (which can also be seen in Section 3 as faster overall decay). This is likely due to the fact that cinnamic acid has an aromatic ring, making it more susceptible to oxidation.

4.2.2.1 Contaminant Concentration

As previously stated, the first order decay constants were analyzed to determine any qualitative trends that arise when varying initial TOC concentration, catalyst concentration, as well as the radiation power. The results follow.

Effect of Initial Concentration

Conventional kinetics suggests that the first order decay rate constant decreases as the initial concentration of the reactant increases. Figure 4.5 displays the decay rate constants for Pump 1 Experiments N through V, all conducted at the same 74.2 W/m^2 radiation intensity. For these experiments, three different levels of initial contaminant concentration and catalyst concentrations were analyzed.

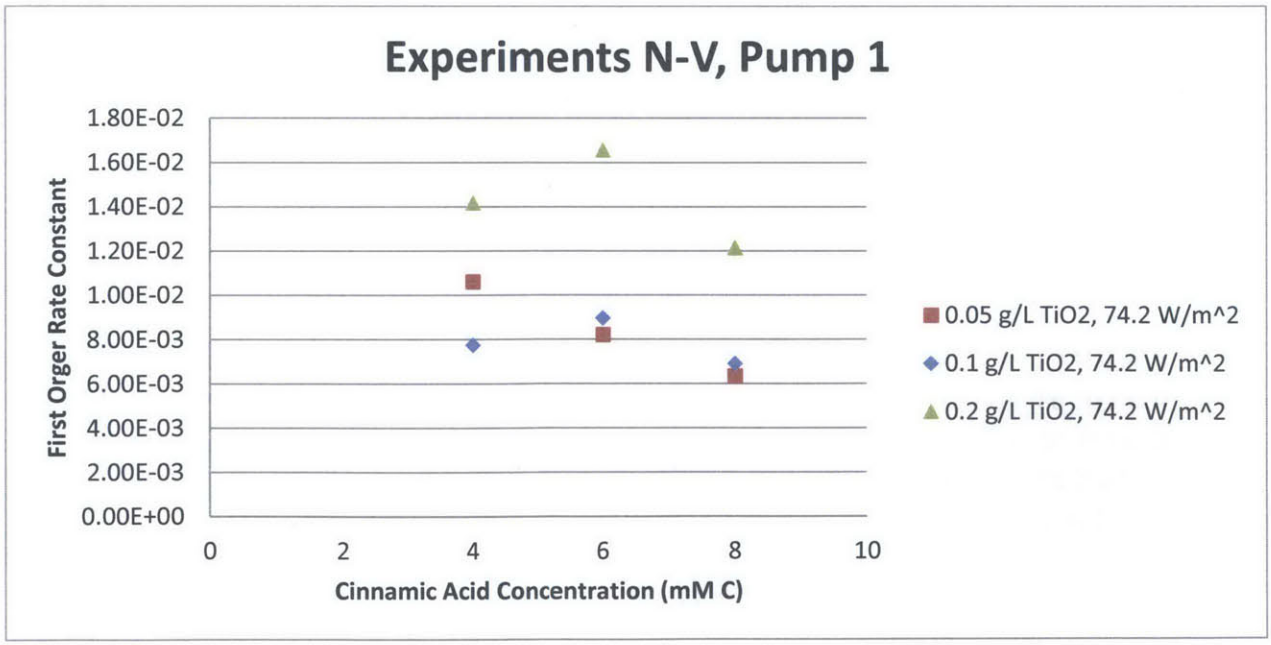

Figure 4.5 Effect of Initial Cinnamic Acid Concentration on Oxidation Rate Constants

From this chart it can be seen that the expected trend does occur for the three experiments with a catalyst concentration of 0.05 g/L. However, this trend of linearly declining decay constants with increasing initial concentration is not observed at the other two catalyst concentrations (0.1 and 0.2 g/L). As previously described, the rate of decay is expected to be directly related to the number of hydroxyl radicals and the number of available oxidation sites. For this reason, one might suspect that the tests at 0.05 g/L TiO_2 were initially hydroxyl radical limited at the low initial concentration of 4 mM. Thus, as the concentration was increased and the number of radicals remained constant, the decay constant was forced to decline. The fact that both the sets of experiments with 0.1 and 0.2 g/L TiO_2 experience a maximum value for the 6 mM initial concentration experiments can also be explained with the same concept. These series of tests suggest that at the low initial contaminant concentrations there was an excess of oxidizing radicals and the decay was therefore limited by the number of sites available for oxidation, which is related to concentration. Therefore, there is a threshold value up to which the concentration of contaminant can be increased while also increasing the decay rate constant; the 6 mM concentration appears to be within this threshold. Thus, due to the decrease in the rate constant from 6 mM to 8 mM, it can be surmised that 8 mM is above that threshold concentration, resulting in a surplus of sites to be oxidized in comparison to the amount of available hydroxyl radicals.

The same trends can be observed in the chart of decay constants for Pump 2 Experiments N through V.

Effect of Catalyst Concentration

Figure 4.6 displays the same data as Figure 4.5, but it has been transformed to more easily display the effects of changing the catalyst concentration.

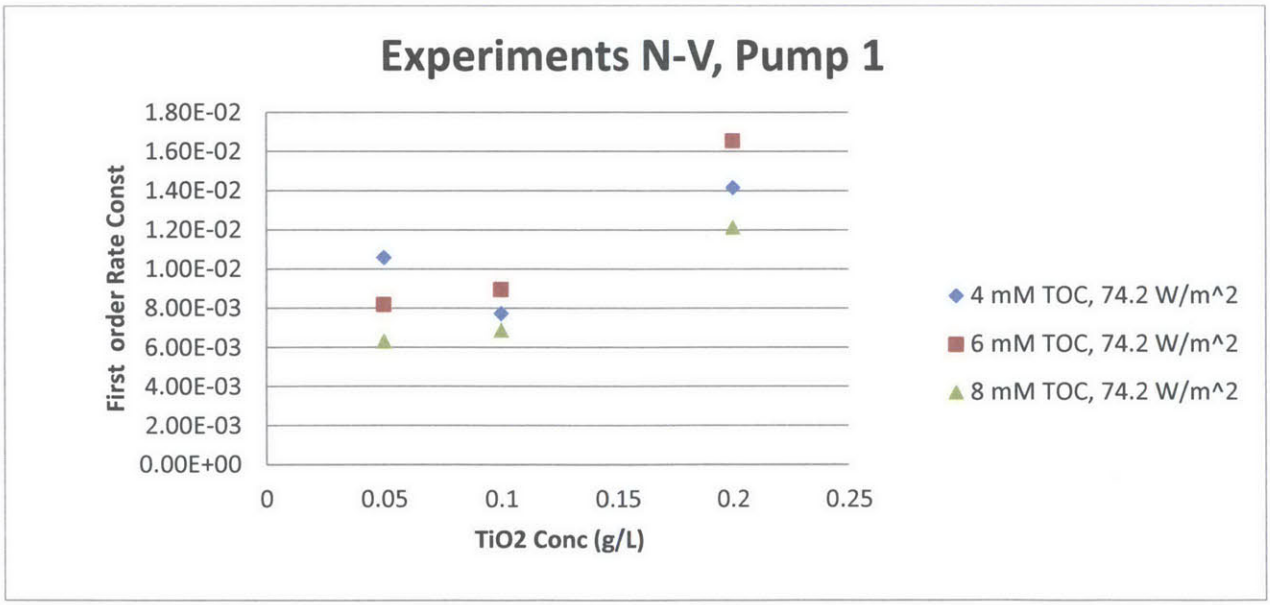

Figure 4.6 Effect of TiO_2 Concentration on Oxidation Rate Constants

The goal of this chart is to evaluate if there exists a general trend of increasing decay rate constant with increasing TiO_2 catalyst concentration. This behavior can once again be described by the concept of available hydroxyl radicals and available oxidation sites. Based on the data from Experiments N through V at constant 74.2 W/m^2 average radiation, this trend can be observed in the experiments with initial concentration of 6 and 8 mM of carbon. However, the set of experiments with an initial concentration of 4 mM does not display this trend, in fact it appears that there may actually be something inhibiting the decay of cinnamic acid at the 0.1 g/L catalyst concentration. Unfortunately, due to the fact that these experiments were not repeated, one might suspect that the results for Experiment Q are not representative of the actual decay behavior for these conditions.

Within Figure 4.6, one can also observe that doubling the catalyst concentration from 0.1 g/L to 0.2 g/L very nearly has a doubling effect on the decay rate constant. This might be expected when considering that doubling the number of oxidizing radicals, while maintaining the number of sites for oxidation, without surpassing some threshold value might lead to a doubling of the rate constant. However, the increase of catalyst concentration from 0.05 to 0.1 g/L does not exhibit this particular trend.

The decay constants for Pump 2 Experiments also showed the same trends as Pump 1.

Effect of Radiation Intensity

To more closely analyze the effect of varying radiation intensity, three experiments (W, X, and Z) were conducted in addition to the nine previously analyzed for initial concentration and catalyst concentration. These experiments were conducted by continuing to vary initial contaminant concentration, but maintaining a constant catalyst concentration of 0.2 g/L at a lower radiation intensity of 46.2 W/m^2.

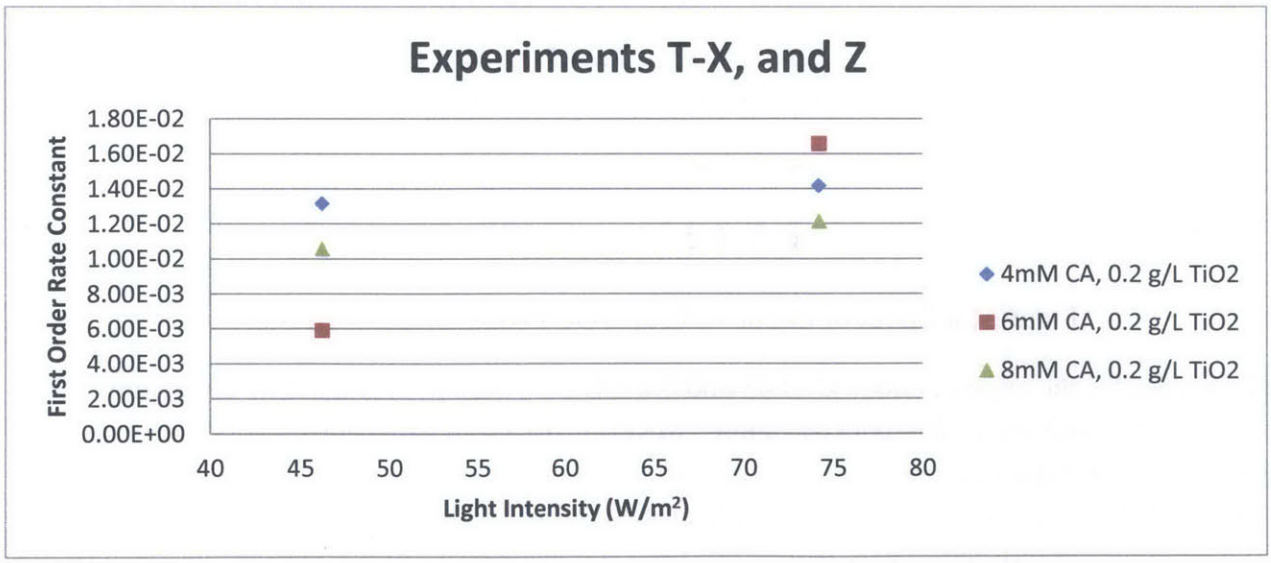

Figure 4.7 Effect of Light Intensity on Oxidation Rate Constants

As is expected for the behavior of photocatalytic oxidation, increasing radiation intensity will increase the rate of oxidation, provided there is a surplus of catalyst. Figure 4.7 shows exactly this trend. The local volumetric rate of photon absorption (LVRPA), to be used in the numerical model in Section 5, is used to quantify the number of photons entering the reactor. These values, computed by Dr. Ruud Timmers equate to 1.6×10^{-7} and 1.3×10^{-7} moles per liter per second, for the 74.2 and 46.2 W/m^2 intensities respectively (both at a catalyst concentration of 0.2 g/L). However, a simple qualitative analysis will show that this increase in LVPRA does not result in a directly proportional increase in the decay rate constant.

4.2.2.2 TOC Concentration

Since the goal of photocatalytic oxidation is to mineralize the organic contaminants, monitoring the rate of decay of the total organic carbon in essential to determining the overall effectiveness of the treatment method.

Effect of Initial Concentration

For the same reasons described above, one would expect that as the concentration of molecules available for oxidation increases (while hydroxyl radical concentration remains constant) the decay rate constant will decline. Figure 4.8 generally displays this behavior.

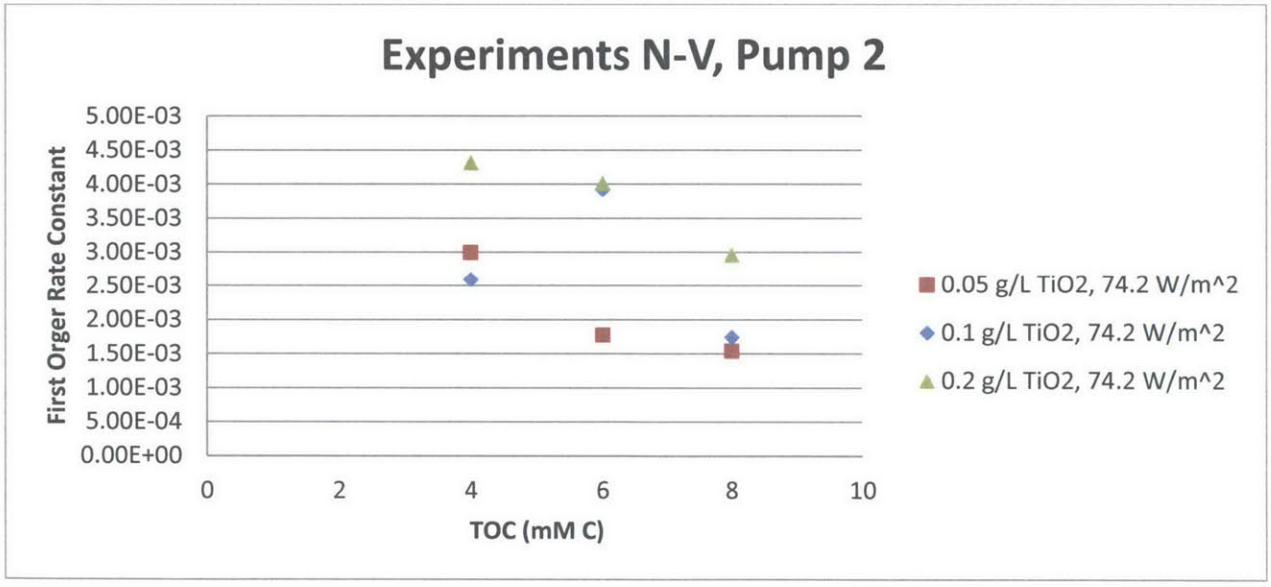

Figure 4.8 Effect of Initial TOC on TOC Oxidation Rate Constants

The results for the experiments with 0.05 and 0.2 g/L TiO_2 display this trend of decreasing decay rate constant with increasing concentration. However, the set of experiments conducted with 0.1 g/L of catalyst displays an increase in decay rate constant when increasing the initial TOC from 4 mM to 6 mM. The irregular behavior of Experiment P does not agree with typical photocatalytic convention, therefore more tests would need to be conducted to prove that this result was not erroneous.

The results for Pump 1 Experiments N through V do not appear to be consistent with these trends. Although there is a decline in rate constants between 4 mM and 8 mM, the values at 6 mM serve as minima for the 0.1 and 0.2 g/L catalyst concentration, while producing a maximum value for the 0.05 g/L TiO_2 concentration.

Effect of Catalyst Concentration

The same data displayed in the previous figure has been reconfigured into Figure 4.9 to better display the effects of varying the catalyst concentration.

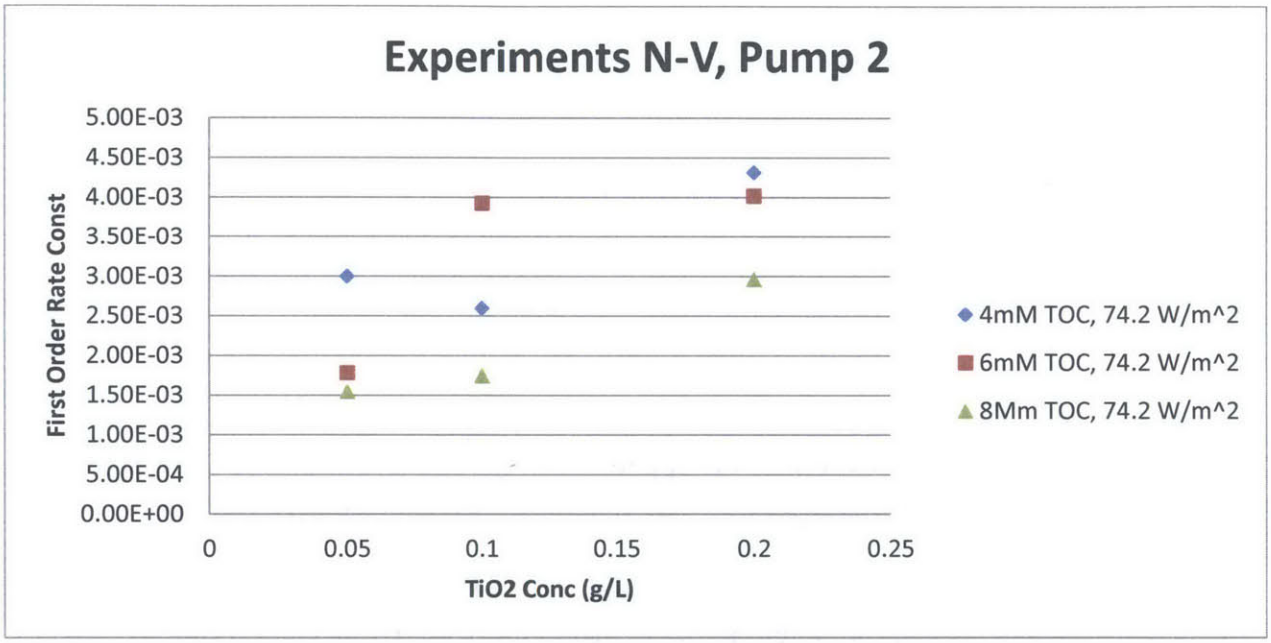

Figure 4.9 Effect of TiO_2 Concentration on TOC Oxidation Rate Constants

As per usual, upon inspection of Figure 4.9, when solely comparing the decay rate constants at 0.05 and 0.2 g/L there is a clear increase in the rate of decay of organic carbon for all initial concentrations. However, at a catalyst concentration of 0.1 g/L, again there is the appearance of a minimum value for the 4 mM initial concentration Experiment N.

Effect of Radiation Intensity

For the same reasons as previously described, one should expect to see an increase in the decay rate constants for the decay of TOC as radiation intensity increases. Figure 4.10 displays the results for Pump 1 Experiments T through X and Z, where radiation is the independent variable of concern.

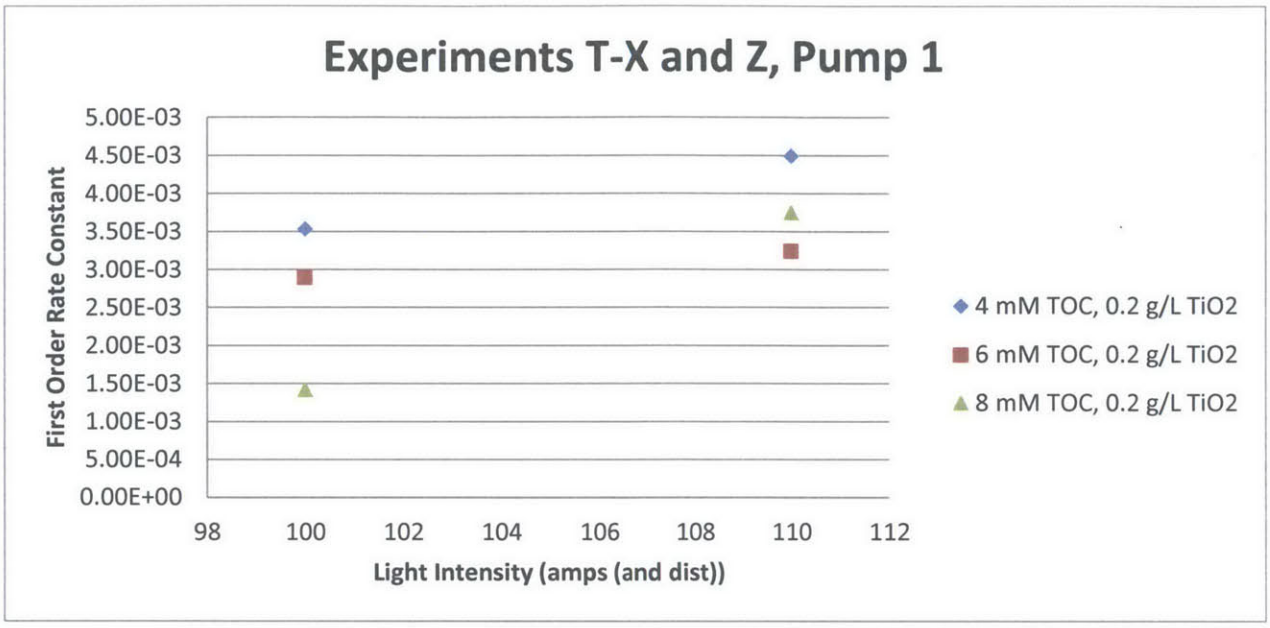

Figure 4.10 Effect of Light Intensity on TOC Oxidation Rate Constants

For each of the initial concentrations tested, it can be seen that the decay rate constants always increase as radiation intensity increases. However, the degree to which the rate constant increases is not the same when comparing the different initial concentrations. It is clear that the decay rate constant of the 8 mM initial concentration experiments increases by a greater degree, than the 4 and 6 mM initial concentrations. This can also be explained by the concept of number of hydroxyl radicals compared to number of sites to be oxidized. At 46.2 W/m^2 there are far too many sites to be oxidized for the number of radicals available, but at 74.2 W/m^2 there is a surplus, allowing the rate constant to be similar to that of the lower initial concentrations.

5 ASSESSMENT OF A NUMERICAL MODEL

The ability to apply photocatalysis to large scale wastewater treatment application depends on the ability of scientists and engineers to effectively predict the behavior of the reaction kinetics that are occurring. In order to do this, a numerical model must be developed to not only predict the decay behavior of a single contaminant, but many. The following chapter will discuss a mathematical model developed by Dr. Javier Marugán, as well as the process and results of numerically fitting this model to the experimental data.

5.1 APPROACH

5.1.1 Developing the Kinetic Model

Section 5.1.1 is a simplified explanation of the process through which Dr. Marugán developed this numerical model for the decay of organic compounds within the photoreactor. The more detailed process, provided directly from a personal correspondence with Dr. Marugán is located in Appendix G.

As mentioned within the introduction, there are a number of reactions that occur within photocatalysis that eventually result in the oxidation of organic molecules. The first reaction to occur is the activation of the TiO_2 catalyst. In this reaction, Step 1 in Table 5.1, the photons (hv) interact with the catalyst to form electrons (e^-) and holes (h^+). Some of these electron hole pairs can recombine, producing heat (Step 2). However, some of the remaining electrons can react with dissolved oxygen to produce O_2^- in a process called electron trapping (Step 3). Similarly, the holes that have not been lost to recombination can react with water, splitting the molecule into hydrogen ions and hydroxyl radicals in a process called hole trapping (Step 4). Finally, Step 5, these hydroxyl radicals can attack the organic compounds, oxidizing them. This process can be further divided into a number of reactions, as many organic molecules require many oxidation reactions before then can be mineralized into carbon dioxide and water. This approach will look at contaminant [A] (methanol or cinnamic acid) and will group all oxidized intermediate compounds into contaminant [B].

Table 5.1 Reaction Processes Required for Photocatalysis

	Step	Reaction
1	Activation	$TiO_2 + hv \rightarrow TiO_2 + e^- + h^+$
2	Recombination	$e^- + h^+ \rightarrow$ heat
3	Electron Trapping	$e^- + O_2 \rightarrow \bullet O_2^-$
4	Hole Trapping	$h^+ + H_2O \rightarrow \bullet OH + h^+$
5	Hydroxyl Attack	$A + n \bullet OH \rightarrow B$ $B + n \bullet OH \rightarrow \ldots \rightarrow CO_2 + H_2O$

By then applying the micro steady state approximation for the concentration of electrons, holes and hydroxyl radicals, an expression for the concentration of holes was developed. Additionally, the volumetric rate of electron/hole generation can be given by the local volumetric rate of photon absorption (LVRPA, e^a) and the primary quantum yield averaged over the wavelength range, both of which can be determined from the solar radiation measurements. These equations can then be developed into an equation for the hydroxyl radical concentration as a function of the concentrations of A and B, as well as the LVRPA and three constant coefficients. Given that the rate of decay of A is defined as $r_A = -k_5[A][\bullet OH]^n$ and the rate for the decay of B is defined as $r_B = k_5[A][\bullet OH]^n - k_6[B][\bullet OH]^n$, the following volumetric rate expressions can be derived.

$$r_A = -\alpha_1 \frac{[A]}{[A]+\alpha_3[B]}\left(-1+\sqrt{1+\alpha_2 e^a}\right) \qquad \text{Eq. 5-1}$$

$$r_B = \alpha_1 \frac{[A]-\alpha_3[B]}{[A]+\alpha_3[B]}\left(-1+\sqrt{1+\alpha_2 e^a}\right) \qquad \text{Eq. 5-2}$$

In these equations, α_1, α_2, α_3, and e^a are constant values for a given experiment, leaving the decay rates of A and B as functions of A and B. Due to the fact that the measurements for A and B were from samples that were being taken from the reservoir tanks, these rate expressions must be integrated over the total volume (assuming fully mixed conditions). Thus the following expressions for the decay of A and B are:

$$\frac{d[A]}{dt} = -\frac{V_r}{V_t}\alpha_1 \frac{[A]}{[A]+\alpha_3[B]}\left(-1+\langle\sqrt{1+\alpha_2 e^a}\rangle_{Vr}\right) \qquad \text{Eq. 5-3}$$

$$\frac{d[B]}{dt} = \frac{V_r}{V_t}\alpha_1 \frac{[A]-\alpha_3[B]}{[A]+\alpha_3[B]}\left(-1+\langle\sqrt{1+\alpha_2 e^a}\rangle_{Vr}\right) \qquad \text{Eq. 5-4}$$

The term V_r represents the irradiated volume of the reactor and the V_t term represents the total reactor volume (including the reservoir). The ratio of V_r/V_t allows for these rate expressions to be adapted to reactors of varying size. The α_1 term, as defined in Appendix G, is said to be dependent on the dissolved oxygen concentration, electron and hole trapping rate constants, and the recombination rate constant. One might expect that the values of α_1 might remain constant for a given set of experiments at the same LVRPA. The α_2 term, by definition, is also a function of the same parameters as α_1, but is also dependent upon the primary quantum yield averaged over the wavelength. This term is also expected to remain constant for any experiments at the same light intensity. The value of α_3 is defined as the ratio of the decay rate constant of B to the decay rate constant of A. Here one would suspect that this value will only remain constant for experiments of the same initial concentration of the contaminant in question.

5.1.2 Fitting the Kinetic Model

In order to attempt to fit the decay expressions to the experimental data, the number of unknown constants (α_1, α_2, α_3) had to be reduced, transforming the decay expressions above into:

$$\frac{d[A]}{dt} = \frac{-a[A]}{[A]+b[B]} \qquad \text{Eq. 5-4}$$

$$\frac{d[B]}{dt} = \frac{a([A]+b[B])}{[A]+b[B]} \qquad \text{Eq. 5-5}$$

where,

$$a = \frac{V_r}{V_t}\alpha_1\left(-1 + \langle\sqrt{1+\alpha_2 e^a}\rangle_{Vr}\right) \qquad \text{Eq. 5-6}$$

$$b = \alpha_3 \qquad \text{Eq. 5-7}$$

Then, using the Euler Method of integration, it was possible to develop equations for the concentrations of A and B at time t = n+1, such as:

$$[A]^{n+1} = [A]^n + \Delta t \times \left(\frac{-a[A]^n}{[A]^n+b[B]^n}\right) \qquad \text{Eq. 5-8}$$

$$[B]^{n+1} = [B]^n + \Delta t \times \left(\frac{-a([A]^n-b[B]^n)}{[A]^n+b[B]^n}\right) \qquad \text{Eq. 5-9}$$

Choosing a time step of ten seconds and the initial concentrations of A and B at time zero, it was possible to choose values for a and b to reproduce plots for the modeled decay of A and B. In order to arrive at this time step value, a balance needed to be found between the accuracy and available computational resources. The choice of a time step of 10 seconds was based on a balance between accuracy and computational time. A time step less than ten seconds would not have produced much more accurate results.

5.1.2.1 Determining Optimal Fit Constants a and b

Fitting the numerical model to the experimental data entailed finding optimal values for the constants a and b. To quantify the degree to which the numerical model fits the experimental data, a measurement of error was developed. At each of the times where experimental data exists, the error was quantified as the square of the difference between the experimental value and the model value. These values were then averaged against the number of samples, resulting in the error for contaminant A. The same was then done for B.

$$Error\ A = \frac{\sum_{i=0}^{n}\left([A]_{i,measured}-[A]_{i,projected}\right)^2}{n} \qquad \text{Eq. 5-10}$$

$$Error\ B = \frac{\sum_{i=0}^{n}([B]_{i,measured} - [B]_{i,projected})^2}{n} \quad \text{Eq. 5-11}$$

In order to find the optimal values of a and b for which the numerical model produces the least amount of error, the error values for A and B were summed.

$$Error\ A + B = ([A]_{measured} - [A]_{projected})^2 + ([B]_{measured} - [B]_{projected})^2 \quad \text{Eq. 5-12}$$

This sum was then used in a data table, which is a function in Microsoft Excel that allows the user to choose a range of values of two independent variables to produce a number of results. This function was used to select ranges of a and b, calculating the combined error that would then result from the fit of A and B. As the minimum value of this combined error would signify the optimal combination of a and b, a conditional format was set up to highlight the lowest value of combined error within the table. A truncated example of this table used in Experiment N Pump 2 is shown as Table 5.2.

Table 5.2 Data Table Function for Optimization of a and b

		a							
Fit errorA+ errorB	0.01739	0	0.00044	0.00045	0.00046	0.00047	0.00048	0.00049	0.0005
b	1.504	0.14978	0.01805	0.01779	0.01761	0.01748	0.01741	0.01739	0.01743
	1.505	0.14978	0.01805	0.01780	0.01761	0.01748	0.01741	0.01739	0.01743
	1.506	0.14978	0.01805	0.01780	0.01761	0.01748	0.01741	0.01739	0.01743
	1.507	0.14978	0.01805	0.01780	0.01761	0.01748	0.01741	0.01739	0.01743
	1.508	0.14978	0.01805	0.01780	0.01761	0.01748	0.01741	0.01739	0.01743
	1.509	0.14978	0.01805	0.01780	0.01761	0.01748	0.01741	0.01739	0.01743
	1.51	0.14978	0.01806	0.01780	0.01761	0.01748	0.01741	0.01739	0.01743
	1.511	0.14978	0.01806	0.01780	0.01761	0.01748	0.01741	0.01739	0.01743
	1.512	0.14978	0.0181	0.01781	0.01761	0.01748	0.01741	0.01739	0.01743

With the intention of determining optimal values for a and b, the range for a and b within the data table was first chosen to be large, and then iterated upon multiple times to find precise values. Often the values for a were found down to the nearest 10^{-5} and b values were found to the nearest 10^{-3}.

5.2 RESULTS & CONCLUSIONS

This section applies the proposed model to the experimental data and also analyzes the fitted parameters a and b for any possible trends. The error bars shown for the concentration measurements in the following charts are based upon the initial concentration error for each measurement, as previously described in Section

5.2.1 Methanol Fitted Model

Following the procedure indicated on Section 5.1.2.1, a series of simulations were computed varying the a and b parameters to find an optimal fit. Using the numerical model, the heuristic method aimed to minimize the error between the projected values for the methanol system and the experimental data sets.

Using the generalized hydroxyl radical attack system on Table 5.1, it is possible to describe the methanol oxidation reactions that take place as a result of photocatalysis. In the methanol system, the [A] values are defined by the methanol content, [B] values are represented by formaldehyde (the only intermediate compound that was found in the experiments), and the [A] + [B] values are the measured TOC. For the analysis, each concentration data set was normalized to the initial target TOC.

The graphs presented in Figure 5.1 and 5.2 show this work for Experiment L data sets. It is relevant to recall that Experiment L was conducted for a target initial methanol equivalent to 8 mM of TOC, 0.05 g/L of titanium dioxide catalyst and radiation flux powered at 74.2 W/m^2. Figure 5.1 shows the measured and projected values for Pump 1, and Figure 5.2 shows the same for Pump 2. The minimized errors were 1.2E-4 and 5.1E-6 for each test, respectively; using a and b values of 3.60E-4 with 1.02 and 2.14E-4 with 0.28, accordingly.

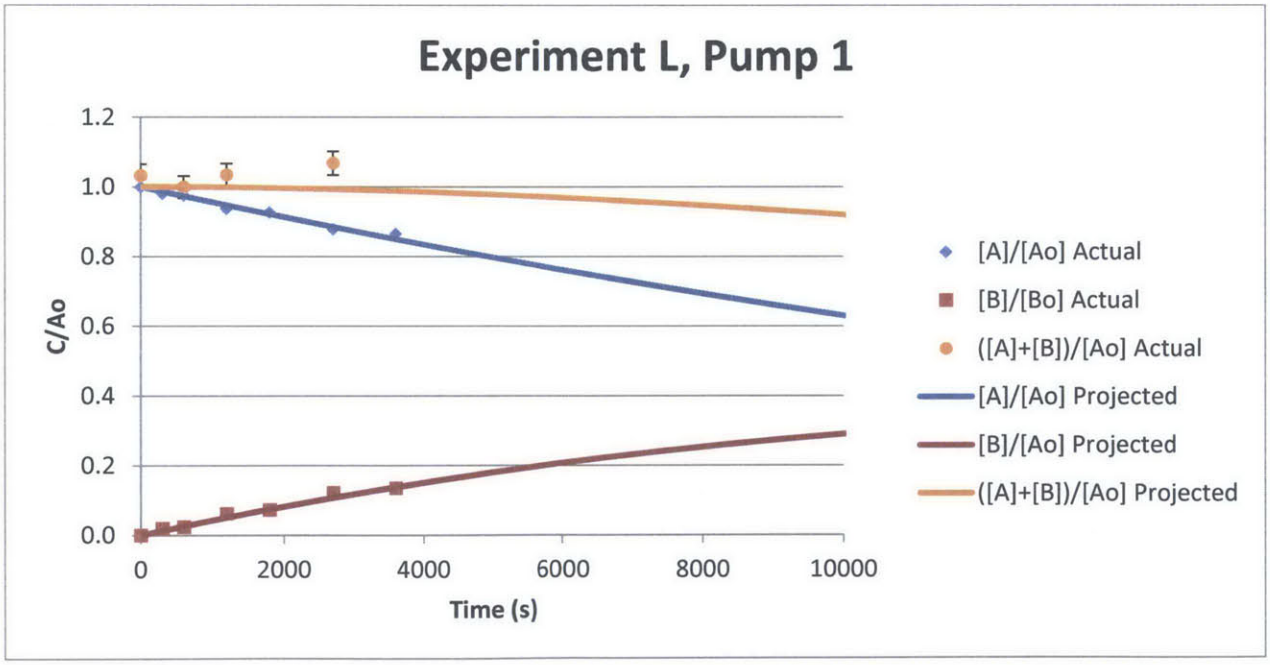

Figure 5.1 Experiment L Pump 1, Actual and Projected Values (a = 3.60E-4; b = 1.02)

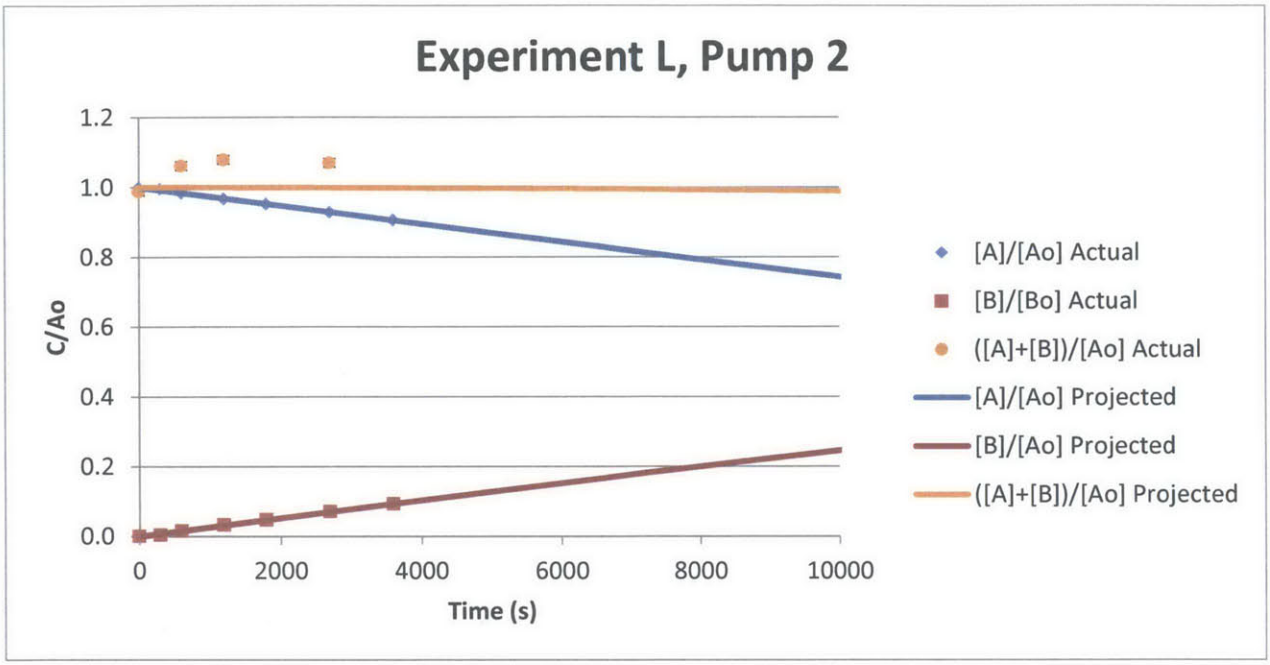

Figure 5.2 Experiment L Pump 2, Actual and Projected Values (a = 2.14E-4; b = 0.28)

When analyzing these graphs, it is noticeable how accurate this model seems to be, as projected values closely predict the behavior observed on the empirical data gathered for the system. It is also pertinent to note that the predicted behavior is consistent with an observation stated in Section 4 of this document: total organic carbon is expected to decrease over time at a very slow rate, converting only to formaldehyde. It is also possible to conclude that (not altering pH conditions), residence times to remove methanol would go over 3 hours (much more than the time assigned for each individual experimentation). The charts displaying the model curves and experimental data for the other methanol experiments are included in Appendix H.

5.2.1.1 Factors Influencing a and b

Given the difficulties to remove methanol by photocatalytic treatment (at least at a neutral pH as during the experiments showed in this research), it is of interest to understand whether or not this factor has an impact on the model parameters a and b. Just as well, because of the nature of photocatalysis, it is relevant to understand the impact of LVRPA on the parameters of the numerical model.

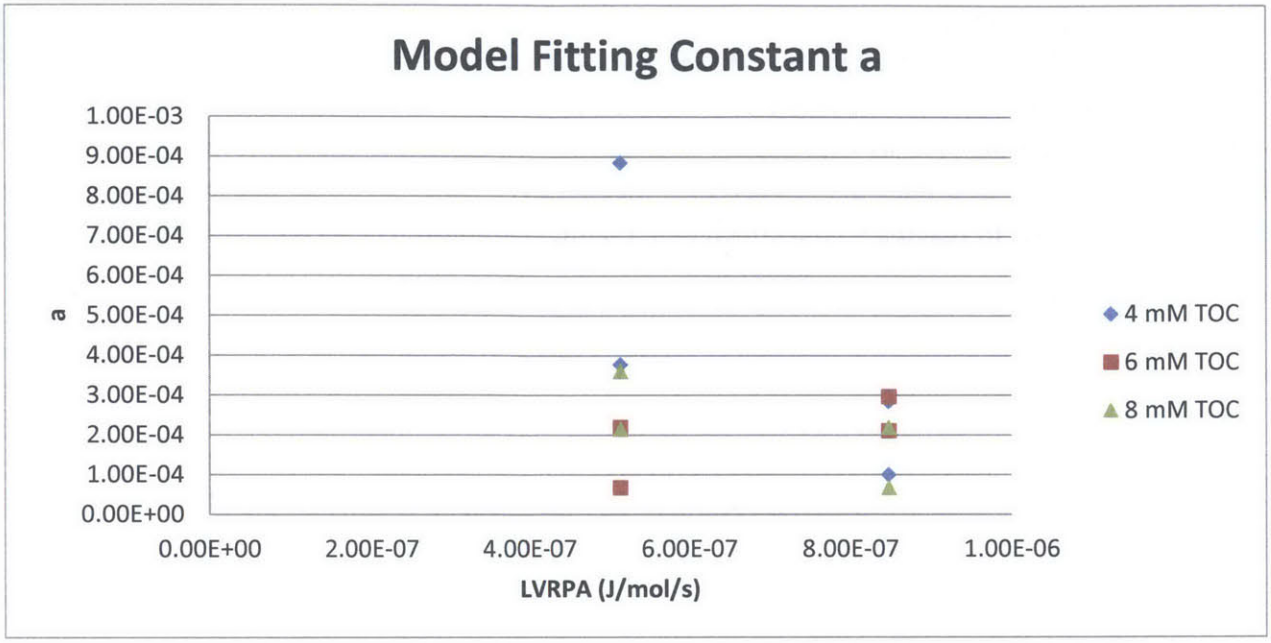

Figure 5.3 Effect of LVRPA on Values of Fitting Constant a

A plot of the a values versus LVRPA, shown on Figure 5.3 above, points to no clear relationship between these two factors.

On the other hand, when analyzing the dependency of the a constant to the initial pollutant concentration, two out of the three times there appears to be a slight correlation. Considering this set of data is not as large as would be desirable, further experimentation is required to either confirm or rule out the relationship.

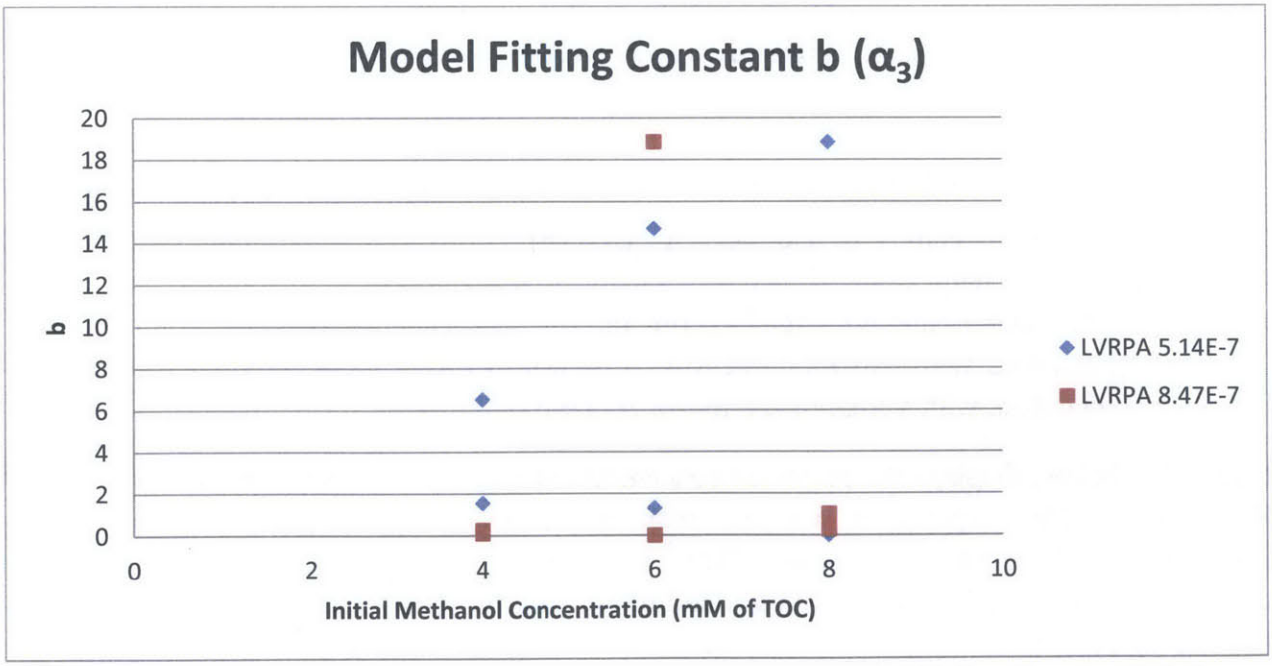

Figure 5.4 Effect of Initial Methanol Concentration on Values of Fitting Constant b (α_3)

For the fitting constant b (α_3), which relates the decay rate constant of B to the decay rate constant of A, Figure 5.4 displays two disagreeing trends: at LVRPA 8.47E-7, b seems to be completely independent from the initial methanol content; and at LVRPA 5.14E-7, there appears to be a large variation of b as the molar concentration of the pollutant increases. Due to this divergent behavior, this analysis is deemed inconclusive, and there is need to repeat the experiments in order to reach a sound conclusion on this relationship or lack thereof.

5.2.2 Cinnamic Acid

After modifying the parameters (a and b) to produce the optimal fit for the proposed model experimental data sets, the model output was plotted against the experimental data.

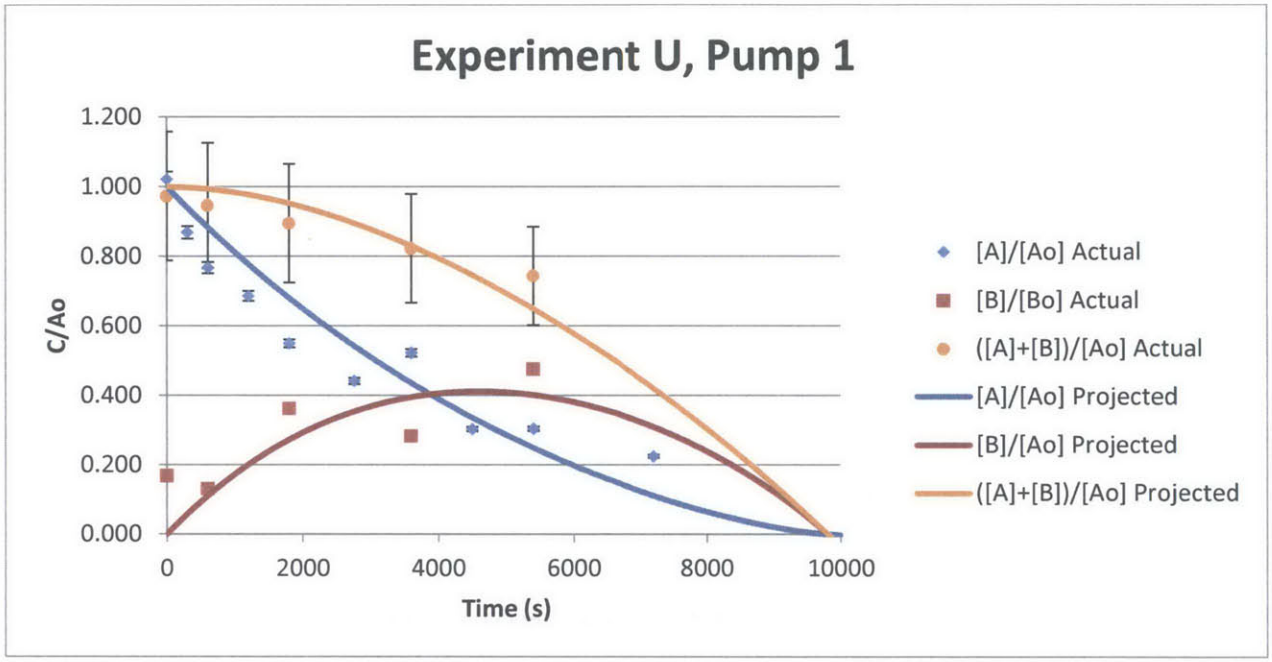

Figure 5.5 Experiment U Pump 1, Actual and Projected Values (a = 0.00163; b = 0.792)

The projected values for the concentration of organic carbon contributed by cinnamic acid, [A]; the intermediate compounds, [B]; and the TOC, [A]+[B] (normalized to the initial target TOC); for Experiment U Pump 1 are shown for values of a and b equal to 1.63E-3 and 0.792 respectively. The initial conditions for Experiment U include an initial concentration of 8 mM, 0.2g/L TiO_2, and 46.2 W/m^2 radiation intensity. It is clear that these values produce a good fit to the experimental data, with a combined error for A and B of 0.019.

Figure 5.6, below, displays the projected concentrations for [A], [B], and TOC for Experiment W, Pump 1. This experiment was run with an initial concentration of 4 mM, catalyst concentration of 0.2 g/L, and at a 46.2 W/m^2 radiation intensity. The values for a and b were determined to be 1.03E-3 and 0.584 for a and b respectively, producing a combined fit error of 0.0154. In particular, the predicted behavior of the organic carbon due to the intermediate compounds is nearly a perfect match to the experimental data.

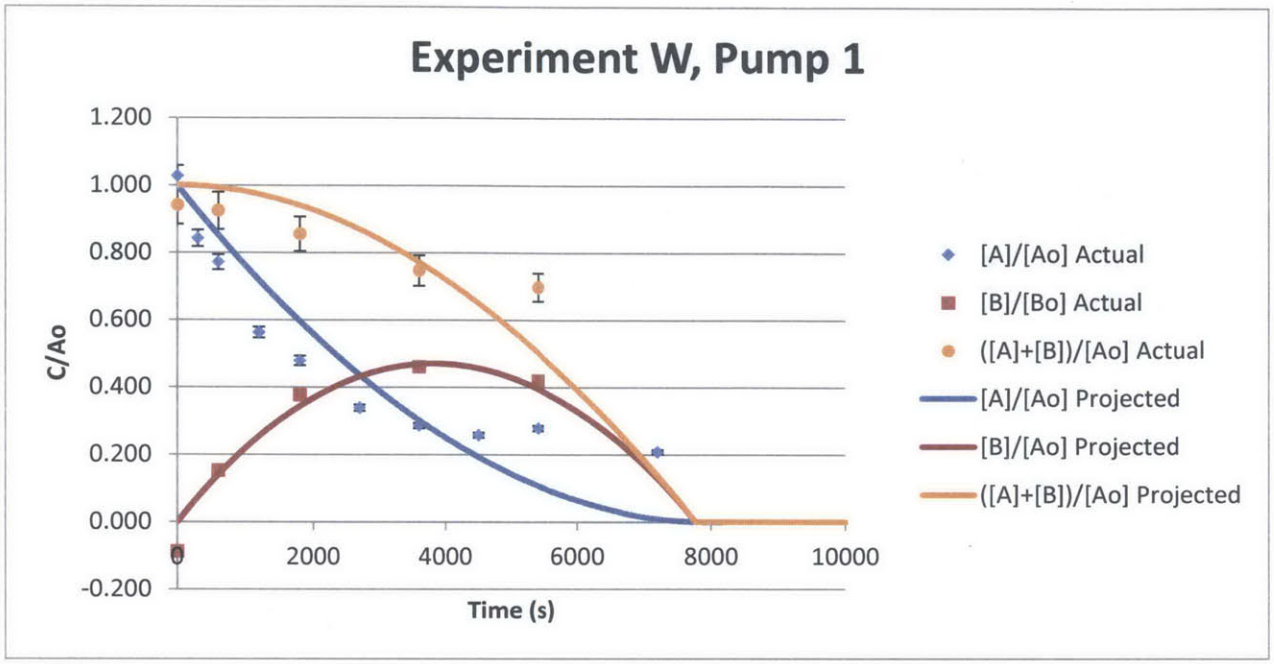

Figure 5.6 Experiment W Pump 1, Actual and Projected Values (a = 0.00103; b = 0.584)

Although these models appear to fit the experimental data quite well, there are some fundamental differences that occur for nearly all of the fitting attempts. For example, as seen in Figures 5.5 and 5.6, the experimental decay of the cinnamic acid initially occurs at a rate faster than the model predicts, but then begins to slow to a rate much less than is predicted. Similarly, the experimental TOC results typically appear to exhibit a linear decay, while the model predicts a behavior in which the decay is continually increasing (as the TOC decreases). For this reason, the model predicts that all of the organic carbon will become mineralized in a period of time that is likely significantly less than it would take in reality. The charts displaying the model curves for each of the experiments are included in Appendix I.

5.2.2.1 Factors Influencing a and b

Although the models show complete removal much sooner than is likely to be the case, it is important to note how the values of a and b affect this time. The higher values of a and b for Experiment U show that they are related to higher initial concentration and radiation intensity, causing the time of complete removal for Experiment U to be much later than the time predicted for Experiment W. This shows that the initial concentration has a larger impact upon the removal than increasing the radiation intensity. Figure 5.7 shows the model fitting constant a plotted versus the LVRPA.

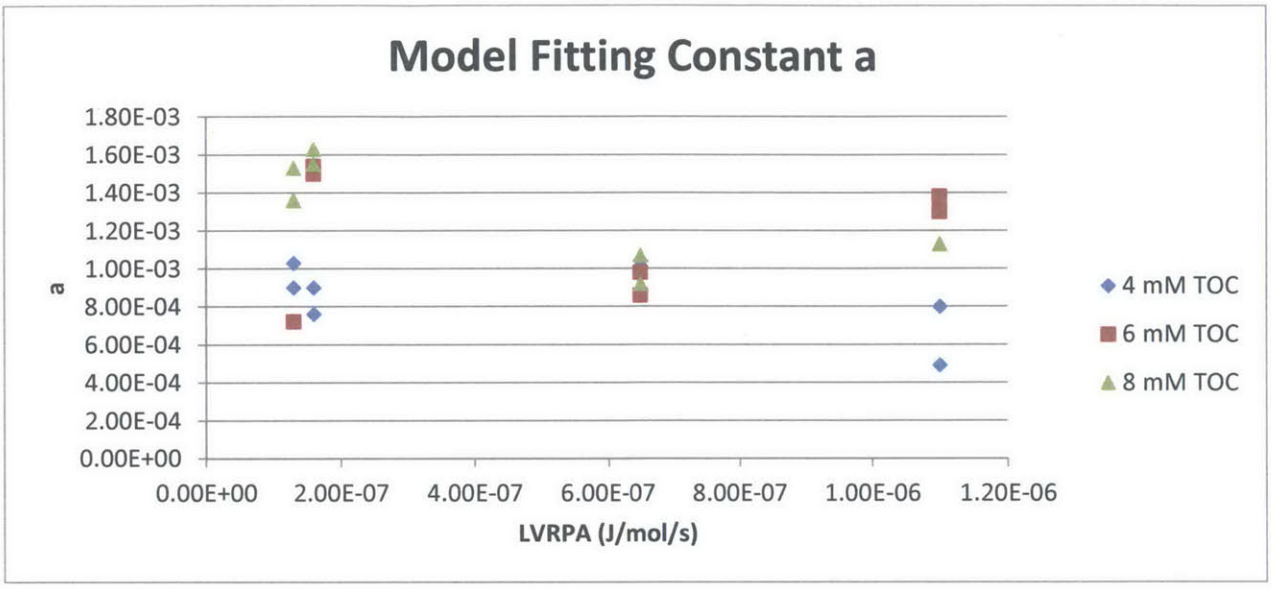

Figure 5.7 Effect of LVRPA on Values of Fitting Constant a

From Figure 5.7, it is clear that there is no obvious correlation between the LVRPA and the value of a. However, one can observe what appears to be a slight correlation between a and the initial concentration of TOC from cinnamic acid.

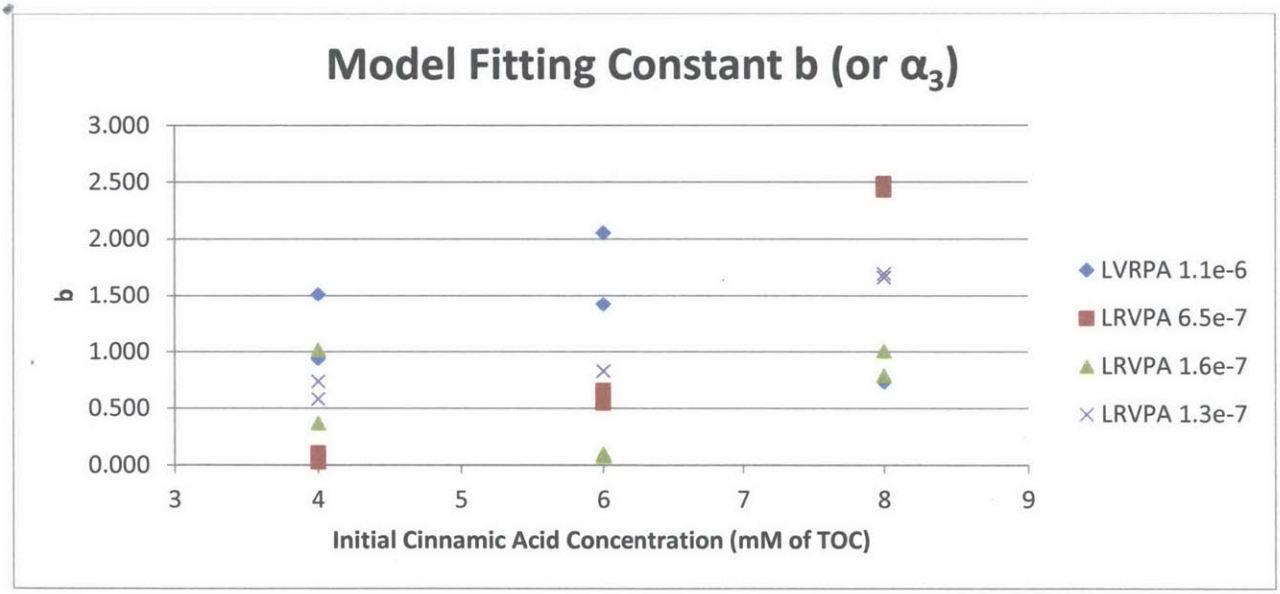

Figure 5.8 Effect of Initial Cinnamic Acid Concentration on Values of Fitting Constant b (α_3)

Figure 5.8 displays the variation of the fitting constant b at different initial contaminant concentrations as well as at different values for the LRVPA. From this chart, one may observe that the values for b show a tendency to increase as the initial TOC concentration increases. This trend can be described with the previously mentioned concept of the decay rate constants, for [A] and [B], being related to the initial TOC concentration. Thus, as initial concentration increases, the decay rate constant for [A] decreases, causing b (α_3) to increase.

6 SUMMARY, CONCLUSIONS AND RECOMMENDATIONS

6.1 SUMMARY AND CONCLUSIONS

Advanced oxidation processes have recently become an important tool to deal with emerging pollutants which have been found to be recalcitrant to traditional wastewater treatment processes. Photocatalytic oxidation is a novel form of AOP that is rapidly gaining interest in the field of water treatment. This technique utilizes a semiconductor catalyst, which upon interaction with light produces hydroxyl radicals that efficiently oxidize these organic emerging pollutants.

For this study, 28 experiments were conducted with a photocatalytic reactor located at Universidad Rey Juan Carlos in Madrid to explore the degradation/inactivation of four model pollutants. *Escherichia coli*, methanol, cinnamic acid, and sulfamethoxazole were all tested under conditions of varying initial concentration, catalyst concentration, and radiation intensity to identify how these variables affect the rate of decay of each contaminant.

Overall, the results from these experiments suggest that photocatalysis is capable of oxidizing these pollutants to varying degrees. The single experiment testing for the inactivation of *E. coli* under natural light conditions displays a five log maximum removal after 45 minutes. This suggests that photocatalysis, even with natural light, is very effective in the inactivation of *E. coli*. The experiments testing the behavior of methanol exhibit some degradation, though much less than initially expected. This behavior is speculated to be a result of the molecular structure of methanol, as well as an unfavorable pH environment. In contrast, results from cinnamic acid experimentation show considerable removal of both cinnamic acid and total organic carbon. This is likely due to the fact that cinnamic acid contains a number of sites for oxidation, including an aromatic ring that is particularly susceptible to photo-oxidation. Finally, the two experiments testing the removal of sulfamethoxazole display complete removal under artificial light conditions (Experiment AA) and reasonable removal with natural light (Experiment AB). The lower removal in Experiment AB might be explained by the fact that this experiment contained 14 other complex organic compounds in addition to lower radiation intensity, resulting in competition for fewer hydroxyl radicals.

A more complete exploration was conducted to determine the decay rate constants for each of the methanol and cinnamic acid experiments. The decay of methanol was found to closely follow zero order degradation kinetics. While the decay of cinnamic acid did not exactly follow first or second order kinetics, an analysis was conducted using the first order decay constants. These rate constants were analyzed to find any correlation between the decay rate constant and the experimental conditions. The experimental data consistently showed that both titanium dioxide concentration and radiation intensity have an effect on the decay rate constants. However, only cinnamic acid experiments appear to show a relationship between the reaction rate constant and the initial concentration. Predicting these decay rate constants is important for applying this technology to a larger scale.

The application of photocatalytic oxidation to the field scale requires the anticipation of reaction kinetic behavior as well as other field parameters. The development of a more complex kinetic model, such as the one described in Section 5, is an important step towards formulating a comprehensive kinetic model. The preliminary results of this model are promising because of its ability to closely represent the behavior of two dissimilar organic chemical groups (alcohols and carboxylic acids).

In order to fit this model to the experimental data, the model fitting parameters a and b were created. However, this simplification does not allow identification of the specific values of α_1 and α_2, which are embedded in the parameter a. The experimental data did not show any trends for a, despite the definition suggesting a relationship with the LRVPA. Nonetheless, the observed trends point to a relation between b (α_3) and initial carbon content, which was expected. Thus, with more experimental data, it may be possible to develop an equation to predict values of a and b given specific initial conditions. If definitive relationships were also found for α_1 and α_2, it may be possible to simulate the degradation behavior of any compound. Being able to predict the behavior of any compound would allow for the scaling up of this technology.

The data and analysis conducted for this research suggests that photocatalytic oxidation can be a viable option for advanced oxidation processes. Further research in the field of photocatalytic reaction kinetics is needed to fully understand the oxidation processes. Moreover, these findings must then be coupled with the development of solar radiation and hydraulic models to produce a comprehensive picture of large scale application of photocatalytic oxidation.

6.2 RECOMMENDATIONS

A continuation of this study might consider the following opportunities to reinforce (or negate) some of the conclusions presented previously.

Future research could benefit from the repetition of some of the experiments conducted within this study, as this would increase the reliability of results.

Additionally, further exploration of other combinations of experimental conditions will improve the understanding of the reaction kinetics of photocatalytic oxidation.

A more intensive study of emerging pollutants is required to be able to model the decay of these complex compounds.

The mathematical model should be refined to better represent the experimental results. Although the model predicts the overall decay fairly well, some adjustments are required to better represent the initial and final decay rates.

A mathematical model should be developed to forecast the values of a and b, based on conceptual and observed dependencies of these fitting parameters. The model could be applied to particular initial conditions and tested at a lab-scale.

REFERENCE MATERIAL

Cited

Agulló-Barceló, M. I. P.-L. (n.d.). Solar Advanced Oxidation Processes as disinfection tertiary treatments for real wastewater: Implications for water reclamation. Applied Catalysis B: Environmental, s 136–137, 341–350. doi:10.1016/j.apcatb.2013.01.069

American Water Works Association (2007). Water resources impact: Contaminants of emerging concern. May 2007, Vol. 9, No. 3

Bennett, D. (March 20, 2014). Researcher explores the use of novel nanomaterials to combat contaminants in water. Retrieved from http://phys.org/news/2014-03-explores-nanomaterials-combat-contaminants.html

Braslavsky, S. E., Braun, A. M. Cassani, A. E., Emeline, A. V., Litter, M. I., Palmisano, L., Parmon, V. N., Serpone, N. (2011). Glossary of terms used in photocatalysis and radiation catalysis (IUPAC Recommendations 2011). Pure Appl. Chem. Vol 84, No. 4 pp 931-1014

Caslake, L. F., Connolly, D. J., Menon, V., Duncanson, C. M., Rojas, R., & Tavakoli, J. (2004). Disinfection of Contaminated Water by Using Solar Irradiation. Applied and Environmental Microbiology, 70(2), 1145–1150. doi:10.1128/AEM.70.2.1145-1150.2004

Dillert, R., Vollmer, S., Schober, M., Theurich, J., Bahnemann, D., Arntz, H.-J., ... Sager, G. (1999). Chemical Engineering & Technology. Vol 22 No 11 pp 931-934

Freudenhammer, H., Bahnemann, D., Bousselmi, L., Geissen, S.-U., Ghrabi, A.,Saleh, F., ... Vogelpohl, A. (1997). Detoxification and recycling of wastewater by solar-catalytic treatment. Water Science and Technology Vol 35 No 3 pp 149-156

Gelover, S., Mondragón, P., and Jiménez, A. J. (2004). Titanium dioxide sol-gel deposited over glass and its application as a photocatalyst for water decontamination. Photochem. Photobiol. A: Chem. 165, 241

Gmelin, L. (1859). Hand-Book of Chemistry Vol. XII, Organic Chemistry, Vol. VII, Organic molecules containing sixteen and eighteen atoms of carbon.Printed for the Cavendish Society. London, England.

Kaan, C. C., Aziz, A. A., Ibrahim, Shaliza, Matheswaran, Manickam, Saravanan, Pichiah (2013) Heterogeneous Photocatalytic Oxidation an Effective Tool for Wastewater

Treatment: A Review. Studies on Water Management Issues, Chapter: 9, Publisher: INTECH OPEN ACCESS, pp.219-236

Kolpin, D., Furlong, E., Meyer, M., Thurman, E., Zaugg, S., Barber, L., & Buxton, H. (2002). Pharmaceuticals, Hormones, and Other Organic Wastewater Contaminants in U.S. Streams, 1999-2000: A National Reconnaissance. Environmental science & technology, 36, 1202-1211.

Legrini, O., Oliveros, E., & Braun, A. M. (1993). Photochemical processes for water treatment. Chemical Reviews, 93(2), 671–698. doi:10.1021/cr00018a003

Malato, S., Fernández-Ibáñez, P., Maldonado, M. I., Blanco, J., & Gernjak, W. (2009). Decontamination and disinfection of water by solar photocatalysis: Recent overview and trends. Catalysis Today, 147(1), 1–59. doi:10.1016/j.cattod.2009.06.018

Malato, S, J. B. (2007). Photocatalytic decontamination and disinfection of water with solar collectors. Catalysis Today, 137–149. doi:10.1016/j.cattod.2007.01.034

Marugán, J., Van Grieken, R. & Pablos C. (2010). Photocatalytic Disinfection of Water. Nova Science Publishers, Inc.

OECD (1999) Guidelines for Testing of Chemicals, Simulation Test-Aerobic Sewage Treatment 303A.

Pablos, C., van Grieken, R., Marugán, J., & Muñoz, A. (2012). Simultaneous photocatalytic oxidation of pharmaceuticals and inactivation of *Escherichia coli* in wastewater treatment plant effluents with suspended and immobilized TiO_2. Water Science & Technology, 65(11), 2016–2023. doi:10.2166/wst.2012.868

Petrovic, M., Radjenovic, J., Postigo, C., Kuster, M., Farre, M., Alda, M. L. de, & Barceló, D. (2008). Emerging Contaminants in Waste Waters: Sources and Occurrence. In D. Barceló & M. Petrovic (Eds.), Emerging Contaminants from Industrial and Municipal Waste (pp. 1–35). Springer Berlin Heidelberg. Retrieved fromhttp://link.springer.com/chapter/10.1007/698_5_106

Schwarzenbach, R., Gschwend, P., Imboden, D., (2003). Environmental Organic Chemistry. Wiley Interscience. Pg 489-

Stinson, B. (n.d.). Contaminants of emerging concern in wastewater streams [PowerPoint slides] Retrieved from http://www.mawaterquality.org/conferences/ edc_03_13_2007/6_Stinson_Wastewater.pdf

Suib, S. L. (2013). *New and Future Developments in Catalysis: Solar Photocatalysis.* Newnes

United Nations Childrens Fund (2013). Water, sanitation and hygiene. Retrieved from http://www.unicef.org/wash/

University of Rhode Island (2011). Emerging contaminants of concern detected throughout Narragansett Bay watershed. U.S. Science Daily. Retrieved from http://www.sciencedaily.com/releases/2011/09/110921154739.htm

U.S. Environmental Protection Agency. (2013). Climate change: international impacts.. Washington, DC: EPA.

U.S. Environmental Protection Agency. (2013). Water: Contaminants of emerging concern. Washington, DC: EPA.

U.S. Environmental Protection Agency (2014). Estimation Programs Interface Suite™ for Microsoft® Windows, v 4.11. United States Environmental Protection Agency, Washington, DC, USA.

U.S. Environmental Protection Agency. (2013). Water: Safe drinking water act (SDWA). Washington, DC: EPA.

U.S. Environmental Protection Agency. (2010). Treating contaminants of emerging concern. Washington, DC: EPA.

U.S. Environmental Protection Agency. (2000). Wastewater Technology Factsheet: Dechlorination. Washington, DC: EPA.

United Nations World Health Organization (2013). Water sanitation health: Drinking water quality. Retrieved from http://www.who.int/water_sanitation_health/dwq/en/

Additional

Chaudhari, R., Ahammed, M. M., & Dave, S. (2013). Solar disinfection of natural waters with modified solar concentrators. Water Science & Technology: Water Supply, 13(2), 462. doi:10.2166/ws.2013.042

Chow, A. T., Leech, D. M., Boyer, T. H., & Singer, P. C. (2008). Impact of simulated solar irradiation on disinfection byproduct precursors. Environmental science & technology, 42(15), 5586–5593.

De la Cruz, N., Esquius, L., Grandjean, D., Magnet, A., Tungler, A., de Alencastro, L. F., & Pulgarín, C. (2013). Degradation of emergent contaminants by UV, UV/H_2O_2 and neutral photo-Fenton at pilot scale in a domestic wastewater treatment plant. Water Research, 47(15), 5836–5845. doi:10.1016/j.watres.2013.07.005

De Laurentiis, E., Minella, M., Sarakha, M., Marrese, A., Minero, C., Mailhot, G., ... Vione, D. (2013). Photochemical processes involving the UV absorber benzophenone-4 (2-hydroxy-4-methoxybenzophenone-5-sulphonic acid) in aqueous solution: Reaction pathways and implications for surface waters. Water Research, 47(15), 5943–5953. doi:10.1016/j.watres.2013.07.017

Fontan-Sainz, M., Gomez-Couso, H., Fernandez-Ibanez, P., & Ares-Mazas, E. (2012). Evaluation of the Solar Water Disinfection Process (SODIS) Against Cryptosporidium parvum Using a 25-L Static Solar Reactor Fitted with a Compound Parabolic Collector (CPC).The American Journal of Tropical Medicine and Hygiene, 86(2), 223–228. doi:10.4269/ajtmh.2012.11-0325

Gosselin, F., Madeira, L. M., Juhna, T., & Block, J. C. (2013). Drinking water and biofilm disinfection by Fenton-like reaction. Water Research,47(15), 5631–5638. doi:10.1016/j.watres.2013.06.036

Gueymard, C. A. (2004). The sun's total and spectral irradiance for solar energy applications and solar radiation models. Solar Energy, (4), 423–453. doi:10.1016/j.solener.2003.08.039

Klamerth, N., Malato, S., Agüera, A., Fernández-Alba, A., & Mailhot, G. (2012). Treatment of municipal wastewater treatment plant effluents with modified photo-Fenton as a tertiary treatment for the degradation of micro pollutants and disinfection. Environmental science & technology, 46(5), 2885–2892. doi:10.1021/es204112d

Mbonimpa, E. G., Vadheim, B., & Blatchley III, E. R. (2012). Continuous-flow solar UVB disinfection reactor for drinking water. Water Research, 46(7), 2344–2354. doi:10.1016/j.watres.2012.02.003

Mtapuri-Zinyowera, S., Midzi, N., Muchaneta-Kubara, C. e., Simbini, T., & Mduluza, T. (2009). Impact of solar radiation in disinfecting drinking water contaminated with Giardia duodenalis and Entamoeba histolytica/dispar at a point-of-use water treatment. Journal of Applied Microbiology, 106(3), 847–852. doi:10.1111/j.1365-2672.2008.04054.x

Oppenländer, T. (2007). Photochemical Processes of Water Treatment. In Photochemical Purification of Water and Air (pp. 101–144). Wiley-VCH Verlag GmbH & Co. KGaA. Retrieved fromhttp://onlinelibrary.wiley.com/doi/10.1002/9783527610884.ch5/summary

Prieto-Rodríguez, L., Oller, I., Klamerth, N., Agüera, A., Rodríguez, E. M., & Malato, S. (2013). Application of solar AOPs and ozonation for elimination of micropollutants

in municipal wastewater treatment plant effluents. Water Research, 47(4), 1521–1528. doi:10.1016/j.watres.2012.11.002

Santiago-Morales, J., Gómez, M. J., Herrera-López, S., Fernández-Alba, A. R., García-Calvo, E., & Rosal, R. (2013). Energy efficiency for the removal of non-polar pollutants during ultraviolet irradiation, visible light photocatalysis and ozonation of a wastewater effluent. Water research, 47(15), 5546–5556. doi:10.1016/j.watres.2013.06.030

APPENDIX A: Procedures to generate calibration curves

The next pages contain the procedures followed by the Universidad Rey Juan Carlos research team to generate some useful calibration curves. The described linear relationships were used to find concentration measurements of methanol and cinnamic acid from the absorbance and TOC tests detailed in Section 2.4 of this document.

In this appendix, the reader will find the following information:

a) Procedure to generate the formaldehyde calibration curve (for the absorbance test)

b) Procedure to generate the cinnamic acid calibration curve (for the absorbance test)

c) Procedure to generate the total organic carbon calibration curve (for the TOC test)

Formaldehyde calibration curve

Instructions to make a calibration curve of Formaldehyde, using Excel and Biochrom Sample Analyzer:

a) Prepare a pattern of a formaldehyde solution at a predefined concentration of formaldehyde. At the Mostoles laboratory of URJC, the pattern solution was a 3 mM dilution of formaldehyde.

b) Using the model compound pattern, prepare dilutions depending on the curve points you want to include in your calibration curve. For the calibration curve used in procedure 2.4.1, solutions of 0.1 through 1 mM concentration where prepared, in increments of 0.1 mM of formaldehyde. A 0 mM sample was prepared too as a blank.

c) Once the dilution mixes have been prepared, measure the absorption of these solutions using the Libra S22 UV/Vis Spectrophotometer and the Biochrom Sample Analyzer software. Record the data points on an Excel sheet for each known solution sample.

d) Using the LINEST or SLOPE functions in Excel, calculate the slope for a linear relation between the measured Absorption values and the predefined Concentration values. Use Absorption as X values and Concentration as Y values.

The calibration curve received from Dr. Ruud Timmers is the following:

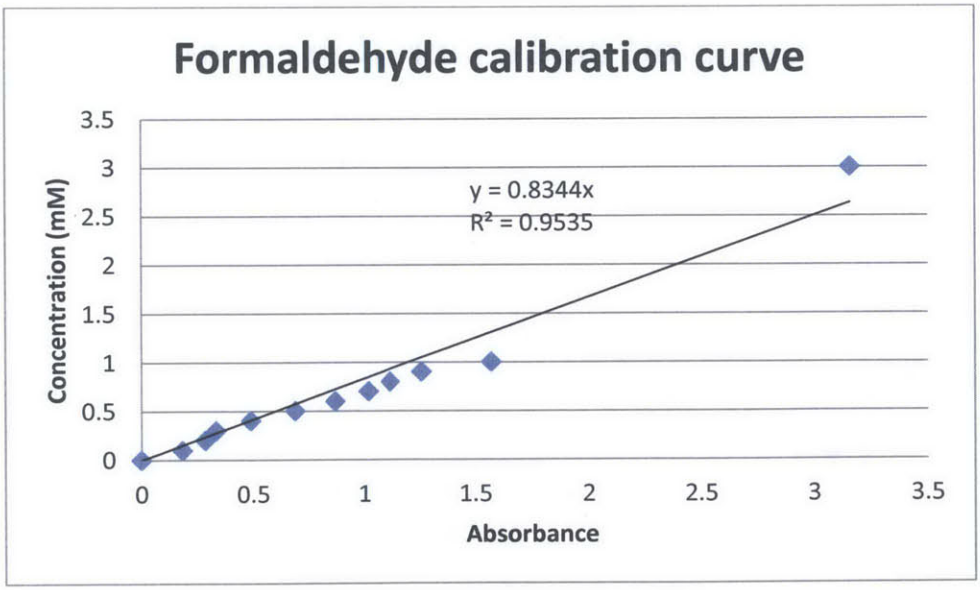

Cinnamic acid calibration curve

Instructions to make a calibration curve of Cinnamic acid, using Excel and Biochrom Sample Analyzer:

a) Prepare a pattern of a cinnamic acid solution at a predefined concentration of cinnamic acid. At the Mostoles laboratory of URJC, the pattern solution was a 10 mg/L dilution of cinnamic acid.

b) Using the model compound pattern, prepare dilutions depending on the curve points you want to include in your calibration curve. For the calibration curve used in procedure 2.4.2, solutions of 1 through 5 mg/L concentration where prepared, in increments of 1 mg/L of cinnamic acid. A 0 mg/L sample was prepared too as a blank.

c) Once the dilution mixes have been prepared, measure the absorption of these solutions using the Libra S22 UV/Vis Spectrophotometer and the Biochrom Sample Analyzer software. Record the data points on an Excel sheet for each known solution sample.

d) Using the LINEST or SLOPE functions in Excel, calculate the slope for a linear relation between the measured Absorption values and the predefined Concentration values. Use Absorption as X values and Concentration as Y values.

The calibration curve received from Dr. Ruud Timmers is the following:

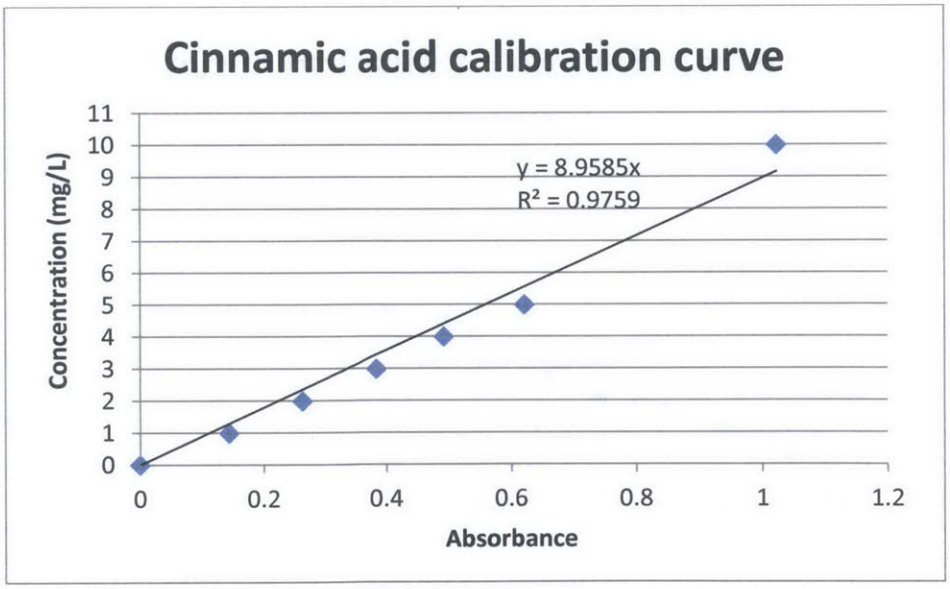

Total organic carbon calibration curve

Instructions to make a calibration curve on the TOC-V CSN Shimadzu Software:

d) Prepare a pattern of a model compound that contains carbon using a predefined concentration of total carbon (it is common that this concentration be 1000 mg/L). At the Mostoles laboratory of URJC, the model compound chosen was potassium hydrogen phthalate.

e) Using the model compound pattern, prepare dilutions depending on the curve points you want to include in your calibration curve.

f) Once the dilution mixes have been prepared, open the Shimadzu Software and manually select on the computer software the points for which you want to calculate the concentration, corresponding to the predetermined dilution patterns.

   For example, for a calibration curve that measures up to 100 mg/L of total organic carbon: Step (a) would be to prepare a potassium hydrogen phthalate pattern at 1000 mg/L of total carbon. Next, step (b) would be to perform a dilution of the 1000 mg/L pattern to a 100 mg/L diluted mix. Then, step (c) would be to program the equipment to do the dilutions to calculate various intermediate points with which the calibration curve will be generated (e.g.: 100, 50, 25, 10, 5 and 1 mg/L dilutions).

g) Once the intermediate points have been selected, define an injection volume for the procedure, the maximum number of replicas and the maximum deviation (error) that will be accepted for the measurements. It is important to choose adequate values, because these numbers are to remain constant for the method and cannot be changed.

   Based on the parameters selected, the equipment will take constant volume samples of varied concentrations. For each sample point, an area will be calculated based on a sensed gasified carbon (CO_2) signal, and the total carbon concentration will be determined as a function of this area. The calibration curve will be generated from these area points and, once it is stored on the Software's library, it can be used to detect TOC concentration value of test samples.

APPENDIX B: Methanol Experimental Results

The following pages contain summary graphs and tables from the results of the methanol experiments. The graphs and charts convey the measured concentrations of the compound after following the test procedures detailed in Section 2.4 of this thesis.

On each page, the reader will find the following information:

a) Experiment name tag

b) Independent variable conditions:

   a. Initial target pollutant concentration

   b. Initial catalyst concentration

   c. Radiation power

c) Concentration of pollutant and intermediates from Absorbance and TOC tests:

   a. Summary table of reported concentrations (TOC tests were not conducted on Experiments A through F)

   b. Graph of normalized concentration values

d) Registered Chemical Oxygen Demand

   a. Summary table of reported COD (COD tests were not conducted on Experiments A through F)

   b. Graph of normalized COD values

Experiment A

Initial Methanol Concentration	Catalyst (TiO_2) Concentration	Radiation Power
100 mM of TOC	0.10 g/L	0 W/m^2

08.A	Pump 1						Pump 2					
Time [min]	TOC [mM C]		Methanol [mM C]		Formaldehyde [mM C]		TOC [mM C]		Methanol [mM C]		Formaldehyde [mM C]	
0	N/A	N/A	99.5	100%	0.489	0%	N/A	N/A	99.5	100%	0.468	0%
5	N/A	N/A	99.4	99%	0.587	1%	N/A	N/A	99.5	99%	0.538	1%
10	N/A	N/A	99.5	100%	0.489	0%	N/A	N/A	99.5	100%	0.482	0%
20	N/A	N/A	99.5	99%	0.510	1%	N/A	N/A	99.5	100%	0.489	0%
30	N/A	N/A	99.5	100%	0.489	0%	N/A	N/A	99.5	99%	0.517	1%
45	N/A	N/A	99.5	100%	0.489	0%	N/A	N/A	99.5	99%	0.510	1%
60	N/A	N/A	99.5	99%	0.524	1%	N/A	N/A	99.5	99%	0.510	1%

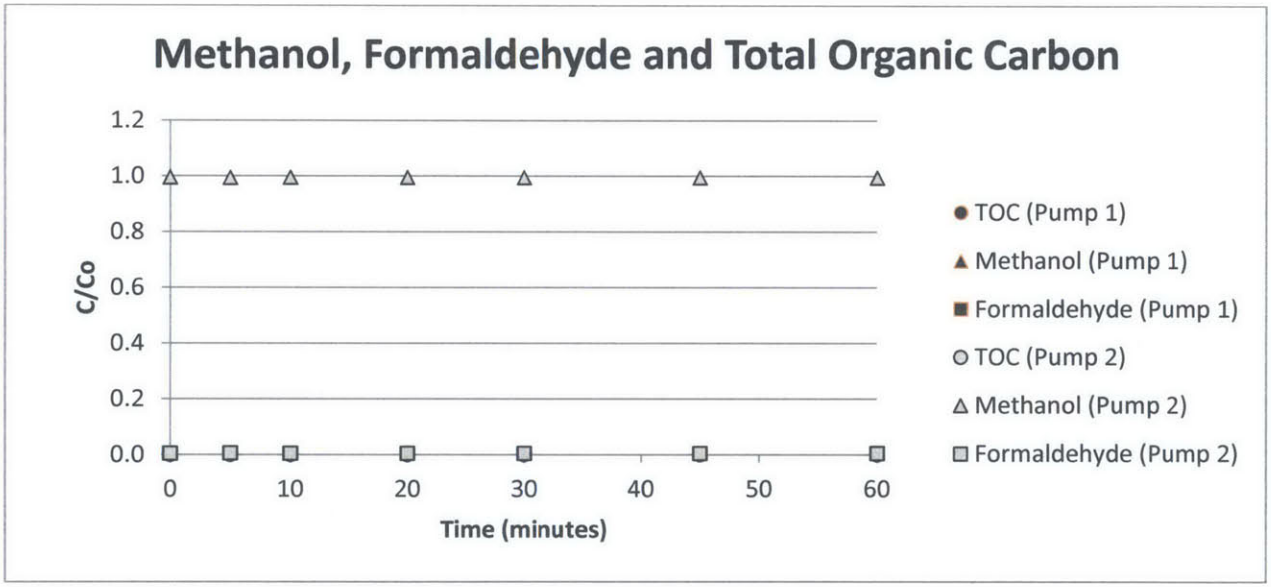

Experiment B

Initial Methanol Concentration	Catalyst (TiO_2) Concentration	Radiation Power
100 mM of TOC	0.0 g/L	83.7 W/m^2

08.B	Pump 1						Pump 2					
Time [min]	TOC [mM C]		Methanol [mM C]		Formaldehyde [mM C]		TOC [mM C]		Methanol [mM C]		Formaldehyde [mM C]	
0	N/A	N/A	100.0	100%	0.035	0%	N/A	N/A	99.5	99%	0.503	1%
5	N/A	N/A	99.9	100%	0.056	0%	N/A	N/A	99.5	99%	0.531	1%
10	N/A	N/A	99.9	100%	0.084	0%	N/A	N/A	99.5	99%	0.538	1%
20	N/A	N/A	99.9	100%	0.056	0%	N/A	N/A	99.4	99%	0.552	1%
30	N/A	N/A	99.9	100%	0.091	0%	N/A	N/A	99.5	99%	0.531	1%
45	N/A	N/A	99.9	100%	0.091	0%	N/A	N/A	99.5	99%	0.531	1%
60	N/A	N/A	100.0	100%	0.049	0%	N/A	N/A	99.4	99%	0.566	1%

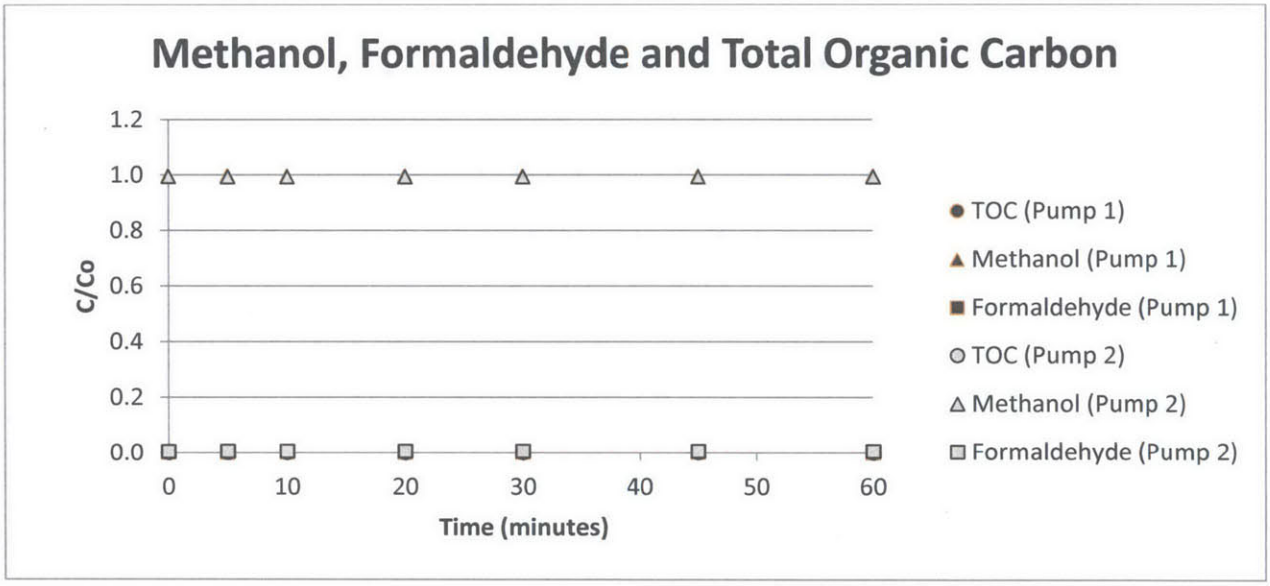

Experiment C

Initial Methanol Concentration	Catalyst (TiO_2) Concentration	Radiation Power
100 mM of TOC	0.10 g/L	83.7 W/m^2

09.C	Pump 1						Pump 2					
Time [min]	TOC [mM C]		Methanol [mM C]		Formaldehyde [mM C]		TOC [mM C]		Methanol [mM C]		Formaldehyde [mM C]	
0	N/A	N/A	100.0	100%	0.028	0%	N/A	N/A	99.9	100%	0.140	0%
5	N/A	N/A	99.3	99%	0.699	1%	N/A	N/A	99.4	99%	0.552	1%
10	N/A	N/A	98.5	99%	1.475	1%	N/A	N/A	98.8	99%	1.153	1%
20	N/A	N/A	97.0	97%	3.006	3%	N/A	N/A	97.9	98%	2.069	2%
30	N/A	N/A	95.3	95%	4.655	5%	N/A	N/A	97.1	97%	2.901	3%
45	N/A	N/A	93.5	93%	6.528	7%	N/A	N/A	96.5	96%	3.537	4%
60	N/A	N/A	90.5	90%	9.534	10%	N/A	N/A	95.5	95%	4.536	5%

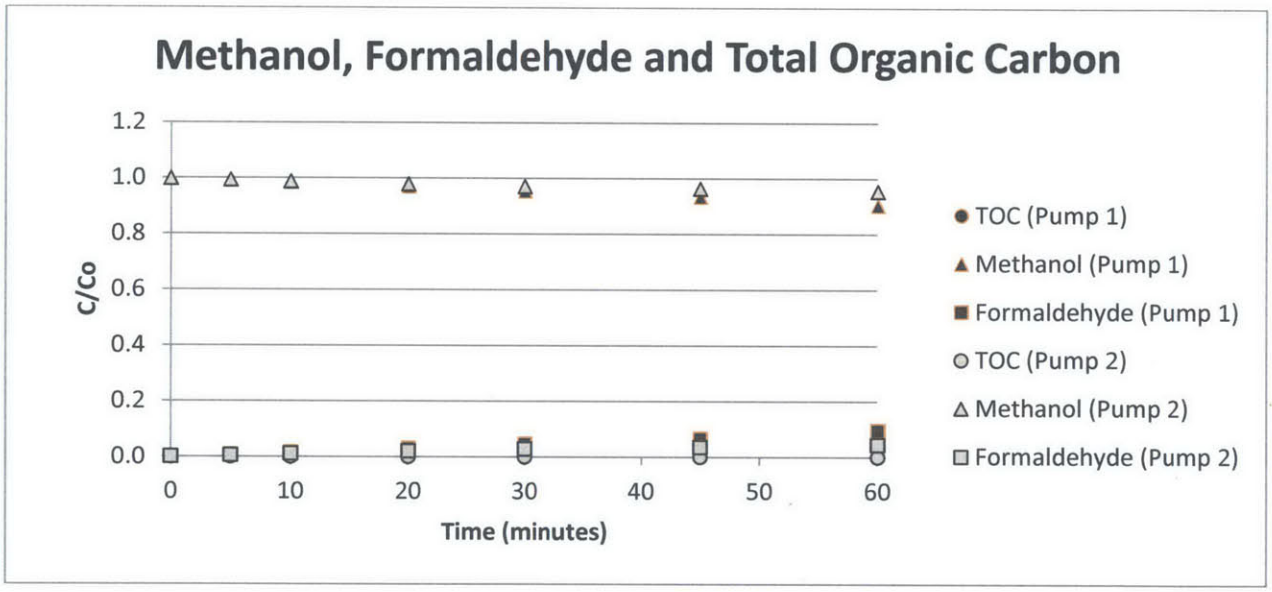

Experiment D

Initial Methanol Concentration	Catalyst (TiO_2) Concentration	Radiation Power
100 mM of TOC	0.0 g/L	83.7 W/m^2

09.D	Pump 1						Pump 2					
Time [min]	TOC [mM C]		Methanol [mM C]		Formaldehyde [mM C]		TOC [mM C]		Methanol [mM C]		Formaldehyde [mM C]	
0	N/A	N/A	100.0	100%	0.007	0%	N/A	N/A	100.0	100%	0.035	0%
5	N/A	N/A	99.8	100%	0.154	0%	N/A	N/A	99.9	100%	0.084	0%
10	N/A	N/A	99.7	100%	0.266	0%	N/A	N/A	99.7	100%	0.315	0%
20	N/A	N/A	99.5	99%	0.531	1%	N/A	N/A	99.6	100%	0.356	0%
30	N/A	N/A	99.2	99%	0.818	1%	N/A	N/A	99.4	99%	0.566	1%
45	N/A	N/A	98.8	99%	1.244	1%	N/A	N/A	99.4	99%	0.636	1%
60	N/A	N/A	98.4	98%	1.622	2%	N/A	N/A	99.1	99%	0.930	1%

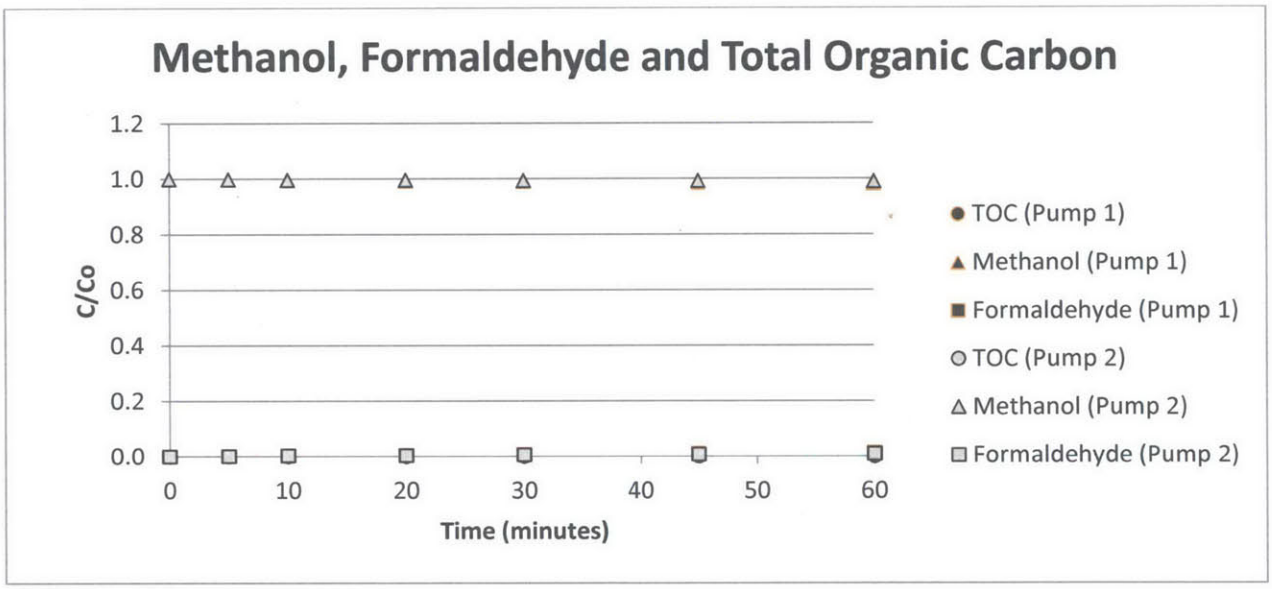

Experiment E

Initial Methanol Concentration	Catalyst (TiO_2) Concentration	Radiation Power
200 mM of TOC	0.0 g/L	83.7 W/m^2

09.E	Pump 1						Pump 2					
Time [min]	TOC [mM C]		Methanol [mM C]		Formaldehyde [mM C]		TOC [mM C]		Methanol [mM C]		Formaldehyde [mM C]	
0	N/A	N/A	199.6	100%	0.398	0%	N/A	N/A	200.0	100%	0.028	0%
5	N/A	N/A	199.9	100%	0.140	0%	N/A	N/A	199.9	100%	0.077	0%
10	N/A	N/A	199.8	100%	0.245	0%	N/A	N/A	199.8	100%	0.154	0%
20	N/A	N/A	199.5	100%	0.503	0%	N/A	N/A	199.7	100%	0.252	0%
30	N/A	N/A	199.2	100%	0.762	0%	N/A	N/A	199.6	100%	0.384	0%
45	N/A	N/A	199.1	100%	0.944	0%	N/A	N/A	199.5	100%	0.531	0%
60	N/A	N/A	198.7	99%	1.293	1%	N/A	N/A	199.2	100%	0.762	0%

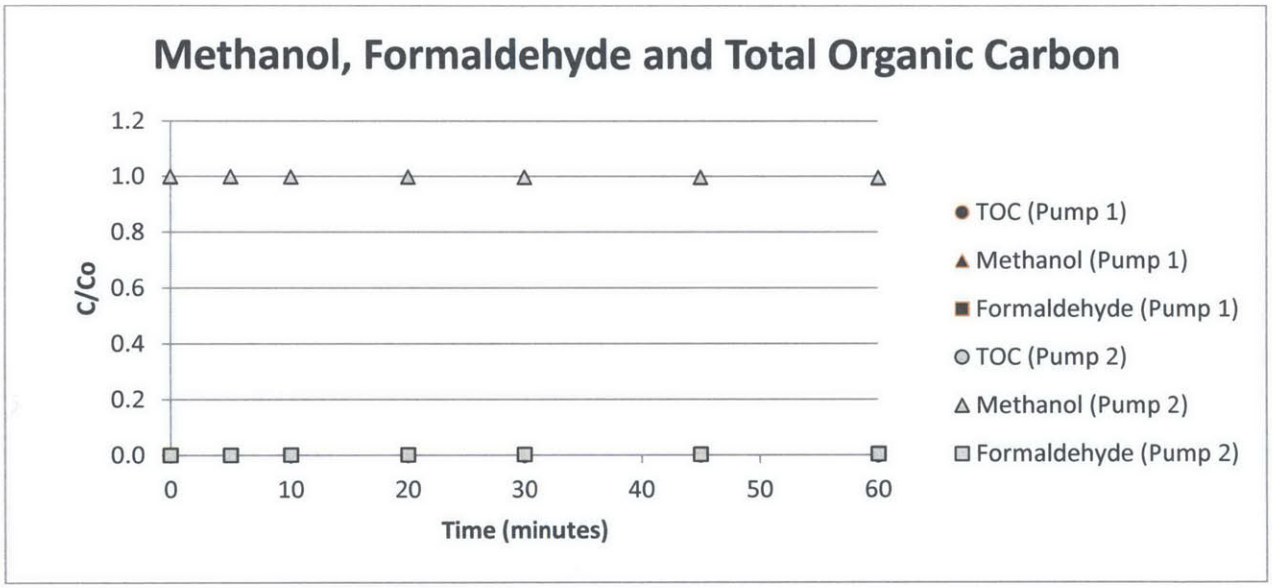

Experiment F

Initial Methanol Concentration	Catalyst (TiO_2) Concentration	Radiation Power
50 mM of TOC	0.0 g/L	83.7 W/m^2

09.F	Pump 1						Pump 2					
Time [min]	TOC [mM C]		Methanol [mM C]		Formaldehyde [mM C]		TOC [mM C]		Methanol [mM C]		Formaldehyde [mM C]	
0	N/A	N/A	50.00	100%	0.000	0%	N/A	N/A	49.90	100%	0.105	0%
5	N/A	N/A	49.96	100%	0.042	0%	N/A	N/A	49.97	100%	0.035	0%
10	N/A	N/A	49.88	100%	0.119	0%	N/A	N/A	49.94	100%	0.063	0%
20	N/A	N/A	49.73	99%	0.273	1%	N/A	N/A	49.92	100%	0.077	0%
30	N/A	N/A	49.60	99%	0.398	1%	N/A	N/A	49.82	100%	0.182	0%
45	N/A	N/A	49.41	99%	0.594	1%	N/A	N/A	49.74	99%	0.259	1%
60	N/A	N/A	49.62	99%	0.377	1%	N/A	N/A	49.18	98%	0.825	2%

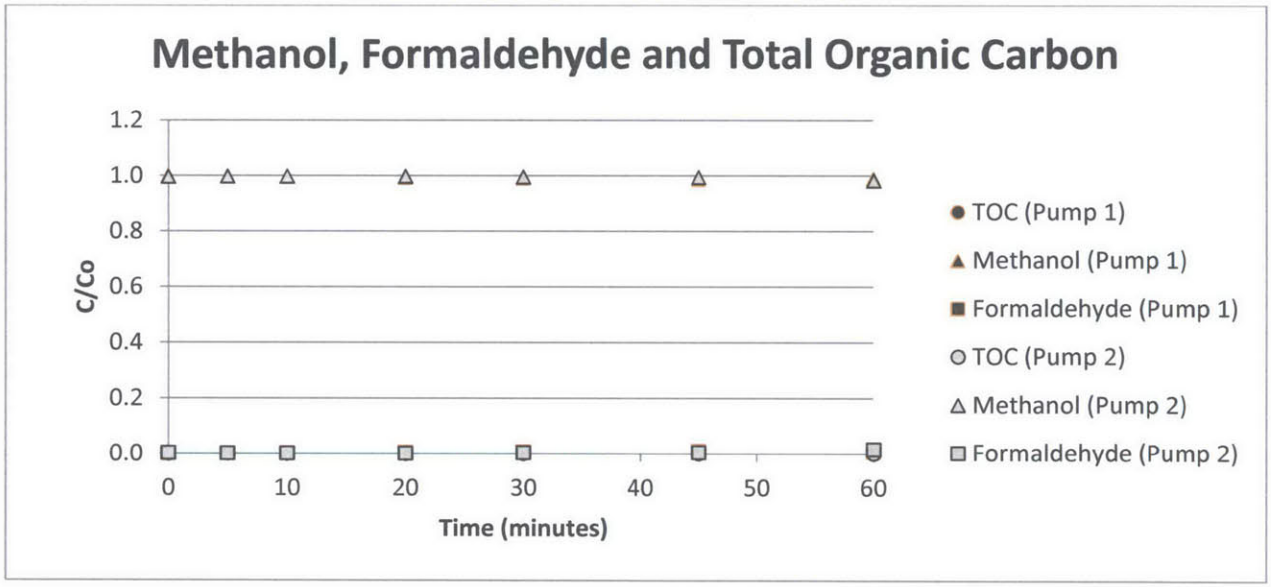

Experiment G

Initial Methanol Concentration	Catalyst (TiO_2) Concentration	Radiation Power
4 mM of TOC	0.0 g/L	83.7 W/m^2

10.G	Pump 1						Pump 2					
Time [min]	TOC [mM C]		Methanol [mM C]		Formaldehyde [mM C]		TOC [mM C]		Methanol [mM C]		Formaldehyde [mM C]	
0	8.567	214%	3.923	98%	0.077	2%	12.497	312%	3.965	99%	0.035	1%
5	0.000	0%	3.930	98%	0.070	2%	0.000	0%	3.951	99%	0.049	1%
10	6.994	175%	3.909	98%	0.091	2%	11.565	289%	3.965	99%	0.035	1%
20	0.000	0%	3.825	96%	0.175	4%	0.000	0%	3.916	98%	0.084	2%
30	7.331	183%	3.734	93%	0.266	7%	11.494	287%	3.846	96%	0.154	4%
45	0.000	0%	3.588	90%	0.412	10%	0.000	0%	3.769	94%	0.231	6%
60	7.614	190%	3.511	88%	0.489	12%	10.765	269%	3.895	97%	0.105	3%

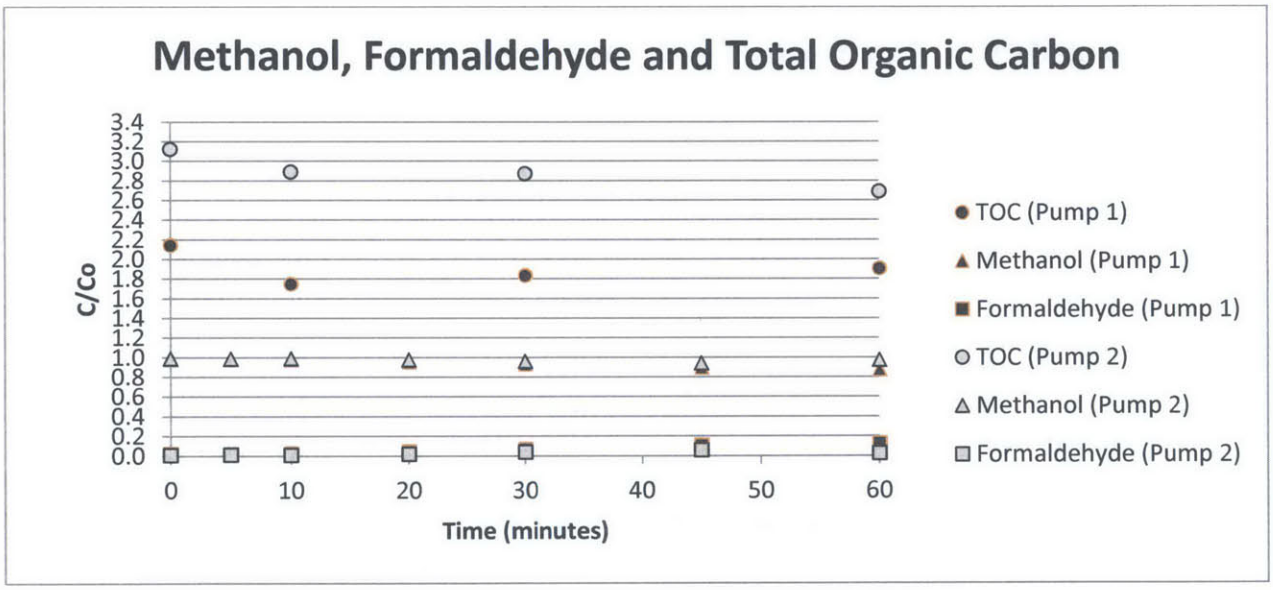

10.G	Pump 1		Pump 2	
Time [min]	COD mg/L	C/Co	COD mg/L	C/Co
0	420	100%	590	100%
5	N/A	N/A	N/A	N/A
10	370	88%	550	93%
15	N/A	N/A	N/A	N/A
20	290	69%	500	85%
30	N/A	N/A	N/A	N/A
45	430	102%	470	80%

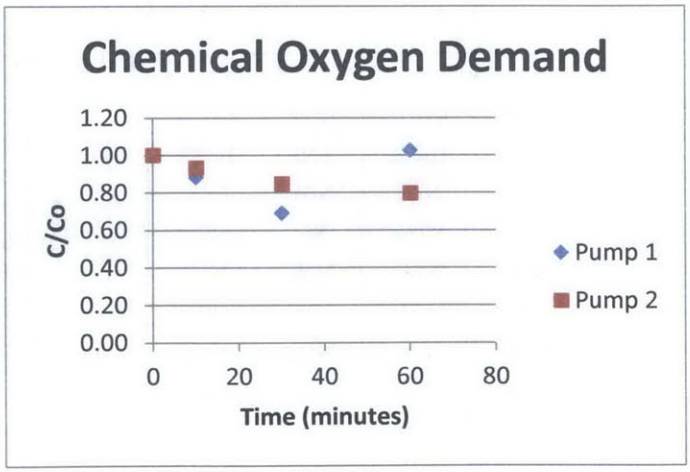

Experiment H

Initial Methanol Concentration	Catalyst (TiO_2) Concentration	Radiation Power
4 mM of TOC	0.10 g/L	74.2 W/m^2

10.H	Pump 1						Pump 2					
Time [min]	TOC [mM C]		Methanol [mM C]		Formaldehyde [mM C]		TOC [mM C]		Methanol [mM C]		Formaldehyde [mM C]	
0	5.250	131%	3.993	100%	0.007	0%	5.095	127%	4.000	100%	0.000	0%
5	0.000	0%	3.832	96%	0.168	4%	0.000	0%	3.951	99%	0.049	1%
10	5.113	128%	3.685	92%	0.315	8%	3.747	94%	3.881	97%	0.119	3%
15	5.757	144%	3.616	90%	0.384	10%	5.585	140%	3.874	97%	0.126	3%
20	0.000	0%	3.476	87%	0.524	13%	0.000	0%	3.825	96%	0.175	4%
30	4.866	122%	3.490	87%	0.510	13%	4.366	109%	3.769	94%	0.231	6%
45	0.000	0%	3.210	80%	0.790	20%	0.000	0%	3.783	95%	0.217	5%

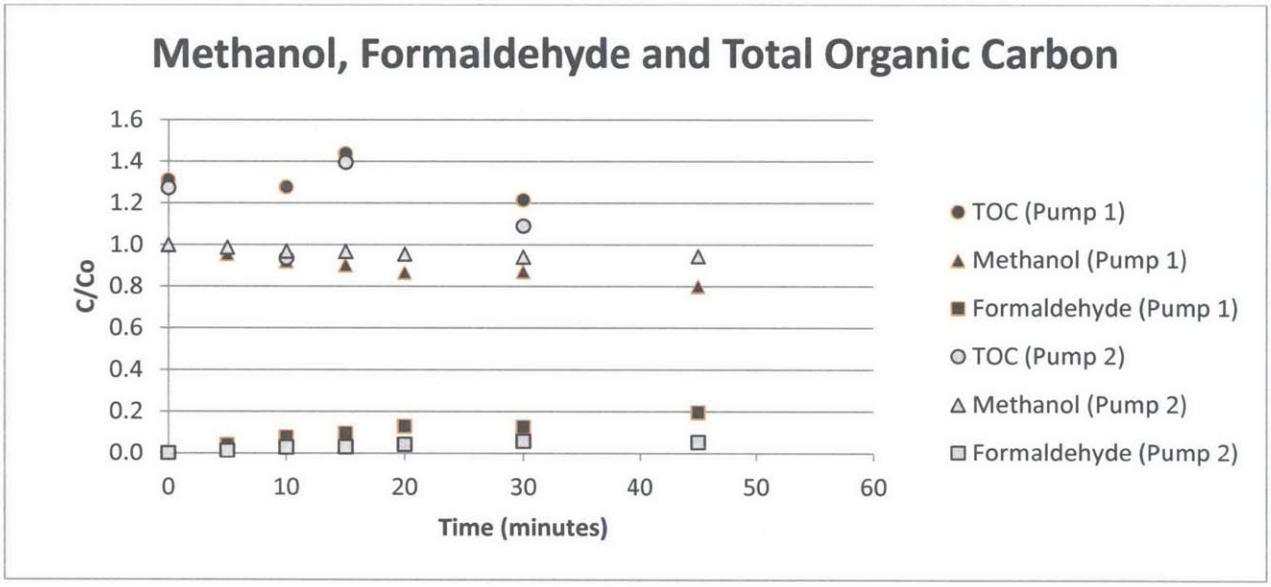

10.H	Pump 1		Pump 2	
Time [min]	COD		COD	
	mg/L	C/Co	mg/L	C/Co
0	156	100%	136	100%
5	N/A	N/A	N/A	N/A
10	136	87%	88	65%
15	N/A	N/A	N/A	N/A
20	172	110%	176	129%
30	N/A	N/A	N/A	N/A
45	136	87%	84	62%

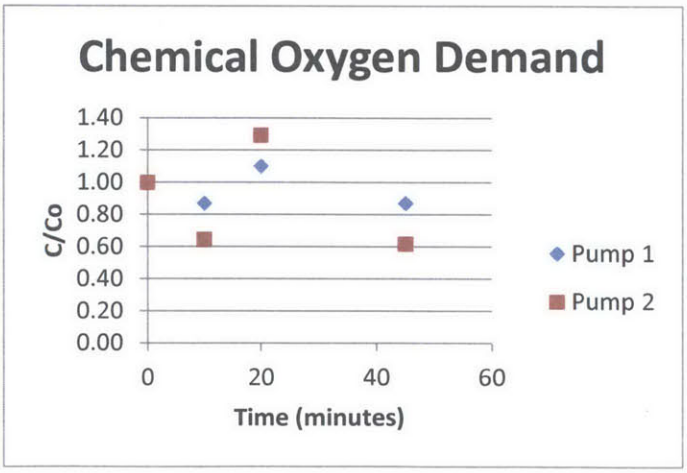

Experiment I

Initial Methanol Concentration	Catalyst (TiO_2) Concentration	Radiation Power
8 mM of TOC	0.10 g/L	74.2 W/m^2

10.I	Pump 1						Pump 2					
Time [min]	TOC [mM C]		Methanol [mM C]		Formaldehyde [mM C]		TOC [mM C]		Methanol [mM C]		Formaldehyde [mM C]	
0	4.164	52%	7.951	99%	0.049	1%	5.195	65%	8.000	100%	0.000	0%
5	0.000	0%	7.769	97%	0.231	3%	0.000	0%	7.895	99%	0.105	1%
10	4.763	60%	7.574	95%	0.426	5%	5.560	70%	7.839	98%	0.161	2%
15	0.000	0%	7.301	91%	0.699	9%	0.000	0%	7.881	99%	0.119	1%
20	5.872	73%	7.105	89%	0.895	11%	6.442	81%	7.699	96%	0.301	4%
30	0.000	0%	7.168	90%	0.832	10%	0.000	0%	7.595	95%	0.405	5%
45	6.337	79%	6.378	80%	1.622	20%	5.036	63%	6.546	82%	1.454	18%

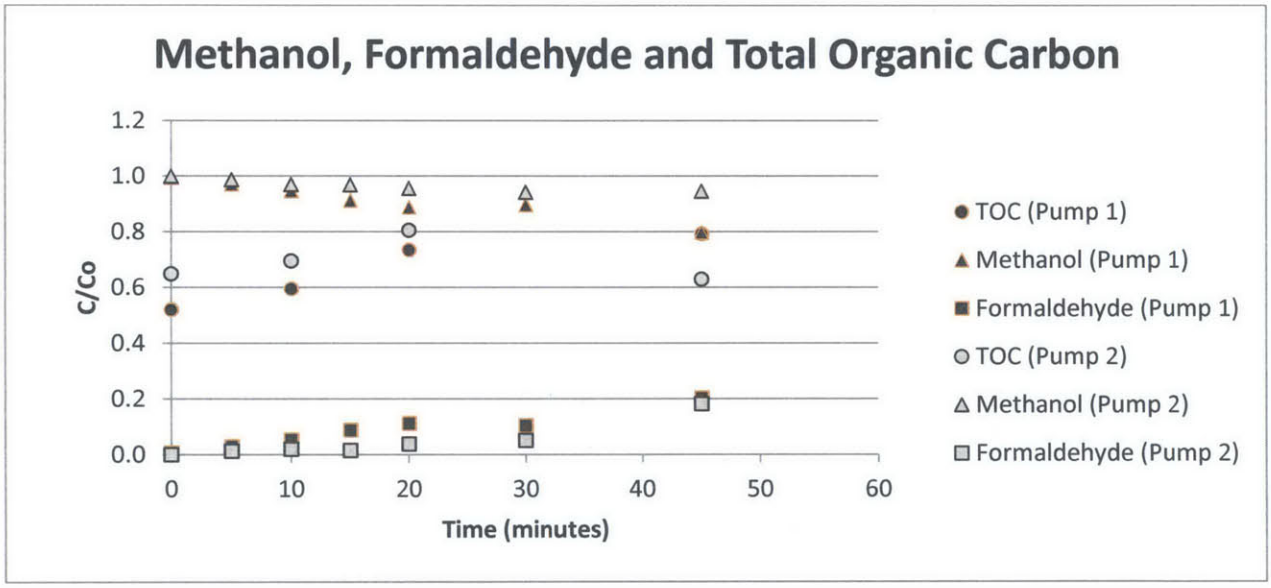

10.I	Pump 1		Pump 2	
Time [min]	COD mg/L	C/Co	COD mg/L	C/Co
0	208	100%	252	100%
5	N/A	N/A	N/A	N/A
10	224	108%	264	105%
15	N/A	N/A!	N/A	N/A
20	260	125%	304	121%
30	N/A	N/A!	N/A	N/A
45	284	137%	224	89%

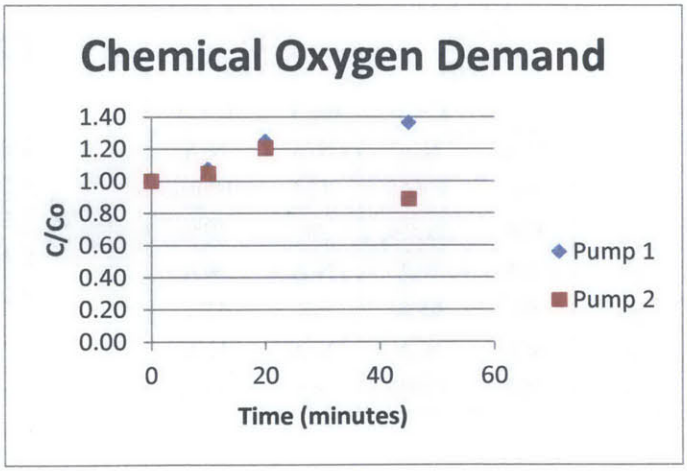

Experiment J

Initial Methanol Concentration	Catalyst (TiO_2) Concentration	Radiation Power
6 mM of TOC	0.10 g/L	74.2 W/m^2

10.J	Pump 1						Pump 2					
Time [min]	TOC [mM C]		Methanol [mM C]		Formaldehyde [mM C]		TOC [mM C]		Methanol [mM C]		Formaldehyde [mM C]	
0	0.000	0%	5.944	99%	0.056	1%	0.000	0%	N/A	N/A	N/A	N/A
5	2.394	40%	5.902	98%	0.098	2%	2.735	46%	5.937	99%	0.063	1%
10	2.538	42%	5.651	94%	0.349	6%	2.035	34%	5.874	98%	0.126	2%
15	0.000	0%	5.595	93%	0.405	7%	0.000	0%	5.839	97%	0.161	3%
20	1.809	30%	5.511	92%	0.489	8%	2.353	39%	5.839	97%	0.161	3%
30	1.914	32%	5.378	90%	0.622	10%	2.520	42%	5.720	95%	0.280	5%
45	0.000	0%	5.077	85%	0.923	15%	0.000	0%	N/A	N/A	N/A	N/A

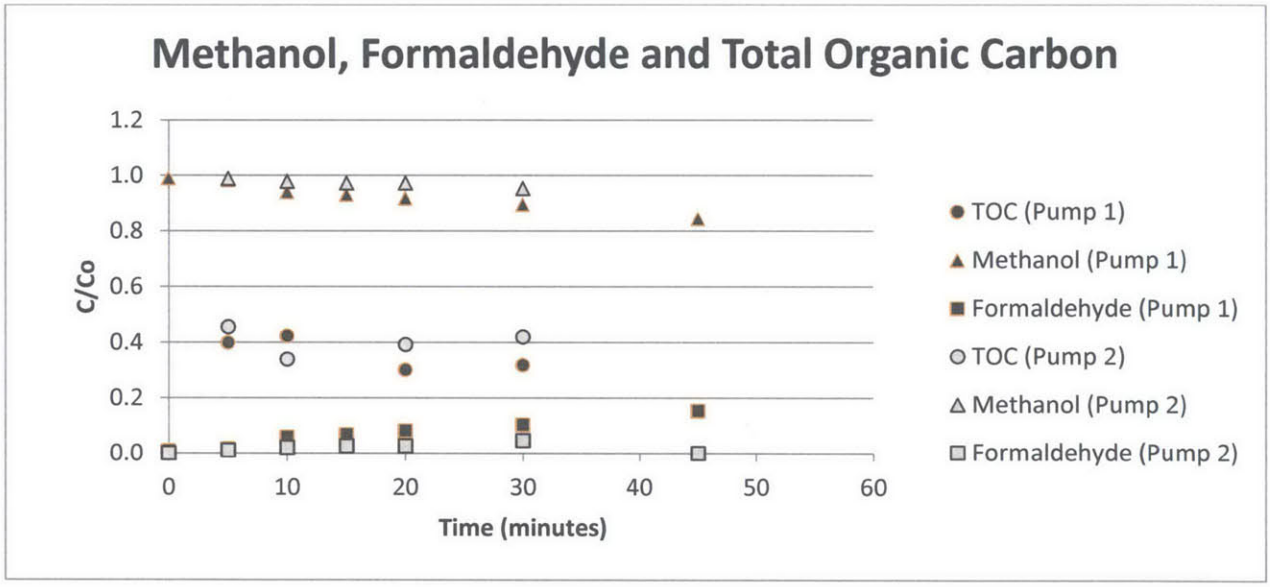

10.J	Pump 1		Pump 2	
Time [min]	COD mg/L	C/Co	COD mg/L	C/Co
0	N/A	N/A	N/A	N/A
5	92	100%	124	100%
10	104	113%	48	39%
15	N/A	N/A	N/A	N/A
20	60	65%	68	55%
30	N/A	N/A	N/A	N/A
45	100	109%	80	65%

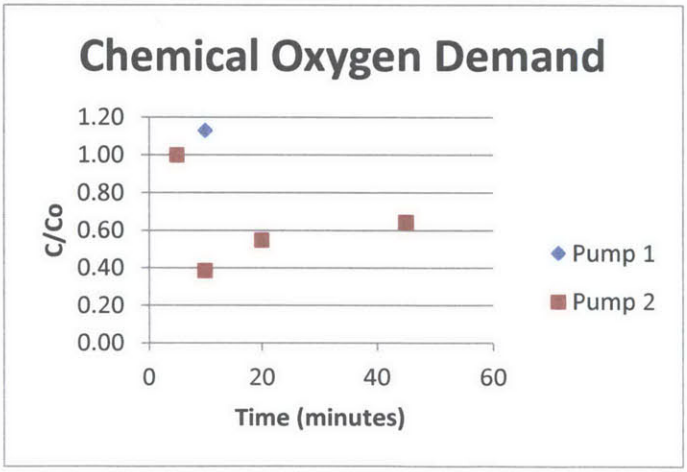

Experiment K

Initial Methanol Concentration	Catalyst (TiO_2) Concentration	Radiation Power
4 mM of TOC	0.05 g/L	74.2 W/m^2

13.K	Pump 1						Pump 2					
Time [min]	TOC [mM C]		Methanol [mM C]		Formaldehyde [mM C]		TOC [mM C]		Methanol [mM C]		Formaldehyde [mM C]	
0	17.417	435%	4.000	100%	0.000	0%	16.525	413%	3.958	99%	0.042	1%
5	0.000	0%	3.720	93%	0.280	7%	0.000	0%	3.797	95%	0.203	5%
10	16.395	410%	3.441	86%	0.559	14%	17.315	433%	3.692	92%	0.308	8%
20	17.584	440%	2.903	73%	1.097	27%	17.037	426%	3.448	86%	0.552	14%
30	0.000	0%	2.483	62%	1.517	38%	0.000	0%	3.448	86%	0.552	14%
45	17.365	434%	1.637	41%	2.363	59%	17.025	426%	3.049	76%	0.951	24%
60	0.000	0%	1.281	32%	2.719	68%	0.000	0%	2.735	68%	1.265	32%

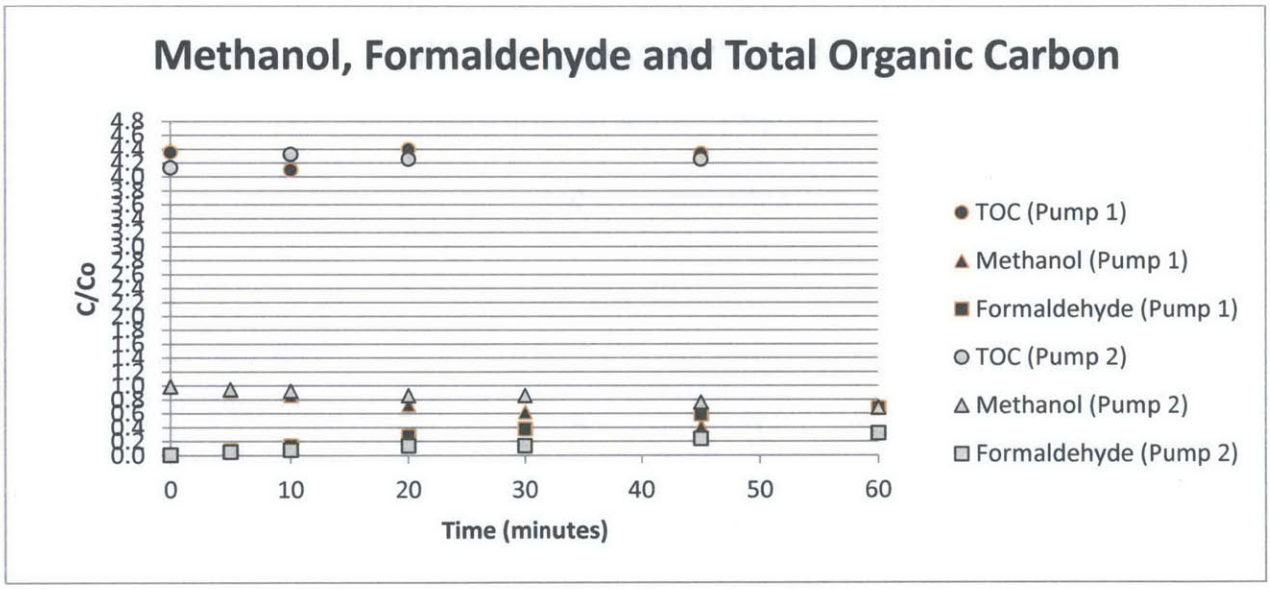

13.K	Pump 1		Pump 2	
Time [min]	COD mg/L	C/Co	COD mg/L	C/Co
0	740	100%	770	100%
5	N/A	N/A	N/A	N/A
10	730	99%	740	96%
15	770	104%	740	96%
20	N/A	N/A	N/A	N/A
30	760	103%	740	96%
45	N/A	N/A	N/A	N/A

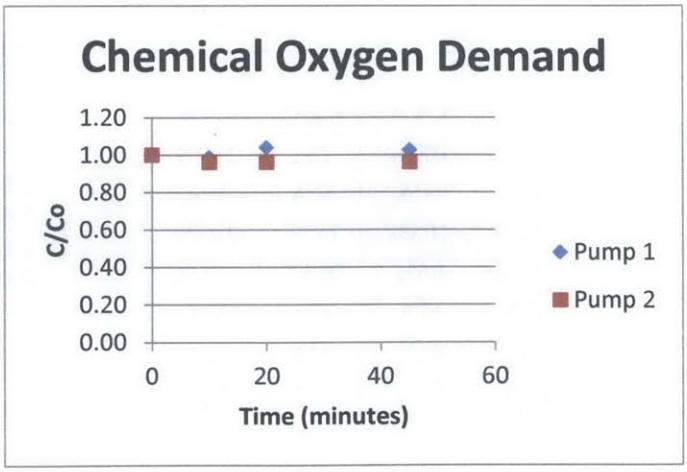

Experiment L

Initial Methanol Concentration	Catalyst (TiO_2) Concentration	Radiation Power
8 mM of TOC	0.05 g/L	74.2 W/m^2

13.L	Pump 1						Pump 2					
Time [min]	TOC [mM C]		Methanol [mM C]		Formaldehyde [mM C]		TOC [mM C]		Methanol [mM C]		Formaldehyde [mM C]	
0	8.255	103%	8.000	100%	0.000	0%	7.903	99%	7.993	100%	0.007	0%
5	0.000	0%	7.846	98%	0.154	2%	0.000	0%	7.965	100%	0.035	0%
10	7.995	100%	7.811	98%	0.189	2%	8.492	106%	7.867	98%	0.133	2%
20	8.273	103%	7.504	94%	0.496	6%	8.632	108%	7.734	97%	0.266	3%
30	0.000	0%	7.420	93%	0.580	7%	0.000	0%	7.616	95%	0.384	5%
45	8.542	107%	7.028	88%	0.972	12%	8.557	107%	7.427	93%	0.573	7%
60	0.000	0%	6.924	87%	1.076	13%	0.000	0%	7.252	91%	0.748	9%

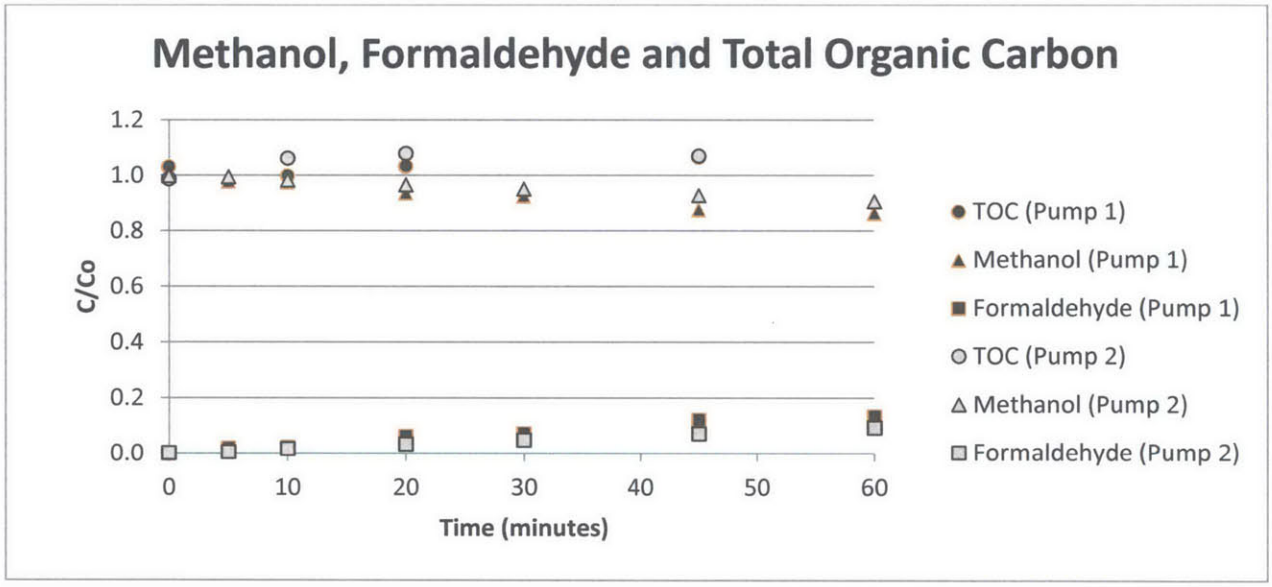

13.L	Pump 1		Pump 2	
Time [min]	COD mg/L	C/Co	COD mg/L	C/Co
0	249.3	100%	252	100%
5	N/A	N/A	N/A	N/A
10	262.7	105%	257.3	102%
15	237.3	95%	266.7	106%
20	N/A	N/A	N/A	N/A
30	240	96%	316	125%
45	N/A	N/A	N/A	N/A

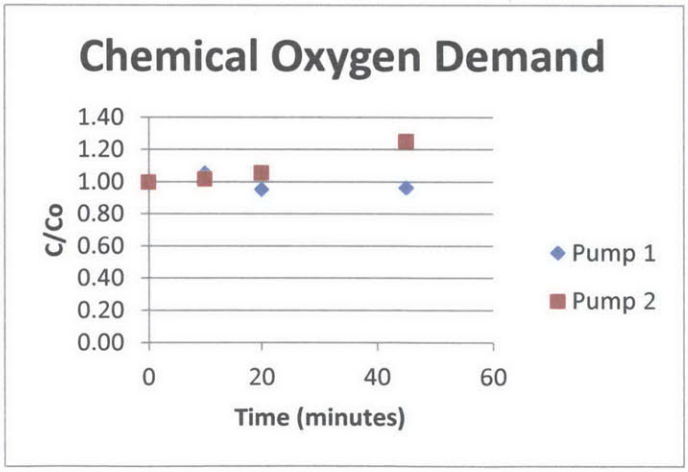

Experiment M

Initial Methanol Concentration	Catalyst (TiO_2) Concentration	Radiation Power
6 mM of TOC	0.05 g/L	74.2 W/m^2

13.L	Pump 1						Pump 2					
Time [min]	TOC [mM C]		Methanol [mM C]		Formaldehyde [mM C]		TOC [mM C]		Methanol [mM C]		Formaldehyde [mM C]	
0	2.466	41%	6.028	100%	-0.028	0%	3.210	53%	6.000	100%	0.000	0%
5	0.000	0%	5.930	99%	0.070	1%	0.000	0%	5.986	100%	0.014	0%
10	2.927	49%	5.846	97%	0.154	3%	2.778	46%	5.930	99%	0.070	1%
20	0.000	0%	6.098	102%	-0.098	-2%	0.000	0%	5.874	98%	0.126	2%
30	2.359	39%	5.560	93%	0.440	7%	2.528	42%	5.825	97%	0.175	3%
45	0.000	0%	5.357	89%	0.643	11%	0.000	0%	5.979	100%	0.021	0%
60	2.403	40%	5.154	86%	0.846	14%	3.205	53%	5.811	97%	0.189	3%

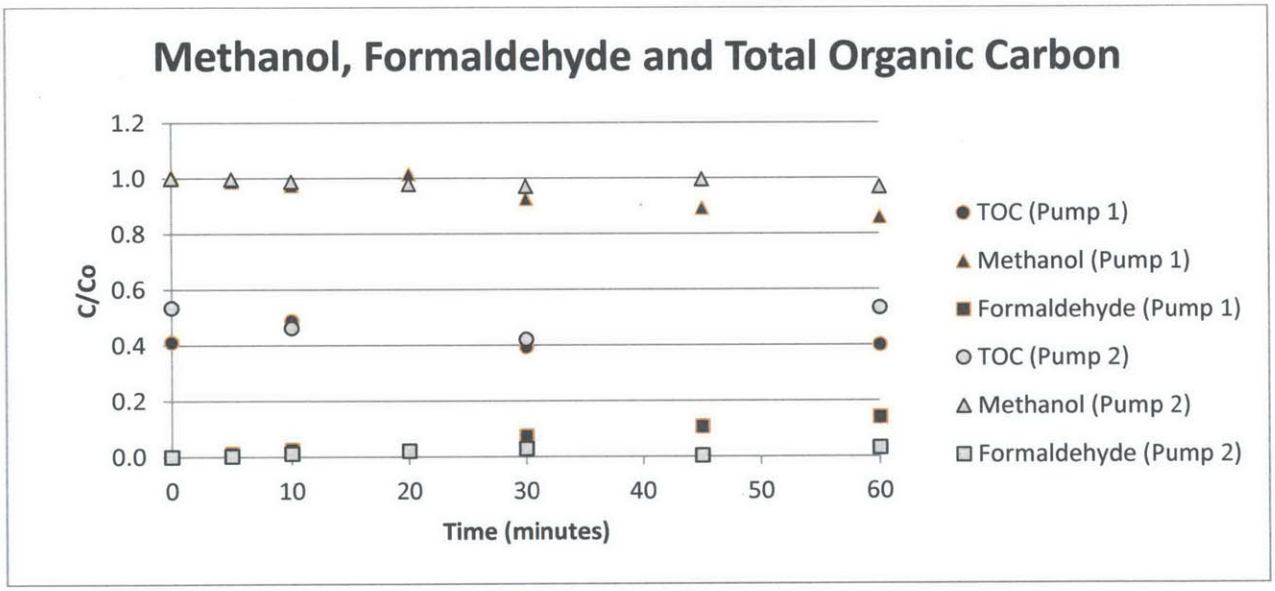

13.M	Pump 1		Pump 2	
Time [min]	COD mg/L	C/Co	COD mg/L	C/Co
0	N/A	N/A	N/A	N/A
5	144	100%	133.3	100%
10	129.3	90%	142.7	107%
15	N/A	N/A	N/A	N/A
20	128	89%	126.7	95%
30	N/A	N/A	N/A	N/A
45	126.7	88%	125.3	94%

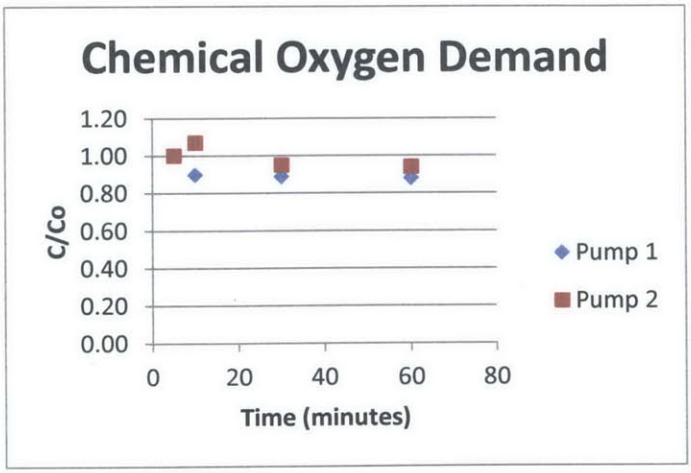

APPENDIX C: Cinnamic Acid Experimental Results

The following pages contain summary graphs and tables from the results of Cinnamic Acid Experiments N-X and Z. The graphs and charts convey the measured concentrations of the compound after following the test procedures detailed in Section 2.4 of this document.

On each page, the reader will find the following information:

a) Experiment name tag

b) Independent variable conditions:

   a. Initial target pollutant concentration

   b. Initial catalyst concentration

   c. Radiation power

c) Concentration of pollutant and intermediates from Absorbance and TOC tests:

   a. Summary table of reported concentrations

   b. Graph of concentrations normalized target values

d) Registered Chemical Oxygen Demand

   a. Summary table of reported COD

   b. Graph of COD values normalized to measurements taken at time zero

Experiment N

Initial CA Concentration	Catalyst (TiO_2) Concentration	Radiation Power
4 mM of TOC	0.10 g/L	74.2 W/m^2

	Pump 1				Pump 2'			
Time (min)	TOC (mM C)		CA (mM C)		TOC (mM C)		CA (mM C)	
0	4.416	110%	4.044	101%	4.678	117%	4.383	110%
5			3.403	85%			3.705	93%
10	4.046	101%	2.987	75%	4.086	102%	3.228	81%
20			2.674	67%			3.018	75%
30	3.774	94%	2.145	54%	4.079	102%	2.879	72%
45			1.960	49%			2.705	68%
60	3.489	87%	1.791	45%	3.432	86%	2.581	65%
75			1.745	44%			2.489	62%
90	3.015	75%	1.668	42%	3.694	92%	2.412	60%
120			1.488	37%			2.222	56%

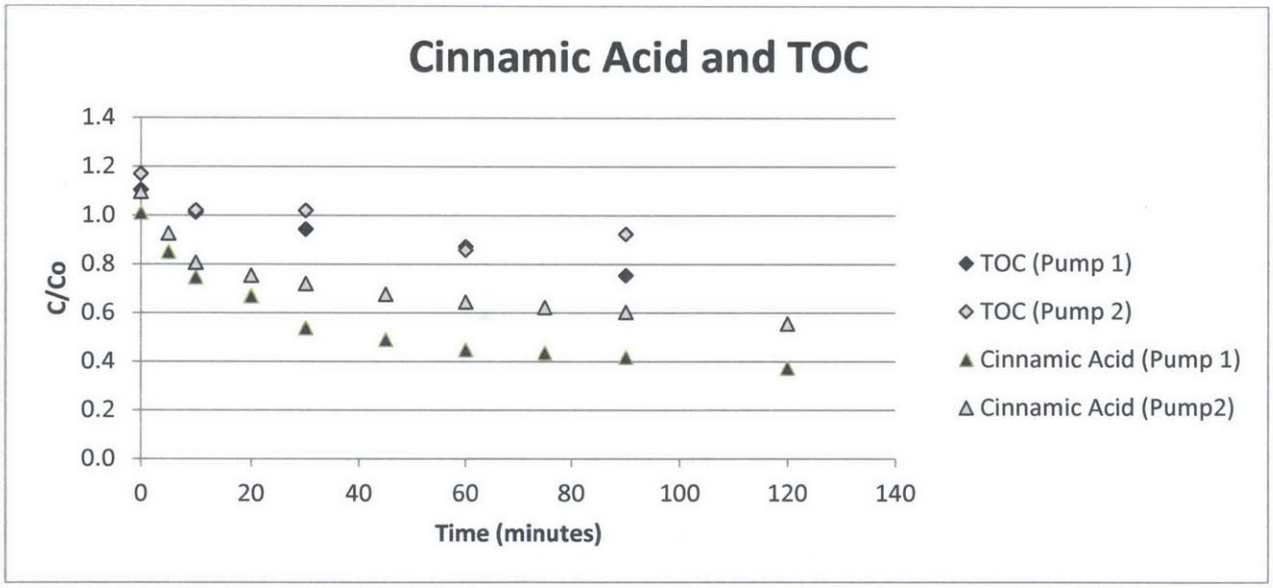

	Pump 1		Pump 2	
Sample	COD (mg/L)	C/Co	COD (mg/L)	C/Co
0	185	1.00	165	1.00
10	195	1.05	190	1.15
30	165	0.89	200	1.21
60	150	0.81	155	0.94
90	150	0.81	120	0.73

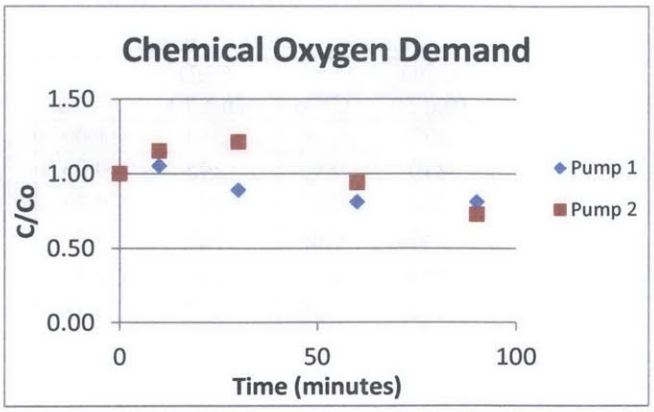

Experiment O

Initial CA Concentration	Catalyst (TiO_2) Concentration	Radiation Power
8 mM of TOC	0.10 g/L	74.2 W/m^2

	Pump 1				Pump 2			
Time (min)	TOC (mM C)		CA (mM C)		TOC (mM C)		CA (mM C)	
0	4.221	53%	7.596	95%	4.034	50%	8.971	112%
5			6.939	87%			7.893	99%
10	3.402	43%	6.025	75%	3.889	49%	6.928	87%
20			4.958	62%			5.707	71%
30	3.230	40%	4.403	55%	3.624	45%	5.173	65%
45			3.829	48%			4.588	57%
60	3.017	38%	4.321	54%	3.684	46%	3.726	47%
75			3.459	43%			3.993	50%
90	3.120	39%	3.274	41%	3.364	42%	4.013	50%
120			3.285	41%			3.726	47%

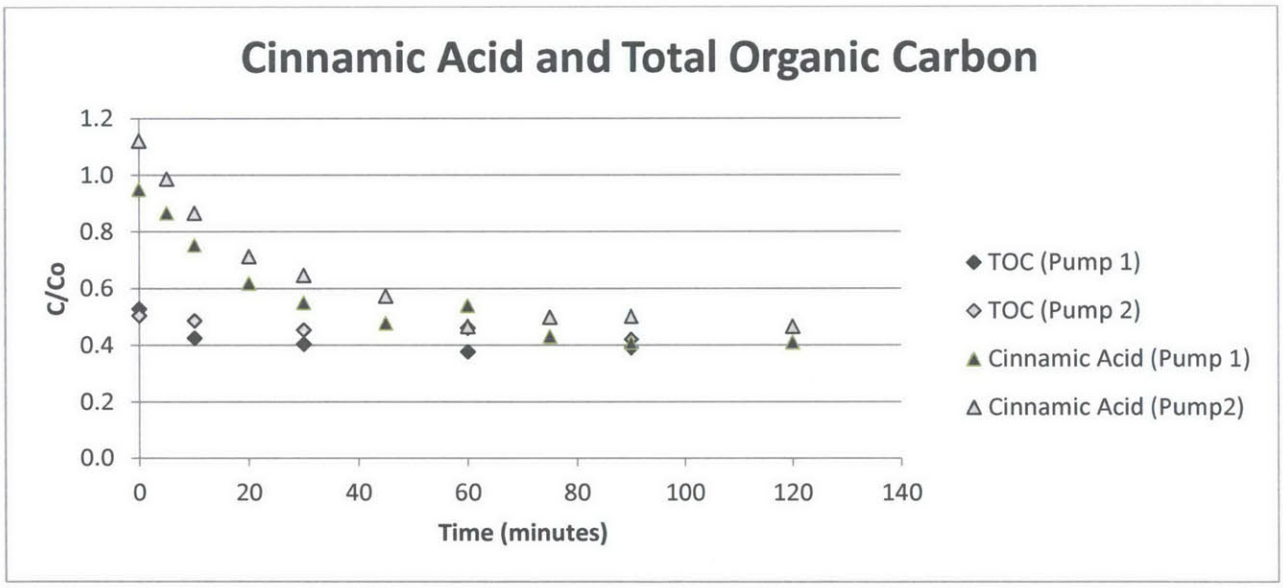

	Pump 1		Pump 2	
Sample	COD (mg/L)	C/Co	COD (mg/L)	C/Co
0	222	1.00	258	1.00
5	210	0.95	245	0.95
10	204	0.92	243	0.94
30	147	0.66	147	0.57
60	135	0.61	135	0.52
90	153	0.69	117	0.45

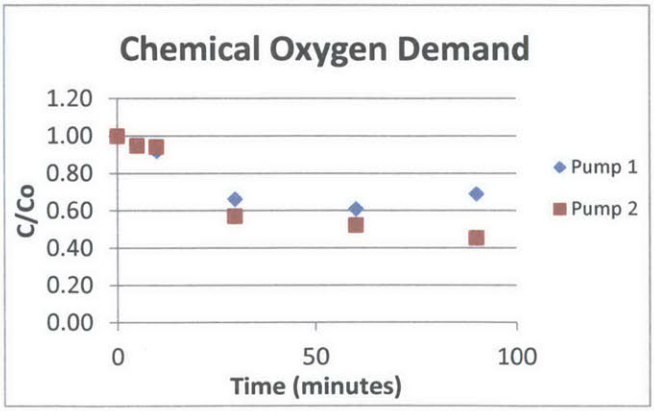

Experiment P

Initial CA Concentration	Catalyst (TiO_2) Concentration	Radiation Power
6 mM of TOC	0.10 g/L	74.2 W/m^2

	Pump 1				Pump 2			
Time (min)	TOC (mM C)		CA (mM C)		TOC (mM C)		CA (mM C)	
0	7.603	127%	8.222	137%	7.873	131%	8.406	140%
5			7.688	128%			7.144	119%
10	7.274	121%	7.010	117%	7.476	125%	6.939	116%
20			6.066	101%			6.220	104%
30	6.624	110%	5.461	91%	6.574	110%	5.563	93%
45			4.681	78%			4.629	77%
60	5.782	96%	3.962	66%	5.982	100%	4.178	70%
75			3.644	61%			3.654	61%
90	6.217	104%	3.346	56%	5.533	92%	3.418	57%
120			2.895	48%			2.977	50%

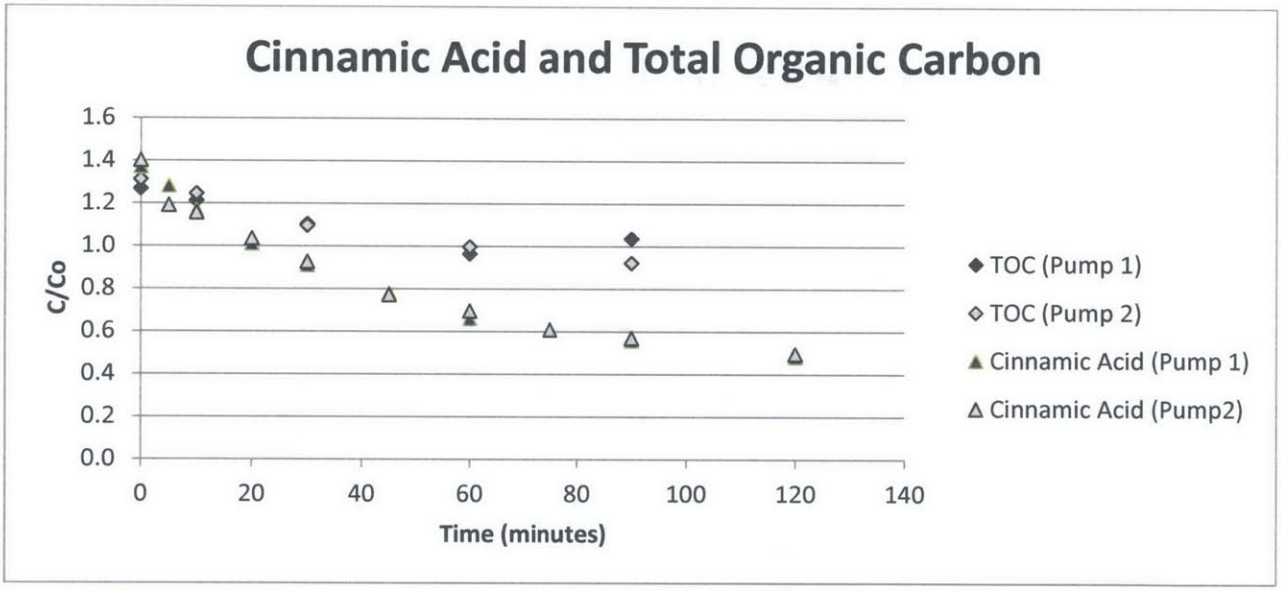

	Pump 1		Pump 2	
Sample	COD (mg/L)	C/Co	COD (mg/L)	C/Co
0	332	1.00	324	1.00
10	296	0.89	292	0.90
20	252	0.76	256	0.79
60	228	0.67	256	0.79
90	256	0.77	248	0.77

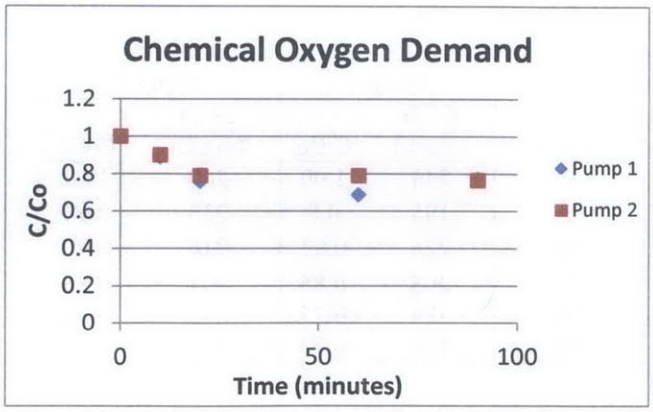

Experiment Q

Initial CA Concentration	Catalyst (TiO_2) Concentration	Radiation Power
4 mM of TOC	0.05 g/L	74.2 W/m^2

	Pump 1				Pump 2			
Time (min)	TOC (mM C)		CA (mM C)		TOC (mM C)		CA (mM C)	
0	5.058	126%	3.120	78%	5.315	133%	3.167	79%
5			2.623	66%			2.684	67%
10	4.923	123%	2.427	61%	5.006	125%	2.438	61%
20			1.919	48%			2.099	52%
30	4.419	110%	1.673	42%	4.716	118%	1.883	47%
45			1.386	35%			1.524	38%
60	4.688	117%	1.201	30%	4.464	112%	1.478	37%
75			1.073	27%			1.134	28%
90	3.929	98%	1.001	25%	3.966	99%	1.032	26%
120			0.862	22%			0.955	24%

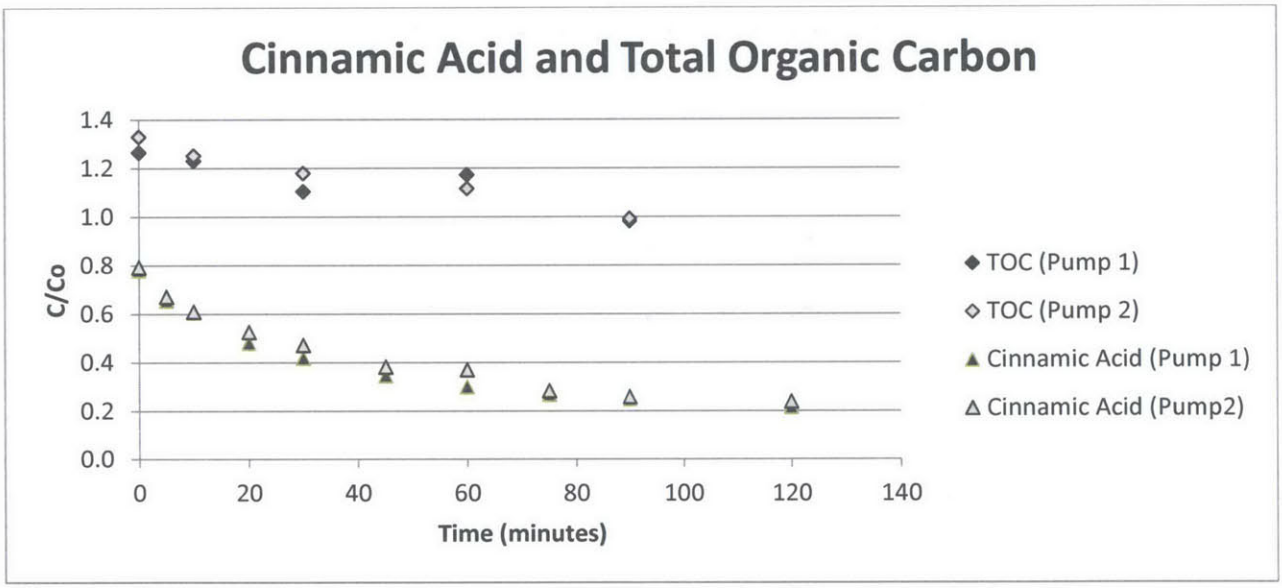

	Pump 1		Pump 2	
Sample	COD (mg/L)	C/Co	COD (mg/L)	C/Co
0	244	1.00	240	1.00
5	195	0.8	235	0.98
10	228	0.93	216	0.90
30	208	0.85	204	0.85
60	184	0.75	212	0.88
90	176	0.72	192	0.8

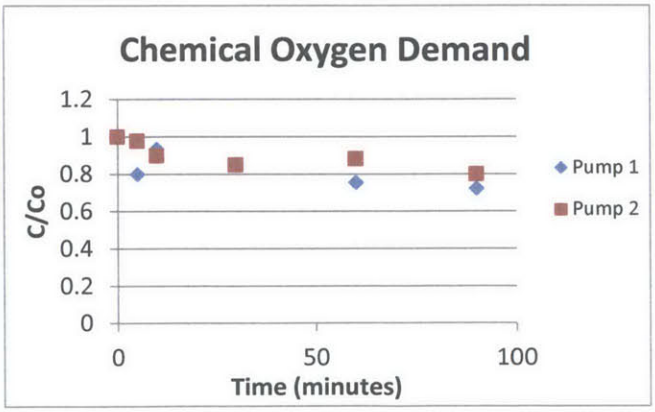

Experiment R

Initial CA Concentration	Catalyst (TiO_2) Concentration	Radiation Power
6 mM of TOC	0.05 g/L	74.2 W/m^2

	Pump 1				Pump 2			
Time (min)	TOC (mM C)		CA (mM C)		TOC (mM C)		CA (mM C)	
0	6.667	111%	6.744	112%	6.442	107%	6.241	104%
5			5.974	100%			5.399	90%
10	8.587	143%	5.091	85%	6.277	105%	5.153	86%
20			4.403	73%			4.516	75%
30	3.799	63%	3.941	66%	6.242	104%	4.065	68%
45			3.449	57%			3.664	61%
60	5.667	94%	2.997	50%	5.785	96%	3.346	56%
75			2.751	46%			3.069	51%
90	5.468	91%	2.371	40%	5.485	91%	2.874	48%
120			2.699	45%			2.207	37%

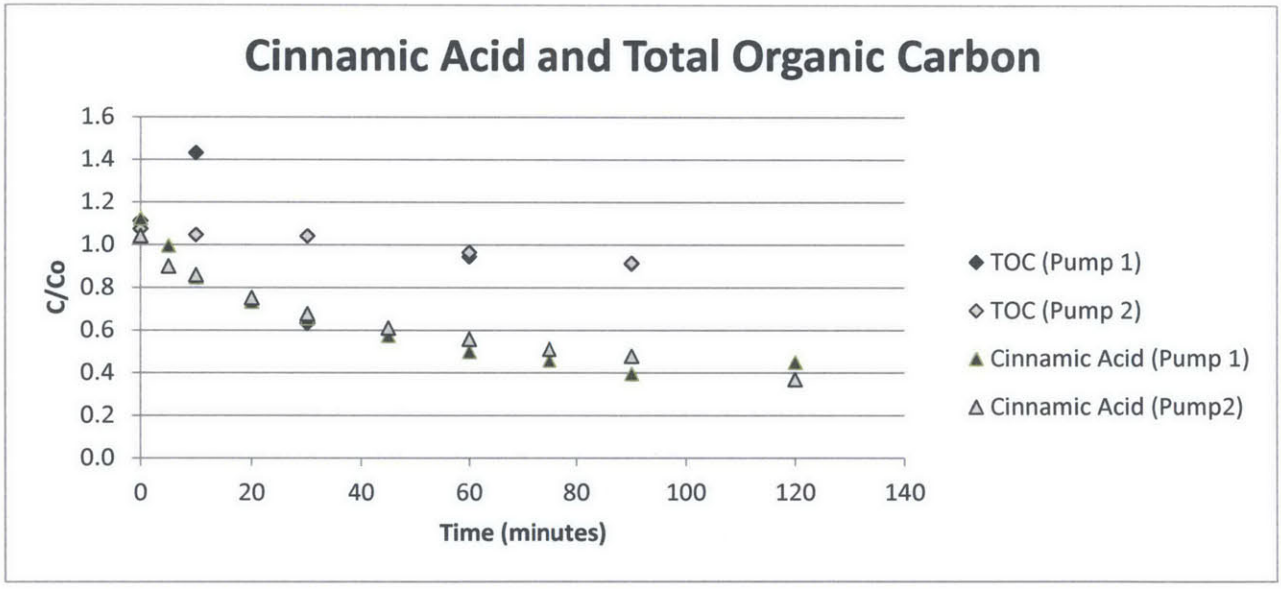

	Pump 1		Pump 2	
Sample	COD (mg/L)	C/Co	COD (mg/L)	C/Co
0	188	1.00	126	1.00
5	180	0.96	230	1.83
10	129	0.69	120	0.95
30	120	0.64	129	1.02
60	108	0.57	117	0.93
90	96	0.51	105	0.83

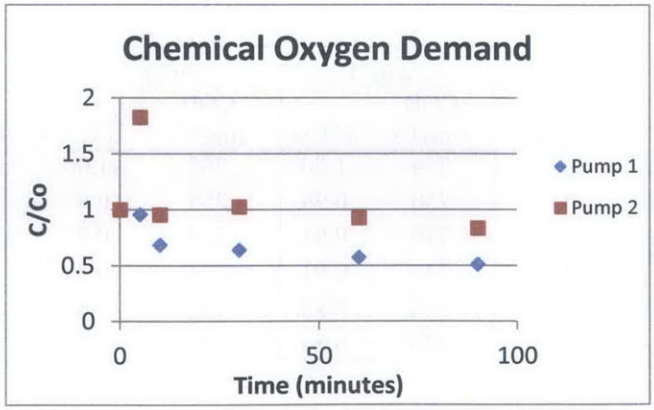

Experiment S

Initial CA Concentration	Catalyst (TiO_2) Concentration	Radiation Power
8 mM of TOC	0.05 g/L	74.2 W/m^2

	Pump 1				Pump 2			
Time (min)	TOC (mM C)		CA (mM C)		TOC (mM C)		CA (mM C)	
0	7.511	94%	--		7.781	97%	--	
5			7.575	95%			7.955	99%
10	7.411	93%	--		7.386	92%	--	
20			6.774	85%			6.980	87%
30	7.011	88%	--		7.026	88%	--	
45			5.461	68%			5.758	72%
60	6.704	84%	--		6.816	85%	--	
75			4.516	56%			4.804	60%
90	6.329	79%	--		6.694	84%	--	
120			3.685	46%			4.198	52%

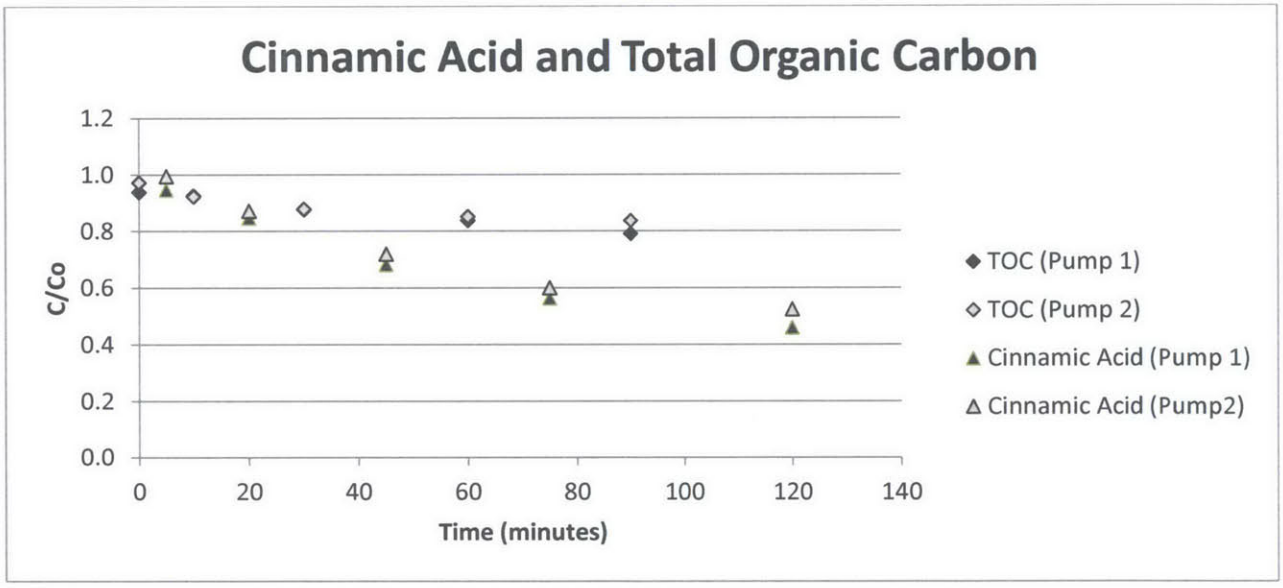

	Pump 1		Pump 2	
Sample	COD (mg/L)	C/Co	COD (mg/L)	C/Co
0	264	1.00	268	1.00
5	250	0.94	255	0.95
10	240	0.91	244	0.91
30	240	0.91	224	0.84
60	224	0.85	184	0.69
90	220	0.83	236	0.88

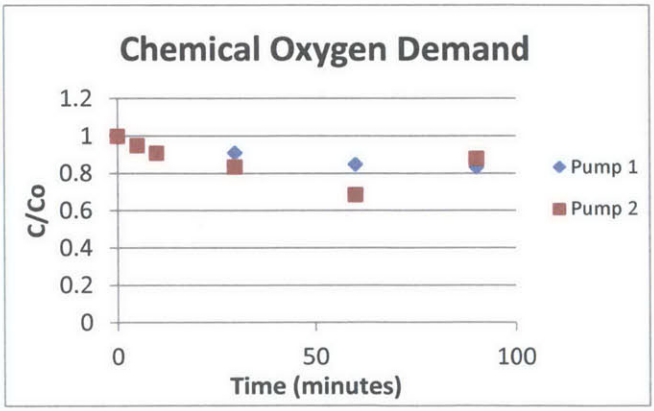

Experiment T

Initial CA Concentration	Catalyst (TiO_2) Concentration	Radiation Power
4 mM of TOC	0.20 g/L	74.2 W/m^2

	Pump 1				Pump 2			
Time (min)	TOC (mM C)		CA (mM C)		TOC (mM C)		CA (mM C)	
0	4.319	108%			4.409	110%		
5			3.028	76%			3.182	80%
10	3.966	99%			3.956	99%		
20			1.919	48%			1.966	49%
30	3.417	85%			3.422	86%		
45			1.032	26%			1.191	30%
60	3.082	77%			3.087	77%		
75			0.754	19%			0.929	23%
90	2.857	71%			2.952	74%		
120			0.565	14%			0.729	18%

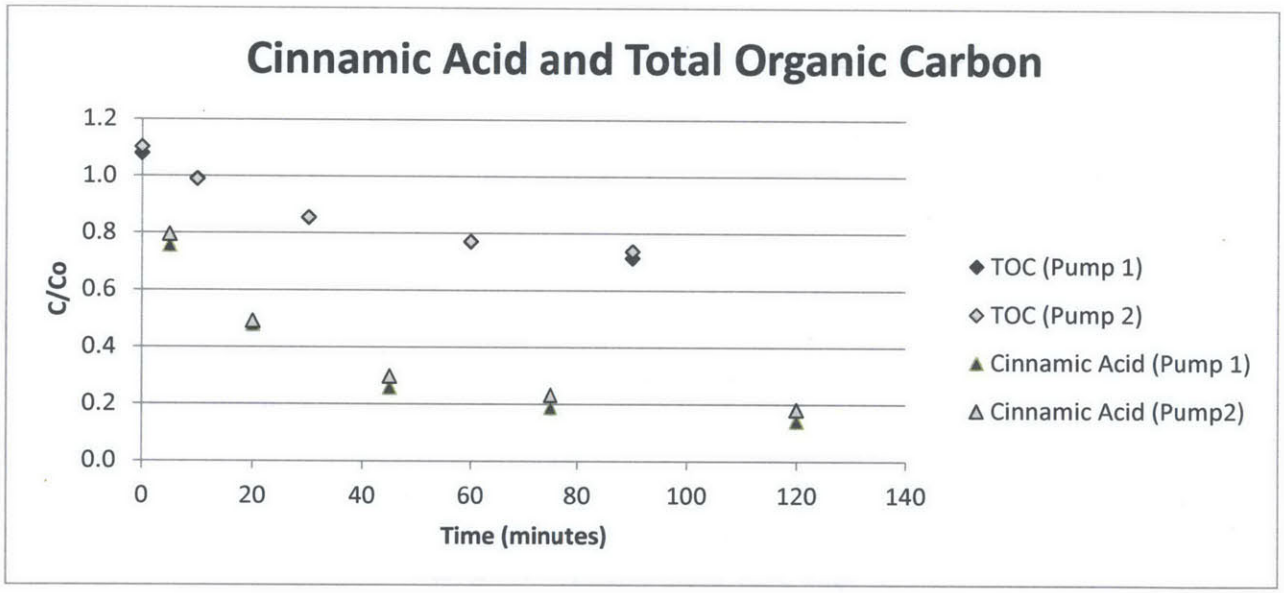

	Pump 1		Pump 2	
Sample	COD (mg/L)	C/Co	COD (mg/L)	C/Co
0	152	1.00	116	1.00
5	135	0.89	150	1.29
10	132	0.87	140	1.21
30	92	0.61	108	0.93
60	44	0.29	100	0.86
90	84	0.55	88	0.76

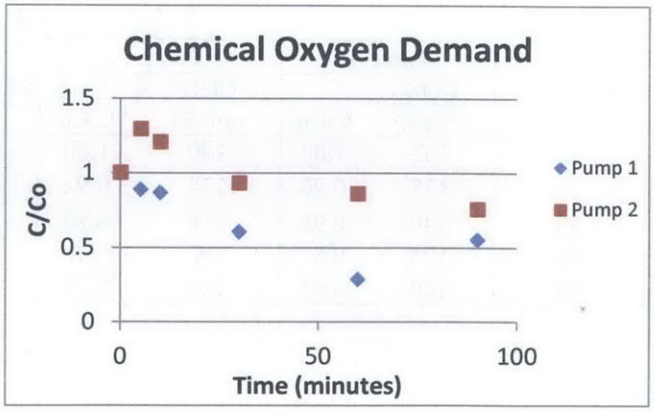

Experiment U

Initial CA Concentration	Catalyst (TiO_2) Concentration	Radiation Power
8 mM of TOC	0.20 g/L	74.2 W/m^2

	Pump 1				Pump 2			
Time (min)	TOC (mM C)		CA (mM C)		TOC (mM C)		CA (mM C)	
0	9.522	119%	8.170	102%	7.786	97%	8.848	111%
5			6.949	87%			8.324	104%
10	7.191	90%	6.138	77%	7.568	95%	6.415	80%
20			5.491	69%			5.183	65%
30	7.293	91%	4.393	55%	7.159	89%	4.650	58%
45			3.531	44%			3.726	47%
60	6.444	81%	4.178	52%	6.579	82%	4.455	56%
75			2.422	30%			2.853	36%
90	6.242	78%	2.433	30%	5.950	74%	2.607	33%
120			1.796	22%			2.320	29%

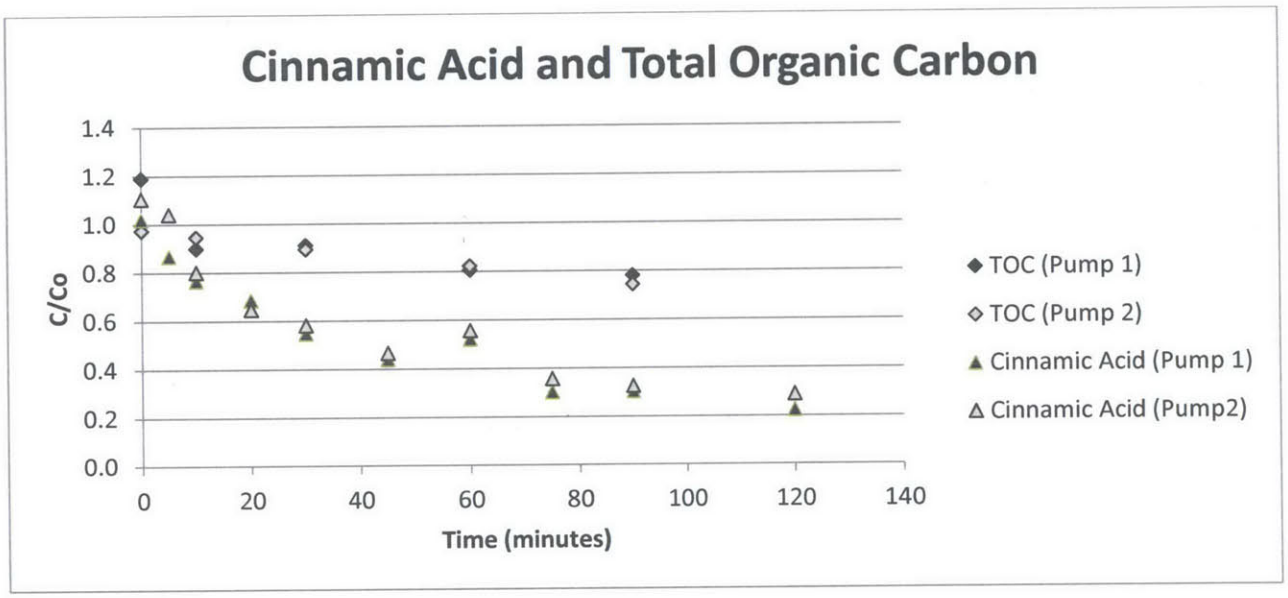

	Pump 1		Pump 2	
Sample	COD (mg/L)	C/Co	COD (mg/L)	C/Co
0	153	1.00	140	1.00
10	138	0.90	128	0.92
30	140	0.91	118	0.85
60	125	0.82	98	0.70
90	100	0.65	108	0.77

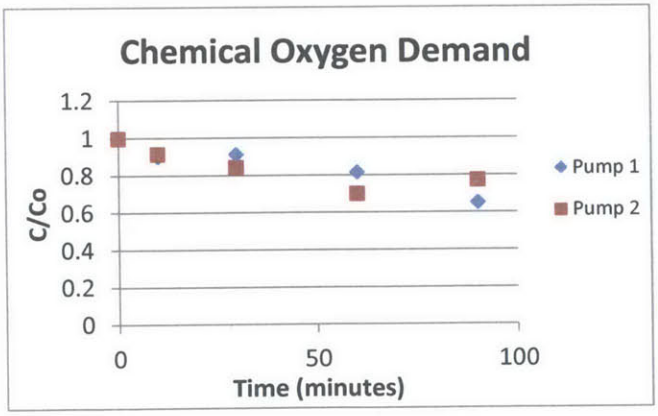

Experiment V

Initial CA Concentration	Catalyst (TiO_2) Concentration	Radiation Power
6 mM of TOC	0.20 g/L	74.2 W/m^2

	Pump 1				Pump 2			
Time (min)	TOC (mM C)		CA (mM C)		TOC (mM C)		CA (mM C)	
0	7.351	123%	6.241	104%	7.556	126%	6.354	106%
5			4.968	83%			5.389	90%
10	7.111	119%	4.147	69%	7.743	129%	4.598	77%
20			3.428	57%			3.634	61%
30	6.886	115%	2.802	47%	7.061	118%	2.966	49%
45			2.094	35%			2.289	38%
60	6.010	100%	1.540	26%	6.304	105%	1.765	29%
75			1.304	22%			1.447	24%
90	5.530	92%	1.047	17%	5.358	89%	1.304	22%
120			0.883	15%			1.119	19%

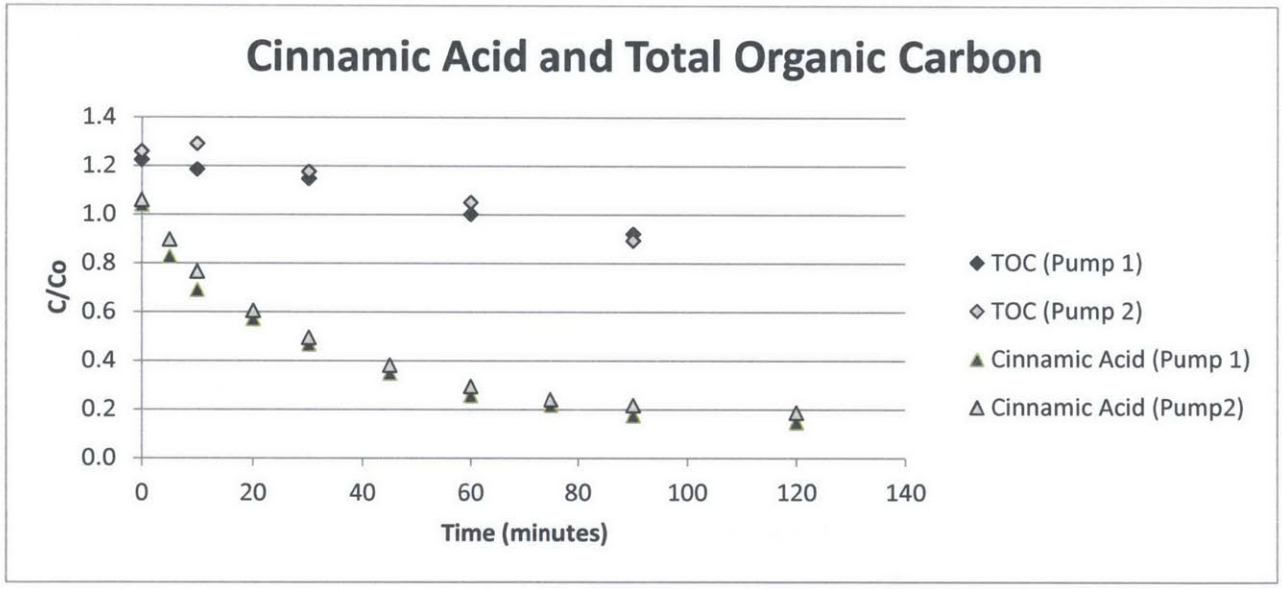

	Pump 1		Pump 2	
Sample	COD (mg/L)	C/Co	COD (mg/L)	C/Co
0	193	1.00	218	1.00
10	185	0.96	208	0.95
30	175	0.91	197	0.90
60	150	0.78	163	0.75
90	118	0.61	147	0.67

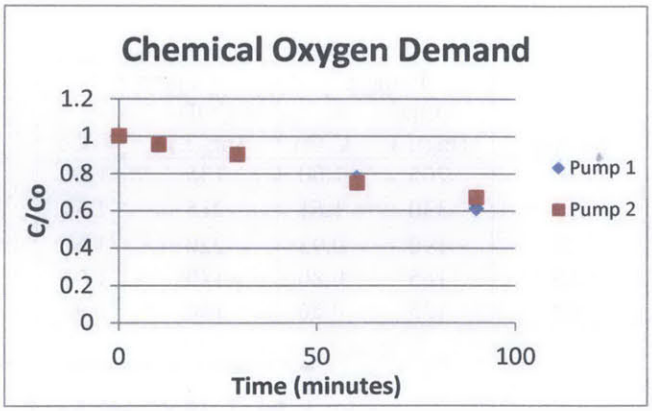

Experiment W

Initial CA Concentration	Catalyst (TiO_2) Concentration	Radiation Power
4 mM of TOC	0.20 g/L	46.2 W/m^2

	Pump 1				Pump 2			
Time (min)	TOC (mM C)		CA (mM C)		TOC (mM C)		CA (mM C)	
0	3.762	94%	4.115	103%	3.877	97%	4.104	103%
5			3.370	84%			3.560	89%
10	3.697	92%	3.087	77%	3.772	94%	2.846	71%
20			2.250	56%			2.481	62%
30	3.422	86%	1.916	48%	3.322	83%	1.973	49%
45			1.356	34%			1.664	42%
60	2.987	75%	1.146	29%	3.080	77%	1.479	37%
75			1.033	26%			1.351	34%
90	2.790	70%	1.115	28%	2.830	71%	1.120	28%
120			0.832	21%			1.161	29%

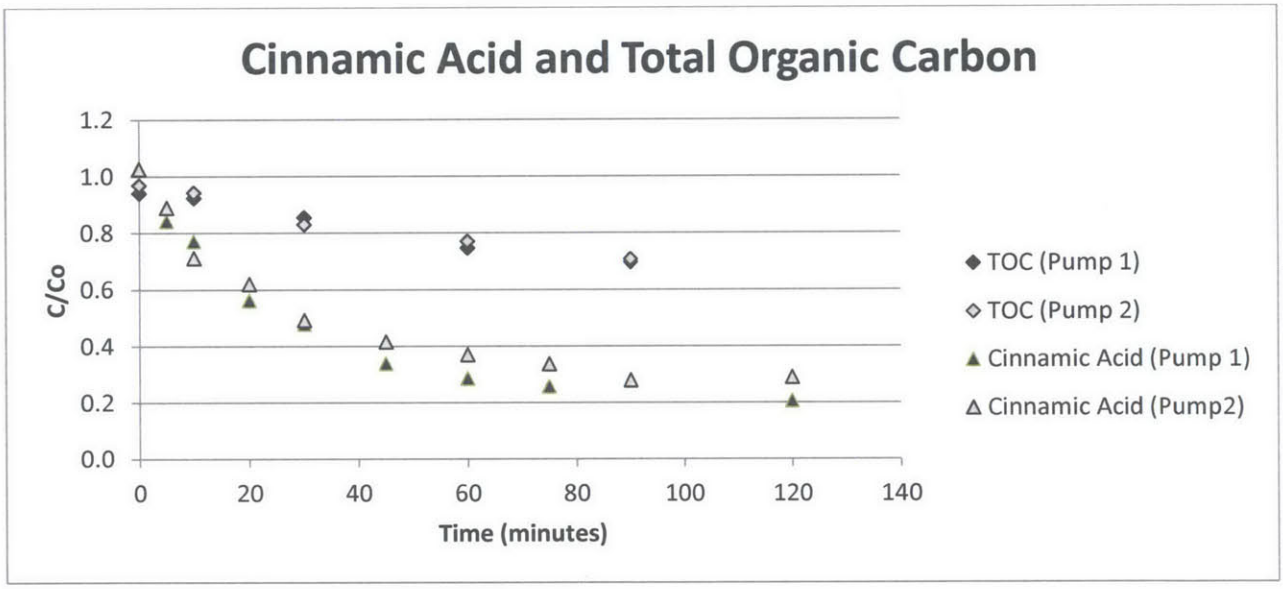

	Pump 1		Pump 2	
Sample	COD (mg/L)	C/Co	COD (mg/L)	C/Co
0	205	1.00	135	1.00
10	330	1.61	215	1.59
30	190	0.93	220	1.62
60	165	0.80	140	1.03
90	135	0.66	130	0.96

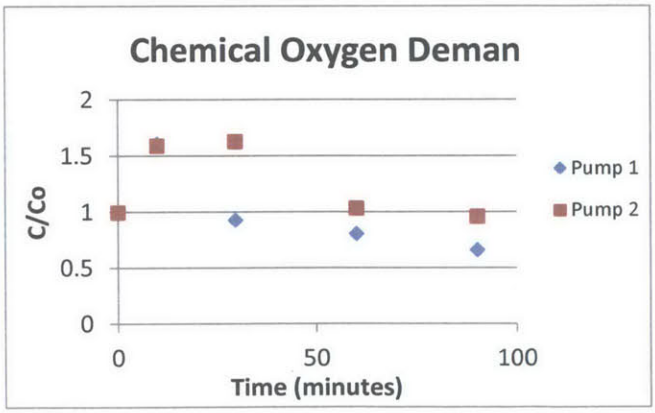

Experiment X

Initial CA Concentration	Catalyst (TiO_2) Concentration	Radiation Power
8 mM of TOC	0.20 g/L	46.2 W/m^2

	Pump 1				Pump 2			
Time (min)	TOC (mM C)		CA (mM C)		TOC (mM C)		CA (mM C)	
0	4.513	56%	8.519	106%	7.978	100%	8.622	108%
5			7.616	95%			7.842	98%
10	8.642	108%	7.082	89%	7.651	96%	7.072	88%
20			6.107	76%			6.333	79%
30	6.884	86%	5.286	66%	6.796	85%	5.584	70%
45			4.578	57%			4.927	62%
60	5.837	73%	3.859	48%	5.875	73%	4.321	54%
75			3.346	42%			3.788	47%
90	5.275	66%	2.977	37%	5.290	66%	3.387	42%
120			2.402	30%			2.802	35%

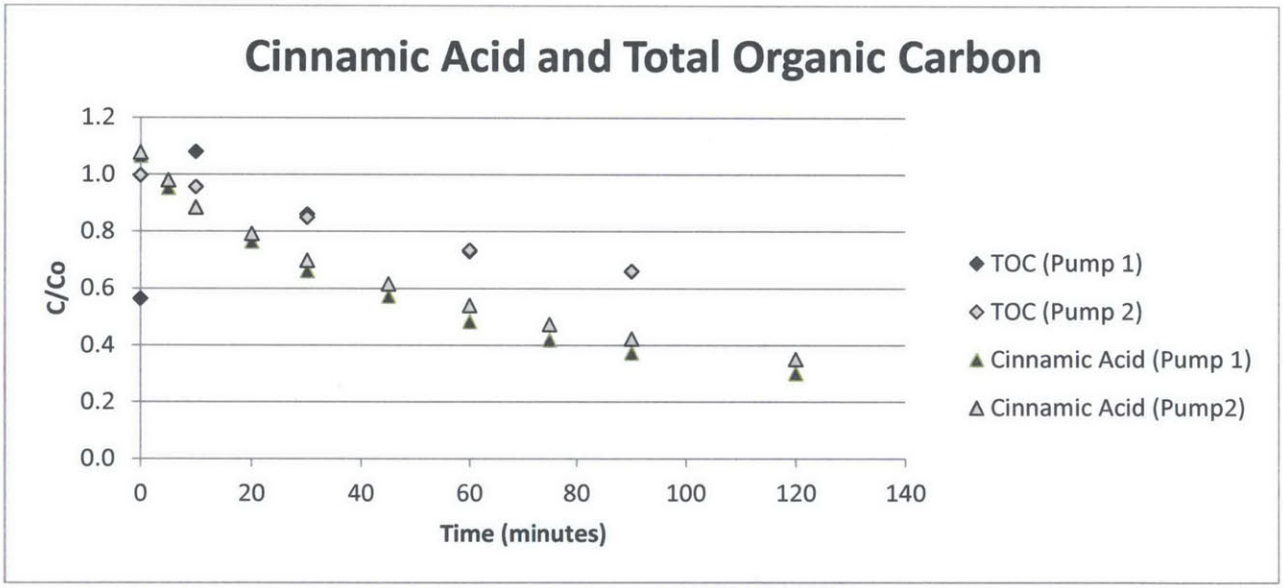

	Pump 1		Pump 2	
Sample	COD (mg/L)	C/Co	COD (mg/L)	C/Co
0	370	1.00	350	1.00
10	335	0.91	350	1.00
30	320	0.86	320	0.91
60	305	0.82	315	0.90
90	265	0.72	270	0.77

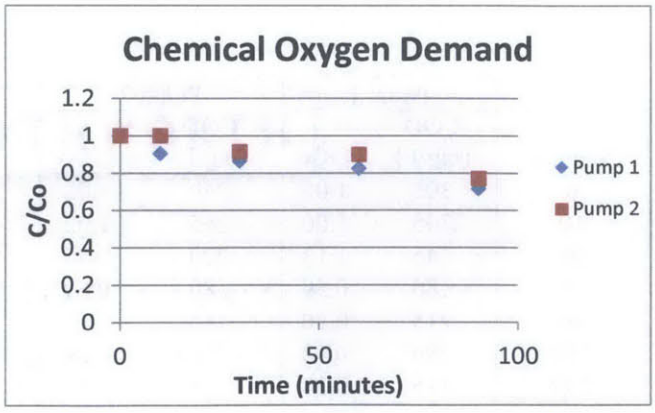

Experiment Z

Initial CA Concentration	Catalyst (TiO_2) Concentration	Radiation Power
6 mM of TOC	0.20 g/L	46.2 W/m^2

	Pump 1				Pump 2			
Time (min)	TOC (mM C)		CA (mM C)		TOC (mM C)		CA (mM C)	
0	6.174	103%	6.302	105%	5.780	96%	6.241	104%
5			5.266	88%			5.563	93%
10	6.057	101%	4.783	80%	5.982	100%	5.153	86%
20			4.054	68%			4.752	79%
30	5.865	98%	5.337	89%	5.343	89%	3.931	66%
45			2.771	46%			3.490	58%
60	4.943	82%	2.422	40%	5.006	83%	3.202	53%
75			2.186	36%			2.833	47%
90	3.999	67%	1.868	31%	4.546	76%	2.884	48%
120			1.909	32%			2.905	48%
150	3.797	63%	2.155	36%	4.074	68%	2.587	43%
180			1.642	27%			3.408	57%
240	3.205	53%	1.468	24%	3.939	66%	2.309	38%

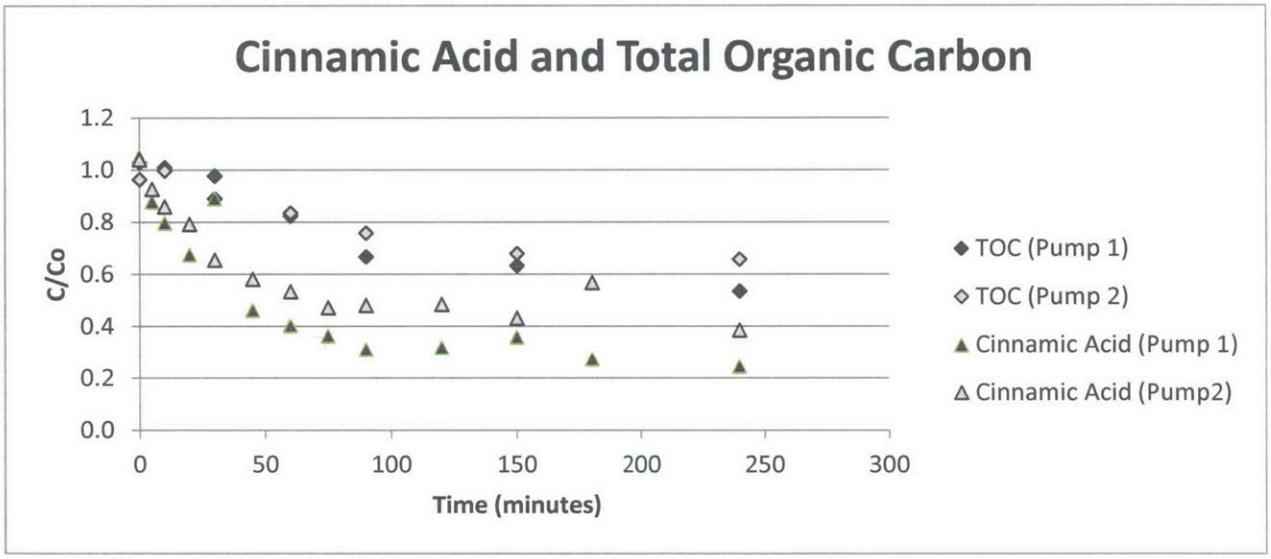

	Pump 1		Pump 2	
Sample	COD (mg/L)	C/Co	COD (mg/L)	C/Co
0	305	1.00	260	1.00
10	305	1.00	265	1.02
30	345	1.13	220	0.85
60	180	0.59	180	0.69
90	215	0.70	165	0.63
150	280	0.92	75	0.29
240	115	0.38	125	0.48

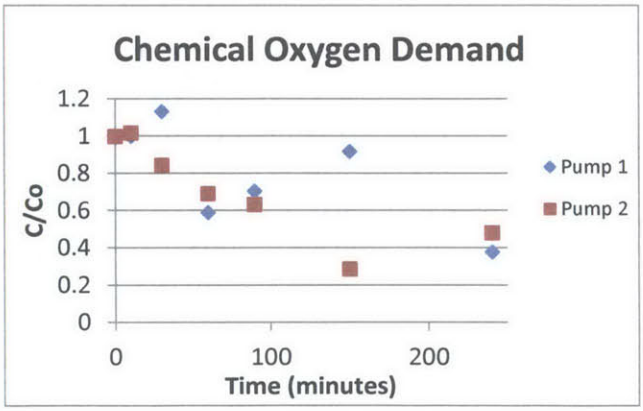

APPENDIX D: Initial Concentration Error

The following pages contain tables displaying the error between the measured initial and the target concentrations for the methanol and cinnamic acid experiments. These values are shown as a percentage and were calculated according to the following equation:

$$Error = \left|\frac{(Target - Measured)}{Target}\right| \times 100\%$$

Initial Concentration Error for Methanol Experiments

Experiment		Methanol Conc	Initial TOC Error	Initial Methanol Error
Label	Pump	[mM Carbon]	[% Error]	[% Error]
A	Pump 1	100	N/A*	0.49%
	Pump 2	100	N/A*	0.47%
B	Pump 1	100	N/A*	0.03%
	Pump 2	100	N/A*	0.50%
C	Pump 1	100	N/A*	0.03%
	Pump 2	100	N/A*	0.14%
D	Pump 1	100	N/A*	0.01%
	Pump 2	100	N/A*	0.03%
E	Pump 1	200	N/A*	0.07%
	Pump 2	200	N/A*	0.01%
F	Pump 1	50	N/A*	0.00%
	Pump 2	50	N/A*	0.07%
G	Pump 1	4	117.99%***	1.75%
	Pump 2	4	215.18%***	0.87%
H	Pump 1	4	31.49%	0.17%
	Pump 2	4	27.39%	0.00%
I	Pump 1	8	47.63%	0.61%
	Pump 2	8	35.06%	0.00%
J	Pump 1	6	59.72%	0.93%
	Pump 2	6	N/A**	N/A**
K	Pump 1	4	335.42%***	0.00%
	Pump 2	4	317.51%***	1.05%
L	Pump 1	8	3.19%	0.00%
	Pump 2	8	1.13%	0.09%
M	Pump 1	6	59.55%	1.63%
	Pump 2	6	46.51%	0.00%
		Average	34.63%	0.36%
		Std. Deviation	21.61%	0.52%

* The initial TOC concentration error for methanol was not calculated for Experiments A through F due to the fact that the samples were not tested for TOC content.

** The initial TOC and Methanol concentration errors were not calculated for Experiment J, Pump 2 due to the fact that the time zero samples could not be tested.

*** Average and standard deviation computations do not include these outliers.

Initial Concentration Error for Cinnamic Acid Experiments

Experiment		CA Conc	Initial TOC Error	Initial CA Error
Label	Pump	[mM Carbon]	[% Error]	[% Error]
N	Pump 1	4	-10.4%	-1.1%
	Pump 2	4	-17.0%	-9.6%
O	Pump 1	8	47.2%	5.1%
	Pump 2	8	49.6%	-12.1%
P	Pump 1	6	-26.7%	-37.0%
	Pump 2	6	-31.2%	-40.1%
Q	Pump 1	4	-26.4%	22.0%
	Pump 2	4	-32.9%	20.8%
R	Pump 1	6	-11.1%	-12.4%
	Pump 2	6	-7.4%	-4.0%
S	Pump 1	8	6.1%	N/A*
	Pump 2	8	2.7%	N/A*
T	Pump 1	4	-8.0%	N/A*
	Pump 2	4	-10.2%	N/A*
U	Pump 1	8	-19.0%	-2.1%
	Pump 2	8	2.7%	-10.6%
V	Pump 1	6	-22.5%	-4.0%
	Pump 2	6	-25.9%	-5.9%
W	Pump 1	4	6.0%	-2.9%
	Pump 2	4	3.1%	-2.6%
X	Pump 1	8	43.6%	-6.5%
	Pump 2	8	0.3%	-7.8%
Z	Pump 1	6	-2.9%	-5.0%
	Pump 2	6	3.7%	-4.0%
		Average	-3.6%	-6.0%
		Std. Deviation	23.0%	14.4%

* The initial concentration error for cinnamic acid was not calculated for Experiments S and T due to the fact that the time zero samples could not be tested for absorbance.

APPENDIX E: Methanol Decay Rate Constants and R^2

The following pages contain tables including the decay rate constants and the R^2 values for the 0^{th}, 1^{st}, and 2^{nd} order rate kinetic linearizations. These decay rate constants were determined according to the processes detailed in Section 4.1.

The general linear regression equations are available below as a guide to the reader. The slope of these equations is equivalent to 0^{th}, 1^{st}, and 2^{nd} order decay rate constants, respectively.

- Zero Order Kinetics

$$[A] = -kt + [A]_0 \qquad \text{Eq. 4-2}$$

- First Order Kinetics

$$ln[A] = -kt + ln[A]_0 \qquad \text{Eq. 4-3}$$

- Second Order Kinetics

$$\frac{1}{[A]} = \frac{1}{[A]_0} + kt \qquad \text{Eq. 4-4}$$

Methanol Decay Rate Constants and R^2 values for 0^{th}, 1^{st}, and 2^{nd} Order Kinetics

Experiment		Zero Order		First Order		Second Order	
Label	Pump	k	R^2	k	R^2	k	R^2
A	Pump 1	-2.51E-06	2.31E-02	-2.51E-06	2.32E-02	-2.52E-08	2.32E-02
	Pump 2	3.47E-06	1.03E-01	3.47E-06	1.03E-01	3.49E-08	1.03E-01
B	Pump 1	2.68E-06	6.98E-02	2.68E-06	6.97E-02	2.69E-08	6.97E-02
	Pump 2	5.98E-06	4.46E-01	5.98E-06	4.46E-01	6.01E-08	4.46E-01
C	Pump 1	1.56E-03	9.96E-01	1.63E-03	9.95E-01	1.71E-05	9.93E-01
	Pump 2	7.28E-04	9.80E-01	7.45E-04	9.81E-01	7.63E-06	9.83E-01
D	Pump 1	2.71E-04	1.00E+00	2.73E-04	1.00E+00	2.75E-06	1.00E+00
	Pump 2	1.41E-04	9.58E-01	1.41E-04	9.58E-01	1.42E-06	9.59E-01
E	Pump 1	8.93E-05	9.17E-01	8.94E-05	9.17E-01	4.49E-07	9.17E-01
	Pump 2	5.99E-05	9.96E-01	6.00E-05	9.96E-01	3.00E-07	9.96E-01
F	Pump 1	1.67E-04	7.28E-01	1.68E-04	7.27E-01	3.37E-06	7.27E-01
	Pump 2	2.15E-04	7.32E-01	2.17E-04	7.31E-01	4.37E-06	7.29E-01
G	Pump 1	1.94E-03	9.81E-01	2.05E-03	9.80E-01	5.49E-04	9.80E-01
	Pump 2	5.83E-04	4.98E-01	5.94E-04	4.94E-01	1.53E-04	4.90E-01
H	Pump 1	3.98E-03	9.23E-01	4.45E-03	9.34E-01	1.25E-03	9.43E-01
	Pump 2	1.24E-03	8.16E-01	1.28E-03	8.19E-01	3.30E-04	8.22E-01
I	Pump 1	4.08E-03	9.39E-01	4.55E-03	9.37E-01	6.39E-04	9.33E-01
	Pump 2	3.65E-03	8.21E-01	4.01E-03	8.07E-01	5.53E-04	7.92E-01
J	Pump 1	3.20E-03	9.70E-01	3.46E-03	9.75E-01	6.30E-04	9.78E-01
	Pump 2	1.33E-03	9.45E-01	1.37E-03	9.45E-01	2.35E-04	9.44E-01
K	Pump 1	1.17E-02	9.88E-01	1.95E-02	9.91E-01	8.88E-03	9.57E-01
	Pump 2	4.87E-03	9.79E-01	5.82E-03	9.76E-01	1.77E-03	9.68E-01
L	Pump 1	2.31E-03	9.75E-01	2.49E-03	9.77E-01	3.36E-04	9.79E-01
	Pump 2	1.58E-03	9.97E-01	1.66E-03	9.98E-01	2.17E-04	9.98E-01
M	Pump 1	2.48E-03	8.40E-01	2.67E-03	8.49E-01	4.78E-04	8.58E-01
	Pump 2	3.63E-04	3.74E-01	3.70E-04	3.75E-01	6.27E-05	3.76E-01

Total Organic Carbon Decay Rate Constants and R^2 values for 0^{th}, 1^{st}, and 2^{nd} Order Kinetics

Experiment		Zero Order		First Order		Second Order	
Label	Pump	k	R^2	k	R^2	k	R^2
A*	Pump1	N/A	N/A	N/A	N/A	N/A	N/A
	Pump2	N/A	N/A	N/A	N/A	N/A	N/A
B*	Pump1	N/A	N/A	N/A	N/A	N/A	N/A
	Pump2	N/A	N/A	N/A	N/A	N/A	N/A
C*	Pump1	N/A	N/A	N/A	N/A	N/A	N/A
	Pump2	N/A	N/A	N/A	N/A	N/A	N/A
D*	Pump1	N/A	N/A	N/A	N/A	N/A	N/A
	Pump2	N/A	N/A	N/A	N/A	N/A	N/A
E*	Pump1	N/A	N/A	N/A	N/A	N/A	N/A
	Pump2	N/A	N/A	N/A	N/A	N/A	N/A
F*	Pump1	N/A	N/A	N/A	N/A	N/A	N/A
	Pump2	N/A	N/A	N/A	N/A	N/A	N/A
G	Pump1	1.34E-03	1.07E-01	1.35E-03	9.10E-02	1.59E-04	7.61E-02
	Pump2	2.76E-03	8.78E-01	2.99E-03	8.93E-01	2.59E-04	9.06E-01
H	Pump1	2.07E-03	1.31E-01	2.18E-03	1.49E-01	4.36E-04	1.68E-01
	Pump2	2.59E-03	4.16E-02	2.65E-03	3.56E-02	5.25E-04	2.87E-02
I	Pump1	-1.16E-02	8.72E-01	-9.19E-03	8.51E-01	-1.77E-03	8.27E-01
	Pump2	1.00E-03	2.56E-02	1.02E-03	3.26E-02	2.01E-04	4.07E-02
J	Pump1	0.00E+00	0.00E+00	0.00E+00	0.00E+00	0.00E+00	0.00E+00
	Pump2	0.00E+00	0.00E+00	0.00E+00	0.00E+00	0.00E+00	0.00E+00
K	Pump1	-3.99E-04	6.21E-02	-4.13E-04	6.29E-02	-2.45E-05	6.37E-02
	Pump2	-3.70E-04	1.29E-01	-3.68E-04	1.33E-01	-2.21E-05	1.38E-01
L	Pump1	-1.06E-03	5.77E-01	-1.05E-03	5.68E-01	-1.27E-04	5.59E-01
	Pump2	-6.85E-04	4.49E-01	-6.72E-04	4.50E-01	-1.70E-04	4.47E-01
M	Pump1	2.11E-03	1.47E-01	2.00E-03	1.52E-01	7.71E-04	1.57E-01
	Pump2	-7.79E-04	2.07E-02	-8.28E-04	1.87E-02	-2.74E-04	1.68E-02

*TOC decay rate constants were not were not calculated for Experiments A-F due to the fact that TOC measurements were not taken.

APPENDIX F: Cinnamic Acid Decay Rate Constants and R^2

The following pages contain tables including the decay rate constants and the R^2 values for the 0^{th}, 1^{st}, and 2^{nd} order rate kinetic linearizations. These decay rate constants were determined according to the processes detailed in Section 4.1.

The general linear regression equations are available below as a guide to the reader. The slope of these equations is equivalent to 0^{th}, 1^{st}, and 2^{nd} order decay rate constants, respectively.

- Zero Order Kinetics

$$[A] = -kt + [A]_0 \qquad \text{Eq. 4-2}$$

- First Order Kinetics

$$ln[A] = -kt + ln[A]_0 \qquad \text{Eq. 4-3}$$

- Second Order Kinetics

$$\frac{1}{[A]} = \frac{1}{[A]_0} + kt \qquad \text{Eq. 4-4}$$

Cinnamic Acid Decay Rate Constants and R^2 values for 0^{th}, 1^{st}, and 2^{nd} Order Kinetics

Test		Zero Order k	R^2	First Order k	R^2	Second Order k	R^2
N	Pump 1	4.57E-03	0.756	7.74E-03	0.848	3.43E-03	0.921
	Pump 2	3.20E-03	0.725	4.67E-03	0.809	1.60E-03	0.882
O	Pump 1	4.38E-03	0.741	6.89E-03	0.810	1.50E-03	0.863
	Pump 2	4.42E-03	0.721	7.13E-03	0.784	1.34E-03	0.828
P	Pump 1	5.43E-03	0.894	8.96E-03	0.959	1.92E-03	0.994
	Pump 2	5.12E-03	0.894	8.59E-03	0.959	1.82E-03	0.993
Q	Pump 1	5.58E-03	0.818	1.06E-02	0.922	7.11E-03	0.985
	Pump 2	5.47E-03	0.859	1.01E-02	0.941	6.38E-03	0.977
R	Pump 1	4.85E-03	0.775	8.19E-03	0.843	2.18E-03	0.875
	Pump 2	4.81E-03	0.902	7.88E-03	0.968	2.20E-03	0.984
S	Pump 1	4.46E-03	0.947	6.33E-03	0.982	1.23E-03	0.998
	Pump 2	4.05E-03	0.919	5.58E-03	0.957	9.95E-04	0.983
T	Pump 1	6.37E-03	0.754	1.42E-02	0.898	1.27E-02	0.986
	Pump 2	5.89E-03	0.737	1.21E-02	0.877	9.14E-03	0.973
U	Pump 1	5.99E-03	0.864	1.21E-02	0.943	3.45E-03	0.946
	Pump 2	5.76E-03	0.792	1.10E-02	0.898	2.69E-03	0.945
V	Pump 1	6.54E-03	0.810	1.66E-02	0.954	8.41E-03	0.992
	Pump 2	6.53E-03	0.812	1.50E-02	0.938	6.53E-03	0.991
W	Pump 1	6.09E-03	0.767	1.32E-02	0.885	8.04E-03	0.954
	Pump 2	5.54E-03	0.764	1.08E-02	0.872	5.68E-03	0.937
X	Pump 1	5.85E-03	0.908	1.06E-02	0.980	2.46E-03	0.999
	Pump 2	5.43E-03	0.912	9.25E-03	0.978	1.97E-03	0.999
Z	Pump 1	2.86E-03	0.651	5.89E-03	0.760	2.18E-03	0.854
	Pump 2	2.08E-03	0.600	3.42E-03	0.661	9.57E-04	0.710

Total Organic Carbon Decay Rate Constants and R^2 values for 0^{th}, 1^{st}, and 2^{nd} Order Kinetics

Test		Zero Order k	R^2	First Order k	R^2	Second Order k	R^2
N	Pump1	3.21E-03	9.68E-01	3.89E-03	0.977	1.08E-03	0.978
	Pump2	2.23E-03	0.672	2.59E-03	0.671	6.48E-04	0.666
O	Pump1	2.29E-03	5.50E-01	2.72E-03	0.574	7.75E-04	0.598
	Pump2	1.59E-03	8.55E-01	1.74E-03	0.859	4.74E-04	0.861
P	Pump1	2.28E-03	7.41E-01	2.58E-03	0.730	3.86E-04	0.715
	Pump2	3.29E-03	9.48E-01	3.92E-03	0.965	6.00E-04	0.980
Q	Pump1	2.09E-03	7.61E-01	2.37E-03	0.759	5.32E-04	0.756
	Pump2	2.59E-03	9.73E-01	3.00E-03	0.977	6.57E-04	0.977
R	Pump1	3.15E-03	1.96E-01	3.01E-03	0.139	4.24E-04	0.083
	Pump2	1.64E-03	9.72E-01	1.78E-03	0.971	3.00E-04	0.970
S	Pump1	1.76E-03	9.89E-01	1.91E-03	0.992	2.77E-04	0.994
	Pump2	1.42E-03	8.52E-01	1.54E-03	0.865	2.16E-04	0.878
T	Pump1	3.64E-03	9.15E-01	4.50E-03	0.942	1.30E-03	0.964
	Pump2	3.49E-03	8.70E-01	4.31E-03	0.900	1.22E-03	0.926
U	Pump1	2.97E-03	6.47E-01	3.75E-03	0.696	5.04E-04	0.746
	Pump2	2.60E-03	1.00E+00	2.96E-03	0.998	4.35E-04	0.994
V	Pump1	2.82E-03	9.85E-01	3.24E-03	0.984	5.10E-04	0.982
	Pump2	3.46E-03	9.70E-01	4.02E-03	0.964	6.24E-04	0.954
W	Pump1	3.06E-03	9.82E-01	3.53E-03	0.986	1.09E-03	0.988
	Pump2	3.04E-03	9.56E-01	3.54E-03	0.970	1.07E-03	0.981
X	Pump1	2.66E-03	7.71E-02	1.42E-03	0.044	1.47E-04	0.018
	Pump2	3.83E-03	9.81E-01	4.68E-03	0.992	7.25E-04	0.998
Z	Pump1	2.13E-03	8.82E-01	2.90E-03	0.919	6.58E-04	0.950
	Pump2	1.49E-03	8.64E-01	1.80E-03	0.892	3.79E-04	0.916

APPENDIX G: Proposed Reaction Kinetics Mathematical Model

The following pages contain documentation provided by Dr. Javier Marugán from Universidad Rey Juan Carlos in Spain. The content herein corresponds to a mathematical model of the reaction kinetics of a pollutant undergoing photocatalysis, and was developed by Dr. Javier Marugán.

Proposed reaction scheme based on hydroxyl radical generation and strong adsorption

STEP	REACTION	RATE
Activation	$TiO_2 + hv \rightarrow TiO_2 + e^- + h^+$	r_g
Recombination	$e^- + h^+ \rightarrow$ heat	$k_2[e^-][h^+]$
Electron trapping	$e^- + O_2 \rightarrow \cdot O_2^-$	$k_3[e^-][O_2]$
Hole trapping	$h^+ + H_2O \rightarrow \cdot OH + H^+$	$k_4[h^+][H_2O]$
Hydroxyl attack	$A + n\cdot OH \rightarrow B$	$k_5[A][\cdot OH]^n$
	$B + n\cdot OH \rightarrow \ldots \rightarrow CO_2 + H_2O$	$k_6[B][\cdot OH]^n$

Derivation of the kinetic model

The kinetic model proposed for the photocatalytic oxidation of organic compounds is based on the reaction scheme summarized in Table 1. By applying the kinetic micro steady state approximation (MSSA) for the concentration of electrons, holes and hydroxyl radicals, we can derive the following expressions:

$$r_{e^-} = \frac{d[e^-]}{dt} = r_g - k_2[e^-][h^+] - k_3[e^-][O_2] \approx 0 \qquad \text{Eq. G-1}$$

$$[e^-] = \frac{r_g}{k_2[h^+]+k_3[O_2]} \qquad \text{Eq. G-2}$$

$$r_{h^+} = \frac{d[h^+]}{dt} = r_g - k_2[e^-][h^+] - k_4[h^+][H_2O] \approx 0 \qquad \text{Eq. G-3}$$

$$[h^+] = \frac{r_g}{k_2[e^-]+k_4[H_2O]} \qquad \text{Eq. G-4}$$

$$r_{\cdot OH} = \frac{d[\cdot OH]}{dt} = k_4[h^+][H_2O] - nk_5[A][\cdot OH]^n - nk_6[B][\cdot OH]^n \approx 0 \qquad \text{Eq. G-5}$$

$$[\cdot OH]^n = \frac{k_4[h^+][H_2O]}{nk_5[A]+nk_6[B]} \qquad \text{Eq. G-6}$$

Introducing equation G-2 into G-3, the expression for the hole concentration is obtained.

$$[h^+] = \frac{r_g}{k_2\frac{r_g}{k_2[h^+]+k_3[O_2]}+k_4[H_2O]} = \frac{r_g}{\frac{k_2 r_g + k_4[H_2O]\,(k_2[h^+]+k_3[O_2])}{k_2[h^+]+k_3[O_2]}}$$

$$[h^+] = \frac{r_g\,(k_2[h^+]+k_3[O_2])}{k_2 r_g + k_4[H_2O]\,(k_2[h^+]+k_3[O_2])}$$

$$[h^+]\left[k_2 r_g + k_4[H_2O]\,(k_2[h^+] + k_3[O_2])\right] - r_g\,(k_2[h^+] + k_3[O_2]) = 0$$

$$[h^+]k_2 r_g + [h^+]k_4[H_2O]\,k_2[h^+] + [h^+]k_4[H_2O]\,k_3[O_2] - r_g\,k_2[h^+] - r_g\,k_3[O_2] = 0$$

$$[h^+]^2 k_4[H_2O]\,k_2 + [h^+]\left(k_2 r_g + k_4[H_2O]\,k_3[O_2] - r_g\,k_2\right) - r_g\,k_3[O_2] = 0$$

$$[h^+]^2 + \frac{k_3[O_2]}{k_2}[h^+] - \frac{r_g\, k_3[O_2]}{k_4[H_2O]\, k_2} = 0 \qquad \text{Eq. G-7}$$

From the solution of equation G-7 (the positive root is the only one that has physical meaning):

$$[h^+] = \frac{-\frac{k_3[O_2]}{k_2} + \sqrt{\left(\frac{k_3[O_2]}{k_2}\right)^2 \left(1 + 4\frac{r_g\, k_3[O_2]}{k_4[H_2O]\, k_2 \left(\frac{k_3[O_2]}{k_2}\right)^2}\right)}}{2}$$

$$[h^+] = \frac{-\frac{k_3[O_2]}{k_2} + \sqrt{\left(\frac{k_3[O_2]}{k_2}\right)^2 \left(1 + \frac{4\, r_g\, k_2}{k_4[H_2O] k_3[O_2]}\right)}}{2}$$

$$[h^+] = \frac{k_3[O_2]}{2\, k_2}\left(-1 + \sqrt{1 + \frac{4\, r_g\, k_2}{k_4[H_2O] k_3[O_2]}}\right) \qquad \text{Eq. G-8}$$

Besides, the volumetric rate of electron-hole generation is given by:

$$r_g = \bar{\Phi} \int_\lambda e^a{}_\lambda(x) d\lambda = \bar{\Phi} e^a(x) \qquad \text{Eq. G-9}$$

where e^arepresents the local volumetric rate of photon absorption (LVRPA) and $\bar{\Phi}$ is the primary quantum yield averaged over the wavelength range.

Then, combining equations G-6, G-8 and G-9 results in:

$$[\cdot OH]^n = \frac{k_4[H_2O]}{nk_5[A] + nk_6[B]} \frac{k_3[O_2]}{2\, k_2}\left(-1 + \sqrt{1 + \frac{4\, k_2 \bar{\Phi} e^a}{k_3 k_4 [H_2O][O_2]}}\right)$$

$$[\cdot OH]^n = \frac{\alpha_1}{k_5[A] + k_6[B]}\left(-1 + \sqrt{1 + \alpha_2 e^a}\right) \qquad \text{Eq. G-10}$$

Where $\alpha_1 = \frac{k_3 k_4 [H_2O][O_2]}{2nk_2}$ and $\alpha_2 = \frac{4\, k_2 \bar{\Phi}}{k_3 k_4 [H_2O][O_2]}$

Introducing equation G-10 into the volumetric rate expression for A, we derive the following equation:

$$r_A = -k_5[A][\cdot OH]^n = -\frac{\alpha_1 k_5[A]}{k_5[A] + k_6[B]}\left(-1 + \sqrt{1 + \alpha_2 e^a}\right)$$

$$r_A = -\alpha_1 \frac{[A]}{[A] + \alpha_3[B]}\left(-1 + \sqrt{1 + \alpha_2 e^a}\right) \qquad \text{Eq. G-11}$$

Where $\alpha_3 = \frac{k_6}{k_5}$

And the volumetric rate expression for B:

$$r_B = k_5[A][\cdot OH]^n - k_6[B][\cdot OH]^n$$

$$r_B = k_5[A]\frac{\alpha_1}{k_5[A]+k_6[B]}\left(-1+\sqrt{1+\alpha_2 e^a}\right) - k_6[B]\frac{\alpha_1}{k_5[A]+k_6[B]}\left(-1+\sqrt{1+\alpha_2 e^a}\right)$$

$$r_B = \frac{\alpha_1(k_5[A]-k_6[B])}{k_5[A]+k_6[B]}\left(-1+\sqrt{1+\alpha_2 e^a}\right)$$

$$r_B = \alpha_1\frac{[A]-\alpha_3[B]}{[A]+\alpha_3[B]}\left(-1+\sqrt{1+\alpha_2 e^a}\right) \qquad \text{Eq. G-12}$$

Limiting case: $\alpha_2 e^a \ll 1$

Under this condition, and taking the first term of the square root Taylor expansion, equations G-11 and G-12 will take the form

$$r_A = -\alpha\frac{[A]}{[A]+\alpha_3[B]}e^a \qquad \text{Eq. G-13}$$

$$r_B = \alpha\frac{[A]-\alpha_3[B]}{[A]+\alpha_3[B]}e^a \qquad \text{Eq. G-14}$$

Where $\alpha = \frac{\alpha_1\alpha_2}{2}$

Limiting case: $\alpha_2 e^a \gg 1$

$$r_A = -\alpha\frac{[A]}{[A]+\alpha_3[B]}\sqrt{e^a} \qquad \text{Eq. G-15}$$

$$r_B = \alpha\frac{[A]-\alpha_3[B]}{[A]+\alpha_3[B]}\sqrt{e^a} \qquad \text{Eq. G-16}$$

Where $\alpha = \alpha_1\sqrt{\alpha_2}$

All these expression correspond to local values of the reaction rate that depends on the values of the Local Volumetric Rate of Photon Absorption (e^a) that is different at every point within the system. To simplify the numerical procedure, instead of solving the differential mass balance of the reactor, the volume-averaged reaction rate can be computed from the volume-averaged term of radiation absorption:

$$\langle r_A\rangle_{V_R} = -\alpha_1\frac{[A]}{[A]+\alpha_3[B]}\left(-1+\langle\sqrt{1+\alpha_2 e^a}\rangle_{V_R}\right) \qquad \text{Eq. G-17}$$

$$\langle r_B\rangle_{V_R} = \alpha_1\frac{[A]-\alpha_3[B]}{[A]+\alpha_3[B]}\left(-1+\langle\sqrt{1+\alpha_2 e^a}\rangle_{V_R}\right) \qquad \text{Eq. G-18}$$

As we are measuring A and B in the reservoir tank, to fit the experimental data we have to consider the mass balance of the whole recirculation system. Assuming that it is a perfectly mixed system, the expressions will be:

$$\left.\frac{d[A]}{dt}\right|_{Tank} = \frac{V_R}{V_T}\langle r_A \rangle_{V_R} \qquad \text{Eq. G-19}$$

$$\left.\frac{d[B]}{dt}\right|_{Tank} = \frac{V_R}{V_T}\langle r_B \rangle_{V_R} \qquad \text{Eq. G-20}$$

So, to fit experimental data it is possible to apply:

$$\left.\frac{d[A]}{dt}\right|_{Tank} = -\frac{V_R}{V_T}\alpha_1 \frac{[A]}{[A]+\alpha_3[B]}\left(-1 + \langle\sqrt{1+\alpha_2 e^a}\rangle_{V_R}\right) \qquad \text{Eq. G-21}$$

$$\left.\frac{d[B]}{dt}\right|_{Tank} = \frac{V_R}{V_T}\alpha_1 \frac{[A]-\alpha_3[B]}{[A]+\alpha_3[B]}\left(-1 + \langle\sqrt{1+\alpha_2 e^a}\rangle_{V_R}\right) \qquad \text{Eq. G-22}$$

Or the corresponding radiation limiting cases.

APPENDIX H: Methanol Model Fitting Results

The following pages contain charts of the results of the model fitting process for Methanol Experiments A through M. The charts contain both the experimental measurements as well as the model predictions. The model predictions are based upon the fitting parameters a and b, as described in section 5.1.

On each page, the reader will find the following information:

a) Experiment name tag

b) Independent variable conditions:

   a. Initial target pollutant concentration

   b. Initial catalyst concentration

   c. Radiation power

c) Plots of experimental and model predicted values for cinnamic acid, intermediate compounds, total organic carbon:

   a. Values for a and b will be given in the title for each plot

   b. The combined error value will also be provided

Experiment A

Initial Methanol Concentration	Catalyst (TiO_2) Concentration	Radiation Power
100 mM of TOC	0.10 g/L	0 W/m^2

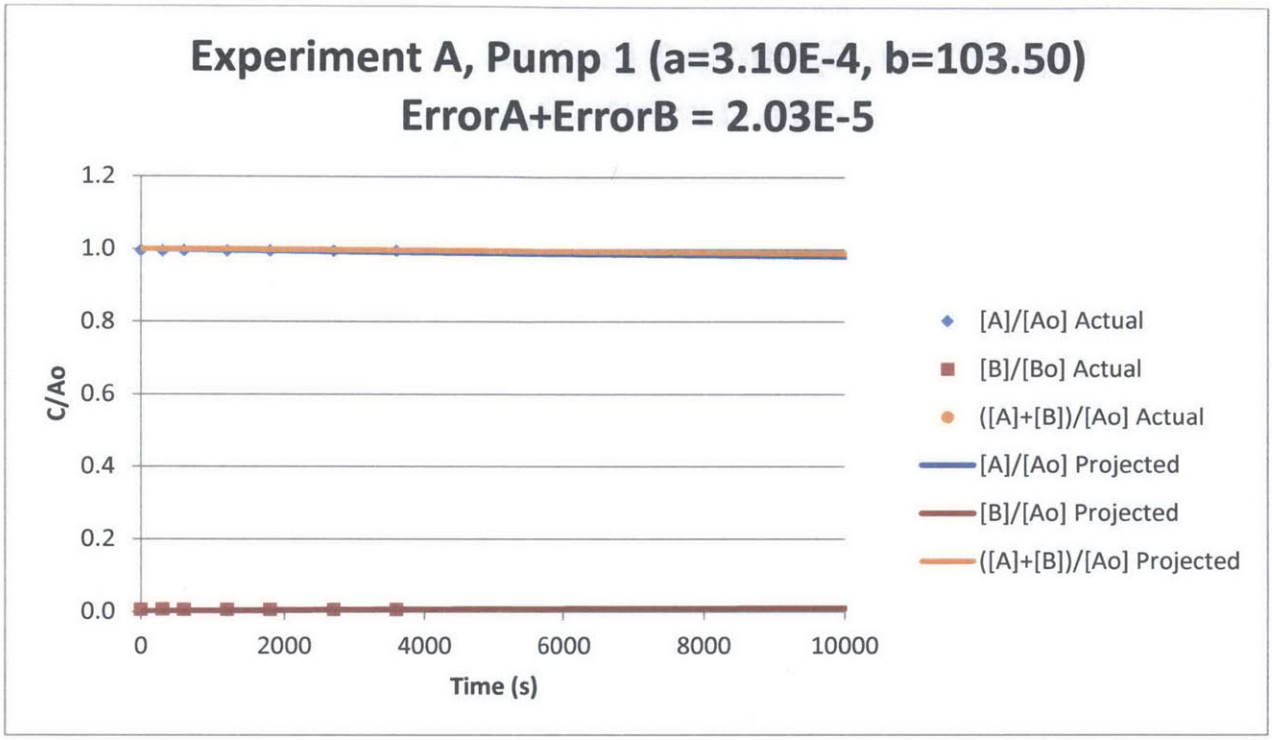

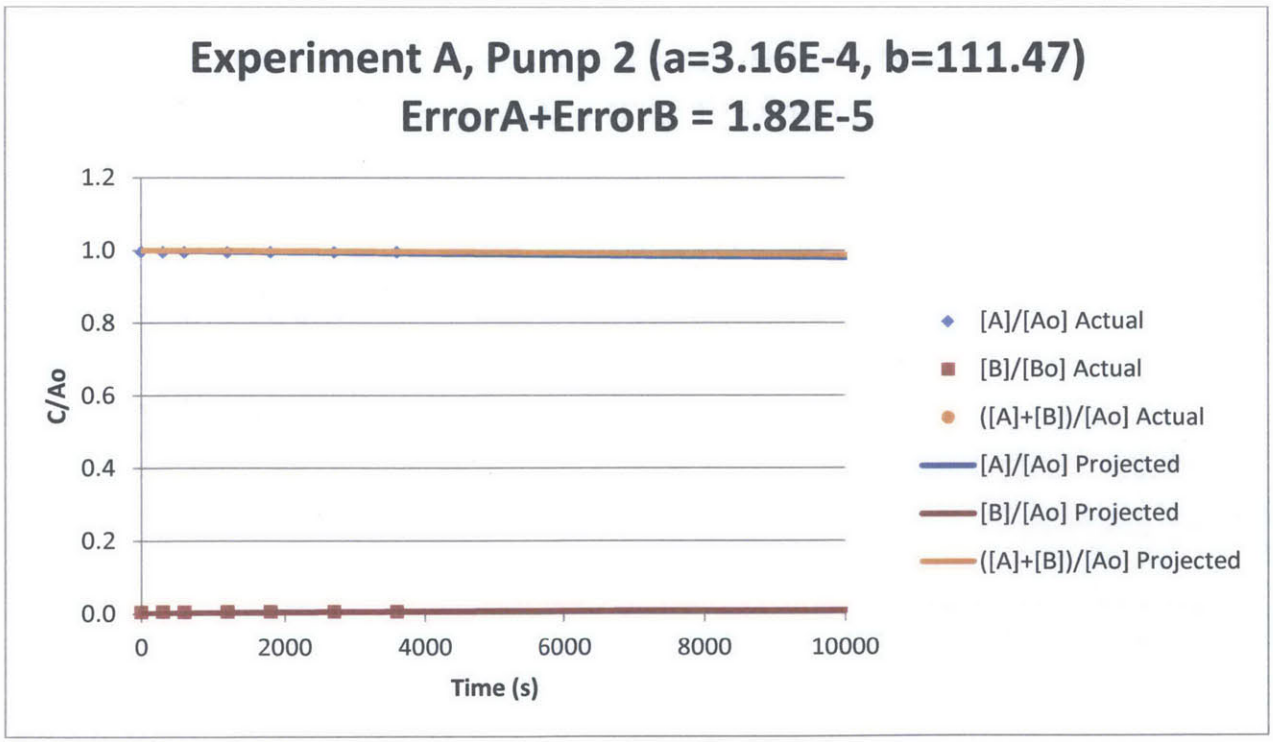

Experiment B

Initial Methanol Concentration	Catalyst (TiO_2) Concentration	Radiation Power
100 mM of TOC	0.0 g/L	83.7 W/m^2

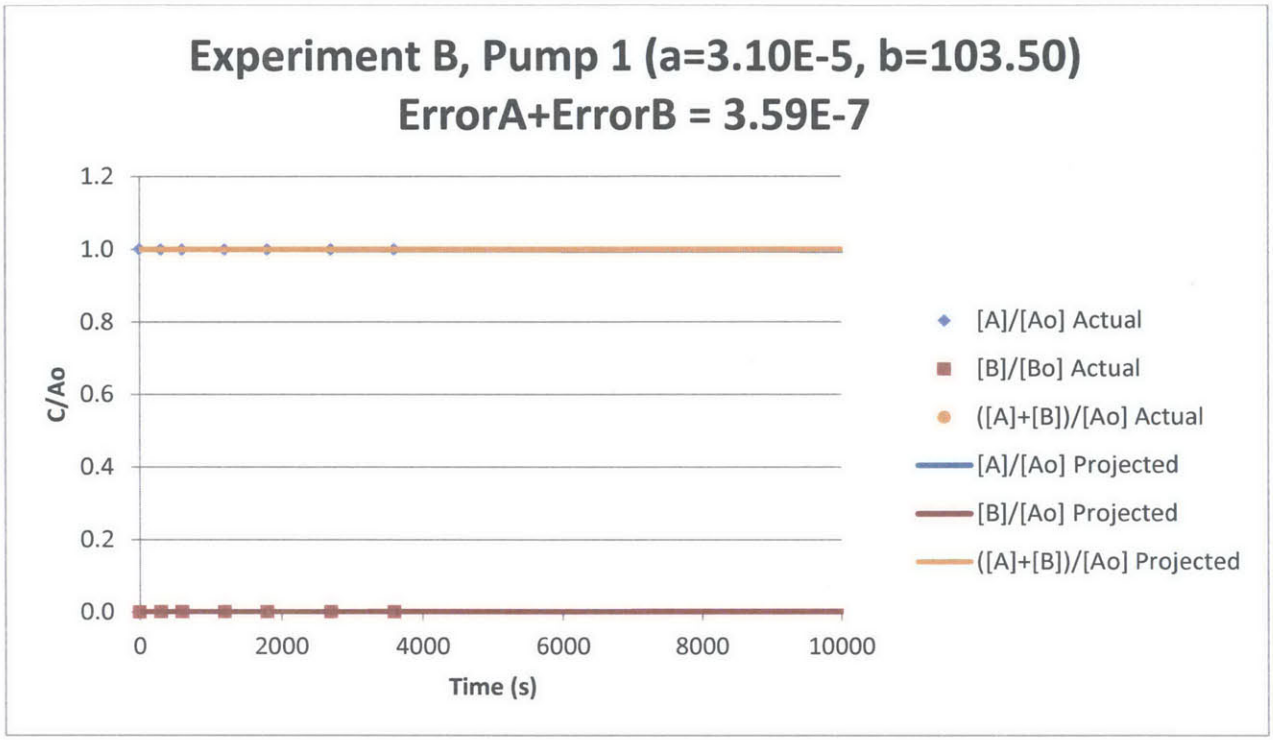

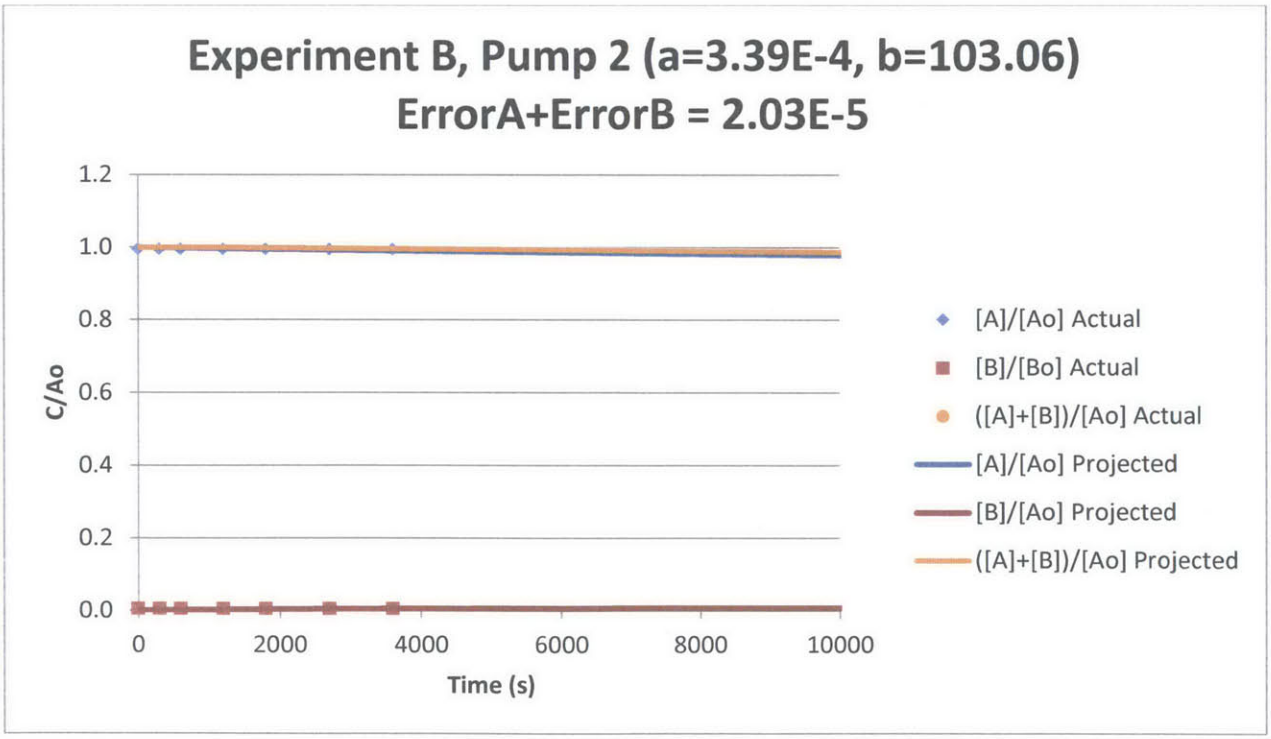

Experiment C

Initial Methanol Concentration	Catalyst (TiO_2) Concentration	Radiation Power
100 mM of TOC	0.10 g/L	83.7 W/m^2

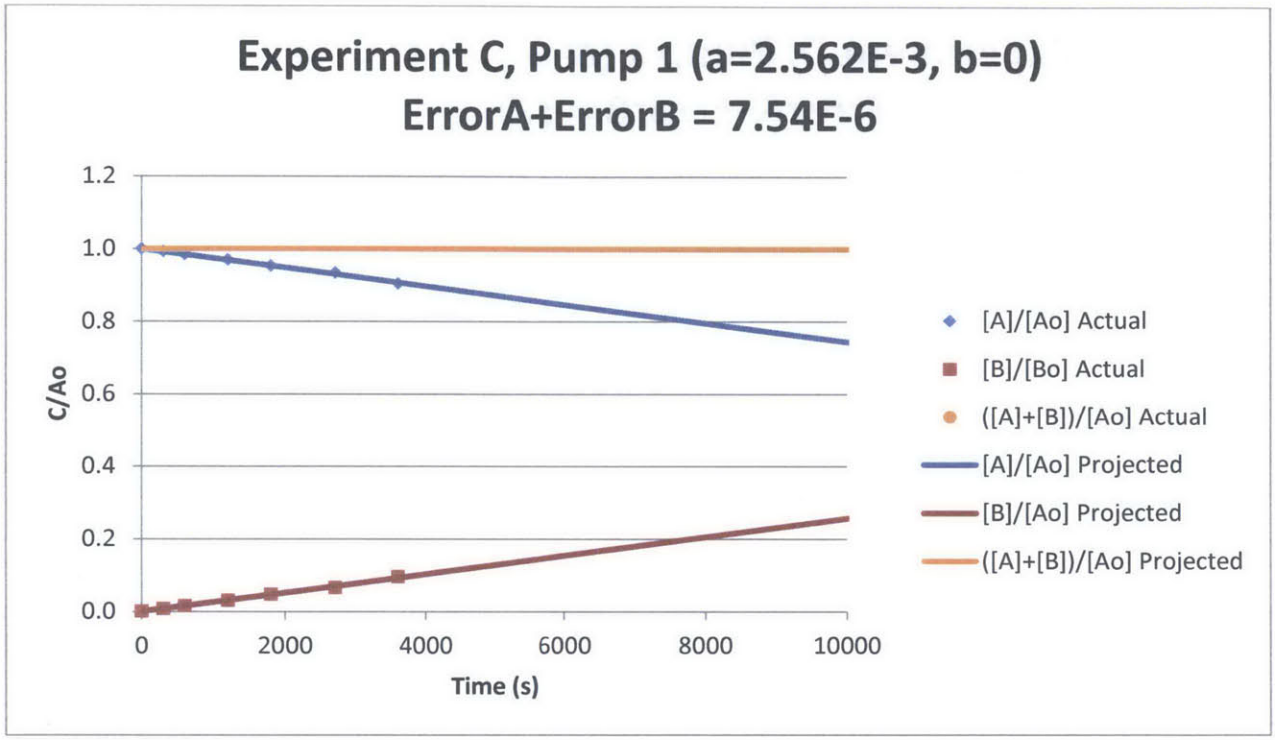

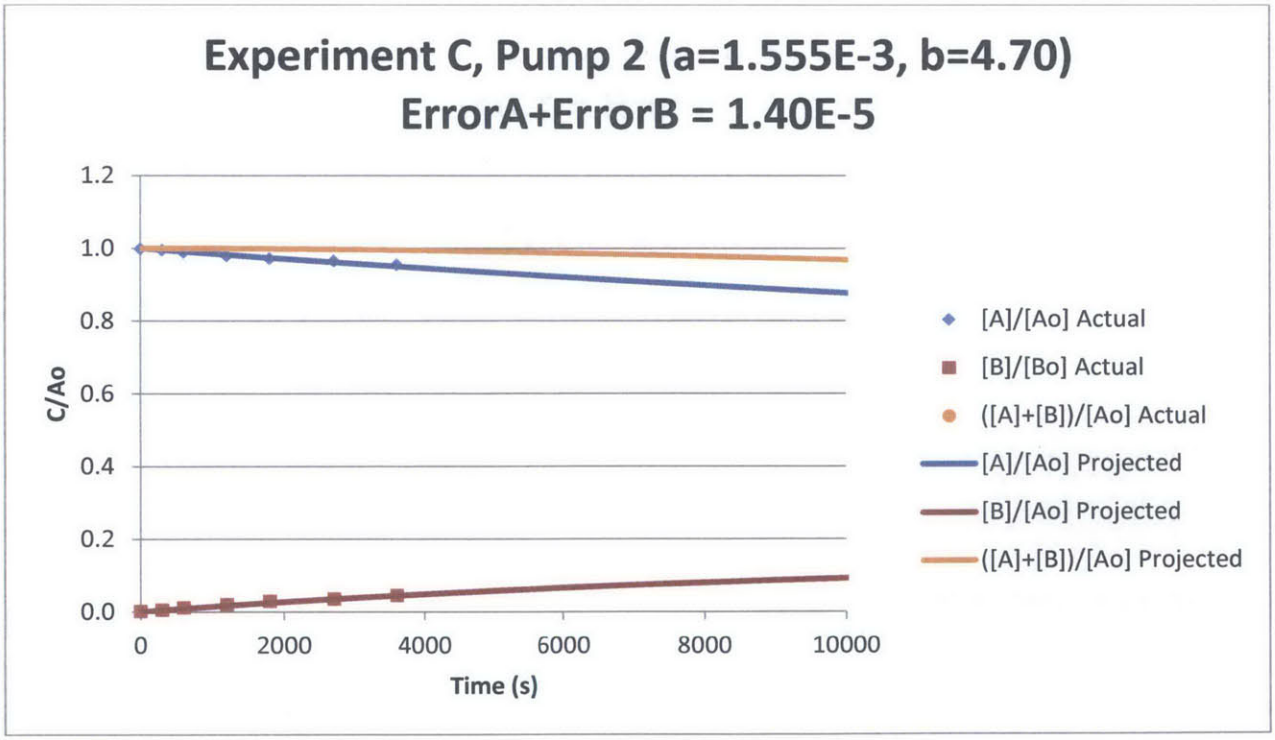

Experiment D

Initial Methanol Concentration	Catalyst (TiO_2) Concentration	Radiation Power
100 mM of TOC	0.0 g/L	83.7 W/m^2

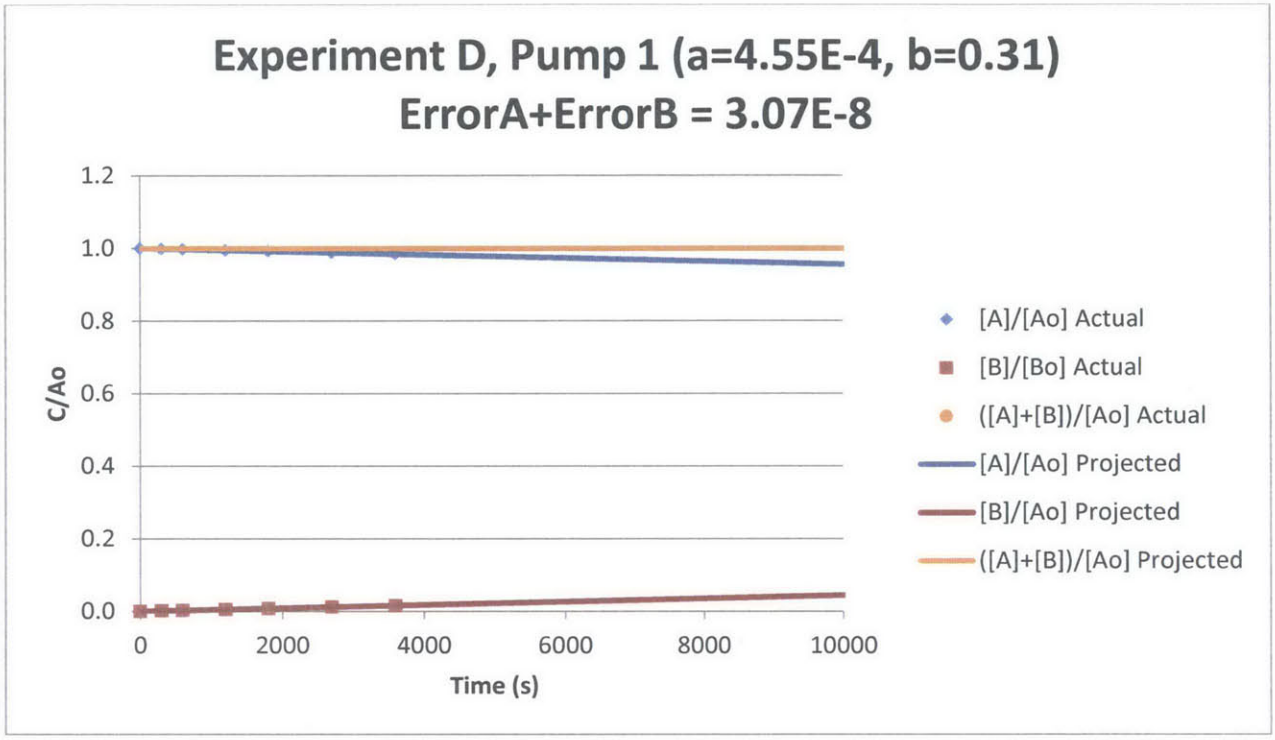

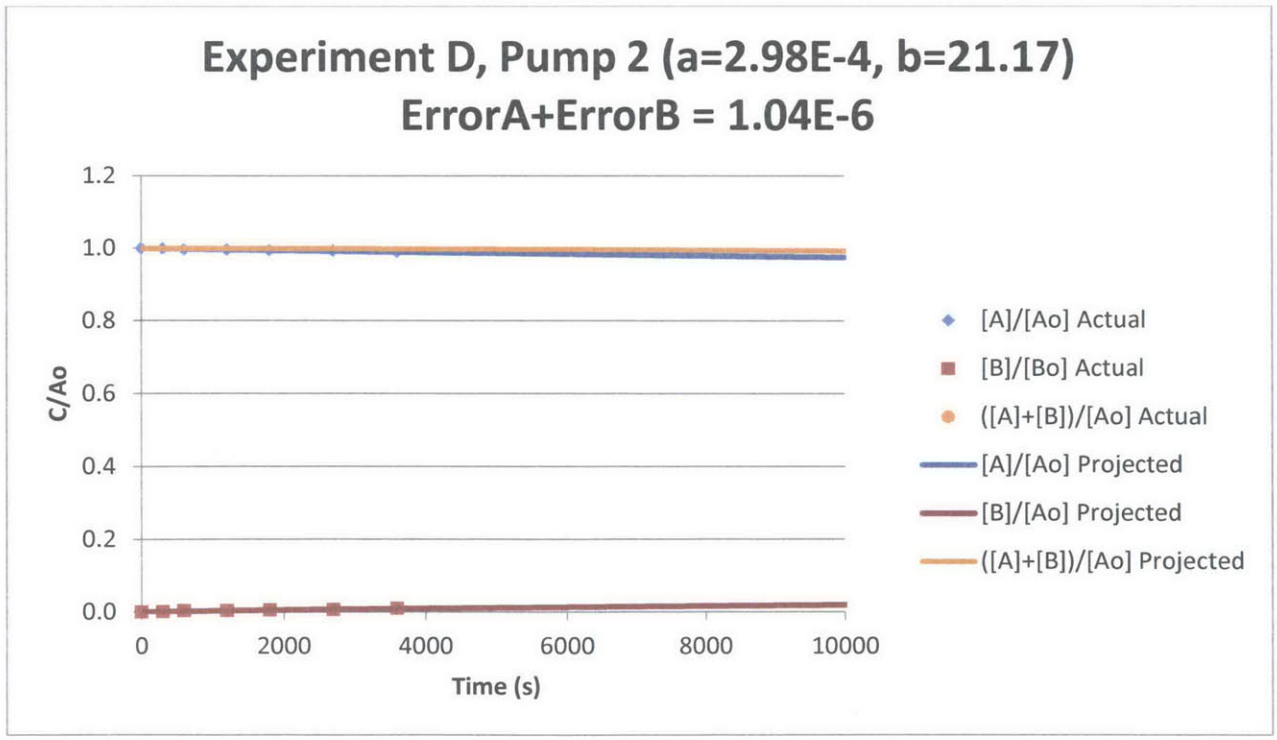

Experiment E

Initial Methanol Concentration	Catalyst (TiO_2) Concentration	Radiation Power
200 mM of TOC	0.0 g/L	83.7 W/m^2

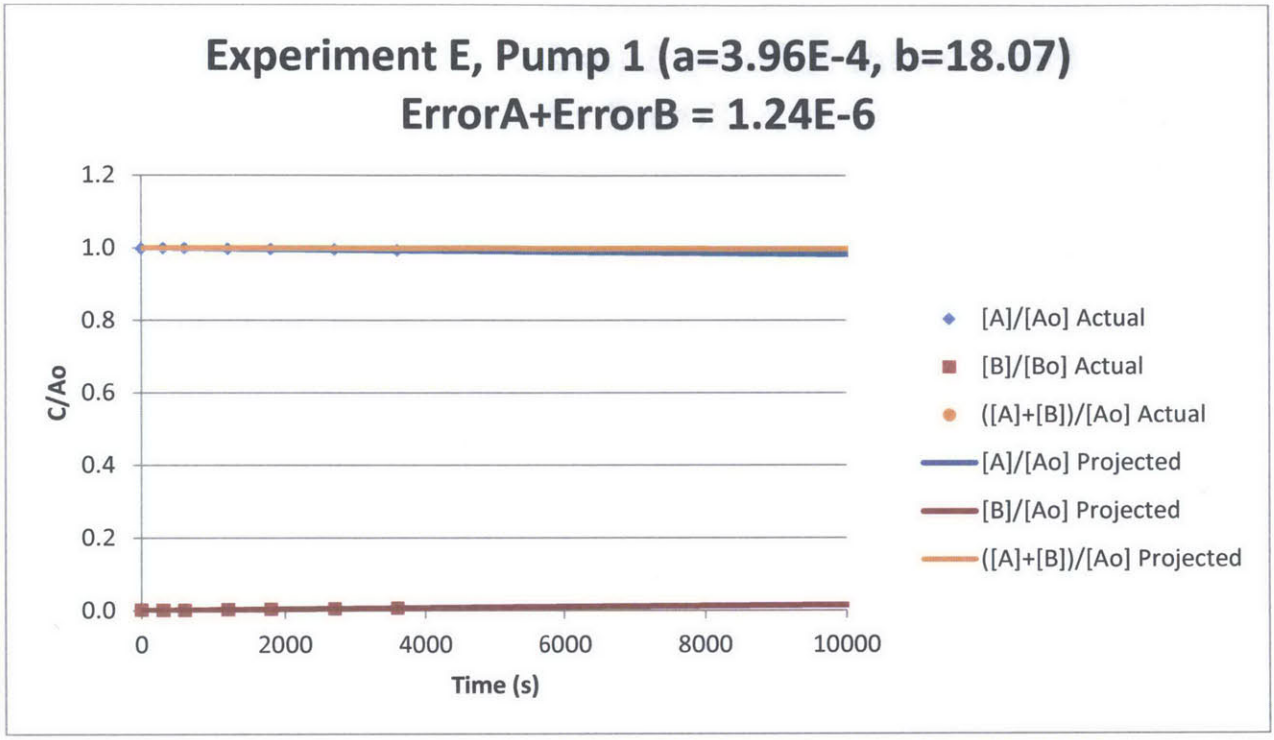

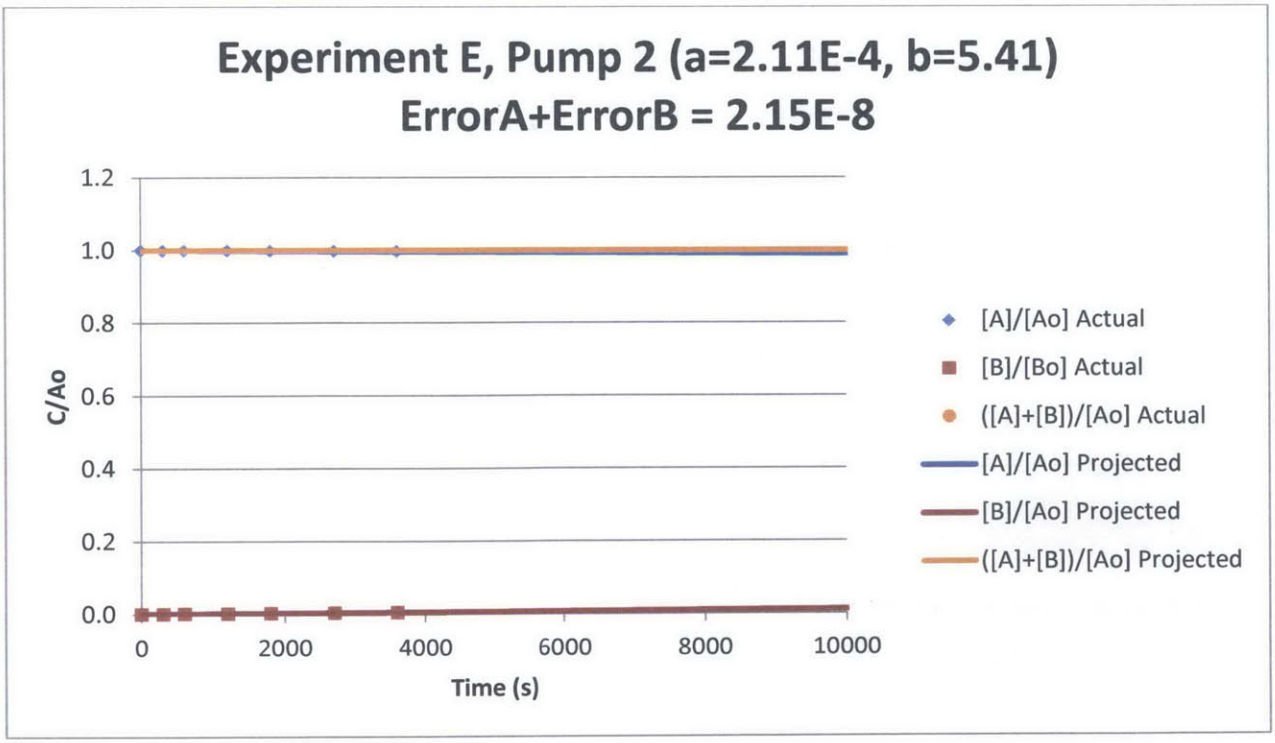

Experiment F

Initial Methanol Concentration	Catalyst (TiO_2) Concentration	Radiation Power
50 mM of TOC	0.0 g/L	83.7 W/m^2

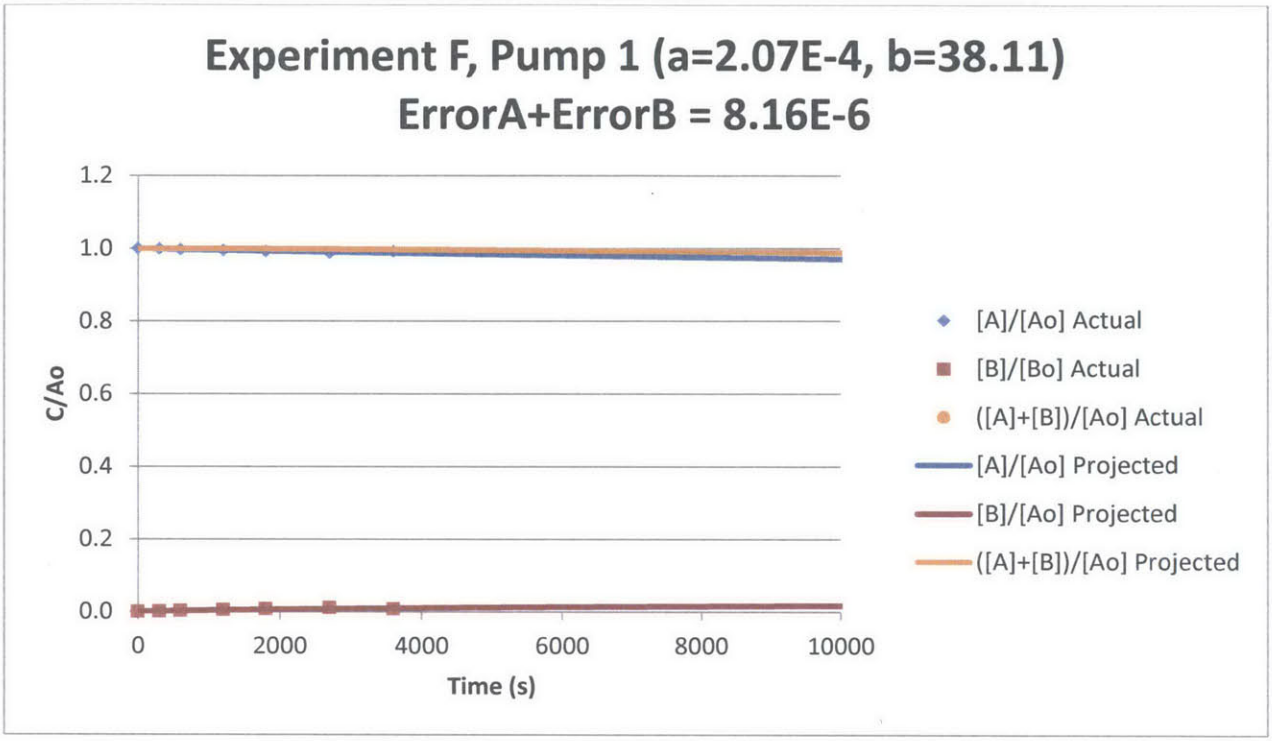

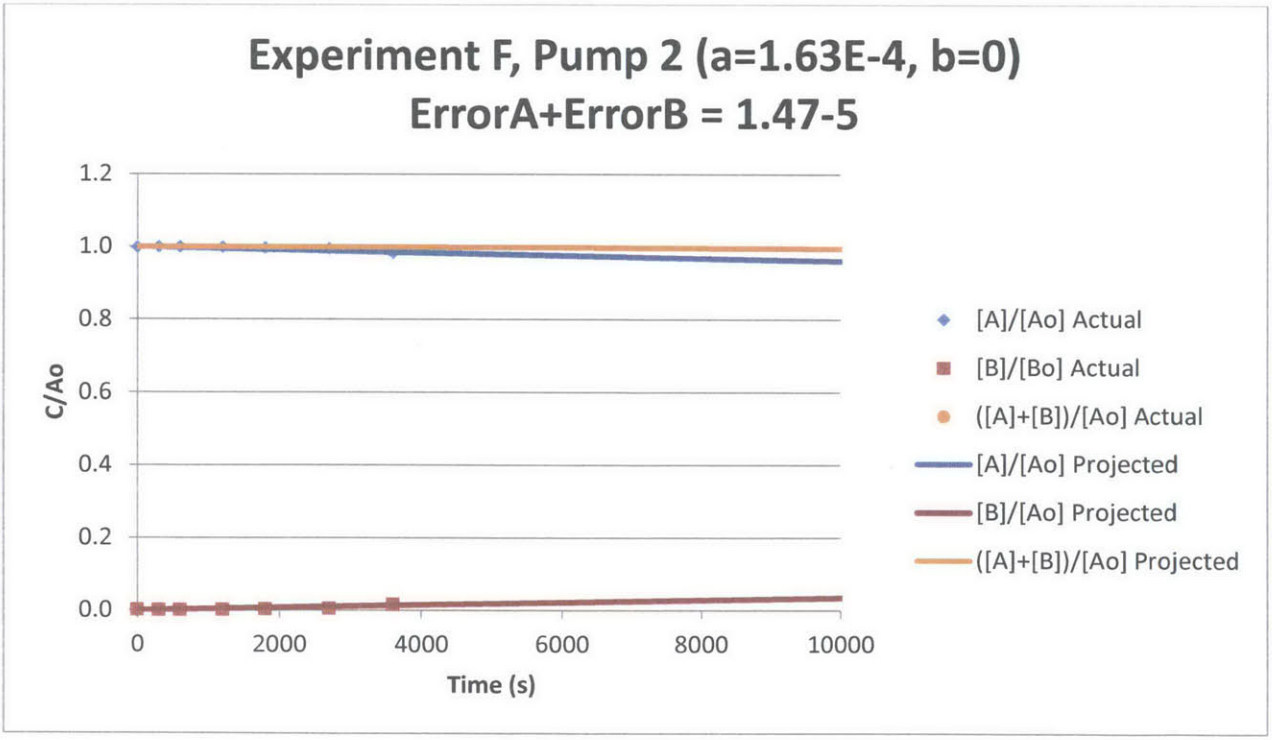

Experiment G

Initial Methanol Concentration	Catalyst (TiO_2) Concentration	Radiation Power
4 mM of TOC	0.0 g/L	83.7 W/m^2

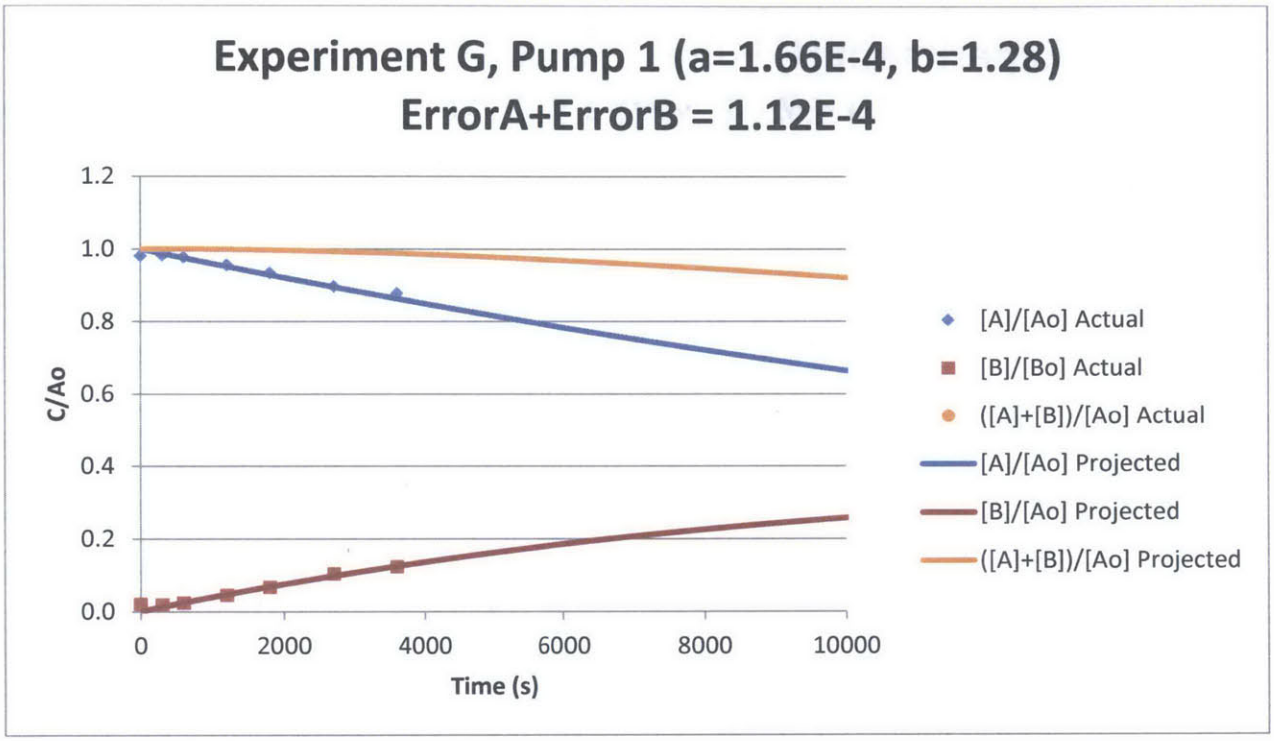

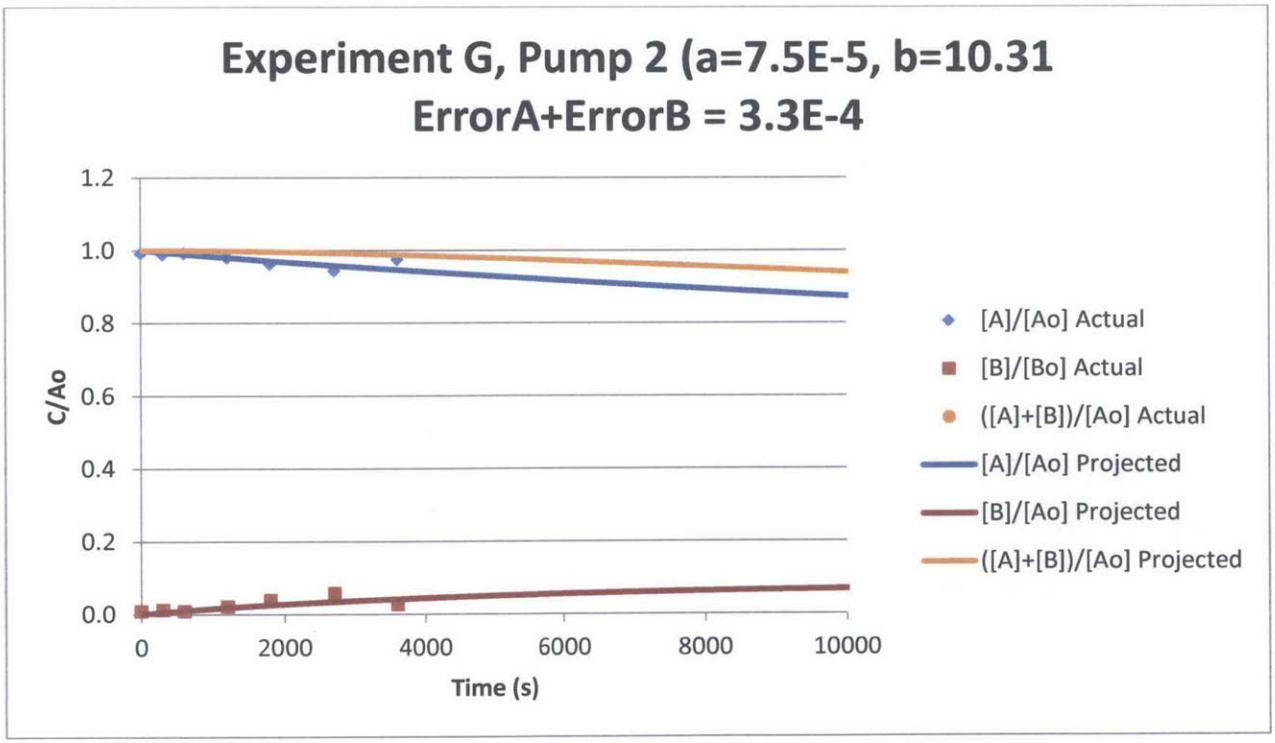

Experiment H

Initial Methanol Concentration	Catalyst (TiO_2) Concentration	Radiation Power
4 mM of TOC	0.10 g/L	74.2 W/m^2

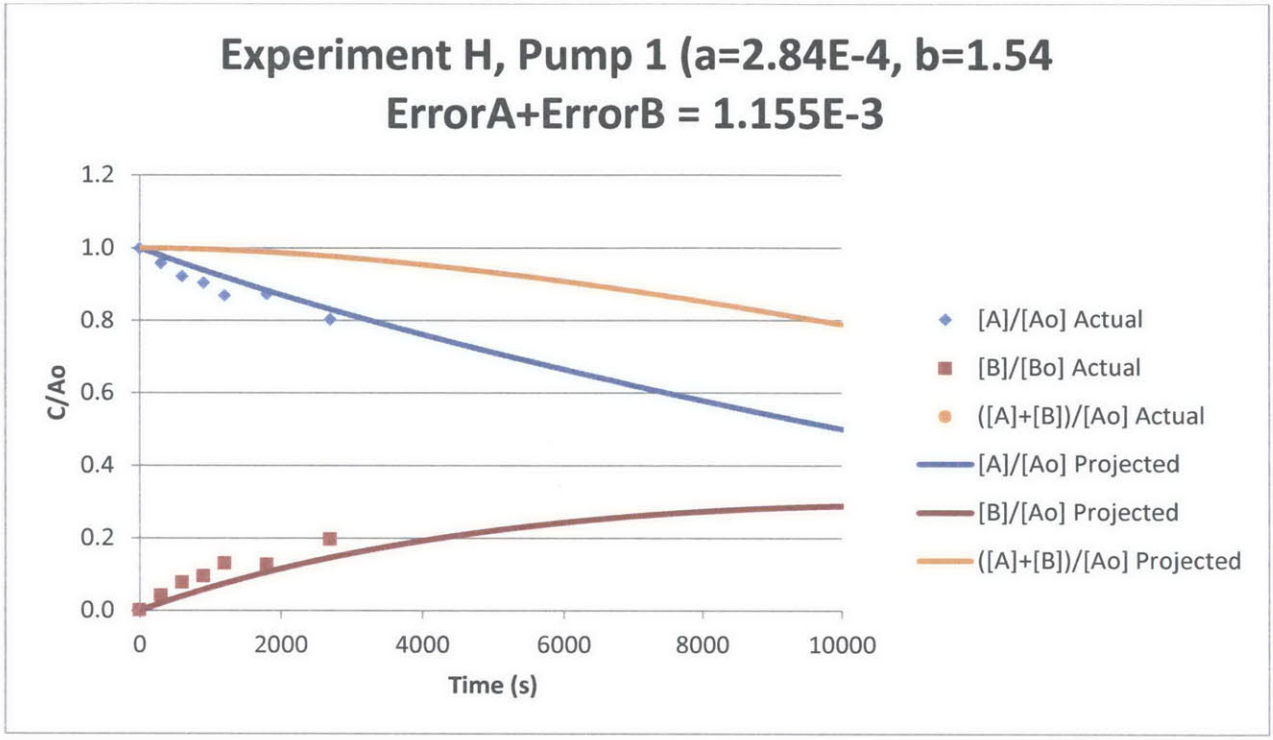

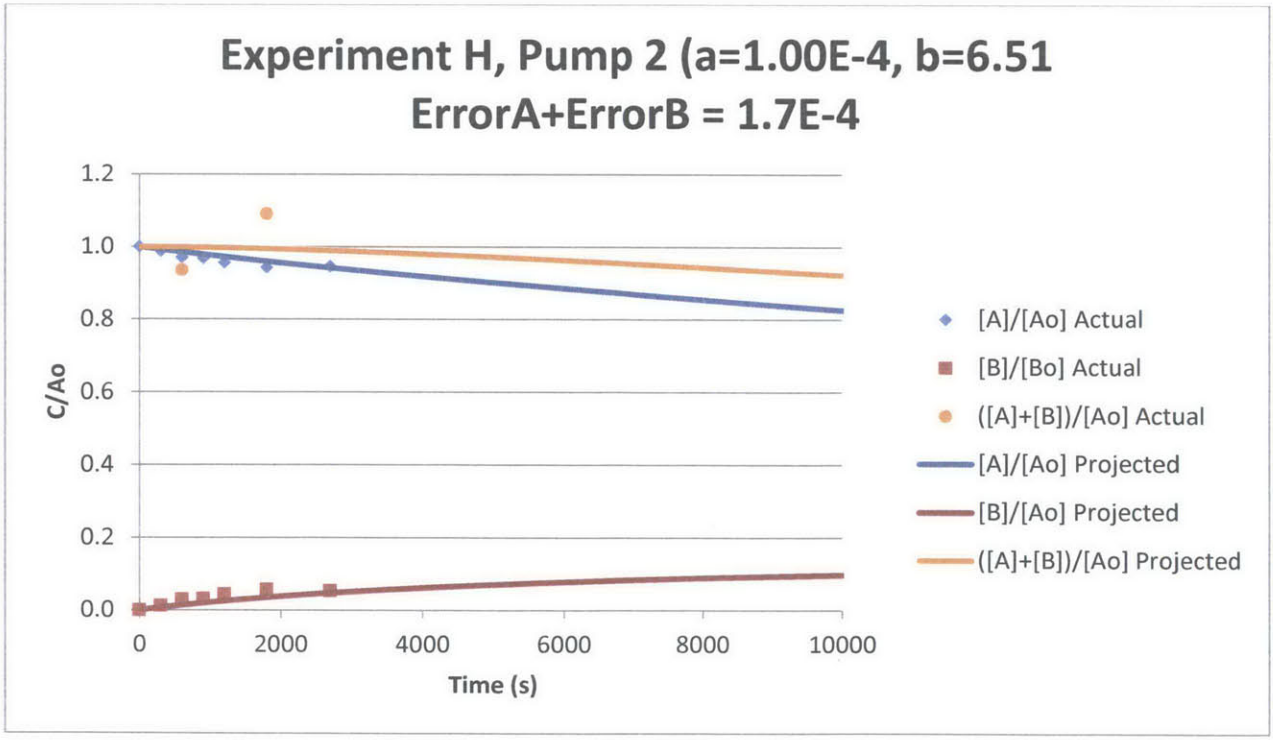

Experiment I

Initial Methanol Concentration	Catalyst (TiO_2) Concentration	Radiation Power
8 mM of TOC	0.10 g/L	74.2 W/m^2

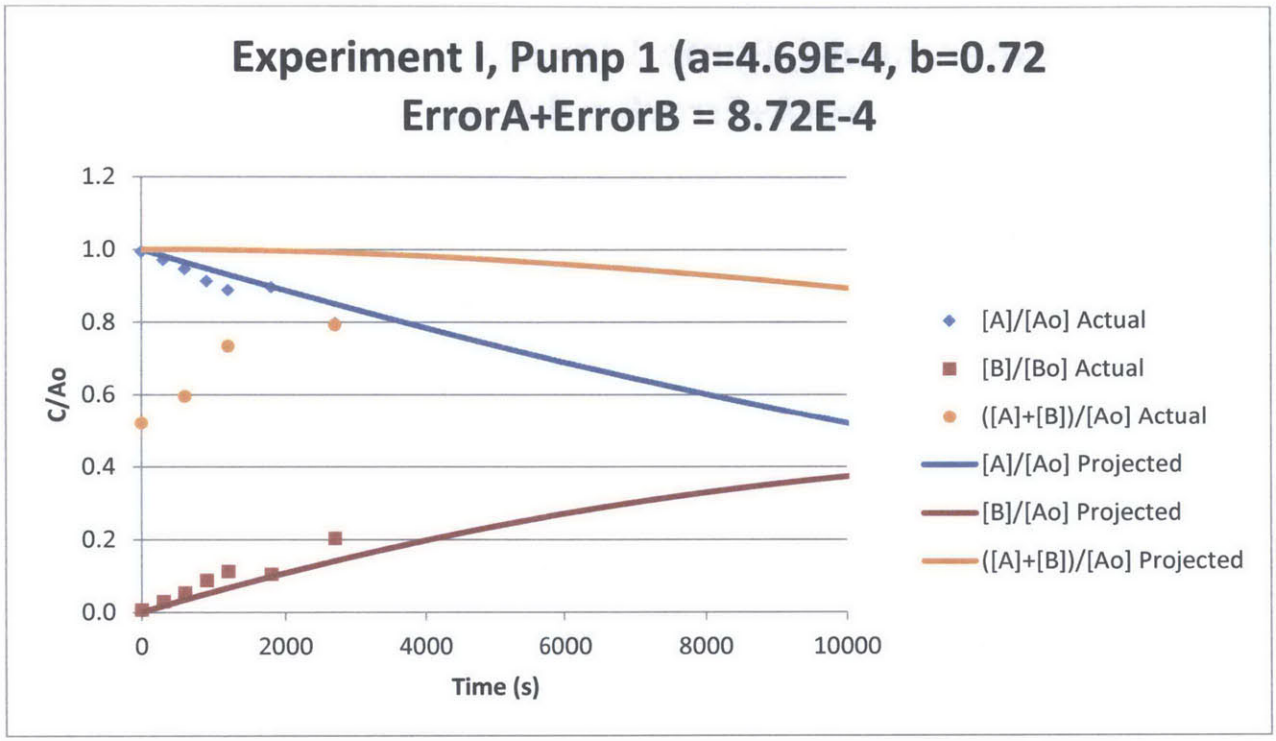

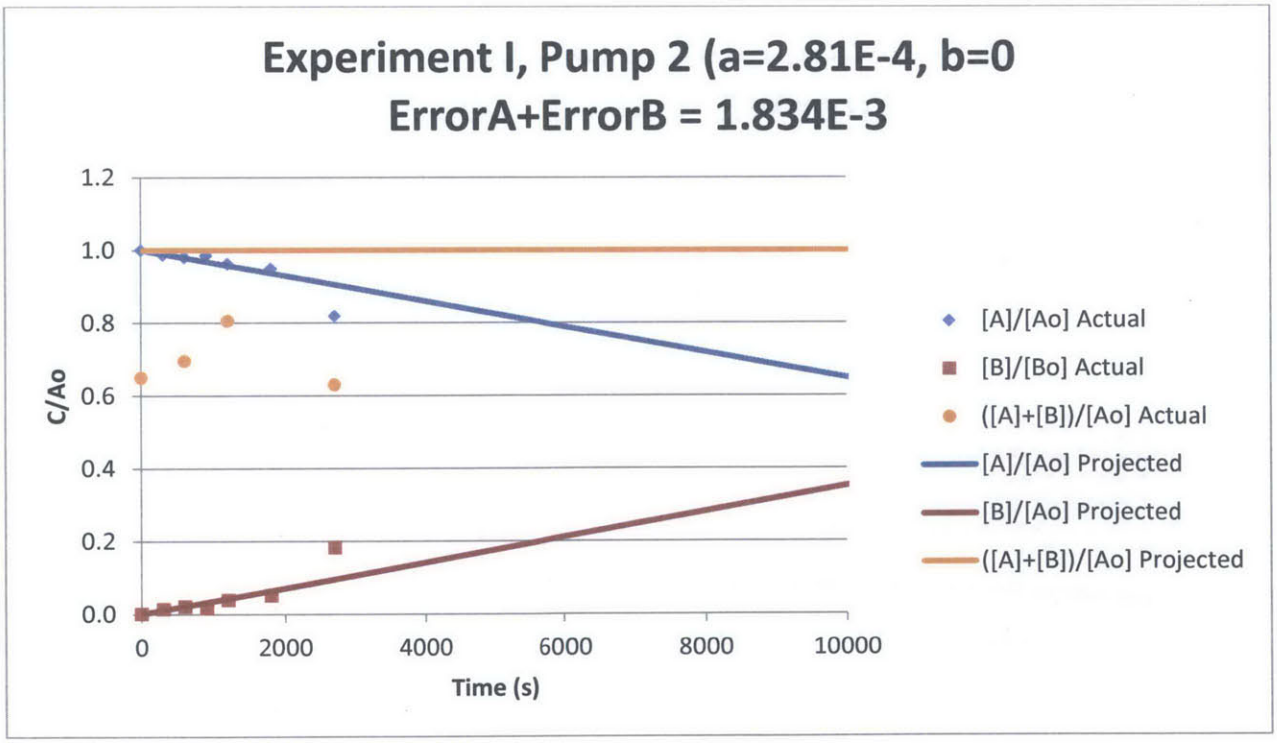

Experiment J

Initial Methanol Concentration	Catalyst (TiO_2) Concentration	Radiation Power
6 mM of TOC	0.10 g/L	74.2 W/m^2

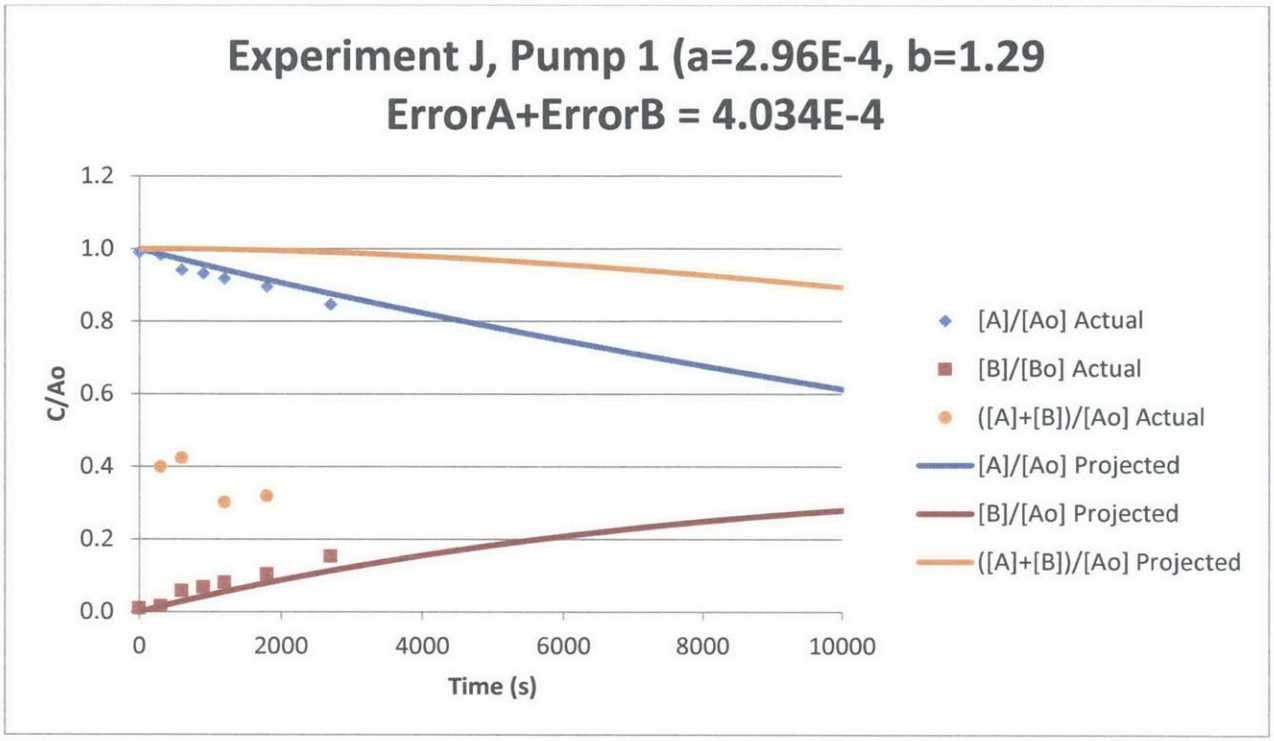

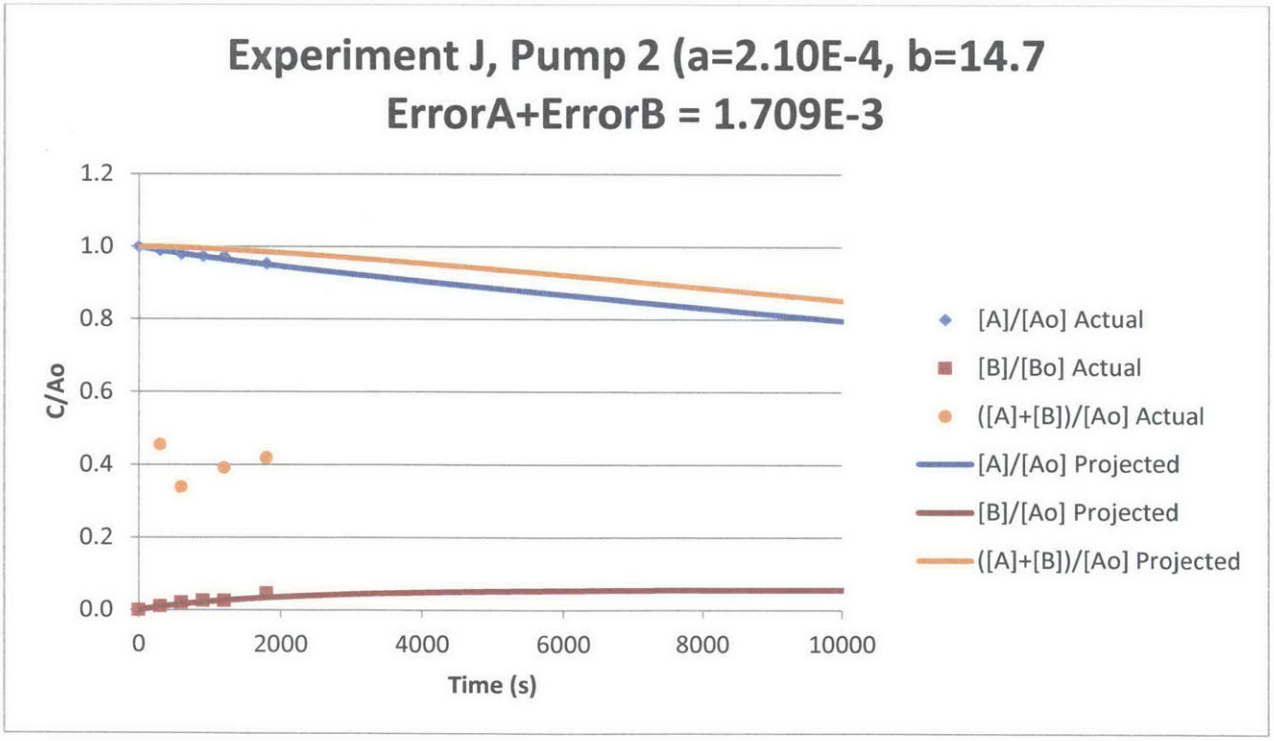

Experiment K

Initial Methanol Concentration	Catalyst (TiO_2) Concentration	Radiation Power
4 mM of TOC	0.05 g/L	74.2 W/m^2

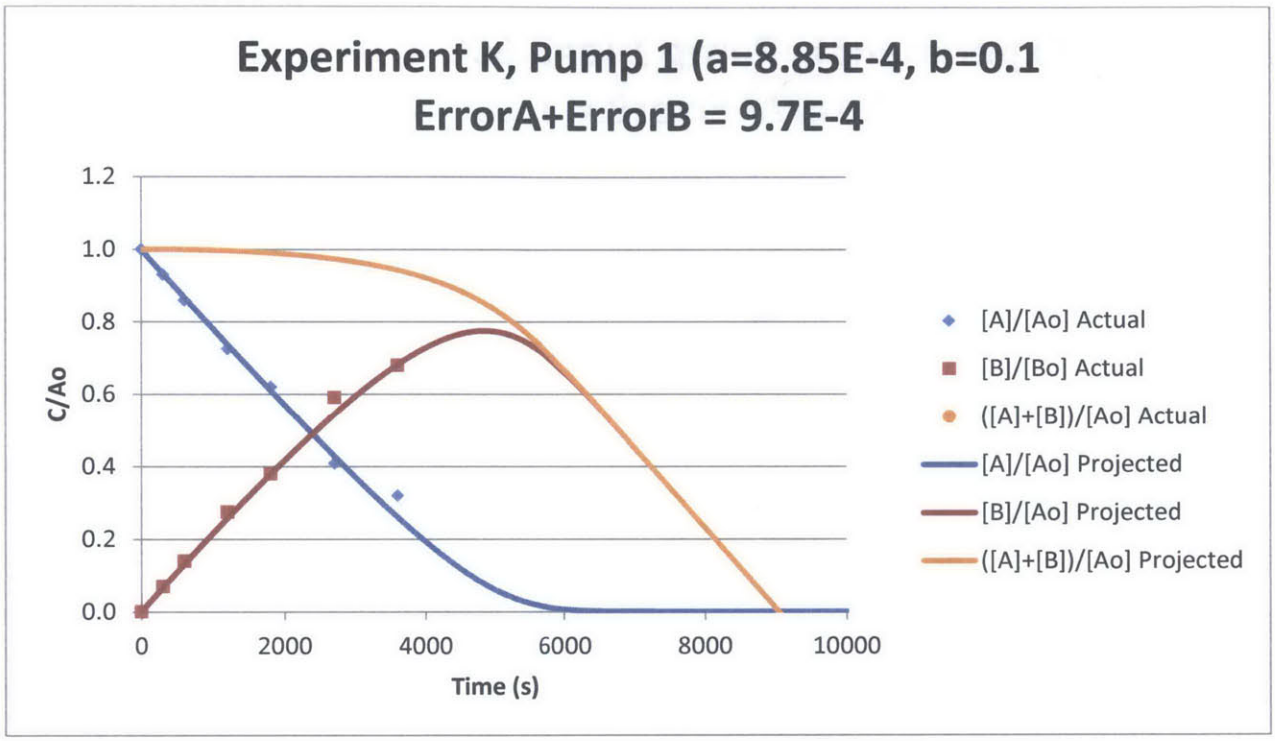

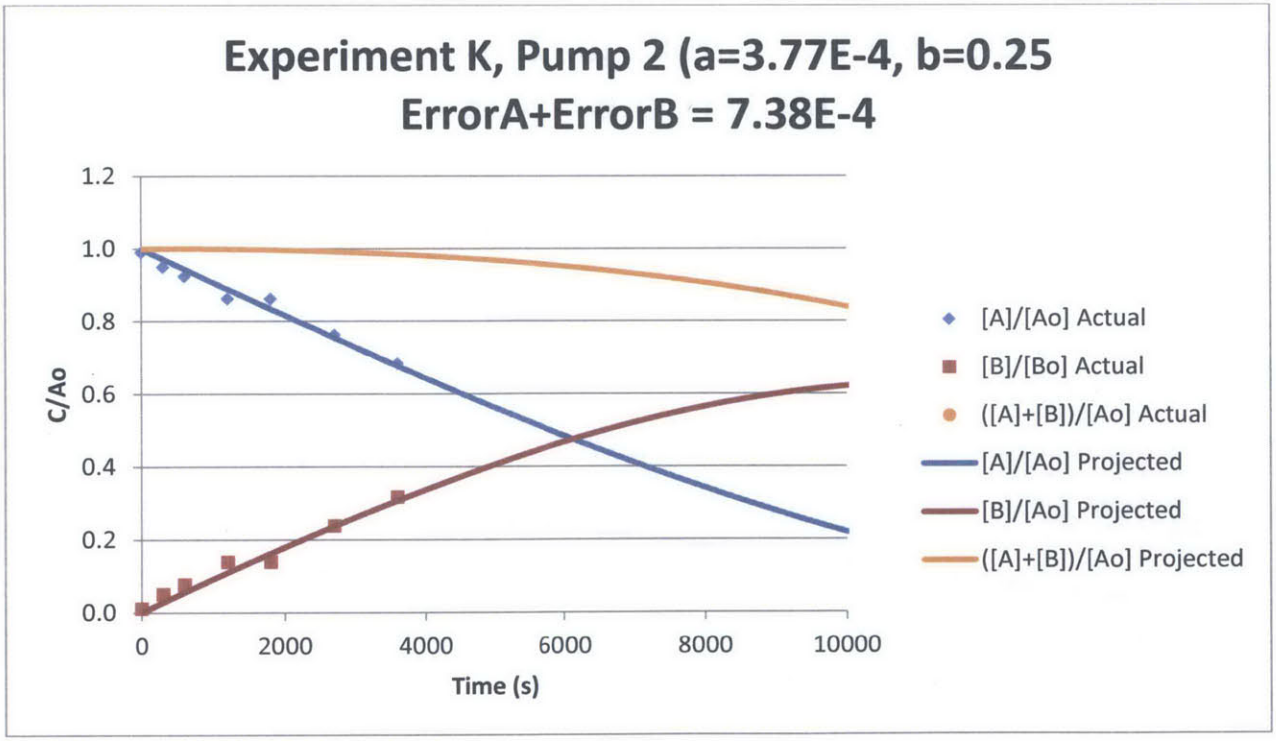

Experiment L

Initial Methanol Concentration	Catalyst (TiO_2) Concentration	Radiation Power
8 mM of TOC	0.05 g/L	74.2 W/m^2

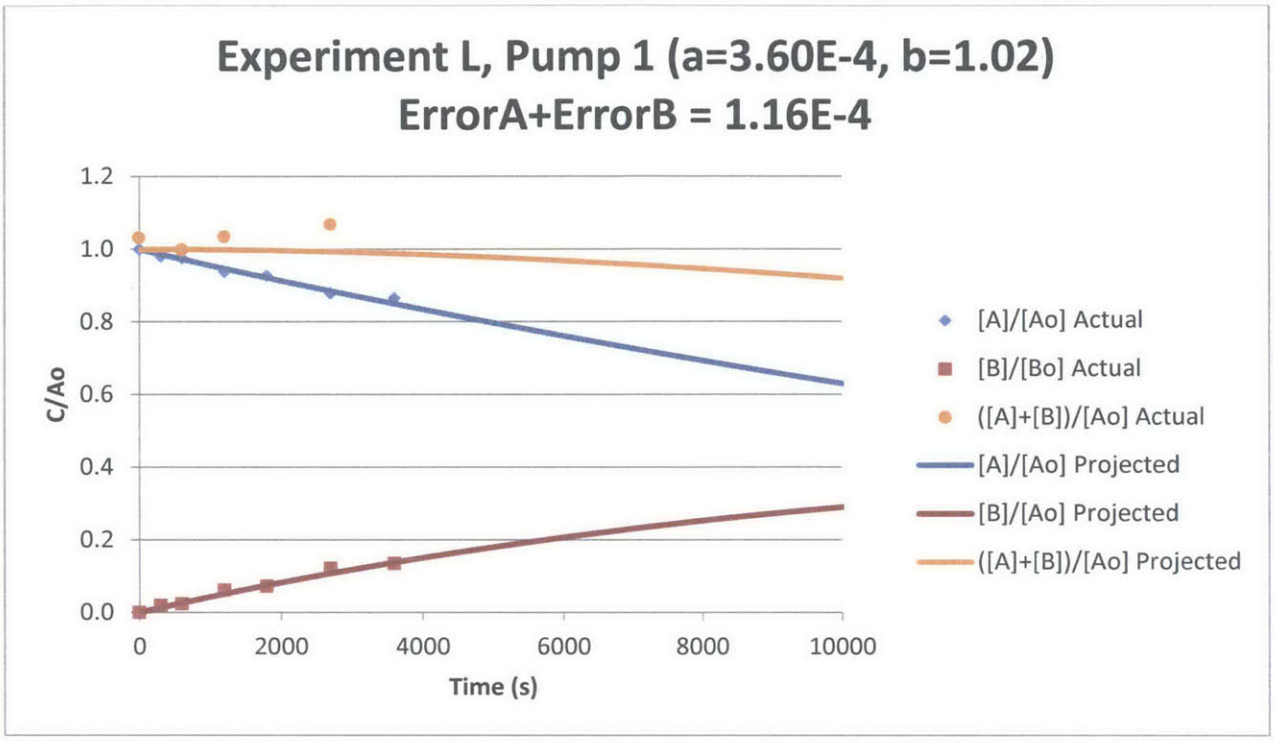

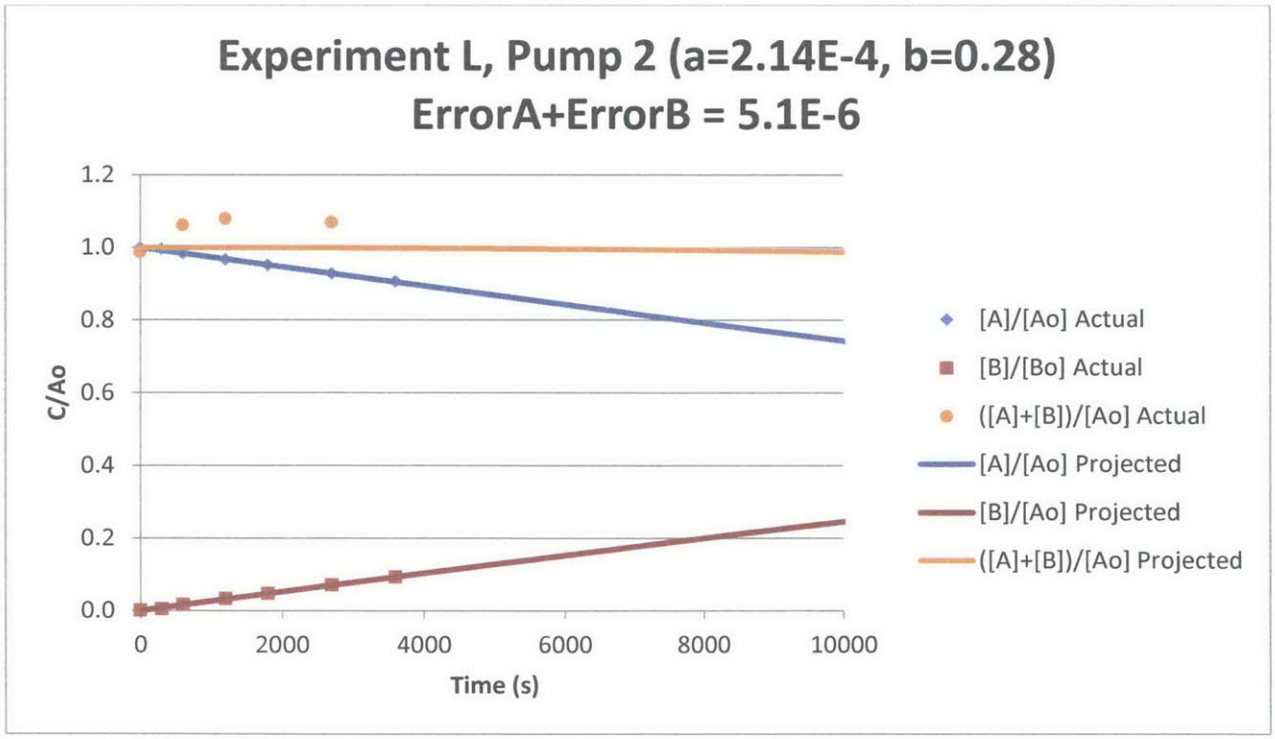

Experiment M

Initial Methanol Concentration	Catalyst (TiO_2) Concentration	Radiation Power
6 mM of TOC	0.05 g/L	74.2 W/m^2

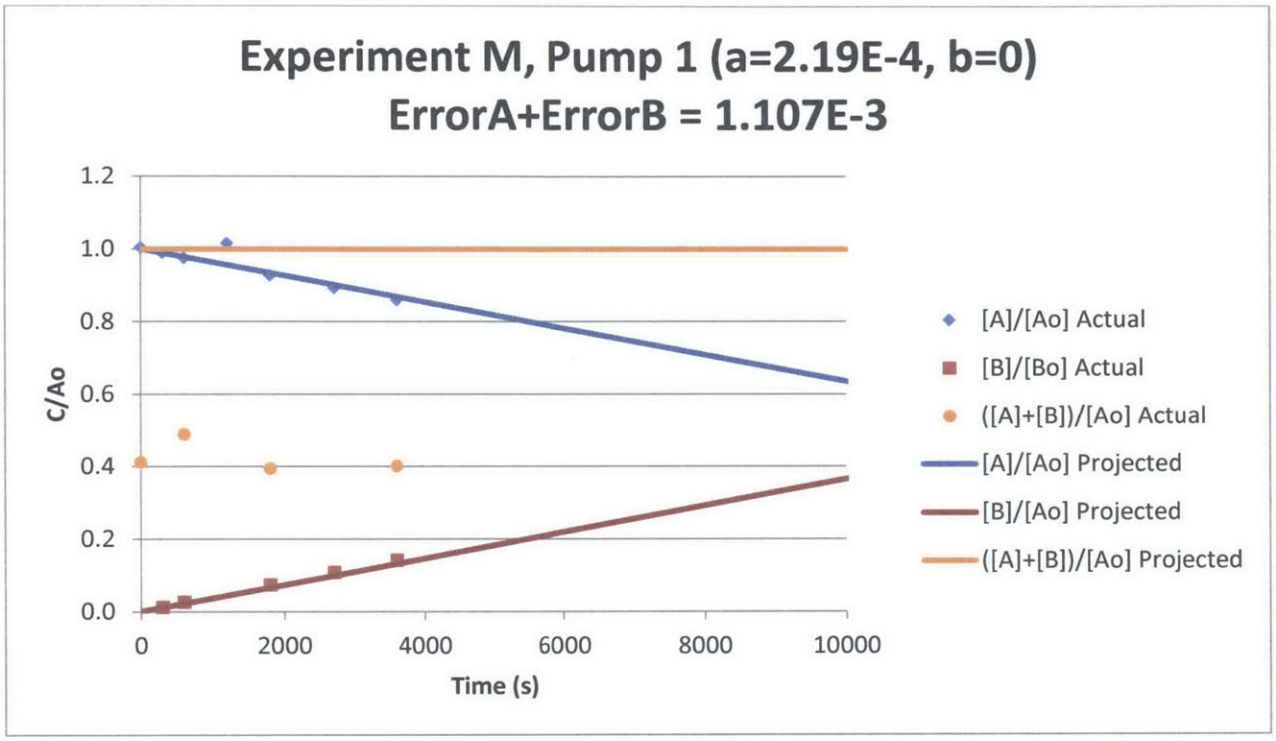

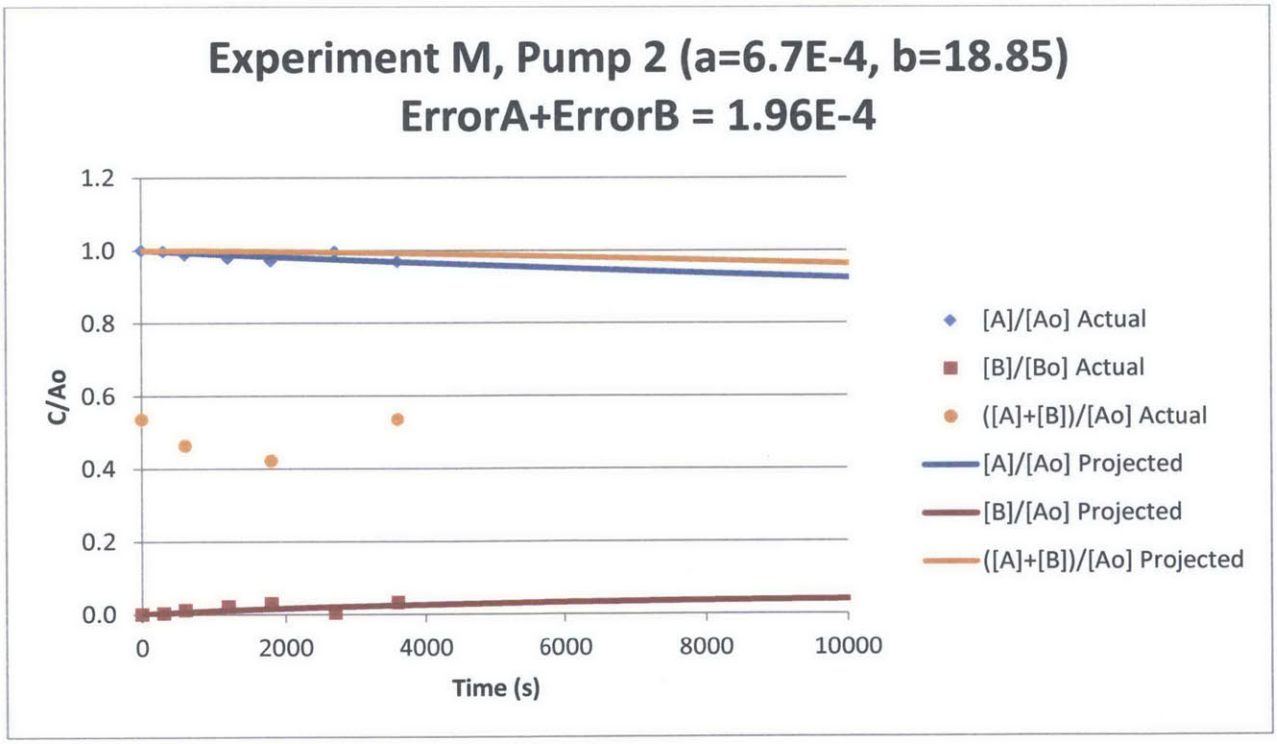

APPENDIX I: Cinnamic Acid Model Fitting Results

The following pages contain charts of the results of the model fitting process for Cinnamic Acid Experiments N-X and Z. The charts contain both the experimental measurements as well as the model predictions. The model predictions are based upon the fitting parameters a and b, as described in section 5.1.

On each page, the reader will find the following information:

a) Experiment name tag

b) Independent variable conditions:

   a. Initial target pollutant concentration

   b. Initial catalyst concentration

   c. Radiation power

c) Plots of experimental and model predicted values for cinnamic acid, intermediate compounds, total organic carbon (all normalized to initial target TOC):

   a. Values for a and b will be given in the title for each plot

   b. The combined error value will also be provided

Experiment N

Initial CA Concentration	Catalyst (TiO_2) Concentration	Radiation Power
4 mM of TOC	0.10 g/L	74.2 W/m^2

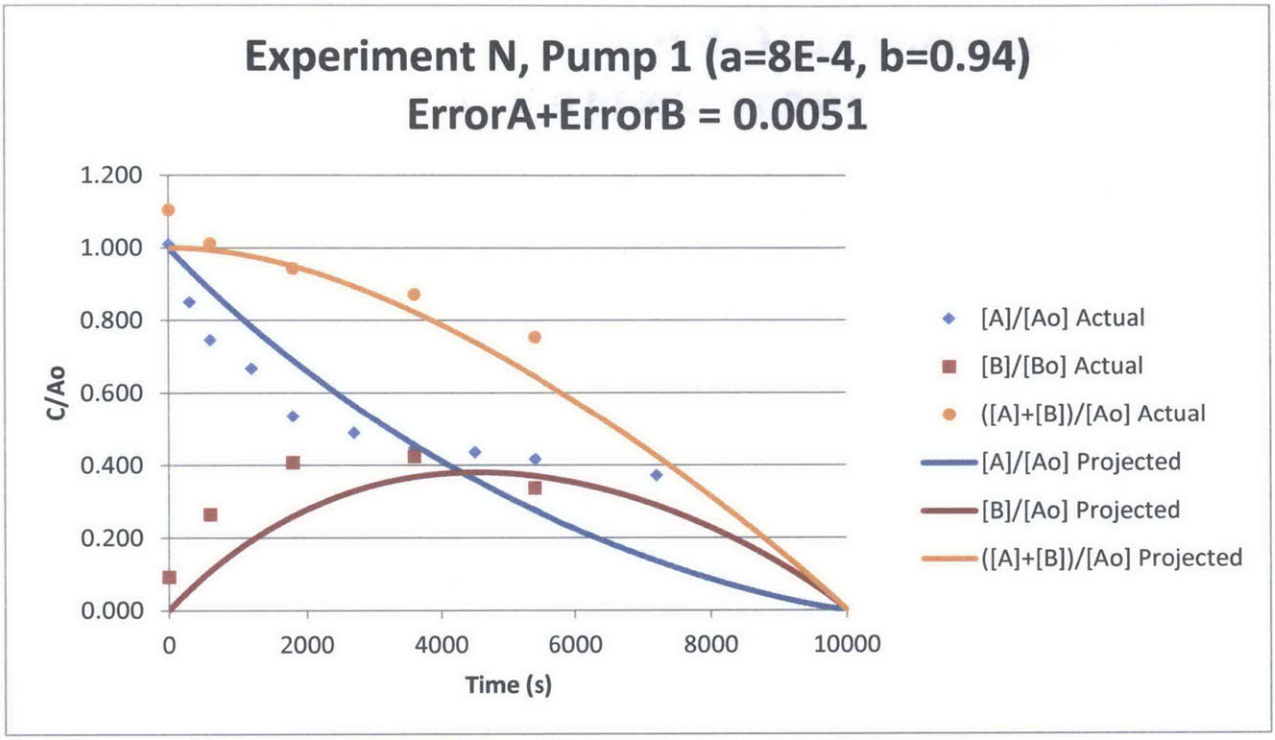

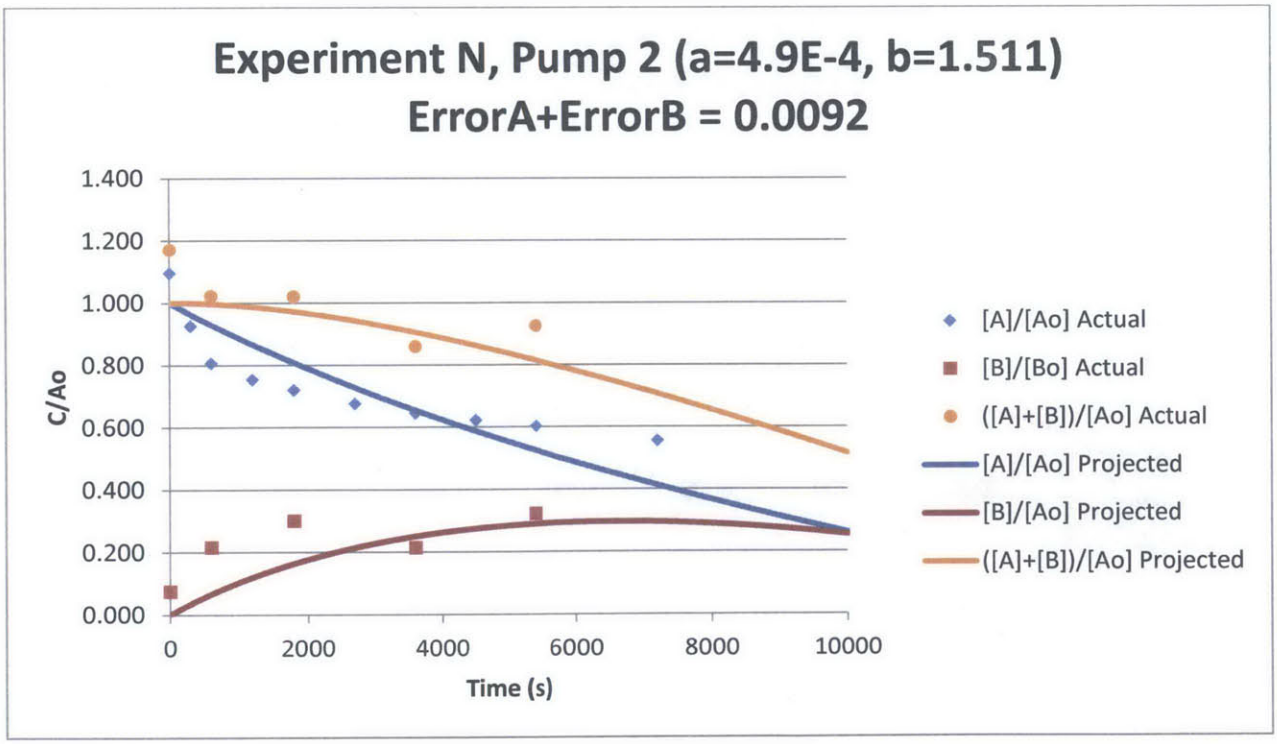

Experiment O

Initial CA Concentration	Catalyst (TiO_2) Concentration	Radiation Power
8 mM of TOC	0.10 g/L	74.2 W/m^2

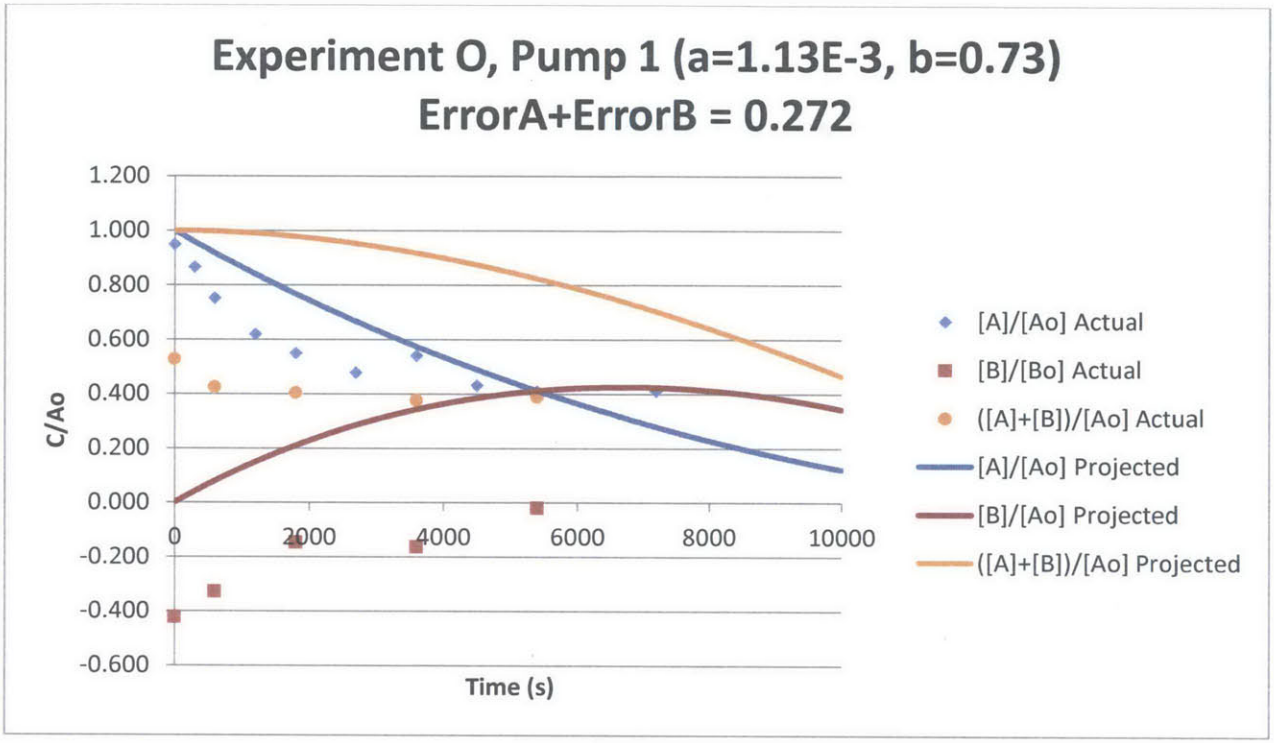

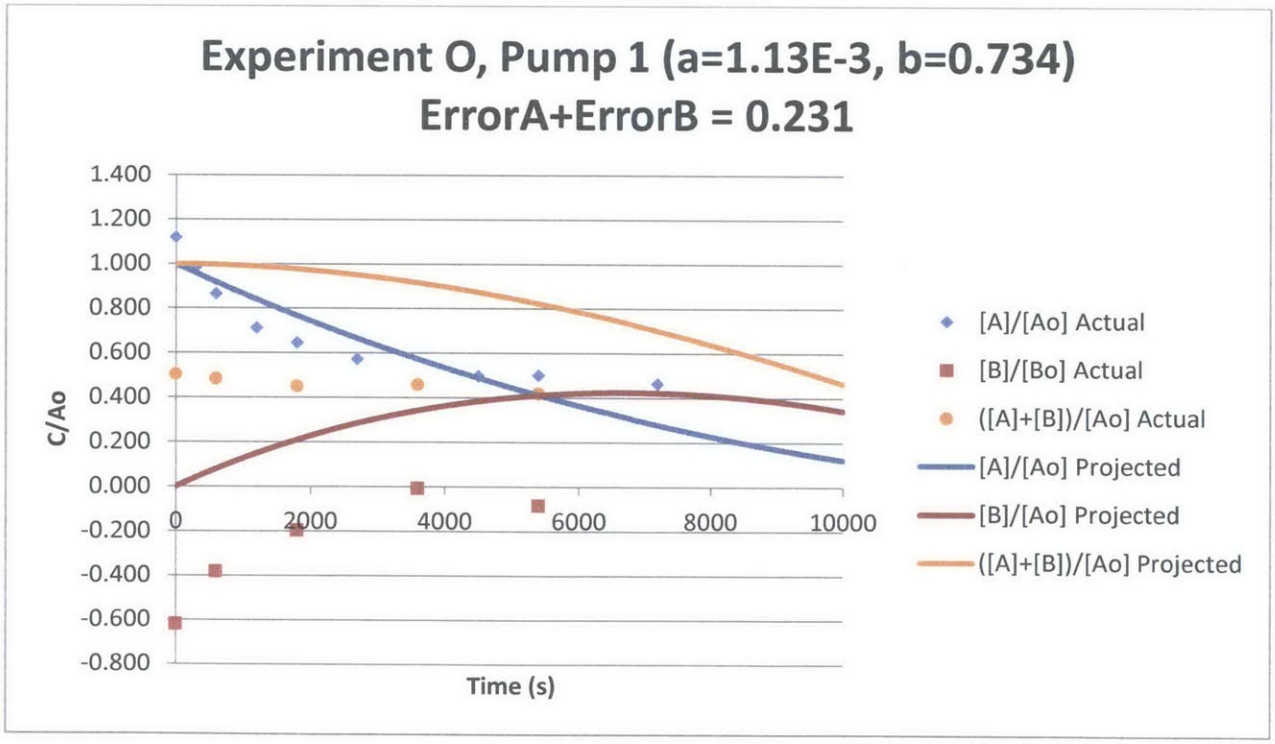

Experiment P

Initial CA Concentration	Catalyst (TiO_2) Concentration	Radiation Power
6 mM of TOC	0.10 g/L	74.2 W/m^2

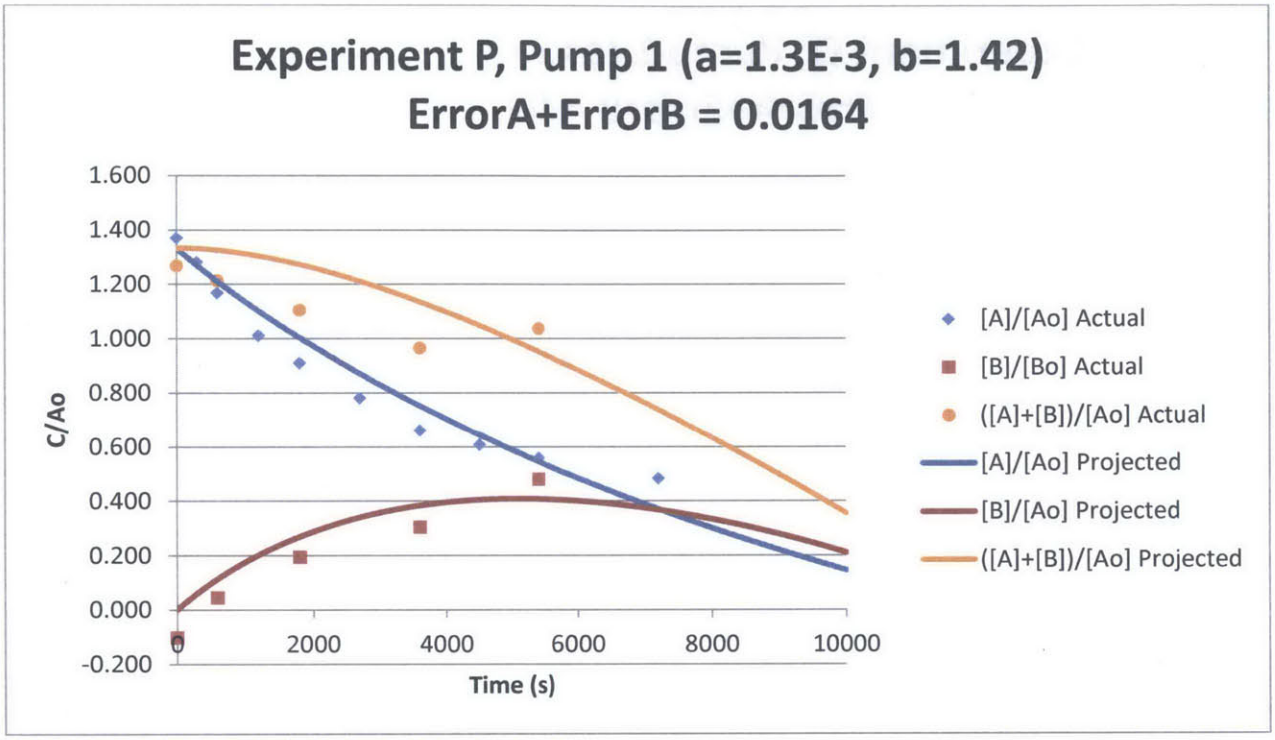

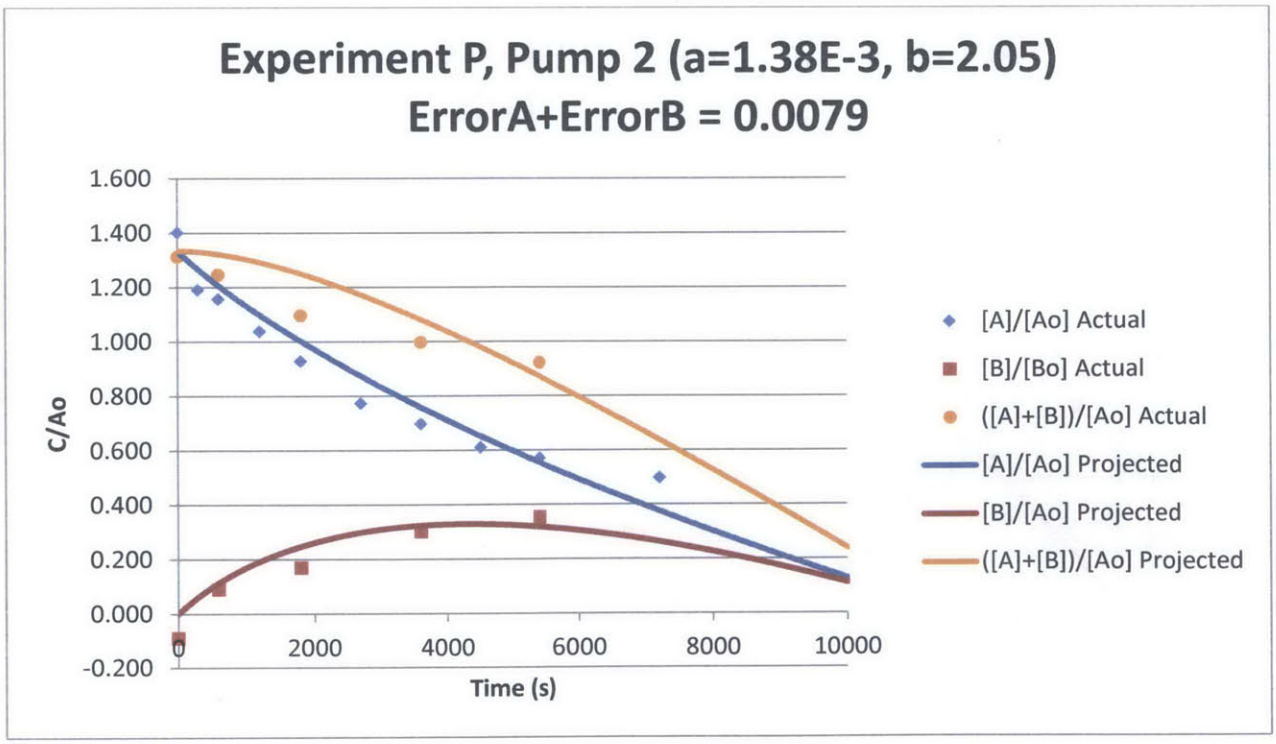

Experiment Q

Initial CA Concentration	Catalyst (TiO_2) Concentration	Radiation Power
4 mM of TOC	0.05 g/L	74.2 W/m^2

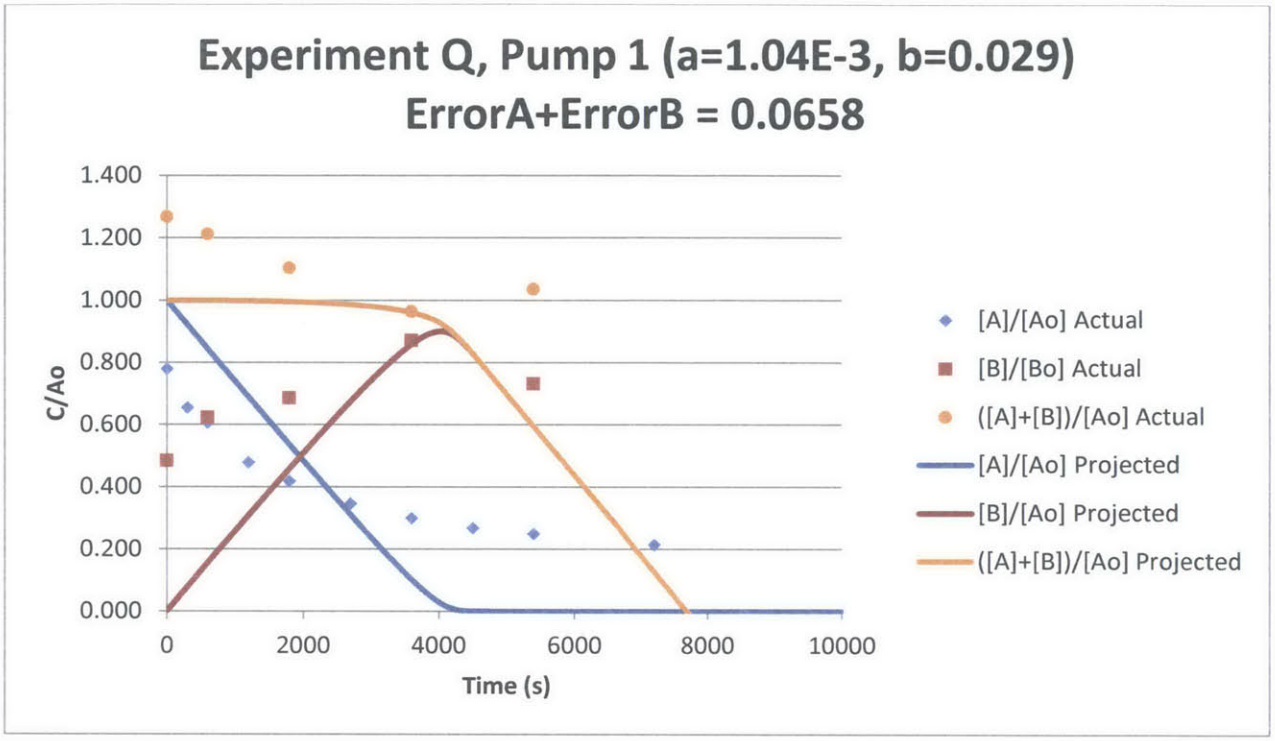

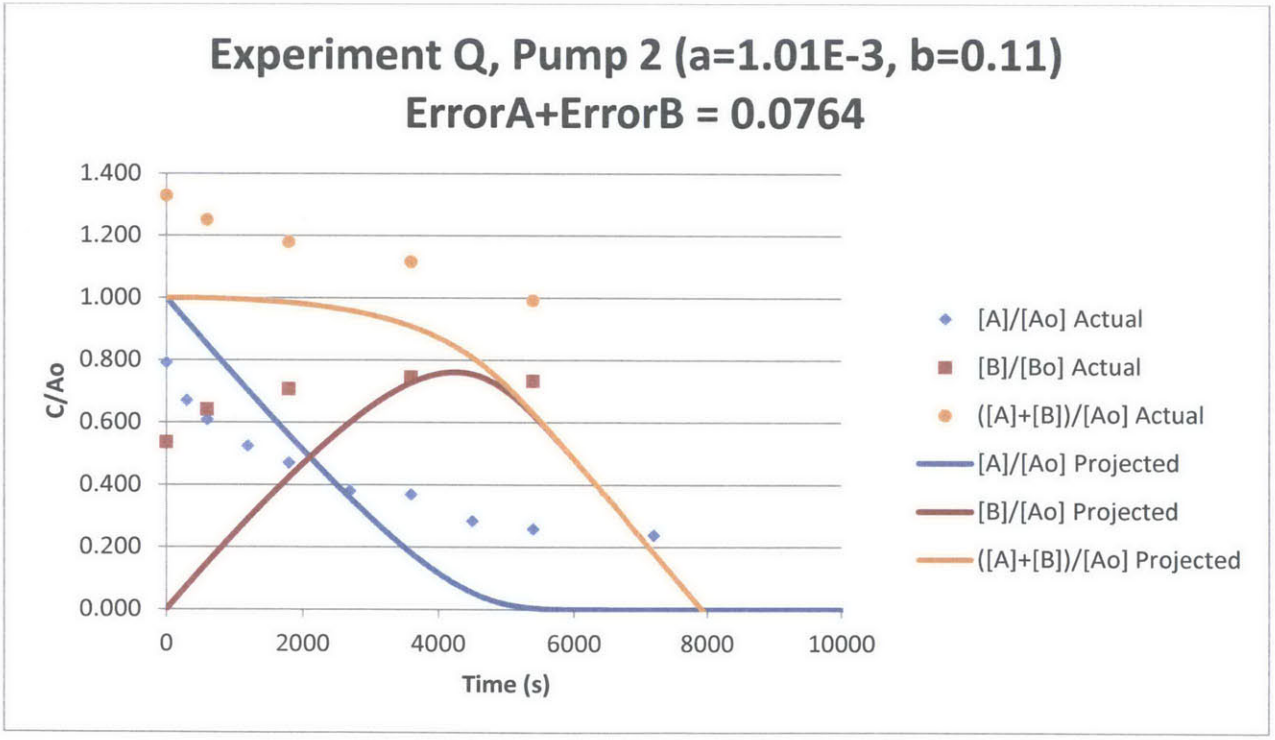

Experiment R

Initial CA Concentration	Catalyst (TiO_2) Concentration	Radiation Power
6 mM of TOC	0.05 g/L	74.2 W/m^2

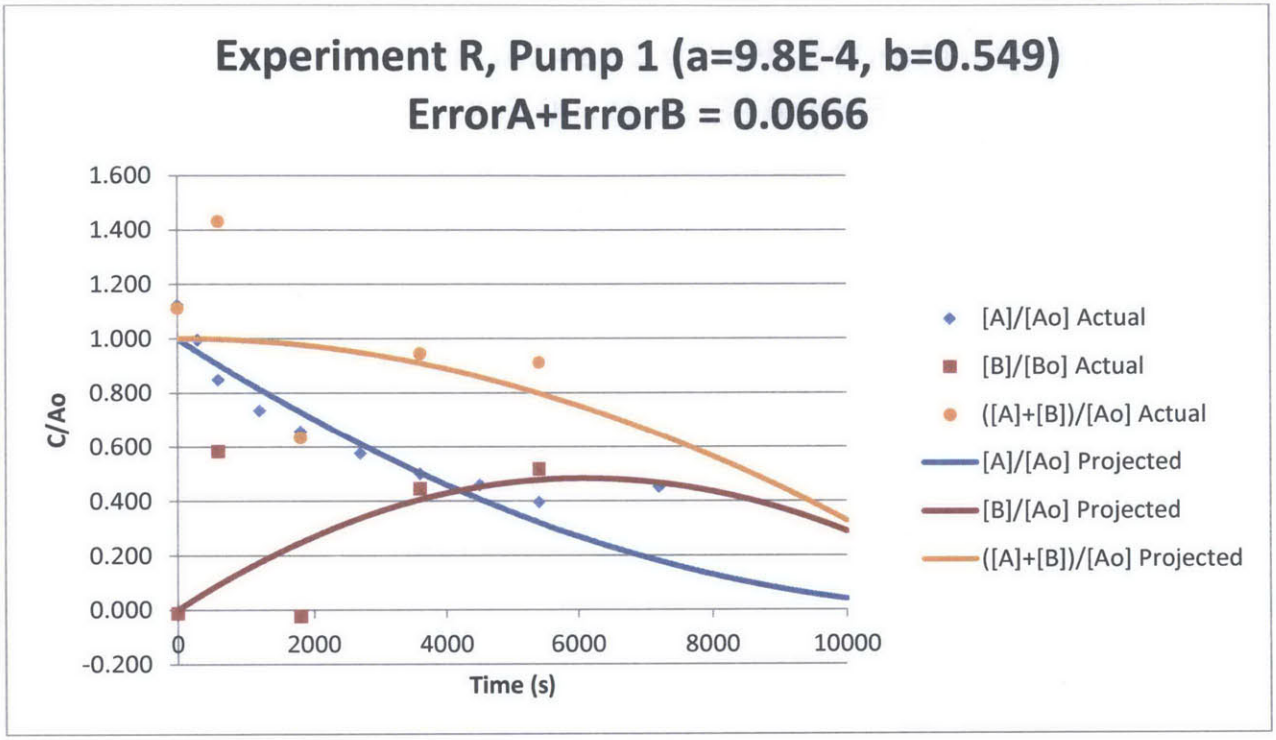

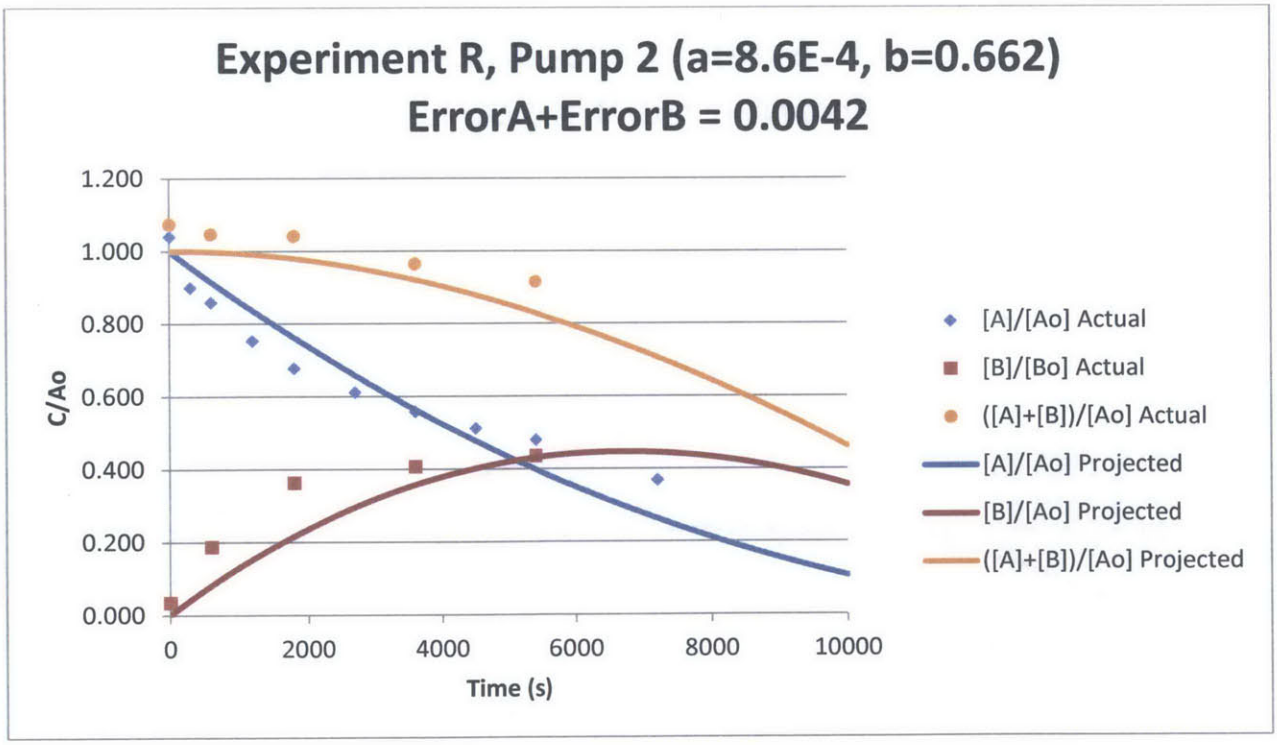

Experiment S

Initial CA Concentration	Catalyst (TiO_2) Concentration	Radiation Power
8 mM of TOC	0.05 g/L	74.2 W/m^2

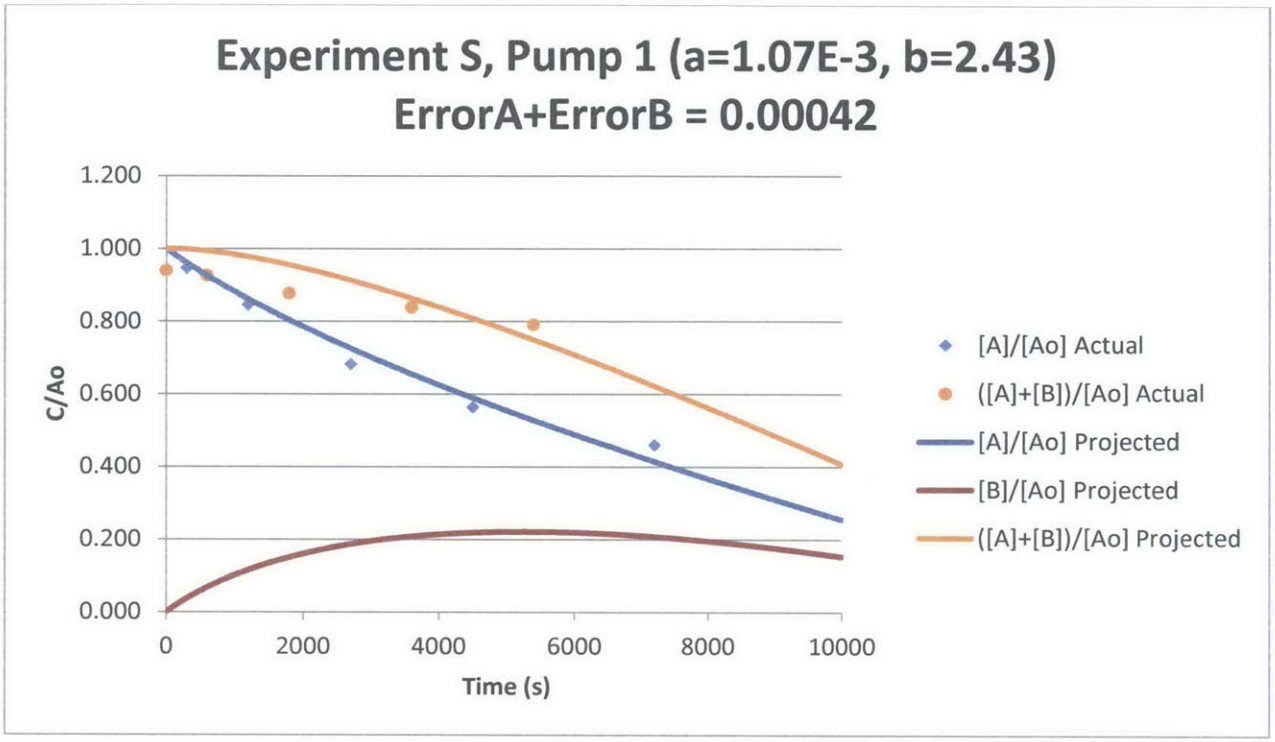

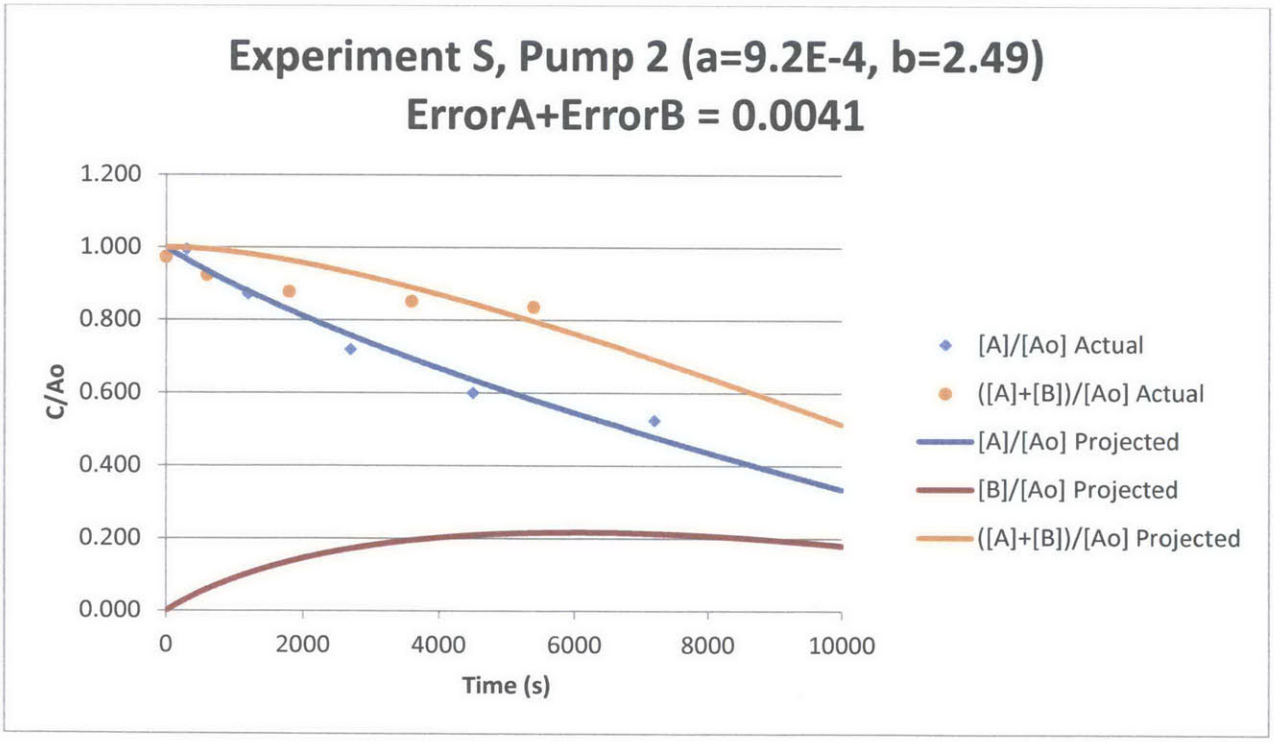

Experiment T

Initial CA Concentration	Catalyst (TiO_2) Concentration	Radiation Power
4 mM of TOC	0.20 g/L	74.2 W/m^2

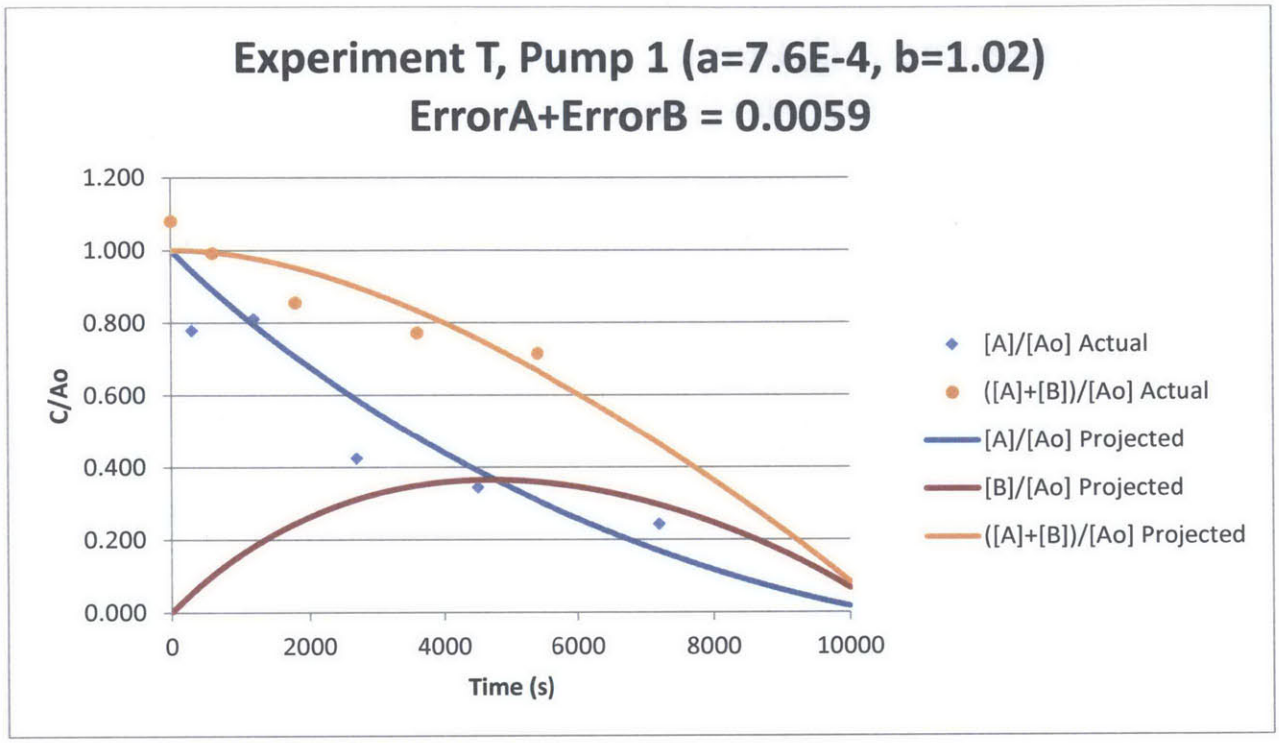

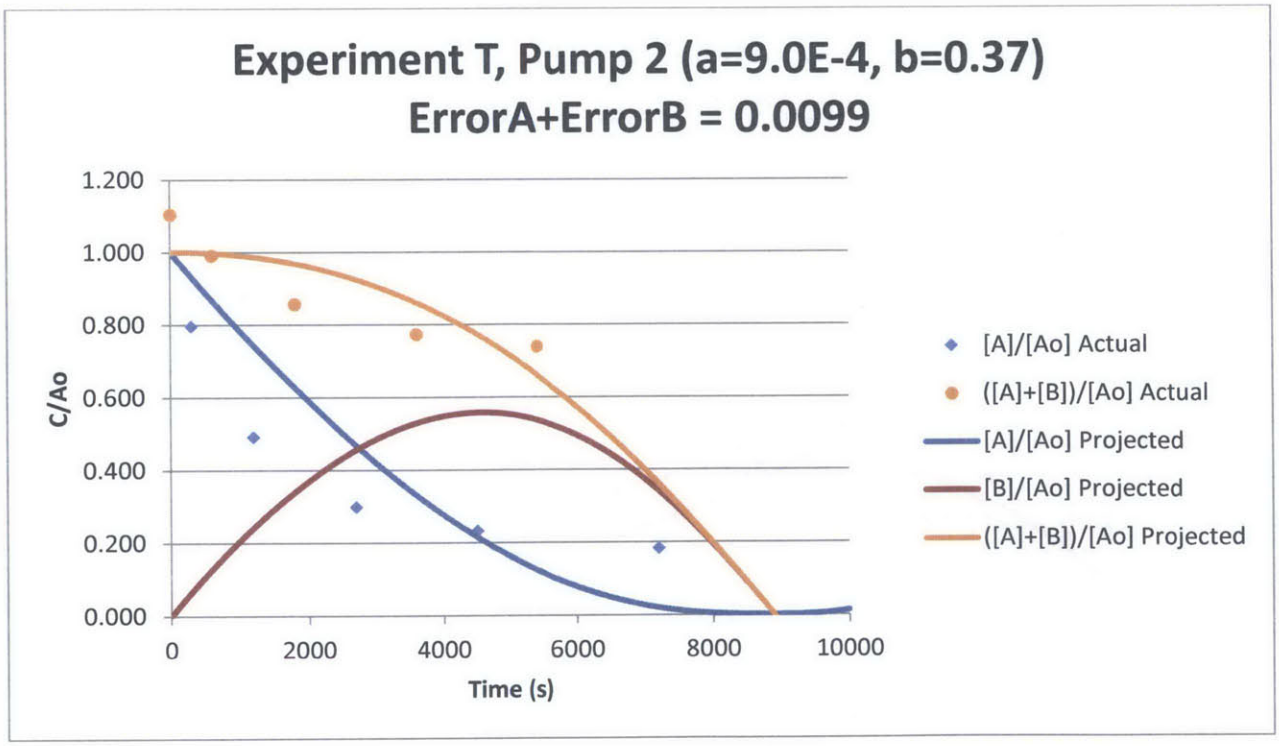

Experiment U

Initial CA Concentration	Catalyst (TiO_2) Concentration	Radiation Power
8 mM of TOC	0.20 g/L	74.2 W/m^2

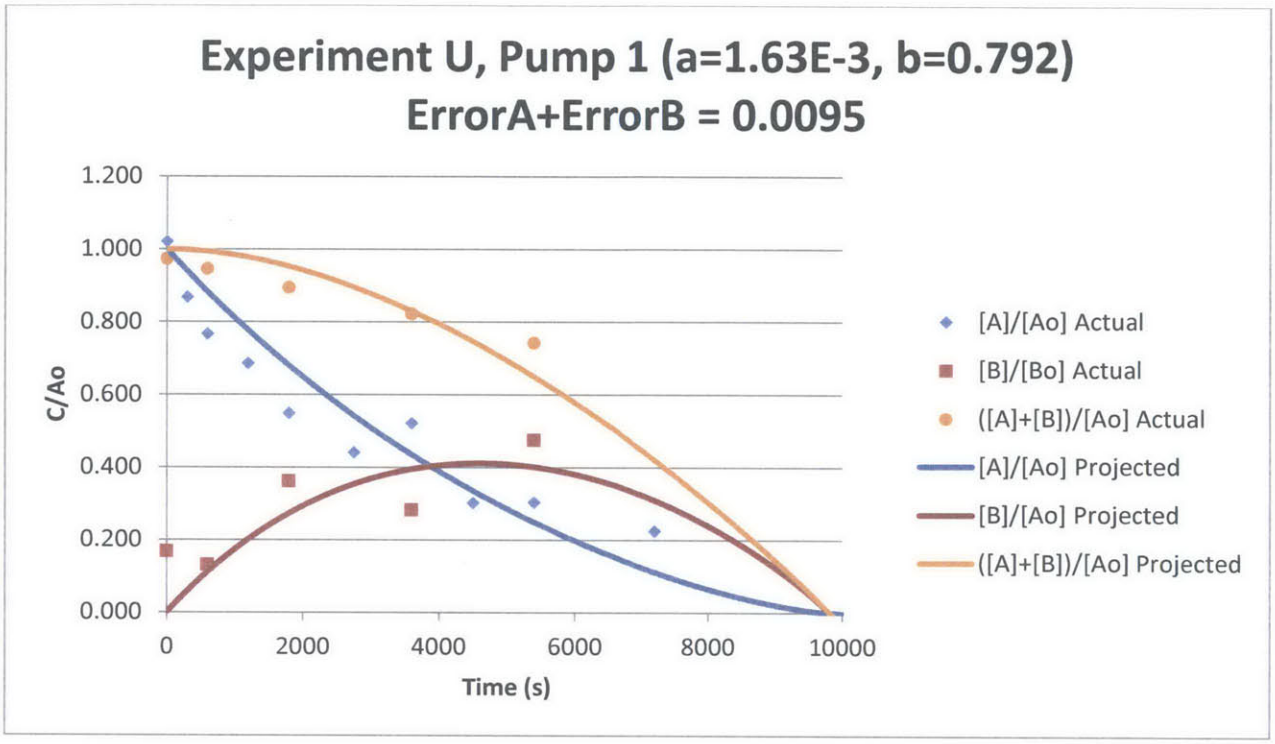

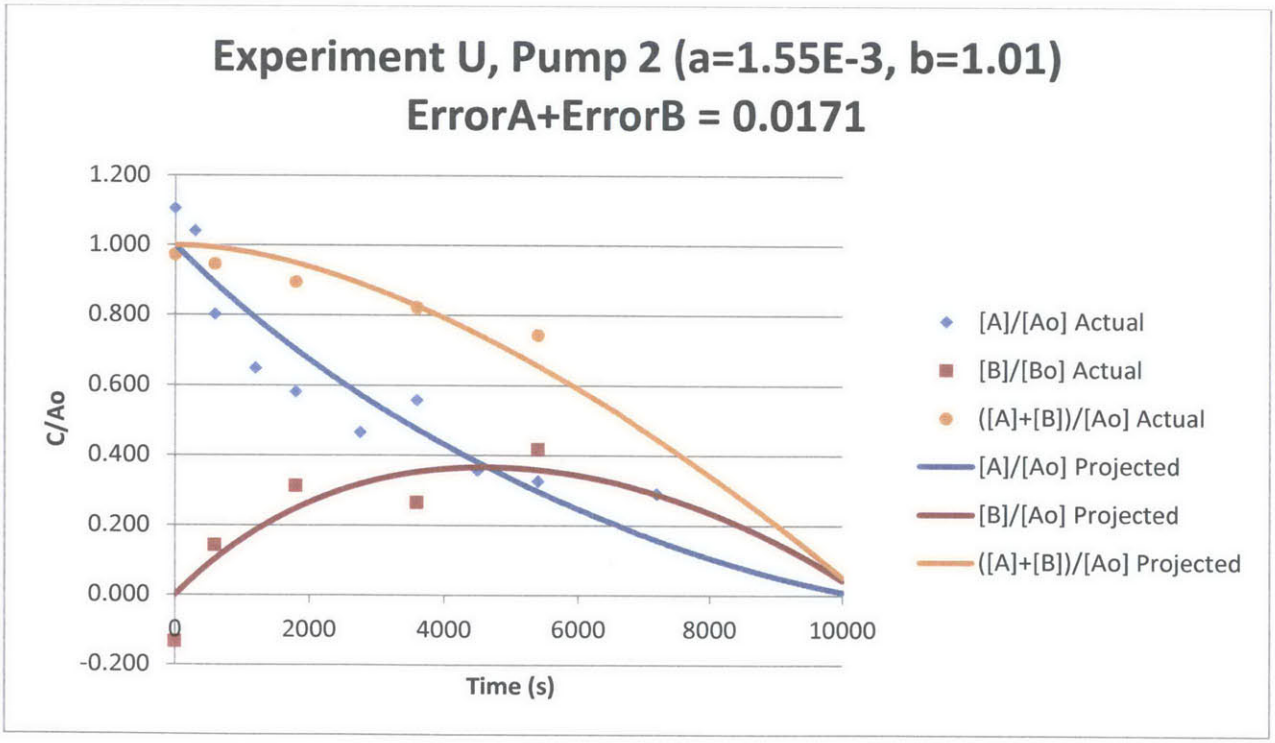

Experiment V

Initial CA Concentration	Catalyst (TiO_2) Concentration	Radiation Power
6 mM of TOC	0.20 g/L	74.2 W/m^2

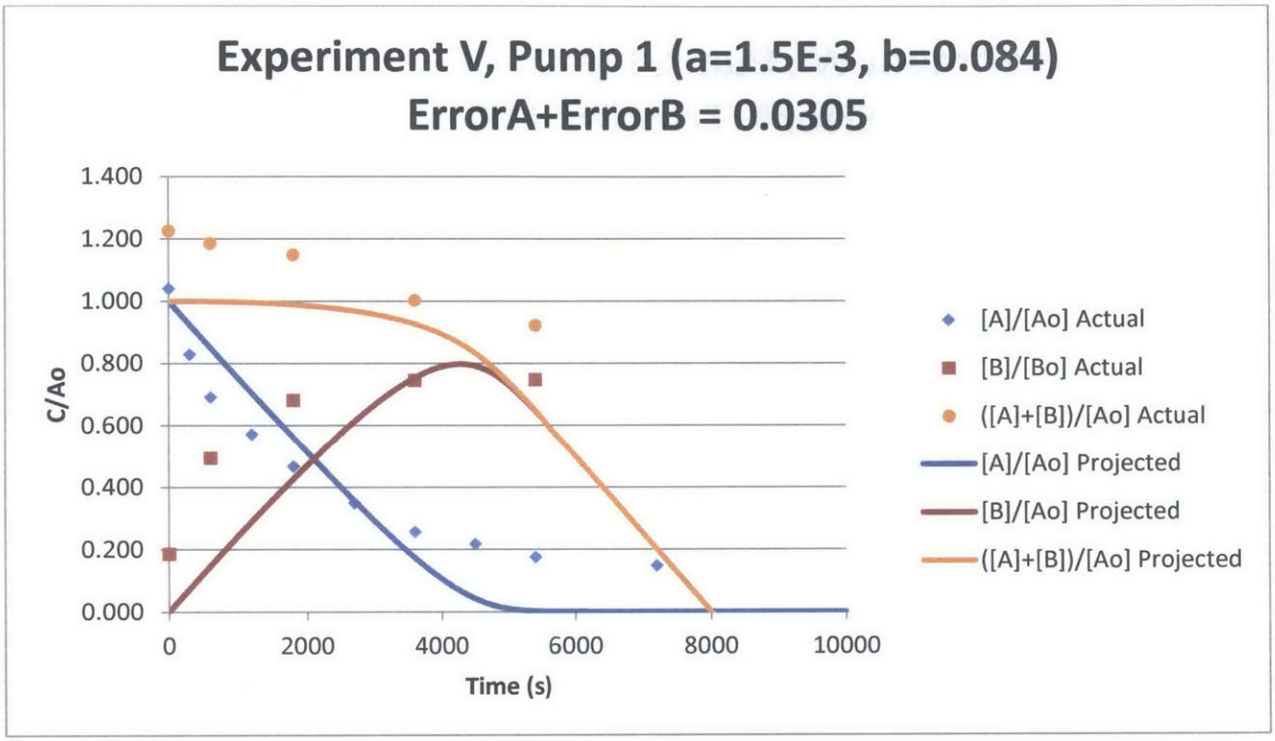

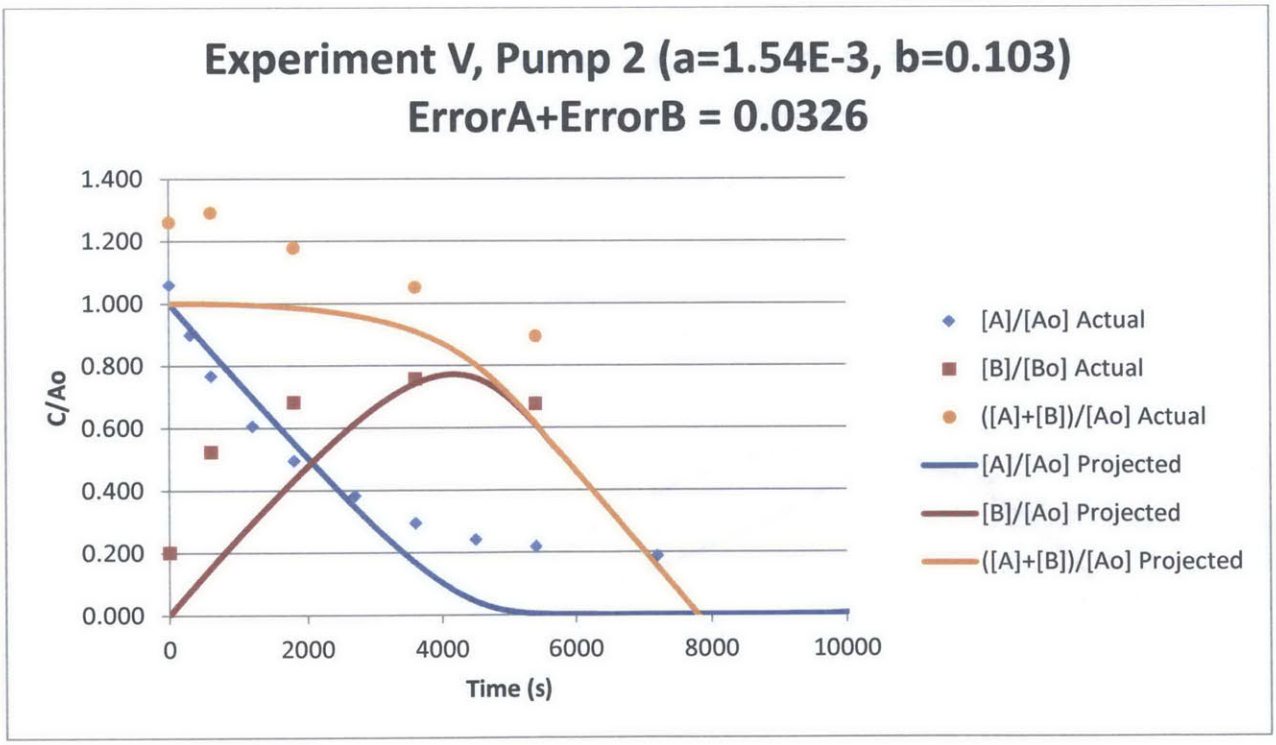

Experiment W

Initial CA Concentration	Catalyst (TiO_2) Concentration	Radiation Power
4 mM of TOC	0.20 g/L	46.2 W/m^2

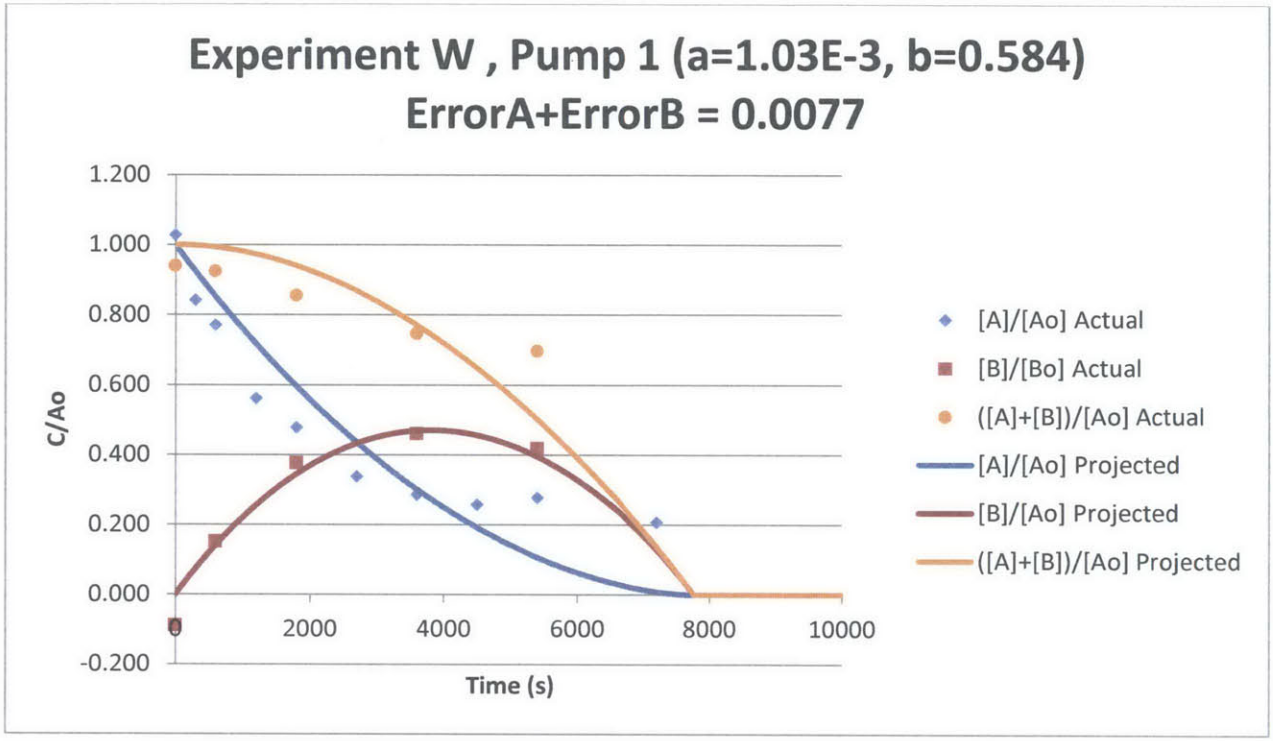

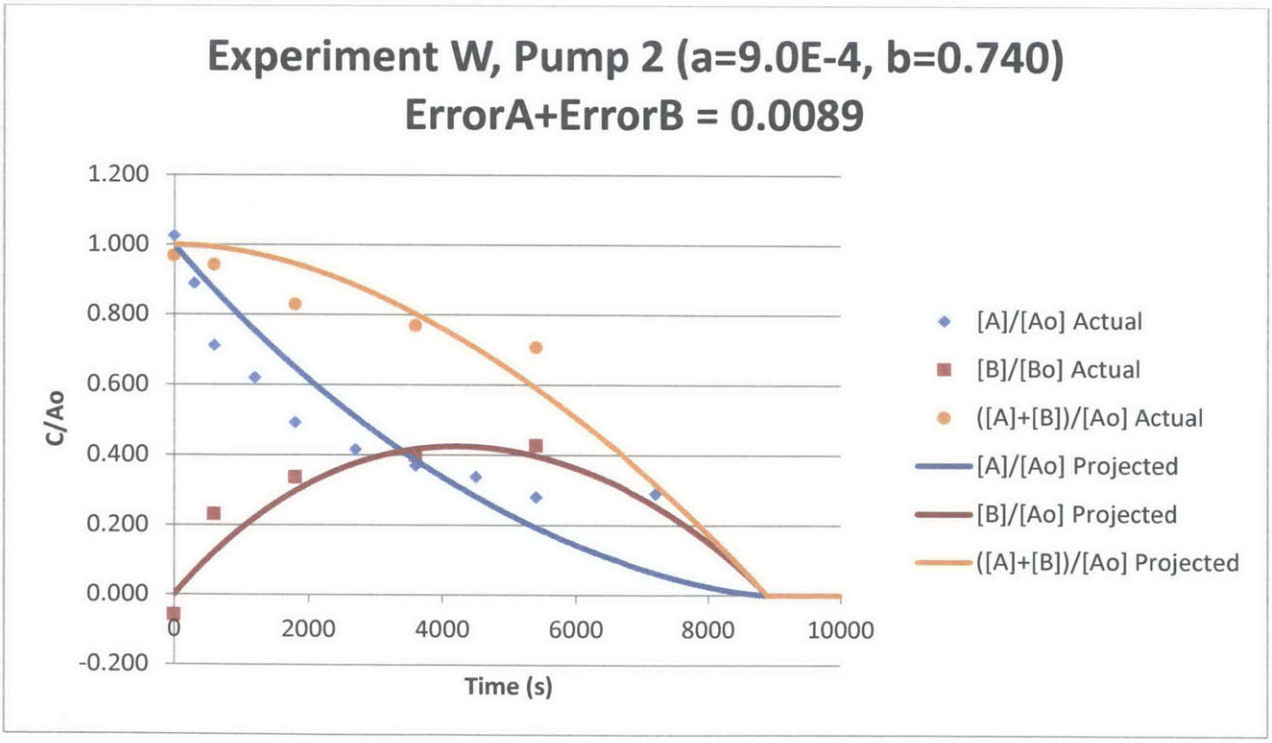

Experiment X

Initial CA Concentration	Catalyst (TiO_2) Concentration	Radiation Power
8 mM of TOC	0.20 g/L	46.2 W/m^2

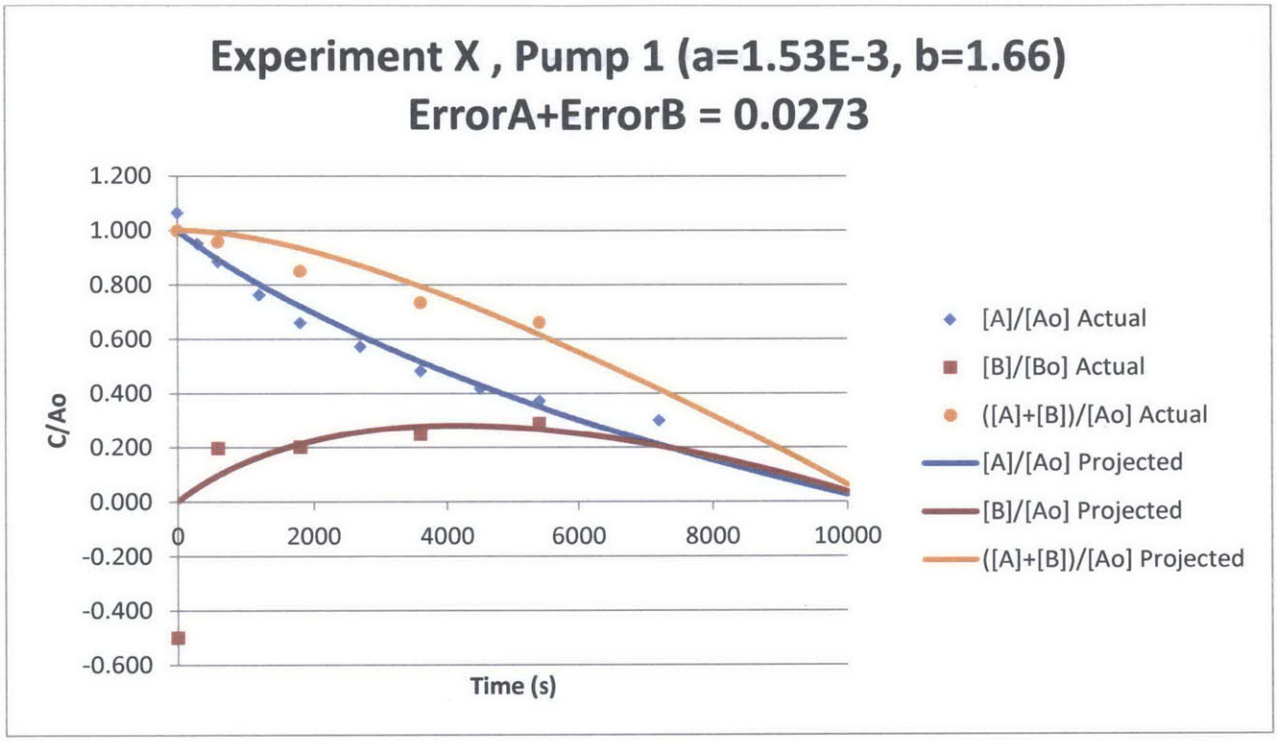

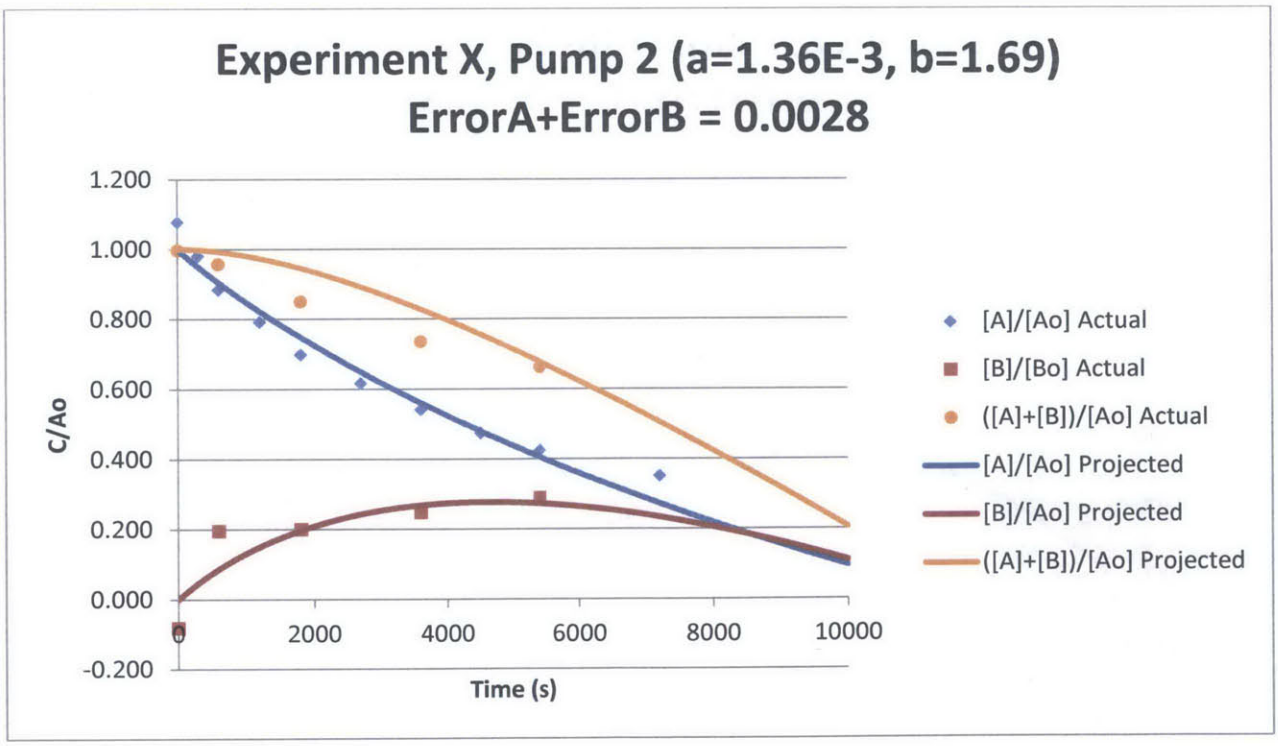

Experiment Z

Initial CA Concentration	Catalyst (TiO_2) Concentration	Radiation Power
6 mM of TOC	0.20 g/L	46.2 W/m^2